



Karin Koch MSc

**Flavoproteins from the yeast
*Saccharomyces cerevisiae***

DISSERTATION

zur Erlangung des akademischen Grades
Doktorin der Naturwissenschaften
eingereicht an der

Technischen Universität Graz

Betreuer

Univ.-Prof. Mag. rer. nat. Dr. rer. nat. Peter Macheroux

Institut für Biochemie
Technische Universität Graz

Graz, März 2017

**All is a riddle,
and the key to a riddle...
is another riddle.**

Ralph Waldo Emerson

Acknowledgements

First of all I want to express my gratitude to my supervisor Prof. Peter Macheroux for giving me the opportunity to work on such interesting research projects. I want to thank him for his support and encouragement throughout the study. Furthermore I am very thankful to the members of the thesis committee (Dr. Karin Athenstaedt, Prof. Karl Gruber and Prof. Sepp-Dieter Kohlwein) for their valuable suggestions.

I want to thank the entire group and institute members for the nice atmosphere inside and outside the lab, for the fruitful discussions and for the nice pasta days we had together. My special thanks go to the people which contributed something to my work. It was a pleasure for me to work with you and learn from you. Karin Athenstaedt and Venugopal Gudipati helped me with various methods and the discussions with them have made me understand yeast a bit better. Emilia Strandback and Wolf-Dieter Lienhart contributed very often new ideas and practical help. Silvia Wallner and Chanakan Tongsook were always helpful with lab equipment and experimental procedures. Eva-Maria Frießer was always motivated to help me with routine work. Altijana Hromic and Karl Gruber for the help with crystallisation and structural biology in general.

During the last years I also had the opportunity to supervise several talented and motivated students during lab courses, project labs and bachelor thesis. Special thanks to Johannes Repelnig, Sarah Stryeck and Marija Sorokina for their contributions to my projects. It was an honor for me to attend you during your first scientific steps. Thanks to all students for the questions which raised me to learn more and more about methods and background stories. Special thanks also to the supervisor team (Peter Augustin, Wolf-Dieter Liehnhart, Barbara Steiner, Marina Toplak, Silvia Wallner) for the good cooperation.

Besides being marvellous working colleagues some people become really good friends within the last years who extended my family, shared new experiences with me and investigated a bit more of our wonderful world together with me. I hope these friendships persist distances and years.

Last but not least, I want to express my gratitude to my dear parents for their love, their constant support and for always believing in me. Without them I would not be able to go this way. Moreover, special thanks to my sister for being one of the most important persons in my life and helping me in difficult situations.

Abstract

Analysis of the flavoproteome of the yeast *Saccharomyces cerevisiae* identified 68 genes encoding flavin-dependent enzymes. This organism is one of the best-investigated eukaryotic model systems for molecular and cell biological studies. Nevertheless many flavoproteins from *Saccharomyces cerevisiae* are poorly characterized. This work was initiated to get a deeper insight into the characteristics of two different flavoproteins, the microtubule-associated Irc15p and the flavodoxin-like protein Pst2p. The proteins were heterologously expressed in *Escherichia coli* and purified for a detailed investigation.

Cell biological studies indicate a functionality of Irc15p on microtubule dynamics and cell cycle progression. In my studies, I could demonstrate that Irc15p is a flavoprotein and its cofactor can be reduced with NAD(P)H and reoxidized by several artificial electron acceptors. Although Irc15p has a high structural similarity to the disulfide reducing lipoamide dehydrogenase, it lacks the protein disulfide but retained the catalytic diad, which are important for the enzymatic activity of lipoamide dehydrogenase. Even though my data do not directly support the disulfide reducing activity of Irc15p it is conceivable that the interaction with other proteins unmask this catalytic activity. Alternatively our findings suggest that Irc15p is efficiently reduced in yeast cells to deliver electrons to an as yet unidentified electron acceptor that is potentially related to Irc15p's function in regulating microtubule dynamics and cell cycle progression.

The yeast genome encodes three highly similar flavodoxin-like proteins, namely Pst2p, Rfs1p and Ycp4p, however none of these proteins were functionally characterized. Therefore I conducted a detailed investigation of Pst2p. It could be demonstrated that Pst2p is a very efficient NAD(P)H:quinone oxidoreductase rapidly reducing quinones *in vitro* and *in vivo*. However, in contrast to other quinone reductases Pst2p displays an unusually positive redox potential. This affects its substrate spectrum as well as its cofactor binding properties. The structure of Pst2p was elucidated by X-ray crystallography and revealed that Pst2p adopts the flavodoxin-like fold and forms tetramers independent of cofactor binding. In summary, my data suggest that Pst2p possesses more similarity to quinone reductases than flavodoxins and that Pst2p enables yeast cells to cope with quinone-induced damage suggesting a role of the enzyme in managing oxidative stress.

Zusammenfassung

Bei einer Analyse des Flavoproteoms der Hefe *Saccharomyces cerevisiae* wurden 68 Gene identifiziert, die ein Flavoprotein kodieren. Diese Hefe ist einer der am besten untersuchten Modelorganismen, dennoch wurden nur wenige Flavoproteine aus *Saccharomyces cerevisiae* eingehend untersucht. Das Hauptziel meiner Arbeit war es einen tieferen Einblick in die Funktion von zwei verschiedenen Flavoproteinen, dem Microtubuli- assoziierten Irc15p und dem Flavodoxin-ähnlichen Protein Pst2p, zu erhalten. Die Proteine wurden heterolog in *Escherichia coli* exprimiert und für eine detaillierte Erforschung gereinigt.

Zellbiologische Studien ergaben, dass Irc15p einen Einfluss auf die Dynamik von Mikrotubuli und den Verlauf des Zellzyklus hat. In meinen Studien konnte ich zeigen, dass es sich bei Irc15p um ein Flavoprotein handelt, dessen Kofaktor mittels NAD(P)H reduziert und mit künstlichen Elektronenakzeptoren reoxidiert werden kann. Obwohl Irc15p eine große strukturelle Ähnlichkeit zu der Disulfid reduzierenden Lipoamiddehydrogenase aufweist, fehlt Irc15p das katalytische Proteindisulfid, die katalytische Diade ist jedoch vorhanden. Beide Funktionen sind unerlässlich für die enzymatische Aktivität der Lipoamiddehydrogenase. Zwar geben meine Daten keinen direkten Hinweis auf die Disulfid reduzierende Aktivität von Irc15p, dennoch ist es möglich, dass Irc15p diese Aktivität erst durch Interaktion mit anderen Proteinen zeigt. Alternativ können meine Resultate auch dahingehend interpretiert werden, dass Irc15p Elektronen an einen bisher nicht identifizierten Elektronenakzeptor liefert, wodurch die Mikrotubulidynamik und der Verlauf des Zellzyklus beeinflusst werden.

Das Hefegenom kodiert drei sehr ähnliche Proteine (Pst2p, Rfs1p, Ycp4p) die der Familie der Flavodoxin-ähnlichen Proteine zugeordnet werden können. Ich führte eine eingehende Untersuchung von Pst2p durch, bei der gezeigt werden konnte, dass es sich bei Pst2p um eine NAD(P)H:Chinonreduktase handelt, welche die Reduktion von Chinonen *in vitro* und *in vivo* katalysiert. Im Vergleich zu anderen Chinonreduktasen weist Pst2p ein sehr positives Redoxpotential auf, wodurch das Substratspektrum und die Bindung des Kofaktors beeinflusst werden. Die Struktur von Pst2p wurde mit Hilfe von X-Ray Kristallographie aufgeklärt und ergab, dass Pst2p eine Flavodoxin-ähnliche Faltung annimmt und unabhängig von der Bindung des Kofaktors als Tetramer vorliegt. Zusammenfassend zeigen meine Daten, dass Pst2p mehr Ähnlichkeiten zu Chinonreduktasen als zu Flavodoxinen aufweist und die Hefezellen durch dieses Protein besser mit Chinon induziertem Stress umgehen können. Dadurch wird eine Funktion von Pst2p im Umgang mit oxidativem Stress nahegelegt.

EIDESSTATTLICHE ERKLÄRUNG

Ich erkläre an Eides statt, dass ich die vorliegende Arbeit selbstständig verfasst, andere als die angegebenen Quellen/Hilfsmittel nicht benutzt, und die den benutzten Quellen wörtlich und inhaltlich entnommenen Stellen als solche kenntlich gemacht habe.

STATUTORY DECLARATION

I declare that I have authored this thesis independently, that I have not used other than the declared sources / resources, and that I have explicitly marked all material which has been quoted either literally or by content from the used sources.

Graz,

Table of Contents

Acknowledgements.....	I
Abstract.....	II
Kurzfassung.....	III
Eidstattliche Erklärung/Statutory declaration.....	IV
Table of Contents.....	V
1 The flavoproteome of the yeast <i>Saccharomyces cerevisiae</i>	1
Abstract.....	3
Introduction to the history of Flavoprotein discovery.....	4
General aspects of the yeast flavoproteome.....	5
Flavoproteins, the stewards of iron.....	11
Flavoprotein families in yeast.....	13
Yeast flavoproteins in redox balancing.....	16
Flavin biosynthesis and transport.....	18
Yeast flavoproteins as models for human diseases.....	21
Concluding remarks.....	25
Methods.....	25
References.....	26
2 The Microtubule-associated flavoprotein Irc15p from <i>Saccharomyces cerevisiae</i> ..	37
Abstract.....	39
Introduction.....	40
Materials and Methods.....	41
Results.....	46
Discussion.....	54
References.....	57

3 Flavodoxin-like proteins and interacting proteins from <i>Saccharomyces cerevisiae</i>	62
3.1 Structure, biochemical and kinetic properties of recombinant Pst2p from <i>Saccharomyces cerevisiae</i> , a FMN-dependent NAD(P)H:quinone oxidoreductase.....	63
Abstract.....	64
Introduction.....	66
Materials and Methods.....	67
Results.....	75
Discussion.....	88
References.....	90
Supplementary Information.....	96
3.2 Expression and purification of the flavodoxin-like proteins Ycp4p and Rfs1p from <i>Saccharomyces cerevisiae</i>	99
Materials and Methods.....	100
Results.....	105
Discussion.....	110
References.....	111
3.3 Overexpression of the yeast bZIP transcription factor Yap4p, an interaction protein of the flavodoxin-like protein Lot6p.....	113
Introduction.....	114
Materials and Methods.....	116
Results.....	121
Discussion.....	127
References.....	129

Appendix.....	135
Additional Publication.....	136
Catalytic competence, structure and stability of the cancer associated R139W variant of the human NAD(P)H:quinone oxidoreductase 1 (NQO1).....	137
Abstract.....	138
Introduction.....	139
Materials and Methods.....	140
Results.....	145
Discussion.....	154
References.....	157
Curriculum vitae.....	162
Publication list.....	164

CHAPTER 1

The flavoproteome of the yeast *Saccharomyces cerevisiae*

The flavoproteome of the yeast *Saccharomyces cerevisiae*

Venugopal Gudipati, Karin Koch, Wolf-Dieter Lienhart, Peter Macheroux*

*From the Graz University of Technology, Institute of Biochemistry, Petersgasse 12,
A-8010 Graz, Austria; Tel.: +43-316-873 6450, Fax: +43-316-873 6952,

Email: peter.macheroux@tugraz.at

Author contributions

P.M. initiated the writing of the review article "*The flavoproteome of the yeast Saccharomyces cerevisiae*"; P.M. wrote the section 1 (introduction to the history of Flavoprotein discovery) and corrected the whole manuscript; K.K. established the list of flavoproteins. K.K. and W.-D.L. wrote sub section 6 (flavin biosynthesis and transport). V.G. revised the list of flavoproteins, wrote the sub section 7 (yeast flavin proteins as models for human diseases) and established the respective list of flavoproteins. All the authors contributed equally to the remaining sections of the manuscript.

Manuscript published

BIOCHIMICA ET BIOPHYSICA ACTA (2014), Volume 1844, Number 3, Pages 534-544.

Abstract

Genome analysis of the yeast *Saccharomyces cerevisiae* identified 68 genes encoding flavin-dependent proteins (1.1% of protein encoding genes) to which 47 distinct biochemical functions were assigned. The majority of flavoproteins operate in mitochondria where they participate in redox processes revolving around the transfer of electrons to the electron transport chain. In addition, we found that flavoenzymes play a central role in various aspects of iron metabolism, such as iron uptake, the biogenesis of iron–sulfur clusters and insertion of the heme cofactor into apocytochromes. Another important group of flavoenzymes is directly (Dus1-4p and Mto1p) or indirectly (Tyw1p) involved in reactions leading to tRNA-modifications. Despite the wealth of genetic information available for *S. cerevisiae*, we were surprised that many flavoproteins are poorly characterized biochemically. For example, the role of the yeast flavodoxins Pst2p, Rfs1p and Ycp4p with regard to their electron donor and acceptor is presently unknown. Similarly, the function of the heterodimeric Aim45p/Cir1p, which is homologous to the electron-transferring flavoproteins of higher eukaryotes, in electron transfer processes occurring in the mitochondrial matrix remains to be elucidated. This lack of information extends to the five membrane proteins involved in riboflavin or FAD transport as well as FMN and FAD homeostasis within the yeast cell. Nevertheless, several yeast flavoproteins, were identified as convenient model systems both in terms of their mechanism of action as well as structurally to improve our understanding of diseases caused by dysfunctional human flavoprotein orthologs.

Introduction to the history of Flavoprotein discovery

The yeast *Saccharomyces cerevisiae* played a central role in the discovery of flavoproteins as Otto Warburg and his collaborators were the first to isolate a “yellow ferment” from yeast cells [1]. Further studies by Theorell led to the concept of reversible association of co-enzyme and apo-enzyme to form the active holo-enzyme [2]. The isolation of other (new) yellow ferments from yeast prompted the renaming of the original ferment in to “old yellow ferment” (old yellow enzyme = OYE) [3]. Although it was demonstrated that OYE is reduced by NADPH [1,4] the physiological electron accepting substrate(s) remains uncertain despite its reported role in the maintenance of the cytoskeleton [5]. This may have contributed to the persistent use of OYE instead of the official classification as NAD(P)H dehydrogenase (EC 1.6.99.1).

Despite the elusive nature of the physiological substrate(s), OYE rapidly developed in to an important model flavoenzyme culminating in the determination of the nucleotide sequence of *oye2* and *oye3* as well as the elucidation of its three-dimensional structure by X-ray crystallography [6–8]. The detailed biochemical characterisation of OYE also led to the identification of a number of artificial substrates, such as N-ethylmaleimide, cyclohex-2-enone and nitroolefins [8–10]. All of these substrates share a common structural motif consisting of an electron-withdrawing group (e.g. a carbonyl or nitro group) in α -position of a carbon–carbon double bond. The remarkably broad range of accepted substrates rendered OYE an ideal tool for biocatalytic applications exploited in numerous studies [11–15]. These efforts were further stimulated by the discovery of OYE homologs in many eubacteria as well as plant species in the 1990s [16–23]. Plant OYE homologs were of particular interest because of their well-defined role in the biosynthesis of the plant hormone jasmonate, which plays a crucial role in the plant's defense response to pathogens [24,25]. In all reported cases, the natural substrates exhibited the structural motif discovered in previous studies with yeast OYE. Hence, the yeast enzyme also became the paradigm for the class of “ene-reductases” now widely used for the synthesis of a variety of useful chemicals. Curiously, the broad range of activated “enes” accepted by OYEs as substrates is in stark contrast to its invoked physiological role as a reductase of disulphide bonds in oxidatively damaged proteins of the cytoskeleton, such as actin [5].

General aspects of the yeast flavoproteome

The yeast genome contains 68 genes encoding for a flavin-dependent protein and thus 1.1% of all yeast proteins (5885 protein-encoding genes [26]) have a requirement for either FMN or FAD. Owing to the presence of several flavoprotein families, which will be discussed further below, these 68 genes give rise to 47 defined biochemical roles. Thirty-five flavoproteins require FAD (74%) and fifteen require FMN (26%). Yeast also possesses three diflavin enzymes, which harbor both FMN and FAD (Table 1). The utilization of FMN and FAD in yeast flavoproteins is very similar to the distribution found in a global analysis across all kingdoms of life [27] and does not have the bias towards FAD as found for the human flavoproteome [28]. Covalent flavinylation, which is statistically found in ca. 10% of flavoproteins, is underrepresented in the yeast flavoproteome with only two enzymes, succinate dehydrogenase (Sdh1p) and l-arabinono-1,4-lactone oxidase (Alo1p) featuring a covalent bond between the N(3)-nitrogen of a histidine residue and the 8-methyl group of the isoalloxazine ring system (Table 1). Both of these enzymes operate in yeast mitochondria and are located in the inner (Sdh1p) and outer (Alo1p) membrane. The scarcity of covalent flavoproteins is linked to the relative absence of the structural clan FAD_PCMH (with the exception of Alo1p), which features many examples of mono- and even bi-covalent flavinylation [27,28].

Table 1. Yeast flavoproteins and genes.

No.	E.C.	Enzyme	Cofactor	Structure clan (family) ^a	Localization	Abbrev.	Syst. name
1	1.1.2.3	l-Lactate:cytochrome c oxidoreductase (flavocytochrome b ₂)	FMN/heme	TIM_barrel (FMN_dh)	Mito. intermembr. sp.	<i>cyb2</i>	YML054C
2	1.1.2.4	d-Lactate dehydrogenase	FAD/heme	–	I. mito. membr. Mito. matrix Cytoplasm	<i>dld1</i> <i>dld2</i> <i>dld3</i>	YDL174C YDL178W YEL071W
3	1.1.3.37	d-Arabino-1,4-lactone oxidase	8α-(N3-His) -FAD	<i>FAD_PCMH</i>	O. mito. membr.	<i>alo1</i>	YML086C
4	1.1.5.3	Glycerol-3-phosphate dehydrogenase	FAD	<i>NADP_Rossmann (DAO)</i>	I. mito. membr.	<i>gut2</i>	YIL155C
5	1.3.1.90	tRNA dihydrouridine synthase	FMN	<i>TIM_barrel (Dus)</i>	Nucleus Nucleus/cytoplasm Nucleus/cytoplasm –	<i>dus1</i> <i>dus2</i> <i>dus3</i> <i>dus4</i>	YML080W YNR015W YLR401C YLR405W
6	1.3.3.1	Dihydroorotate dehydrogenase	FMN	<i>TIM_barrel (DHO_dh)</i>	Cytoplasm	<i>ura1</i>	YKL216W
7	1.3.3.4	Protoporphyrinogen IX oxidase	FAD	<i>NADP_Rossmann (Amino_oxidase)</i>	I. mito. membr.	<i>hem14</i>	YER014W
8	1.3.3.6	Acyl-CoA oxidase	FAD	<i>Acyl-CoA_dh (ACOX, acyl-CoA_dh_1)</i>	Peroxisome	<i>pox1</i>	YGL205W
9	1.3.5.1	Succinate dehydrogenase	8α-(N3-His) -FAD/2Fe-2S/	<i>NAPH_Rossmann (FAD_binding_2)</i>	I. mito. membr.	<i>sdh1</i> <i>sdh1b</i>	YKL148C YJL045W
–	–	Protein required for flavinylation of <i>sdh</i>	–	–	I. mito. membr.	<i>emi5</i>	YOL071W
10	1.4.1.14	NAD-dependent glutamate synthase	FMN/3Fe-4S	<i>Glu_synthase/Glu_syn_central</i>	Mito. matrix	<i>glt1</i>	YDL171C

The flavoproteome of the yeast *Saccharomyces cerevisiae*

No.	E.C.	Enzyme	Cofactor	Structure clan (family) ^a	Localization	Abbrev.	Syst. name
11	1.4.3.5	Pyridoxal 5'-phosphate oxidase Pyridoxine 5'-phosphate oxidase	FMN	FMN-binding (Pyridox_oxidase)	Mito. intermembr. sp.	<i>pdx3</i>	YBR035C
12	1.4.3.17	Polyamine oxidase	FAD	NADP_Rossmann (FAD_binding_2)	cytoplasm	<i>fms1</i>	YMR020W
13	1.5.1.20	Methylenetetrahydrofolate reductase	FAD	<i>FAD_oxidored (MTHFR)</i>	– Mito.	<i>met12</i> <i>met13</i>	YPL023C YGL125W
14	1.5.5.1	Electron-transferring flavoprotein-ubiquinone oxidoreductase	FAD/4Fe-4S	<i>4Fe-4S (ETF_QO)</i>	I. mito. membr.	<i>cir2</i>	YOR356W
15	–	Electron transferring flavoprotein	FAD	<i>FAD_DHS (ETF_alpha)</i>	Mito. matrix	<i>aim45</i>	YPR004C
16	1.5.99.8	Proline dehydrogenase	FAD	<i>FAD_oxidored (Pro_dh)</i>	Mito. matrix	<i>put1</i>	YLR142W
17	1.6.2.2	Cytochrome-b5 reductase	FAD	<i>FAD_Lum_binding</i> (<i>FAD_binding_6</i>)	ER & o. mito. membr. ER & plasma membr.	<i>cbr1</i> <i>pga3</i>	YIL043C YML125C
18	1.6.2.4	NADPH-hemoprotein reductase (cytochrome P450 reductase)	FMN/heme FAD	Flavoprotein (Flavodoxin_1) <i>FAD_Lum_binding</i> (<i>FAD_binding_1</i>)	O. mito. membr., ER & plasma membr.	<i>ncp1</i>	YHR042W
19	1.6.5.2	NAD(P)H quinone oxidoreductase	FMN	Flavoprotein (Flavodoxin_2)	cytoplasm	<i>lot6</i>	YLR011W
20	1.6.5.9	NADH-ubiquinone oxidoreductase (rotenone-insensitive)	FAD/Fe-S	NADP_Rossmann (Pyr_redox_2)	I. mito. membr.	<i>ndi1</i>	YML120C
21	1.6.99.1	NADPH dehydrogenase	FMN	TIM_barrel (Oxidored_FMN)	Cytoplasm	<i>oye2</i> <i>oye3</i>	YHR179W YPL171C
22	1.–.–.–	External NADH dehydrogenase	FAD	–	I. mito. membr. I. mito. membr.	<i>nde1</i> <i>nde2</i>	YMR145C YDL085W
23	1.6.–.–	NADPH-dep. diflavin oxidoreductase	FMN FAD	<i>Flavoprotein (Flavodoxin_1)</i> <i>FAD_Lum_binding</i>	Mito. matrix	<i>tah18</i>	YPR048W

The flavoproteome of the yeast *Saccharomyces cerevisiae*

No. E.C.	Enzyme	Cofactor	Structure clan (family) ^a	Localization	Abbrev.	Syst. name
			(<i>FAD_binding_1</i>)			
24 –	5-Carboxymethylaminomethylation of uridine (heterodimer with Mss1p)	FAD	<i>GIDA</i>	Mito.	<i>mto1</i>	YGL236C
25 –	Wybutosine biosynthesis, a tRNA-modification	FMN/4Fe–4S	<i>Flavoprotein</i>	ER	<i>tyw1</i>	YPL207W
26 1.8.1.2	Sulphite reductase (beta subunit)	FMN/heme FAD	<i>Flavoprotein (Flavodoxin_1)</i> <i>FAD_Lum_binding</i> (<i>FAD_binding_1</i>)	Cytoplasm	<i>met5</i>	YJR137C
27 1.8.1.4	Dihydrolipoyl dehydrogenase	FAD	NADP_Rossmann (Pyr_redox_2)	Mito. matrix	<i>lpd1</i>	YFL018C
28 1.8.1.7	Glutathione-disulfide reductase	FAD	NADP_Rossmann (Pyr_redox_2)	Cytoplasm & mito.	<i>glr1</i>	YPL091W
29 1.8.1.9	Thioredoxin-disulfide reductase	FAD	NADP_Rossmann (Pyr_redox_2)	Cytoplasm & mito. intermembr. sp.	<i>trr1</i>	YDR353W
30 –	Microtubule associated protein	FAD	<i>NADP_Rossmann?</i> (<i>Pyr_redox_2</i>)	Cytoplasm & mito. cytoplasm microtubule	<i>trr2</i> <i>irc15</i>	YHR106W YPL017C
31 1.8.3.2	Sulfhydryl oxidase	FAD/Fe–S cluster/ Heme	<i>Erv1_Alr</i>	Mito. intermembr. sp.	<i>erv1</i>	YGR029W
32 1.8.4.-	Endoplasmic oxidoreductin 1	FAD	<i>Ero1</i>	ER membr.	<i>erv2</i>	YPR037C
33 1.14.12.17	Nitric oxide oxidoreductase (flavo-hemoglobin)	FAD/heme	<i>FAD_Lum_Binding</i> (<i>FAD_binding_6</i>)	ER & ER membr.e Cytoplasm Mito. matrix	<i>ero1</i> <i>yhb1</i>	YML130C YGR234W
34 1.14.13.–	Oxidase of thiols in the ER	FAD	–	ER membr.	<i>fmo1</i>	YHR176W

The flavoproteome of the yeast *Saccharomyces cerevisiae*

No.	E.C.	Enzyme	Cofactor	Structure clan (family) ^a	Localization	Abbrev.	Syst. name
35	1.14.13.9	Kynurenine 3-monooxygenase	FAD	NADP_Rossmann (FAD_Binding_3)	O. mito. membr.	<i>bn4</i>	YBL098W
36	1.14.99.7	Squalene monooxygenase	FAD	–	ER membr.	<i>erg1</i>	YGR175C
37	1.14.99.-	Monooxygenase in coenzyme Q biosyn.	FAD	–	I. mito. membr.	<i>coq6</i>	YGR255C
38	1.-.-.-	Ferric reductase	FAD/heme	–	Plasma membr.	<i>fre1</i>	YLR214W
					Plasma membr.	<i>fre2</i>	YKL220C
					Plasma membr.	<i>fre3</i>	YOR381W
					Plasma membr.	<i>fre4</i>	YNR060W
					Plasma membr.	<i>fre5</i>	YOR384W
					Vacuole membr.	<i>fre6</i>	YLL051C
					Plasma membr.	<i>fre7</i>	YOL152W
					–	<i>fre8</i>	YLR047C
39	1.-.-.-	NADPH oxidase	FAD/heme	–	Perinucl. ER membr.	<i>aim14</i>	YGL160W
40	1.-.-.-	NAD(P)H-dep. heme reductase	FAD	–	Inner mito. membr.	<i>cyc2</i>	YOR037W
41	2.2.1.6	Acetolactate synthase	FAD/TPP	FAD_DHS (TPP_enzyme_M)	Mito.	<i>ilv2</i>	YMR108W
42	2.3.1.86	Fatty acid synthase, subunit β , chain I	FMN	Not reported	Cytoplasm & mito.	<i>fas1</i>	YKL182W
43	4.1.1.36	4'-Phosphopantothenoylecysteine decarboxylase (forms a heterotrimeric complex with Sis2p and Vhs3p)	FMN	<i>Flavoprotein</i>	Cytoplasm	<i>cab3</i>	YKL088W
44	4.1.99.3	Deoxyribodipyrimidine photo-lyase	FAD	<i>HUP (DNA_photolyase)</i>	Cytoplasm, mito. & nucleus	<i>phr1</i>	YOR386W
45	4.2.3.5	Chorismate synthase	FMN	Chorismate_synt	Cytoplasm	<i>aro2</i>	YGL148W
46	–	Flavodoxin-like protein	FMN	<i>Flavoprotein (Flavodoxin_1)</i>	Cytoplasm, mito.	<i>pst2</i>	YDR032C
	–	Flavodoxin-like protein	FMN	<i>Flavoprotein (Flavodoxin_1)</i>	Cytoplasm	<i>rfs1</i>	YBR052C

The flavoproteome of the yeast *Saccharomyces cerevisiae*

No. E.C.	Enzyme	Cofactor	Structure clan (family) ^a	Localization	Abbrev.	Syst. name
–	flavodoxin-like protein	FMN	<i>Flavoprotein (Flavodoxin_1)</i>	Cytoplasm, mito. O. mito. membr., plasma membr. & nucleus	<i>ycp4</i>	YCR004C
47 –	Apoptosis-inducing factor	FAD	–		<i>aif1</i>	YNR074C

Abbreviations used in Table 1: biosyn., biosynthesis; dh, dehydrogenase; degr., degradation; dep., dependent; i., inner; ER, endoplasmic reticulum; mito., mitochondrion; o., outer; perinucl., perinuclear; red., reductase; sp., space.

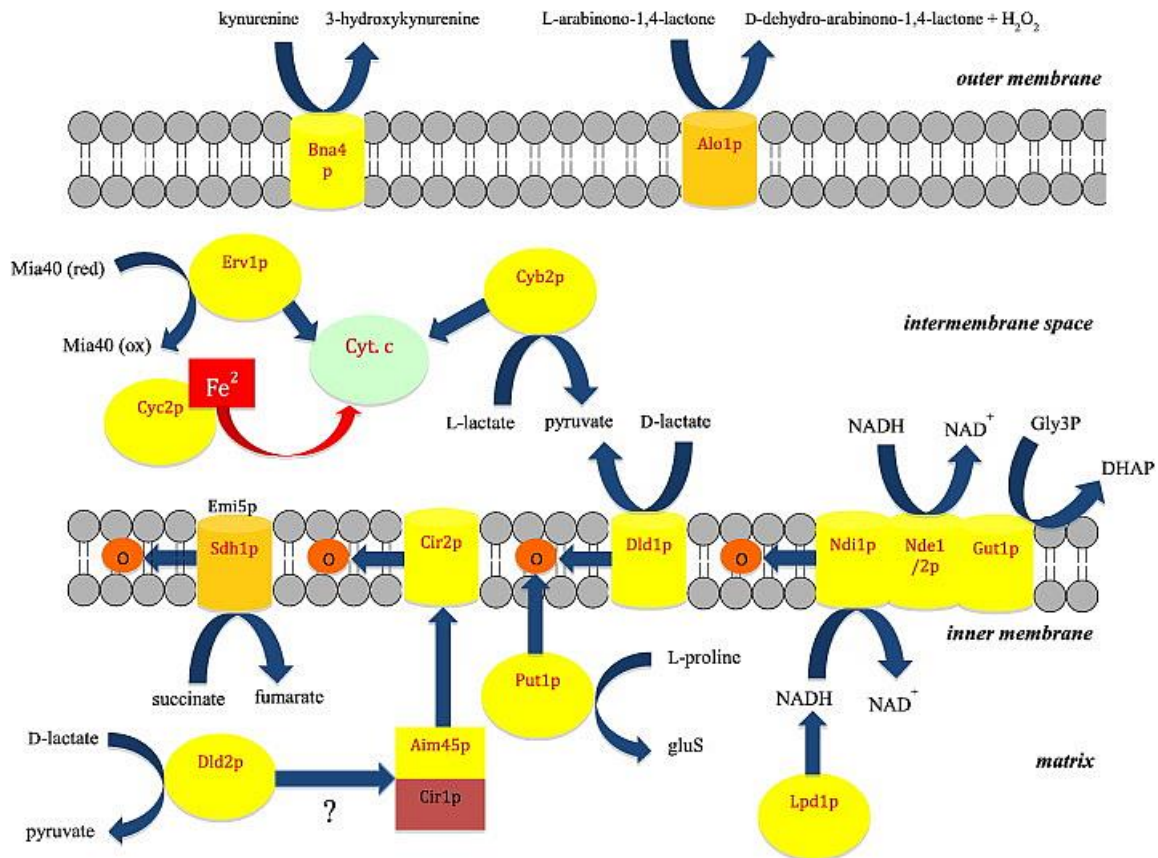
^aPfam classification given in plain text is for yeast proteins and those in italics are for homologs from other species.

Structural information through X-ray crystallographic analysis is available for about one third of yeast flavoproteins listed in Table 1 (plain font in column “Structure clan/family”). In addition, the three-dimensional structure can be inferred from the known structure of homologs from other species (*italics* in column “Structure clan/family”). In some cases the structure of yeast flavoproteins served as paradigms for a family of enzymes, for example yeast OYEs [6,29] and more recently kynurenine monooxygenase [30]. The general difficulties to elucidate the structure of integral or membrane associated proteins is also seen for flavoproteins (see Table 1).

Table 1 also provides information on the localisation of flavoproteins in the yeast cell. More than half of yeast flavoproteins (36 entries in Table 1) operate in the mitochondrion. Many of these are directly participating in redox reactions connected to the electron transport chain (ETC) (see also next section). Seventeen flavoproteins are located in the cytoplasm and only a few in the nucleus (Dus1-4p, Phr1p, Aif1p), endoplasmic reticulum (Aim14p, Cbr1p, Erg1p, Ero1p, Erv2p, Fmo1p, Ncp1p, Pga3p, Tyw1p) or the peroxisome (Pox1p). Requirement for the same flavoenzyme activity in different cellular compartments is either satisfied by expression of isozymes (e.g. Dld1-3p are found in either the cytoplasm, the inner mitochondrial membrane or the matrix) or the same flavoenzyme is present in multiple compartments (e.g. Cbr1p, Pga3p, Ncp1p, Trr1/2p, Yhb1p, Fas1p, Phr1p, Aif1p).

Flavoproteins, the stewards of iron

A remarkable result of our analysis concerns the multi-layered relationship between flavins and iron. As discussed in more detail in the next section, flavin-dependent ferric reductases (Fre1p-8p) are essential for reduction of ferric iron (and copper), which is prerequisite for iron (and copper) uptake by yeast transporters (permeases). Moreover, in several flavoproteins the flavin is responsible for the reduction of either heme iron or an iron–sulfur cluster (Table 1 and Scheme 1).



Scheme 1. Flavoproteins in mitochondrial redox processes. Flavoproteins are represented by yellow spheres (soluble flavoproteins in the matrix or intermembrane space) or barrels (inner or outer mitochondrial membrane). Flavoproteins with a covalently bound FAD (Sdh1p in the inner and Alo1p in the outer membrane) are shown in light orange. Cytochrome c is shown as a light green sphere. Curved blue arrows indicate redox reactions and straight arrows electron transfer. For further explanations and comments see main text. Several flavoproteins appear to participate in a multi-protein complex in the inner mitochondrial membrane [57]. For clarity, we have shown only a complex consisting of Ndi1p, Nde1/2p and Gut1p. Abbreviations used are: DHAP, dihydroxy acetone phosphate; Gly3p, glycerol 3-phosphate; GluSA, γ -glutamic acid semialdehyde; Mia(40), mitochondrial intermembrane space import and assay/oxidoreductase 40 (ox, oxidized; red, reduced); Q, ubiquinone.

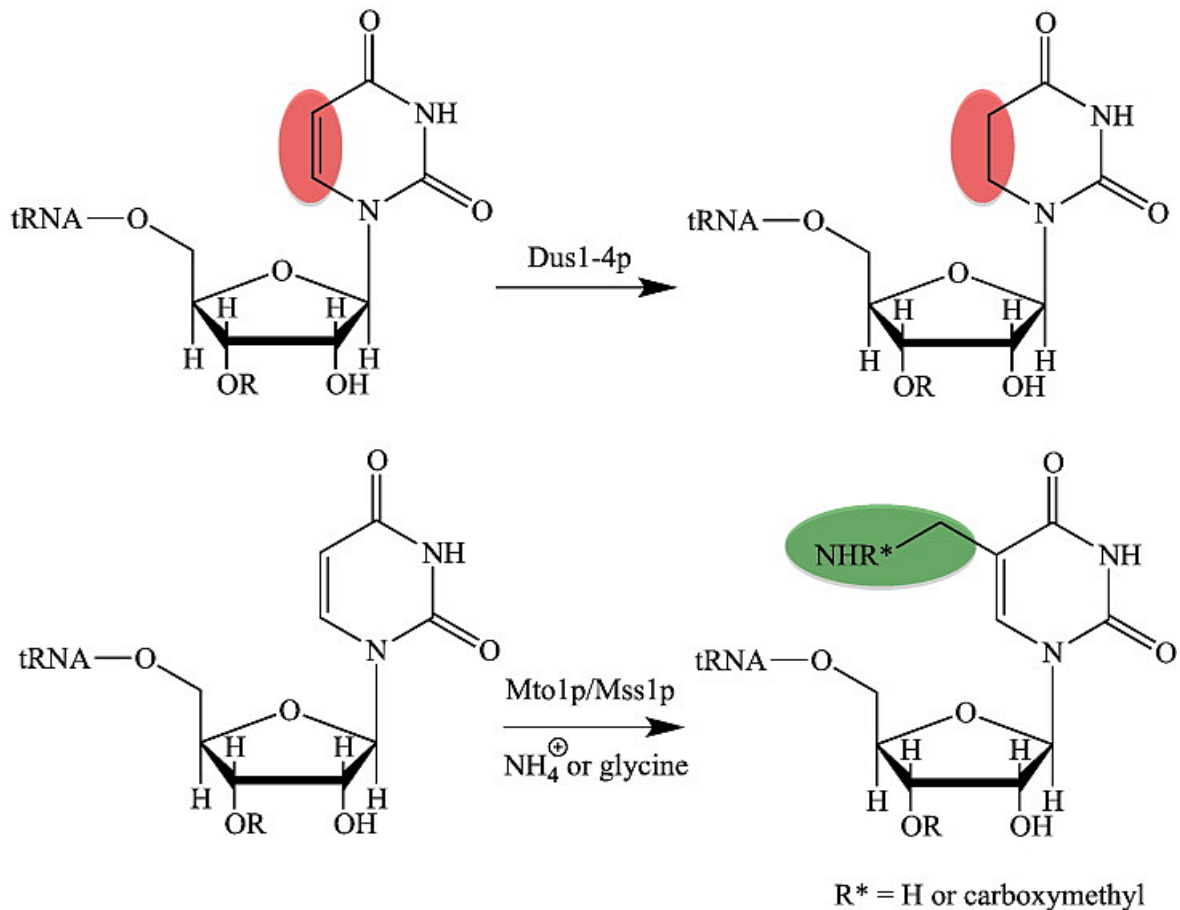
Prominent examples include succinate dehydrogenase (Sdh1p), (Aim1p), nitric oxide oxidoreductase and L-lactate:cytochrome c oxido reductase (flavocytochrome b2). In addition to this intramolecular electron transfer, two yeast flavoproteins, Cyc2p and Tah18p, are involved in intermolecular electron transfer. In the case of Cyc2p, which is located in the inner mitochondrial membrane with its FAD-containing active site exposed to the intermembrane space, the enzyme reduces Fe(III) and participates in the incorporation of the heme prosthetic group into apocytochrome c and c1 [31,32]. Similarly, the diflavin reductase Tah18p forms a complex with Dre2p and provides

electrons derived from NADPH to support the biosynthesis of two iron–sulfur clusters [33]. Recently, Tah18p was reported to be involved in NO generation in yeast and hence it is conceivable that it has more clients than Dre2p [34]. Thus flavoproteins fulfill various crucial tasks ranging from iron uptake, delivery of electrons to the mitochondrial electron transport chain, reduction of cytochrome-dependent reductases, biogenesis of iron–sulfur clusters and insertion of the heme cofactor into apocytochromes.

Flavoprotein families in yeast

As mentioned above, the yeast flavoproteome contains several families of flavoproteins, which catalyze identical or similar reactions. The largest group are the ferric/cupric reductases encoded by *fre1-8* (see Table 1, entry 38). *Fre1* and *fre2* are metalloregulated by either iron or copper availability and the encoded metalloreductases reduce Fe(III) and Cu(II) at the expense of NADPH [35]. In addition to *fre1* and *fre2*, the yeast genome contains six homologous genes, termed *fre3-8*. *Fre3-6* are regulated by iron whereas *fre7* is copper-regulated [36,37]. *Fre8* and the homologous *aim14* are not regulated by iron or copper suggesting a different role for these proteins [36]. Recently, it was demonstrated that *aim14* encodes an NADPH-oxidase, which produces superoxide in the endoplasmic reticulum [38] and it is thus conceivable that *fre8* also encodes an enzyme with similar properties. This notion is also supported by pair-wise sequence alignments showing the highest identity (30.6%) and similarity (56.5%) on the amino acid level between *fre8* and *aim14* within this family of flavoproteins [36]. Again, these functions highlight the importance of flavoenzymes for iron uptake and reduction as introduced in the previous section.

The second largest family comprise four tRNA-dihydrouridine synthases encoded by *dus1-4* (Table 1, entry 5). The reduction of uracils to dihydrouridines in tRNA is one of the most common modifications of nucleosides in tRNA in all kingdoms of life [39]. A recent mechanistic study employing *Dus2p* revealed that reduction of uracil to dihydrouracil (see Scheme 2, top) is promoted by other tRNA modifications suggesting that tRNA maturation may occur in an ordered fashion [40].



Scheme 2. Flavoproteins in tRNA-modification. Top, reaction catalyzed by tRNA-dihydrouridine synthase (Dus1-4p); Bottom, reaction catalyzed by Mto1p/Mss1p. Depending on the co-substrate, ammonia or glycine, the side chain in position 5' of the uracil base is aminomethyl or carboxymethylaminomethyl. "R" represents the next 3'-nucleotide in the tRNA molecule.

Cytoplasmic tRNA in *S. cerevisiae* contains dihydrouridine in the D loop at positions 16, 17, 20, 20A, 20B and at the base of the variable arm at position 47. The four yeast enzymes exclusively reduce uracils in specific positions in tRNA: Dus1p reduces uracils in positions 16 and 17, Dus2p in position 20, Dus3p in position 47 and Dus4p in positions 20a and 20b. Thus these four enzymes are sufficient to generate all dihydrouridine modifications known in yeast [41]. In humans, only one dihydrouridine synthase homologous to yeast Dus2p (42% identity) was identified so far, which reduces uracil in tRNA for phenylalanine [28,42]. The human enzyme appears to be upregulated in malignant tissues resulting in higher levels of dihydrouridine [42]. Despite its putative role in malignancy the specificity and exact role of the human enzyme remains unclear.

In addition to reduction of uracil, the flavoenzyme Mto1p (also termed GidA) is involved in the biosynthesis of modifications at the C5-position of the uracil base in tRNAs [43,44]. Depending on the nitrogen source, ammonia or glycine, this reaction leads to the formation of either 5-aminomethyl- or 5-carboxymethylamino-methyluridine (Scheme 2, bottom). This modification occurs at the wobble position in mitochondrial tRNAs for lysine, glutamate and glutamine [44]. Detailed characterization of the bacterial protein complex of MnmE and MnmG (homolog of Mto1p) led to a mechanistic proposal in which the FAD-dependent MnmG serves a dual function during the reaction [43,45]. In this model, methylene tetrahydrofolate bound to MnmE reacts with either ammonia or glycine to form a methylene amino group at N-5 of the tetrahydrofolate cofactor. Then, FAD oxidizes the carbon–nitrogen bond to yield an imine, which is then nucleophilically attacked by the uracil base of the tRNA substrate. In the next step the reduced FAD transfers a hydride to the imine to reduce the carbon–nitrogen double bond thus completing the biosynthesis of the C-5 side chain (see Scheme 2). Thus MnmG combines two canonical flavin-dependent reactions – oxidation of amines and reduction of double bonds – to catalyze the biosynthesis of the amino methyl or carboxymethylamino-methyl side chain.

Recently, yet another flavin-dependent enzyme encoded by *tyw1* (Table 1, entry 25) was discovered that catalyzes the second step in the biosynthesis of wybutosine-modified tRNA [46]. This enzyme belongs to the radical SAM superfamily characterized by the presence of a [4Fe–4S] cluster and a S-adenosylmethionine (SAM) domain [47]. Catalytic activity requires reduction of the [4Fe–4S] cluster in order to initiate one-electron transfer for reductive cleavage of SAM to generate the 5'-deoxyadenosyl radical [48]. In vivo, flavodoxins or ferredoxins might act as potential electron donors to convert [4Fe–4S]²⁺ to [4Fe–4S]⁺ and therefore it is conceivable that the N-terminal flavodoxin domain of Tyw1p relays electrons from an external electron donor such as NAD(P)H or an electron transfer protein to the [4Fe–4S] cluster. Such a functional role is supported by the finding that deletion of the flavodoxin domain abolishes TYW1p activity [49].

Interestingly, the yeast genome contains three homologous genes, *pst1*, *rfs1* and *ycp4* encoding three highly similar flavodoxin-like proteins (Table 1, entry 46) [50]. Although none of the proteins was functionally characterized with respect to their electron transfer properties and physiological redox partners they were found to

act as transcriptional regulators of *spi1*, a gene responding to various environmental stimuli [51]. The lack of information on yeast flavodoxins is very surprising in view of the abundance of structural (148 structures of wild-type and variants in the pdb) and biochemical studies available for bacterial flavodoxins. Therefore, the current state of affairs for yeast flavodoxin-like proteins is very unsatisfactory and clearly warrants further investigations to define their biochemical and structural properties.

The family of d-lactate dehydrogenases comprising three enzymes, Dld1-3p, will be discussed in the context of redox processes in the next section.

Yeast flavoproteins in redox balancing

More than a quarter of yeast flavoproteins listed in Table 1 participate in redox reactions in the mitochondrion. As shown in Scheme 1, transfer of electrons into the ETC can either occur through electron donation to cytochrome c (cyt. c) in the intermembrane space or directly by reduction of ubiquinone to ubiquinol in the inner mitochondrial membrane. The latter route is clearly the dominating process in yeast mitochondria. Electrons transferred to NAD^+ in the isocitrate, α -ketoglutarate and malate dehydrogenase reactions of the tricarboxylic acid cycle enter the ETC. via the NADH:ubiquinone oxidoreductase Ndi1p (“internal NADH dehydrogenase”). In contrast to complex I of higher eukaryotes this membrane-bound enzyme does not engage in proton translocation resulting in lower phosphorylation efficiency. The oxidation of succinate to fumarate is catalyzed by a canonical membrane-bound succinate dehydrogenase in which the covalently linked FAD becomes reduced by the substrate and the electrons are passed on to ubiquinone via an iron–sulfur cluster and heme relay system. The Sdh1p subunit of yeast succinate dehydrogenase (complex II) is one of only two flavin-dependent proteins exhibiting a covalent linkage (see Table 1, entry 9). Typically, covalent flavinylation is a spontaneous co- or posttranslational process. However, in the case of Sdh1p the assistance of Emi1p (Sdh5p) is required, which is conserved in higher eukaryotes and hence appears to be essential for complex II assembly [52,53]. Yeast also possesses a heterodimeric electron transfer flavoprotein (Aim45p/Cir1p) located in the mitochondrial matrix, which communicates with a membrane-bound electron transferring flavoprotein ubiquinone oxidoreductase (Cir2p). The latter flavoprotein feeds electrons received

from Aim45p/Cir1p into the ETC. The clients for Aim45p/Cir1p, however, remain elusive as most electron donor proteins, such as the acyl-Co dehydrogenases involved in β -oxidation or amino acid degradation, are not present in *S. cerevisiae*. A potential candidate, l-proline dehydrogenase (Put1p), evidently feeds electrons from l-proline oxidation directly into the ETC. by reduction of ubiquinone to ubiquinol (see Scheme 1) [54].

Cytosolic NADH generated for example by the glycolytic enzyme glyceraldehyde 3-phosphate dehydrogenase is oxidized by either Nde1p or Nde2p (“external NADH:ubiquinone oxidoreductases”) and the electrons serve to reduce ubiquinone (Scheme 1). The mitochondrial ETC. can also be fuelled by the glycerol 3-phosphate shuttle: glycerol is first phosphorylated by glycerol kinase (Gut1p) in the cytosol and then transported to the intermembrane space to become oxidized by the membrane-bound glycerol 3-phosphate dehydrogenase (Gut2p) [55,56]. Several of the membrane-bound flavoproteins involved in substrate oxidation and electron transfer form a large supramolecular complex containing Nde1p, Nde2p and Gut2p and therefore inter-protein electron transfer may also occur prior to ubiquinone reduction [57].

Yeast possesses three d-lactate dehydrogenases (Dldp1-3, see Table 1), which operate in different compartments of the cell: Dld1p is located in the inner mitochondrial membrane, Dld2p in the matrix and Dld3 in the cytosol [58,59]. d-lactate is produced by the glyoxalase pathway that detoxifies methylglyoxal adventitiously generated by non-enzymatic elimination of hydrogen and phosphate from the enediol intermediate of triose phosphates [60]. Since this detoxification pathway is active in the cytosol and the mitochondrial matrix d-lactate dehydrogenase activity is required in these compartments to oxidize d-lactate to pyruvate (Scheme 1). Oxidation of d-lactate by the d-lactate dehydrogenase (Dld2p) localized in the mitochondrial matrix is coupled to ATP synthesis and therefore Dld2p apparently donates substrate-derived electrons to the ETC [61]. However, it is currently unknown whether electrons are directly used to reduce ubiquinone or transferred to the heterodimeric Aim45p/Cir2p electron transfer complex (Scheme 1).

The involvement of flavoproteins in central mitochondrial redox processes is also reflected by the fact that the flavin oxidation state oscillates in synchronized aerobically grown yeast cultures. During the oxidative phase of the culture the increase of flavin fluorescence indicates that more flavoproteins become oxidized

whereas in the reductive phase of the internal rhythm a decrease of flavin fluorescence indicates a shift to the reduced state [62,63].

Flavin biosynthesis and transport

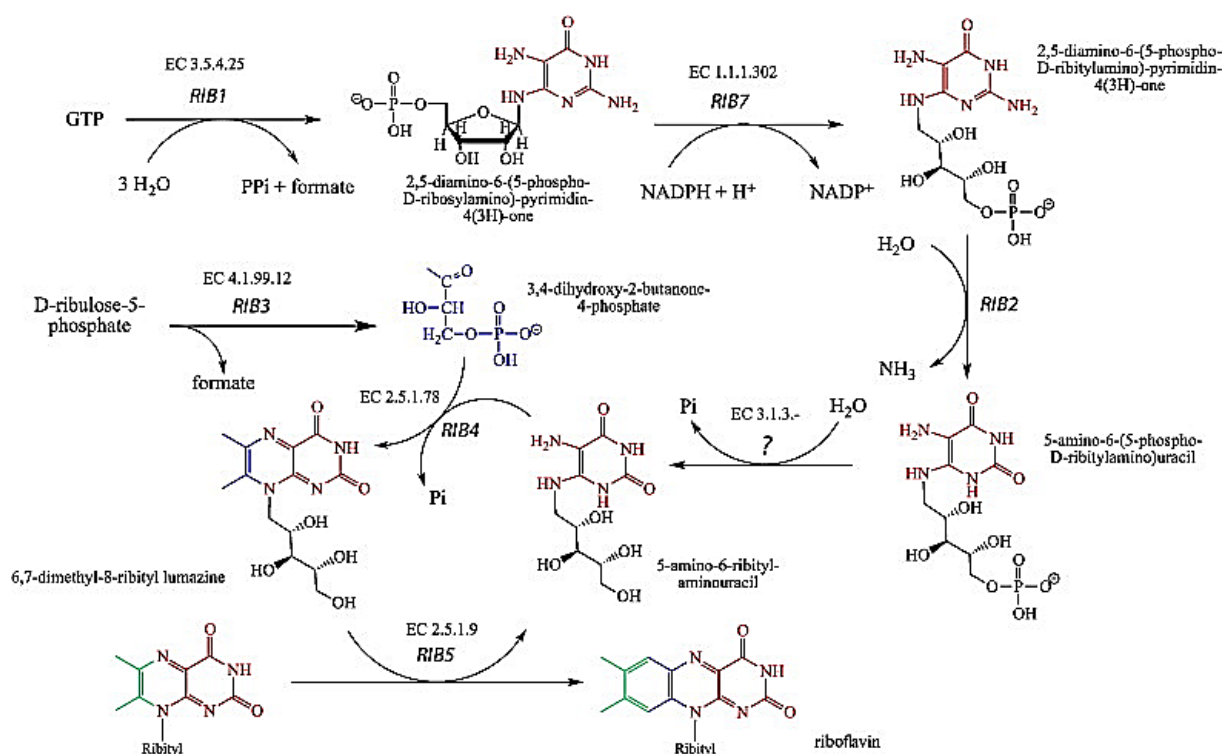
The biosynthesis of riboflavin in *S. cerevisiae* utilizes the canonical precursors, GTP and ribulose 5-phosphate. However, riboflavin biosynthesis deviates from the bacterial pathway in that deamination and reduction of the initial metabolite, 2,5-diamino-6-(ribosylamino)-4-(3H)-pyrimidinone 5'-phosphate (DRAP), take place in reverse order (www.kegg.jp). Briefly, in the first step GTP is converted by GTP cyclohydrolase II, encoded by *rib1*, to DRAP, which is reduced by Rib7p to 2,5-diamino-6-(ribitylamino)-4-(3H)-pyrimidinone 5'-phosphate (Table 2 and Scheme 3). This reaction is followed by deamination to 5-amino-6-ribitylamino-2,4-(1H,3H)-pyrimidinedione 5'-phosphate catalyzed by Rib2p [64]. After dephosphorylation by an unidentified phosphatase condensation with 3,4-dihydroxy-2-butanone-4-phosphate (DHAB) occurs. The latter metabolite is synthesized from ribulose 5-phosphate by DHBP synthase (encoded by *rib3*). The condensation reaction is catalyzed by lumazine synthase (encoded by *rib4*) and yields 6,7-dimethyl-8-(1-d-ribityl)lumazine [65,66]. In the final reaction, riboflavin synthase (encoded by *rib5*) uses two molecules of 6,7-dimethyl-8-(1-d-ribityl)-lumazine where one acts as donor and the other as acceptor of four carbon atoms leading to the generation of the isoalloxazine ring of one molecule of riboflavin [67]. The coenzyme forms of riboflavin, FMN and FAD, are synthesized from riboflavin by riboflavin kinase (Fmn1p) and FAD synthetase (Fad1p), respectively [68,69].

Table 2. Yeast flavin transporters and biosynthesis.

No.	E.C.	Protein/enzyme	Substrate/ligand	Structure clan (family) ^a	Abbrev.	Syst. name
<i>Transporters</i>						
1	–	FAD transmembrane transporter	FAD	–	<i>flx1</i>	YIL134W
2	–	FAD transporter (into ER)	FAD	–	<i>flc1</i>	YPL221W
3	–	FAD transporter (into ER)	FAD	–	<i>flc2</i>	YAL053W
4	–	FAD transporter (into ER)	FAD	–	<i>flc3</i>	YGL139W
5	–	Plasma-membrane riboflavin transporter	Riboflavin	–	<i>mch5</i>	YOR306C
<i>Biosynthesis of riboflavin, FMN and FAD</i>						
1	3.5.4.25	GTP cyclohydrolase II (1st step)	–	<i>GTP cyclohydrolase II</i>	<i>rib1</i>	YBL033C
2	1.1.1.302	DRAP reductase (2nd step)	–	DHFred (RibD_C)	<i>rib7</i>	YBR153W
3	–	Deaminase (3rd step)	–	<i>DHFred (RibD_C)</i>	<i>rib2</i>	YOL066C
4	4.1.99.12	DHBP synthase (4th step)	–	<i>DHBP_synthase</i>	<i>rib3</i>	YDR487C
5	2.5.1.78	Lumazine synthase (5th step)	–	DMRL_synthase	<i>rib4</i>	YOL143C
6	2.5.1.9	Riboflavin synthase (6th step)	–	<i>FAD_Lum_binding (Lum_binding)</i>	<i>rib5</i>	YBR256C
7	2.7.1.26	Riboflavin kinase	Riboflavin	<i>Flavokinase</i>	<i>fmn1</i>	YDR236C
8	2.7.7.2	FAD-adenylyl transferase (synthetase)	FMN	HUP (PAPS_reduct)	<i>fad1</i>	YDL045C

Abbreviations used in Table 2 are: DHBP, 3,4-dihydroxy-2-butanone-4-phosphate; DRAP, 2,5-diamino-6-ribosylamino-4(3H)-pyrimidinone 5'-phosphate.

^aPfam classification given in plain text is for yeast proteins and those in italics are for homologs from other species.



Scheme 3. Biosynthesis of riboflavin in *S. cerevisiae*. GTP and d-ribulose-5-phosphate serve as building blocks for the biosynthesis of 5-amino-6-ribityl-aminouracil and 3,4-dihydroxy-2-butanone-4-phosphate, respectively. These two compounds are then used by Rib4p to synthesize 6,7-dimethyl-8-ribityl lumazine. Two molecules 6,7-dimethyl-8-ribityl lumazine are converted by Rib5p to riboflavin and 5-amino-6-ribityl-aminouracil which serves again as substrate for Rib4p. This way all atoms of the dimethylbenzene moiety are derived from 3,4-dihydroxy-2-butanone-4-phosphate (colored in blue and green) while remainder of riboflavin is derived from GTP (colored in red).

In addition to de novo biosynthesis, yeast is also capable of riboflavin uptake from the medium and it was shown that a plasma membrane flavin transporter, encoded by *mch5*, is regulated by the proline-dependent transcription factor Put3p [70,71]. Since proline utilization depends on the FAD-dependent proline dehydrogenase Put1p (Table 1) upregulation of *Mch5p* suggests that riboflavin uptake is necessary under these conditions to meet the cellular demand for flavin coenzymes.

Despite the wealth of genetic and biochemical information available on riboflavin biosynthesis in the cytosol, transport to other compartments, in particular the mitochondrion as the dominant organelle for flavoenzyme catalyzed reactions, remains controversial [53]. Based on the finding that yeast mitochondria possess riboflavin kinase but no FAD synthetase activity, Tzagaloff et al. [72] proposed a model according to which the carrier protein Flx1p acts as a “flavin antiporter” by exchanging FMN from the mitochondrial matrix with FAD from the cytosol. In contrast

to this model, Barile and coworkers claim that riboflavin is transported into mitochondria where both FMN and FAD can be synthesized and are even exported back to the “extramitochondrial phase” [73,74]. More recent data from Pallotta indicated that mitochondria can also hydrolyze FAD and FMN to riboflavin and are thus capable of balancing the pools of riboflavin, FMN and FAD [75]. Yeast FAD synthetase (Fad1p) is essential and deletion of *fad1* makes yeast unviable. The localization of yeast FAD1p is still unclear, although recent studies on human FAD synthetase isoform 1 (hFADS1) suggest a mitochondrial localization in eukaryotes [76].

In addition to *flx1* and *mch5*, yeast possesses three *flc* genes encoding putative transporters of flavins (Table 2). These transporters are responsible for FAD transport into the endoplasmic reticulum (ER) where several flavoenzymes (e. g. *Ero1p*, *Erv2p* and *Fmo1p*) are involved in the redox balance of thiols and disulfide linkages [77]. However, the exact role and localisation of *Flc1-3p* in yeast are currently not fully understood.

An alternative mechanism for assembling the holo-flavoenzyme is realized for the sole peroxisomal flavoenzyme, acyl-CoA oxidase (*Pox1p*). In this case, the holo-enzyme is formed in the cytosol, then binds to the import receptor *Pex5p* and, following an unknown import pathway, is transported into the peroxisome [78,79].

Yeast flavoproteins as models for human diseases

The yeast *S. cerevisiae* has been used as a model organism for studying fundamental biological processes for some time [80]. In 1997, Botstein and colleagues showed that nearly 31% of yeast open reading frames (ORF) have a homologue in mammalian genomes [81]. Since the number of annotated ORFs has almost doubled since 1997 this percentage is likely to have risen significantly. Moreover, an estimated 30% of human genes implicated in human diseases have a yeast homologue [82]. In a recent review, we have documented that fifty human flavoproteins are implicated in human diseases [28]. As shown in Table 3, nearly half of the disease-related human flavoproteins possess a yeast homologue. Interestingly, the majority of disease-related human flavoproteins operate in the mitochondrion [28]. Owing to the similarity of mitochondrial processes in eukaryotes it is conceivable

that the yeast homologs located in mitochondria (see Table 3) may be particularly suitable as models for an improved understanding of human mitochondrial diseases.

Functional assignments based on sequence similarity generated ambiguities for several flavoproteins. For example, the yeast d-lactate dehydrogenases (Dld1-3p) show remarkable similarity to human d-2-hydroxyglutarate dehydrogenase and to a much lesser degree to alkyldihydroxyacetone phosphate synthase. Similarly, the yeast glutamate synthase, Glt1p, exhibits similarity to human dihydropyrimidine dehydrogenase (see Table 3). On the other hand the yeast NAD(P)H:quinone oxidoreductase Lot6p shows only a very low similarity to the human ortholog (P = 1) although it possesses a similar structure and function [83–86]. These examples illustrate the need for biochemical characterization to provide a solid basis for comparative functional studies.

Yeast deletion strains were also used as convenient models to investigate the impact of mutations discovered in human genes. Examples are deletions of the genes *ura1*, *sdh1*, *ldp1* and *coq6*, leading to auxotrophic yeast strains, which were complemented with the orthologous human gene to investigate the functional impairment of mutations [87–90]. Yeast was also utilized as a host for heterologous expression of the human gene encoding 3 β -hydroxysterol Δ 24-reductase (DHCR24). Desmosterolosis, a rare autosomal recessive disorder is caused by mutations in the gene encoding DHCR24. Heterologous expression of the human DHCR24 gene bearing different missense mutations confirmed their role in desmosterolosis [91].

A genetic screen in yeast suggested that kynurenine 3-monooxygenase may be a useful therapeutic target for Huntington disease [92]. This has prompted structural studies with the yeast enzyme leading to the elucidation of its X-ray crystal structure, which may serve as a model to investigate the structural basis of inhibitor binding [30]. Similarly, the crystal structure of the yeast flavin-containing monooxygenase Fmo1p proved useful as a model to understand the effect of mutations in human FMO3 that cause trimethylaminuria (“fish-odor” syndrome) [93].

Table 3. Yeast flavoproteins as human disease models.

No.	E.C.	Human enzyme	Disease	OMIM	Yeast homolog	E value ^a
1	1.1.5.3	Glycerol 3-phosphate dh	<i>Diabetes mellitus, type 2</i>	138430	Gut2p	7.3 e – 124
2	1.1.99-	d-2-Hydroxyglutarate dh	d-2-Hydroxyglutaric aciduria	605176	Dld1p Dld2p Dld3p	1.9 e – 39 8.7 e – 128 3.3 e – 112
3	1.3.1.2	Dihydropyrimidine dh	Deficiency	612779	Glt1p	2.7 e – 14
4	1.3.5.2	Dihydroorotate dh	Miller syn.	126064	Ura1p	2.0 e – 6
5	1.3.3.4	Protoporphyrinongen IX ox.	Variegate porphyria	600923	Hem1p	7.2 e – 20
6	1.3.3.6	Acyl-CoA ox.	Deficiency	609751	Pox1p	2.0 e – 45
7	1.3.5.1	Succinate dh	Complex II deficiency,	600857	Sdh1p	3.9 e – 219
		Flavoprotein subunit A	Leigh syn., paraganglioma 5		Sdh1bp	3.0 e – 214
8	1.4.3.4	Monoamine ox	Brunner syn., antisocial behavior, autism	309850	Fms1p	7.8 e – 11
9	1.4.3.5	Pyridoxine 5'-phosphate ox.	Encephalopathy	603287	Pdx3p	5.1 e – 36
10	1.5.1.20	Methylenetetrahydrofolate red.	Homocystinuria, neural tube	607093	Met12p	2.9 e – 98
			Defects, schizophrenia		Met13p	7.5 e – 122
11	1.5.5.1	Electron-transferring flavo-protein ubiquinone oxidored.	Glutaric academia IIC	231675	Cir2p	8.0 e – 157
12	–	Electron-transferring flavoprot.	Glutaric acidemia IIA	608053	Aim45p	8.5 e – 66

The flavoproteome of the yeast *Saccharomyces cerevisiae*

No.	E.C.	Human enzyme	Disease	OMIM	Yeast homolog	E value ^a
			Glutaric acidemia IIB	130410		
13	1.5.99.8	Proline dh	Hyperprolinemia type I, schizophrenia	606810	Put1p	8.7 e – 12
14	1.6.2.2	Cytochrome-b5 red.	Methemoglobinemia types I & II	613213	Cbr1p	1.9 e – 30
15	1.6.2.4	NADPH-hemoprotein red. (cytochrome P450 red.)	Antley–Bixler syn.,	124015	Ncp1p	2.4 e – 86
16	1.6.5.2	NAD(P)H:quinone oxidored.	Benzene toxicity, breast cancer	125860	Lot6p	1
17	1.8.1.4	Dihydrolipoyl dh	Leigh syn., maple syrup urine disease	238331	Lpd1p	2.8 e – 147
18	1.8.1.7	Glutathione-disulfide red.	Hemolytic anemia	138300	Glr1p	1.4 e – 104
19	1.14.13.8	Flavin-containing monooxy.	Trimethylaminuria	136132	Fmo1p	4.8 e – 27
20	1.14.13.39	Nitric-oxide synthase	Hypertension	163729	Tah18p	9.6 e – 27
				163730		
21	1.14.99.-	Monooxy. in coenzyme Q	Deficiency, nephrotic syn.	614647	Coq6p	7.0 e – 55
22	1.16.1.8	Methionine synthase red.	Homocystinuria, neural tube	602568	Met5p	0.24
23	2.5.1.26	Alkyldihydroxyacetone Phosphate synthase	Rhizomelic chondrodysplasia Punctata type 3	603051	Dld1p Dld2p Dld3p	2.1 e – 25 4.4 e – 16 1.1 e – 15
24	–	Apoptosis inducing protein	Combined oxidative phosphorylation deficiency	300169	Aif1p	8.8 e – 4

Abbreviations used in Table 3: dh, dehydrogenase; flavoprot., flavoprotein; monooxy., monooxygenase; ox, oxidase; oxidored., oxidoreductase; red., reductase; syn., syndrome.

^aE value; expect value, was generated by searching of *Saccharomyces* Genome Database (SGD; <http://www.yeastgenome.org>) open reading frames (DNA or protein) against human protein sequences using the SGD WU_Blast2 program.

Concluding remarks

Our analysis of the yeast flavoproteome has highlighted the importance of flavin-dependent enzymes in mitochondrial redox processes. Many of these mitochondrial enzymes have human homologs involved in diseases and thus genetically manipulated yeast strains (e.g. gene deletions) have potential as convenient model systems. On the other hand, many yeast flavoenzymes are barely characterized with regard to their biochemical properties, such as substrate specificity, kinetic parameters and reaction partners. This deficit is clearly illustrated by the yeast flavodoxin-like proteins and the electron-transferring flavoprotein, none of which were characterized in any biochemical or structural detail. Similarly, our understanding of riboflavin uptake and trafficking between cellular compartments as well as flavin homeostasis are at an early stage necessitating further studies. Since these processes are also poorly understood in humans, yeast lends itself as a valuable model organism to gain insight into uptake, transport and trafficking of this vital vitamin.

Methods

The names and gene abbreviations of yeast flavoproteins were recently compiled for a review article [27]. This list of flavoproteins was updated using the information available in the *Saccharomyces* genome database (<http://www.yeastgenome.org/>). This database was also used to extract information on viability of gene knock-outs and localisation of flavoproteins in the yeast cell. Structural information was obtained from the protein database (<http://www.pdb.org>).

Acknowledgments

We thank the Austrian Research Fund (FWF) for financial support through project P22361 and the PhD program “Molecular Enzymology” (W901).

References

- [1] O. Warburg, W. Christian, Über das gelbe Ferment und seine Wirkungen, *Biochem. Z.* 266 (1933) 377–392.
- [2] H. Theorell, O. Warburg, Reindarstellung (Kristallisation) des gelben Atmungsfermentes und die reversible Spaltung desselben, *Biochem. Z.* 272 (1934) 155–156.
- [3] E. Haas, O. Warburg, Isolierung eines neuen gelben Ferments, *Biochem. Z.* 298 (1938) 378–390.
- [4] V. Massey, L.M. Schopfer, Reactivity of old yellow enzyme with alpha-NADPH and other pyridine nucleotide derivatives, *J. Biol. Chem.* 261 (1986) 1215–1222.
- [5] B.K. Haarer, D.C. Amberg, Old yellow enzyme protects the actin cytoskeleton from oxidative stress, *Mol. Biol. Cell.* 15 (2004) 4522–4531.
- [6] K.M. Fox, P.A. Karplus, Old yellow enzyme at 2 Å resolution: overall structure, ligand binding, and comparison with related flavoproteins, *Structure* 2 (1994) 1089–1105.
- [7] Y.S. Niino, S. Chakraborty, B.J. Brown, V. Massey, A new old yellow enzyme of *Saccharomyces cerevisiae*, *J. Biol. Chem.* 270 (1995) 1983–1991.
- [8] K. Stott, K. Saito, D.J. Thiele, V. Massey, Old yellow enzyme. The discovery of multiple isozymes and a family of related proteins, *J. Biol. Chem.* 268 (1993) 6097–6106.
- [9] Y. Meah, V. Massey, Old yellow enzyme: stepwise reduction of nitro-olefins and catalysis of aci-nitro tautomerization, *Proc. Natl. Acad. Sci. USA.* 97 (2000) 10733–10738.
- [10] A.D. Vaz, S. Chakraborty, V. Massey, Old yellow enzyme: aromatization of cyclic enones and the mechanism of a novel dismutation reaction, *Biochemistry.* 34 (1995) 4246–4256.

- [11] M. Hall, C. Stueckler, W. Kroutil, P. Macheroux, K. Faber, Asymmetric bioreduction of activated alkenes using cloned 12-oxophytodienoate reductase isoenzymes OPR-1 and OPR-3 from *Lycopersicon esculentum* (tomato): a striking change of stereoselectivity, *Angew. Chem. Int. Ed.* 46 (2007) 3934–3937.
- [12] A. Muller, R. Sturmer, B. Hauer, B. Rosche, Stereospecific alkyne reduction: novel activity of old yellow enzymes, *Angew. Chem. Int. Ed.* 46 (2007) 3316–3318.
- [13] R. Stuermer, B. Hauer, M. Hall, K. Faber, Asymmetric bioreduction of activated C 000000000000 000000000000 000000000000 111111111111 000000000000 111111111111 000000000000 000000000000 000000000000 C bonds using enoate reductases from the old yellow enzyme family, *Curr. Opin. Chem. Biol.* 11 (2007) 203–213.
- [14] R.E. Williams, N.C. Bruce, 'New uses for an old enzyme' — the old yellow enzyme family of flavoenzymes, *Microbiology.* 148 (2002) 1607–1614.
- [15] R.E. Williams, D.A. Rathbone, N.S. Scrutton, N.C. Bruce, Biotransformation of explosives by the old yellow enzyme family of flavoproteins, *Appl. Environ. Microbiol.* 70 (2004) 3566–3574.
- [16] F. Schaller, E.W. Weiler, Molecular cloning and characterization of 12-oxophytodienoate reductase, an enzyme of the octadecanoid signaling pathway from *Arabidopsis thaliana*. Structural and functional relationship to yeast old yellow enzyme, *J. Biol. Chem.* 272 (1997) 28066–28072.
- [17] J. Strassner, A. Fürholz, P. Macheroux, N. Amrhein, A. Schaller, A homolog of old yellow enzyme in tomato: Spectral properties and substrate specificity of the recombinant protein, *J. Biol. Chem.* 274 (1999) 35067–35073.
- [18] C.E. French, N.C. Bruce, Bacterial morphinone reductase is related to old yellow enzyme, *Biochem. J.* 312 (1995) 671–678.
- [19] T.B. Fitzpatrick, N. Amrhein, P. Macheroux, Characterization of YqjM, an old yellow enzyme homolog from *Bacillus subtilis*, *J. Biol. Chem.* 278 (2003) 19891–19897.

- [20] O. Adachi, K. Matsushita, E. Shinagawa, M. Ameyama, Occurrence of old yellow enzyme in *Gluconobacter suboxydans*, and the cyclic regeneration of NADP, *J. Biochem.* 86 (1979) 699–709.
- [21] C.E. French, S. Nicklin, N.C. Bruce Sequence and properties of pentaerythritol tetranitrate reductase from *Enterobacter cloacae* PB2, *J. Bacteriol.* 178 (1996) 6623–6627.
- [22] J.R. Snape, N.A. Walkley, A.P. Morby, S. Nicklin, G.F. White, Purification, properties, and sequence of glycerol trinitrate reductase from *Agrobacterium radiobacte*., *J. Bacteriol.* 179 (1997) 7796–7802.
- [23] D.S. Blehert, B.G. Fox, G.H. Chambliss, Cloning and sequence analysis of two *Pseudomonas* flavoprotein xenobiotic reductases, *J. Bacteriol.* 181 (1999) 6254–6263.
- [24] J. Strassner, F. Schaller, U. Frick, G.A. Howe, E.E. Weiler, N. Amrhein, P. Macheroux, A. Schaller, Characterization and cDNA-microarray expression analysis of 12-oxophytodienoate reductases reveals differential roles for octadecanoid biosynthesis in the local versus the systemic wound response, *Plant J.* 32 (2002) 585–601.
- [25] A. Stintzi, J. Browse, The *Arabidopsis* male-sterile mutant, opr3, lacks the 12-oxophytodienoic acid reductase required for jasmonate synthesis, *Proc. Natl. Acad. Sci. USA* 97 (2000) 10625–10630.
- [26] A. Goffeau, B.G. Barrell, H. Bussey, R.W. Davis, B. Dujon, H. Feldmann, F. Galibert, J.D. Hoheisel, C. Jacq, M. Johnston, E.J. Louis, H.W. Mewes, Y. Murakami, P. Philippsen, H. Tettelin, S.G. Oliver, Life with 6000 genes, *Science.* 274 (1996) 546 (563–547).
- [27] P. Macheroux, B. Kappes, S.E. Ealick, Flavogenomics—a genomic and structural view of flavin-dependent proteins, *FEBS J.* 278 (2011) 2625–2634.
- [28] W.D. Lienhart, V. Gudipati, P. Macheroux, The human flavoproteome, *Arch. Biochem. Biophys.* 535 (2013) 150–162.

- [29] K.M. Fox, P.A. Karplus, Crystallization of old yellow enzyme illustrates an effective strategy for increasing protein crystal size, *J. Mol. Biol.* 234 (1993) 502–507.
- [30] M. Amaral, C. Levy, D.J. Heyes, P. Lafite, T.F. Outeiro, F. Giorgini, D. Leys, N.S. Scrutton, Structural basis of kynurenine 3-monooxygenase inhibition, *Nature.* 496 (2013) 382–385.
- [31] D.G. Bernard, S. Quevillon-Cheruel, S. Merchant, B. Guiard, P.P. Hamel, Cyc2p, a membrane-bound flavoprotein involved in the maturation of mitochondrial c-type cytochromes, *J. Biol. Chem.* 280 (2005) 39852–39859.
- [32] V. Corvest, D.A. Murrey, M. Hirasawa, D.B. Knaff, B. Guiard, P.P. Hamel, The flavoprotein Cyc2p, a mitochondrial cytochrome c assembly factor, is a NAD(P)H-dependent haem reductase, *Mol. Microbiol.* 83 (2012) 968–980.
- [33] N. Soler, E. Delagoutte, S. Miron, C. Facca, D. Baille, B. d'Autreaux, G. Craescu, Y.M. Frapart, D. Mansuy, G. Baldacci, M.E. Huang, L. Vernis, Interaction between the reductase Tah18 and highly conserved Fe–S containing Dre2 C-terminus is essential for yeast viability, *Mol. Microbiol.* 82 (2011) 54–67.
- [34] A. Nishimura, N. Kawahara, H. Takagi, The flavoprotein Tah18-dependent NO synthesis confers high-temperature stress tolerance on yeast cells, *Biochem. Biophys. Res. Commun.* 430 (2013) 137–143.
- [35] A. Dancis, D.G. Roman, G.J. Anderson, A.G. Hinnebusch, R.D. Klausner, Ferric reductase of *Saccharomyces cerevisiae*: molecular characterization, role in iron uptake, and transcriptional control by iron, *Proc. Natl. Acad. Sci. U. S. A.* 89 (1992) 3869–3873.
- [36] E. Georgatsou, D. Alexandraki, Regulated expression of the *Saccharomyces cerevisiae* Fre1p/Fre2p Fe/Cu reductase related genes, *Yeast.* 15 (1999) 573–584.
- [37] L.J. Martins, L.T. Jensen, J.R. Simon, G.L. Keller, D.R. Winge, Metalloregulation of FRE1 and FRE2 homologs in *Saccharomyces cerevisiae*. *J. Biol. Chem.* 273 (1998) 23716–23721.

- [38] M. Rinnerthaler, S. Buttner, P. Laun, G. Heeren, T.K. Felder, H. Klinger, M. Weinberger, K. Stolze, T. Grousl, J. Hasek, O. Benada, I. Frydlova, A. Klocker, B. Simon-Nobbe, B. Jansko, H. Breitenbach-Koller, T. Eisenberg, C.W. Gourlay, F. Madeo, W.C. Burhans, M. Breitenbach, Yno1p/Aim14p, a NADPH-oxidase ortholog, controls extramitochondrial reactive oxygen species generation, apoptosis, and actin cable formation in yeast, *Proc. Natl. Acad. Sci. USA* 109 (2012) 8658–8663.
- [39] M. Sprinzl, C. Steegborn, F. Hubel, S. Steinberg, Compilation of tRNA sequences and sequences of tRNA genes, *Nucleic Acids Res.* 24 (1996) 68-72.
- [40] L.W. Rider, M.B. Ottosen, S.G. Gattis, B.A. Palfey, Mechanism of dihydrouridine synthase 2 from yeast and the importance of modifications for efficient tRNA reduction, *J. Biol. Chem.* 284 (2009) 10324–10333.
- [41] F. Xing, S.L. Hiley, T.R. Hughes, E.M. Phizicky, The specificities of four yeast dihydrouridine synthases for cytoplasmic tRNAs, *J. Biol. Chem.* 279 (2004) 17850–17860.
- [42] T. Kato, Y. Daigo, S. Hayama, N. Ishikawa, T. Yamabuki, T. Ito, M. Miyamoto, S. Kondo, Y. Nakamura, A novel human tRNA-dihydrouridine synthase involved in pulmonary carcinogenesis, *Cancer Res.* 65 (2005) 5638–5646.
- [43] M.E. Armengod, I. Moukadiri, S. Prado, R. Ruiz-Partida, A. Benitez-Paez, M. Villarroya, R. Lomas, M.J. Garzon, A. Martinez-Zamora, S. Meseguer, C. Navarro-Gonzalez, Enzymology of tRNA modification in the bacterial MnmEG pathway *Biochimie* 94 (2012) 1510–1520.
- [44] X. Wang, Q. Yan, M.X. Guan, Mutation in MTO1 involved in tRNA modification impairs mitochondrial RNA metabolism in the yeast *Saccharomyces cerevisiae*, *Mitochondrion* (2009) 180–185.
- [45] I. Moukadiri, S. Prado, J. Piera, A. Velazquez-Campoy, G.R. Bjork, M.E. Armengod, Evolutionarily conserved proteins MnmE and GidA catalyze the formation of two methyluridine derivatives at tRNA wobble positions, *Nucleic Acids Res.* 37 (2009) 7177–7193.

- [46] L. Li, X. Jia, D.M. Ward, J. Kaplan, Yap5 protein-regulated transcription of the TYW1 gene protects yeast from high iron toxicity, *J. Biol. Chem.* 286 (2011) 38488–38497.
- [47] H.J. Sofia, G. Chen, B.G. Hetzler, J.F. Reyes-Spindola, N.E. Miller; Radical SAM, a novel protein superfamily linking unresolved steps in familiar biosynthetic pathways with radical mechanisms: functional characterization using new analysis and information visualization methods; *Nucleic Acids Res.* 29 (2001) 1097–1106.
- [48] S.C. Wang, P.A. Frey, S-adenosylmethionine as an oxidant: the radical SAM superfamily, *Trends Biochem. Sci.* 32 (2007) 101–110.
- [49] Y. Suzuki, A. Noma, T. Suzuki, M. Senda, T. Senda, R. Ishitani, O. Nureki, Crystal structure of the radical SAM enzyme catalyzing tricyclic modified base formation in tRNA, *J. Mol. Biol.* 372 (2007) 1204–1214.
- [50] R. Grandori, J. Carey, Six new candidate members of the alpha/beta twisted open-sheet family detected by sequence similarity to flavodoxin, *Protein Sci.* 3 (1994) 2185–2193.
- [51] F. Cardona, H. Orozco, S. Friant, A. Aranda, M. del Olmo, The *Saccharomyces cerevisiae* flavodoxin-like proteins Ycp4 and Rfs1 play a role in stress response and in the regulation of genes related to metabolism, *Arch. Microbiol.* 193 (2011) 515–525.
- [52] H.X. Hao, O. Khalimonchuk, M. Schraders, N. Dephoure, J.P. Bayley, H. Kunst, P. Devilee, C.W. Cremers, J.D. Schiffman, B.G. Bentz, S.P. Gygi, D.R. Winge, H. Kremer, J. Rutter, SDH5, a gene required for flavination of succinate dehydrogenase, is mutated in paraganglioma, *Science* 325 (2009) 1139–1142.
- [53] H.J. Kim, D.R. Winge, Emerging concepts in the flavinylation of succinate dehydrogenase, *Biochim. Biophys. Acta.* 1827 (2013) 627–636.
- [54] J. Lopes, M.J. Pinto, A. Rodrigues, F. Vasconcelos, R. Oliveira, The *Saccharomyces cerevisiae* genes, AIM45, YGR207c/CIR1 and

- YOR356w/CIR2, are involved in cellular redox state under stress conditions, *Open Microbiol. J.* 4 (2010) 75–82.
- [55] R. Ansell, K. Granath, S. Hohmann, J.M. Thevelein, L. Adler, The two isoenzymes for yeast NAD⁺-dependent glycerol 3-phosphate dehydrogenase encoded by GPD1 and GPD2 have distinct roles in osmoadaptation and redox regulation, *EMBO J.* 16 (1997) 2179–2187.
- [56] M. Grauslund, J.M. Lopes, B. Ronnow, Expression of GUT1, which encodes glycerol kinase in *Saccharomyces cerevisiae*, is controlled by the positive regulators Adr1p, Ino2p and Ino4p and the negative regulator Opi1p in a carbon source-dependent fashion, *Nucleic Acids Res.* 27 (1999) 4391–4398.
- [57] X. Grandier-Vazeille, K. Bathany, S. Chaignepain, N. Camougrand, S. Manon, J.M. Schmitter, Yeast mitochondrial dehydrogenases are associated in a supramolecular complex, *Biochemistry* 40 (2001) 9758–9769.
- [58] A. Chelstowska, Z. Liu, Y. Jia, D. Amberg, R.A. Butow, Signalling between mitochondria and the nucleus regulates the expression of a new d-lactate dehydrogenase activity in yeast, *Yeast.* 15 (1999) 1377–1391.
- [59] E.E. Rojo, B. Guiard, W. Neupert, R.A. Stuart, Sorting of d-lactate dehydrogenase to the inner membrane of mitochondria. Analysis of topogenic signal and energetic requirements, *J. Biol. Chem.* 273 (1998) 8040–8047.
- [60] M.J. Penninckx, C.J. Jaspers, M.J. Legrain, The glutathione-dependent glyoxalase pathway in the yeast *Saccharomyces cerevisiae*, *J. Biol. Chem.* 258 (1983) 6030–6036.
- [61] M.L. Pallotta, D. Valenti, M. Iacovino, S. Passarella, Two separate pathways for d-lactate oxidation by *Saccharomyces cerevisiae* mitochondria which differ in energy production and carrier involvement, *Biochim. Biophys. Acta* 1608 (2004) 104–113.
- [62] D.B. Murray, K. Haynes, M. Tomita, Redox regulation in respiring *Saccharomyces cerevisiae*, *Biochim. Biophys. Acta* 1810 (2011) 945–958.

- [63] D.B. Murray, S. Roller, H. Kuriyama, D. Lloyd, Clock control of ultradian respiratory oscillation found during yeast continuous culture, *J. Bacteriol.* 183 (2001) 7253–7259.
- [64] A. Urban, I. Ansmant, Y. Motorin, Optimisation of expression and purification of the recombinant Yol066 (Rib2) protein from *Saccharomyces cerevisiae*, *J. Chromatogr. B Anal. Technol. Biomed. Life Sci.* 786 (2003) 187–195.
- [65] C. Jin, A. Barrientos, A. Tzagoloff, Yeast dihydroxybutanone phosphate synthase, an enzyme of the riboflavin biosynthetic pathway, has a second unrelated function in expression of mitochondrial respiration, *J. Biol. Chem.* 278 (2003) 14698–14703.
- [66] J.J. Garcia-Ramirez, M.A. Santos, J.L. Revuelta, The *Saccharomyces cerevisiae* RIB4 gene codes for 6,7-dimethyl-8-ribityllumazine synthase involved in riboflavin biosynthesis. Molecular characterization of the gene and purification of the encoded protein. *J. Biol. Chem.* 270 (1995) 23801–23807.
- [67] M.A. Santos, J.J. Garcia-Ramirez, J.L. Revuelta, Riboflavin biosynthesis in *Saccharomyces cerevisiae*. Cloning, characterization, and expression of the RIB5 gene encoding riboflavin synthase, *J. Biol. Chem.* 270 (1995) 437–444.
- [68] M.A. Santos, A. Jimenez, J.L. Revuelta, Molecular characterization of FMN1, the structural gene for the monofunctional flavokinase of *Saccharomyces cerevisiae*, *J. Biol. Chem.* 275 (2000) 28618–28624.
- [69] M. Wu, B. Repetto, D.M. Glerum, A. Tzagoloff, Cloning and characterization of FAD1, the structural gene for flavin adenine dinucleotide synthetase of *Saccharomyces cerevisiae*, *Mol. Cell. Biol.* 15 (1995) 264–271.
- [70] P. Reihl, J. Stolz, The monocarboxylate transporter homolog Mch5p catalyzes riboflavin (vitamin B2) uptake in *Saccharomyces cerevisiae*, *J. Biol. Chem.* 280 (2005) 39809–39817.
- [71] A. Spitzner, A.F. Perzlmaier, K.E. Geillinger, P. Reihl, J. Stolz, The proline-dependent transcription factor Put3 regulates the expression of the riboflavin transporter MCH5 in *Saccharomyces cerevisiae*, *Genetics* 180 (2008) 2007–2017.

- [72] A. Tzagoloff, J. Jang, D.M. Glerum, M. Wu, FLX1 codes for a carrier protein involved in maintaining a proper balance of flavin nucleotides in yeast mitochondria, *J. Biol. Chem.* 271 (1996) 7392–7397.
- [73] M.L. Pallotta, C. Brizio, A. Fratianni, C. De Virgilio, M. Barile, S. Passarella, *Saccharomyces cerevisiae* mitochondria can synthesise FMN and FAD from externally added riboflavin and export them to the extramitochondrial phase, *FEBS Lett.* 428 (1998) 245–249.
- [74] V. Bafunno, T.A. Giancaspero, C. Brizio, D. Bufano, S. Passarella, E. Boles, M. Barile, Riboflavin uptake and FAD synthesis in *Saccharomyces cerevisiae* mitochondria: involvement of the Flx1p carrier in FAD export, *J. Biol. Chem.* 279 (2004) 95–102.
- [75] M.L. Pallotta, Evidence for the presence of a FAD pyrophosphatase and a FMN phosphohydrolase in yeast mitochondria: a possible role in flavin homeostasis, *Yeast.* 28 (2011) 693–705.
- [76] E.M. Torchetti, C. Brizio, M. Colella, M. Galluccio, T.A. Giancaspero, C. Indiveri, M. Roberti, M. Barile, Mitochondrial localization of human FAD synthetase isoform 1, *Mitochondrion* 10 (2010) 263–273.
- [77] O. Protchenko, R. Rodriguez-Suarez, R. Androphy, H. Bussey, C.C. Philpott, A screen for genes of heme uptake identifies the FLC family required for import of FAD into the endoplasmic reticulum, *J. Biol. Chem.* 281 (2006) 21445–21457.
- [78] A.T. Klein, M. van den Berg, G. Bottger, H.F. Tabak, B. Distel, *Saccharomyces cerevisiae* acyl-CoA oxidase follows a novel, non-PTS1, import pathway into peroxisomes that is dependent on Pex5p. *J. Biol. Chem.* 277 (2002) 25011–25019.
- [79] S. Subramani, Hitchhiking fads en route to peroxisomes, *J. Cell Biol.* 156 (2002) 415–417.
- [80] D. Drubin, The yeast *Saccharomyces cerevisiae* as a model organism for the cytoskeleton and cell biology, *Cell Motil. Cytoskeleton* 14 (1989) 42–49.

- [81] D. Botstein, S.A. Chervitz, J.M. Cherry, Yeast as a model organism, *Science* 277 (1997) 1259–1260.
- [82] F. Foury, Human genetic diseases: a cross-talk between man and yeast, *Gene* 195 (1997) 1–10.
- [83] R. Li, M.A. Bianchet, P. Talalay, L.M. Amzel, The three-dimensional structure of NAD(P)H:quinone reductase, a flavoprotein involved in cancer chemoprotection and chemotherapy: Mechanism of the two-electron reduction, *Proc. Natl. Acad. Sci. USA* 92 (1995) 8846–8850.
- [84] D. Liger, M. Graille, C.-Z. Zhou, N. Leulliot, S. Quevillon-Cheruel, K. Blondeau, J. Janin, H. van Tilbeurgh, Crystal structure and functional characterization of yeast YLR011wp, an enzyme with NAD(P)H-FMN and ferric iron reductase activities, *J. Biol. Chem.* 279 (2004) 34890–34897.
- [85] S. Sollner, R. Nebauer, H. Ehammer, A. Prem, S. Deller, B.A. Palfey, G. Daum, P. Macheroux, Lot6p from *Saccharomyces cerevisiae* is a FMN-dependent reductase with a potential role in quinone detoxification, *FEBS J.* 274 (2007) 1328–1339.
- [86] S. Sollner, P. Macheroux, New roles of flavoproteins in molecular cell biology: an unexpected role for quinone reductases as regulators of proteasomal degradation, *FEBS J.* 276 (2009) 4313–4324.
- [87] N. Burnichon, J.J. Briere, R. Libe, L. Vescovo, J. Riviere, F. Tissier, E. Jouanno, X. Jeunemaitre, P. Benit, A. Tzagoloff, P. Rustin, J. Bertherat, J. Favier, A.P. Gimenez-Roqueplo, SDHA is a tumor suppressor gene causing paraganglioma, *Hum. Mol. Genet.* 19 (2010) 3011–3020.
- [88] S.F. Heeringa, G. Chernin, M. Chaki, W. Zhou, A.J. Sloan, Z. Ji, L.X. Xie, L. Salviati, T.W. Hurd, V. Vega-Warner, P.D. Killen, Y. Raphael, S. Ashraf, B. Ovunc, D.S. Schoeb, H.M. McLaughlin, R. Airik, C.N. Vlangos, R. Gbadegesin, B. Hinkes, P. Saisawat, E. Trevisson, M. Doimo, A. Casarin, V. Pertegato, G. Giorgi, H. Prokisch, A. Rotig, G. Nurnberg, C. Becker, S. Wang, F. Ozaltin, R. Topaloglu, A. Bakkaloglu, S.A. Bakkaloglu, D. Muller, A. Beissert, S. Mir, A. Berdeli, S. Varpizen, M. Zenker, V. Matejas, C. Santos-Ocana, P. Navas, T. Kusakabe, A. Kispert, S. Akman, N.A. Soliman, S. Krick,

- P. Mundel, J. Reiser, P. Nurnberg, C.F. Clarke, R.C. Wiggins, C. Faul, F. Hildebrandt, COQ6 mutations in human patients produce nephrotic syndrome with sensorineural deafness, *J. Clin. Invest.* 121 (2011) 2013–2024.
- [89] J. Rainger, H. Bengani, L. Campbell, E. Anderson, K. Sokhi, W. Lam, A. Riess, M. Ansari, S. Smithson, M. Lees, C. Mercer, K. McKenzie, T. Lengfeld, B. Gener Querol, P. Branney, S. McKay, H. Morrison, B. Medina, M. Robertson, J. Kohlhase, C. Gordon, J. Kirk, D. Wieczorek, D.R. Fitzpatrick, Miller (Genee-Wiedemann) syndrome represents a clinically and biochemically distinct subgroup of postaxial acrofacial dysostosis associated with partial deficiency of DHODH, *Hum. Mol. Genet.* 21 (2012) 3969–3983.
- [90] R.A. Vaubel, P. Rustin, G. Isaya, Mutations in the dimer interface of dihydrolipoamide dehydrogenase promote site-specific oxidative damages in yeast and human cells, *J. Biol. Chem.* 286 (2011) 40232–40245.
- [91] H.R. Waterham, J. Koster, G.J. Romeijn, R.C. Hennekam, P. Vreken, H.C. Andersson, D.R. FitzPatrick, R.I. Kelley, R.J. Wanders, Mutations in the 3beta-hydroxysterol Delta24-reductase gene cause desmosterolosis, an autosomal recessive disorder of cholesterol biosynthesis, *Am. J. Hum. Genet.* 69 (2001) 685–694.
- [92] F. Giorgini, P. Guidetti, Q. Nguyen, S.C. Bennett, P.J. Muchowski, A genomic screen in yeast implicates kynurenine 3-monooxygenase as a therapeutic target for Huntington disease, *Nat. Genet.* 37 (2005) 526–531.
- [93] C.K. Yeung, E.T. Adman, A.E. Rettie, Functional characterization of genetic variants of human FMO3 associated with trimethylaminuria, *Arch. Biochem. Biophys.* 464 (2007) 251–259.

CHAPTER 2

**The microtubule-associated flavoprotein Irc15p from
*Saccharomyces cerevisiae***

Microtubule-associated Irc15p from Saccharomyces cerevisiae is an FAD-dependent NADH dehydrogenase

Karin Koch and Peter Macheroux*

*From the Graz University of Technology, Institute of Biochemistry, Petersgasse 12,

A-8010 Graz, Austria; Tel.: +43-316-873 6450, Fax: +43-316-873 6952,

Email: peter.macheroux@tugraz.at

Author contributions

P.M. initiated the project; K.K. and P.M. designed the experiments and interpreted the data. K.K. expressed and purified Irc15p and performed analytical, biochemical and enzymatic experiments. K.K. and P.M. wrote the manuscript. The authors appreciate the help of Chaitanya R. Tabib for his support with HPLC analysis and Eva-Maria Frießer for the help with routine work, as protein expression and purification.

Abstract

The genome of the yeast *Saccharomyces cerevisiae* encodes a canonical lipoamide dehydrogenase (Lpd1p) as part of the pyruvate dehydrogenase complex and a highly similar protein termed Irc15p (increased recombination centers 15). In contrast to Lpd1p, Irc15p lacks a pair of redox active cysteine residues required for the reduction of lipoamide and thus it is very unlikely that Irc15p performs a similar dithiol-disulfide exchange reaction as reported for lipoamide dehydrogenases. In the present study, we heterologously expressed *IRC15* in *Escherichia coli* and purified the produced protein to conduct a detailed biochemical and enzymatic characterization. Here, we show that Irc15p is a dimeric protein with one FAD per protomer. Photoreduction of the protein generates the fully reduced hydroquinone without the occurrence of a flavin semiquinone radical. Similarly, reduction with NADH or NADPH yields the flavin hydroquinone without the occurrence of intermediates as observed for lipoamide dehydrogenase. The redox potential of Irc15p was -313 ± 1 mV and is thus similar to lipoamide dehydrogenase. Surprisingly, reduced Irc15p is oxidized by several artificial electron acceptors, such as potassium ferricyanide, 2,6-dichlorophenol-indophenol, 3-(4,5-dimethyl-2-thiazolyl)-2,5-diphenyl-2*H*-tetrazolium bromide and menadione. However, disulfides, such as cysteine, glutathione and lipoamid were unable to react with reduced Irc15p. Taken together our findings suggest that Irc15p is efficiently reduced in yeast cells to deliver electrons to an as yet unidentified electron acceptor that is potentially related to Irc15p's function in regulating microtubule dynamics.

Keywords:

flavin adenine dinucleotide; lipoamide dehydrogenase; microtubule-binding protein; UV/visible absorption spectroscopy;

Abbreviations:

DCPIP, 2,6-dichlorophenol-indophenol; DTT, dithiothreitol; *E. coli*, *Escherichia coli*; Irc15, increased recombination centers 15; LPD, lipoamide dehydrogenase; MQ, menadione; MTT, 3-(4,5-Dimethyl-2-thiazolyl)-2,5-diphenyl-2*H*-tetrazolium bromide; *S. cerevisiae*, *Saccharomyces cerevisiae*; STH, soluble pyridine nucleotide transhydrogenases;

Introduction

The genome of the yeast *Saccharomyces cerevisiae* (*S. cerevisiae*) features 68 genes that were identified to encode a flavoprotein. Despite being a widely utilized model organism biochemical information on the flavoproteome is rather limited. For example, Irc15p (increased recombination centers 15) has a sequence similarity of 59% to the FAD-containing yeast lipoamide dehydrogenase 1 (Lpd1p) [1]. Although it was demonstrated that Irc15p is associated with microtubules and regulates their dynamics [2], it is currently unclear whether the protein carries a flavin cofactor not to mention the potential properties and function of the putative enzymatic activity. This lack of information prompted us to recombinantly produce Irc15p and study its properties.

Lipoamide dehydrogenases (LPDs) orchestrate the reversible transfer of electrons between dihydrolipoamide to the enzyme-bound FAD cofactor and NAD⁺. Generally, LPDs possess a second redox active group that is composed of two cysteine residues capable of forming an internal disulfide. This internal dithiol-disulfide exchange communicates the electrons between the lipoamide and the FAD cofactor and is thus an essential asset of LPDs [3,4]. Interestingly, Irc15p lacks the two essential cysteines required for the formation of a disulfide and therefore it is most unlikely that Irc15p is a redundant LPD or even exhibits similar enzymatic properties. Apparently, *IRC15* evolved after the whole genome duplication of *S. cerevisiae* and the duplicated *LPD1* sequence subsequently evolved to attain a new function (“neofunctionalization”) [5,6]. This new function appears to be connected to the regulation of microtubule dynamics and chromosome segregation [2]. However, it is not known what exactly this function is let alone whether this function is compatible with the properties of a putative LPD homolog.

LPDs are members of the family of flavoprotein disulfide reductases that catalyze the NAD(P)H-dependent reduction of disulfide containing substrates. To perform this reaction the enzymes are equipped with a flavin cofactor and another non-flavin redox center. Initially only three members, namely LPD, glutathione reductase and thioredoxin reductase composed the enzyme family, which has expanded significantly in recent years [3]. In 2012, family was classified according to the nature and position of the non-flavin redox center into five sub groups [4]. Group one comprises the flavoprotein disulfide reductases with the classical sequence motif

CXXXXC, such as LPD. Members of group two are structurally related but contain a second cysteine based redox center. Enzymes from group three contain only one cysteine, which either forms a cysteine sulfenic acid or a cysteine-coenzyme A mixed disulfide during the reaction. Members of group four contain the classical sequence motif but catalyze a non-disulfide reductase reaction. Finally, members of group five feature two cysteines that are widely separated in the primary sequence.

In addition to these five sub-groups, several proteins described in the literature exhibit high sequence similarity with flavoprotein disulfide reductases, but lack some significant features. For example, pyridine nucleotide transhydrogenases (STH) catalyzes the reversible transfer of electrons between NADH and NADP⁺ and lack at least one of the redox active cysteines and a histidine residue essential for catalytic activity [3,7]. These enzymes are also closely related to LPD, for example, STH from *E. coli* exhibits 27% identity and 45% similarity to several LPDs [8]. However, also LPDs themselves are able to catalyze transhydrogenase reactions [9]. Another example is LpdA from *Mycobacterium tuberculosis*, which lacks as well one cysteine and the catalytic histidine and glutamate. Like STH the protein is not able to catalyze the reduction of disulfides but instead features quinone reductase activity. The physiological relevance of this protein is unknown [10].

In the present work we recombinantly produced Irc15p in *Escherichia coli*. The purified Irc15p shows the typical characteristics of a flavoenzyme. We have shown that Irc15p is efficiently reduced by NADH but lacks disulfide reductase activity. However, reduced Irc15p reduces a range of artificial electron acceptors, such as potassium ferricyanide, 2,6-dichlorophenol-indophenol (DCPIP) and quinones. The potential role of Irc15p as a microtubule-associated protein is discussed in light of our findings concerning the enzymatic properties.

Materials and Methods

Materials

All chemicals, reagents and enzymes were of highest quality and from Sigma-Aldrich (St. Louis, USA), Roth (Karlsruhe, Germany) or Thermo Fisher Scientific (Waltham, USA), unless otherwise noted. Columns for affinity chromatography (Ni-NTA-sepharose), size exclusion chromatography (Superdex 200 10/300 GL) and buffer

exchange (PD-10 desalting column) were from GE Healthcare (Little Chalfont, UK). The *E. coli* strains Top10 and Rosetta™(DE3) were from Invitrogen (Carlsbad, USA) and Merck (Darmstadt, Germany), respectively. The plasmid pET21d was from Merck (Darmstadt, Germany).

Cloning of IRC15 for large scale expression in E. coli

All strains were generated using standard genetic techniques [11,12]. Briefly, genomic DNA from *S. cerevisiae* was extracted with the yeast DNA extraction kit from VWR (Radnor, USA). According to the sequence for *IRC15* from the *Saccharomyces* genome database [13] the following primers were designed and synthesized from VBC (Vienna, Austria): fw_5'-GAACCATGGCAATGGGAGGTGAA GACGAAATATTAAGCAC-3'; rev_5'-GAGCCTCGAGTTAATGGTGATGATGGTGAT GATGATGATGTTCCCGGACATGTACGCCAG-3'. To construct the heterologous expression vector pET21d(+)/*IRC15* introducing an additional C-terminal 9x-histidine tag the restriction enzymes NcoI/XhoI were used. Individual clones were sequenced before transforming the plasmid into *Escherichia coli* Rosetta™(DE3) cells.

Heterologous production and purification of Irc15p

A single colony of *E. coli* Rosetta(DE3) comprising pET21d(+)/*IRC15* was used to inoculate a pre-culture that was aerobically incubated (37 °C, 16 h, 150 rpm) in terrific broth media (bacto-tryptone 12 g/L, bacto-yeast extract 24 g/L, glycerol 4g/L, KH₂PO₄ 2.31 g/L and K₂HPO₄ 12.54 g/L) supplemented with 100 µg·mL⁻¹ ampicillin and 20 µg·mL⁻¹ chloramphenicol. 1% pre-culture was used to inoculate the main-culture supplemented with 100 µg·mL⁻¹ ampicillin and 10 µg·mL⁻¹ chloramphenicol, which was incubated aerobically at 37 °C with agitation at 150 rpm until a OD₆₀₀ of ~0,6 was reached. Production of the recombinant protein was induced by addition of 0.5 mM isopropyl-thio-β-D-galactoside and the culture was further incubated for 16 h at 20 °C. Cells were harvested by centrifugation at 4.500 g at 4 °C and washed once with 1% saline solution. Cell pellets were resuspended in 4 mL/g pellet buffer A [50 mM Hepes, 150 mM NaCl, 1 mM dithiothreitol, pH 7.0) supplemented with 30 mM imidazole, 1 mM phenylmethylsulfonyl fluoride dissolved in dimethylsulfoxide, 10 µM flavin adenine dinucleotide disodium salt hydrate. Furthermore, 1 µL of protease inhibitor cocktail for the purification of histidine-tagged proteins from Sigma-Aldrich (St. Louis, USA) was added per 1 g of cell pellet. Cell disruption was achieved by sonication with a Labsonic L instrument from Braun biotechnoly international (Berlin,

Germany) with 120 Watt for 3 x 3 min in an ice-water bath with 3 min pauses between each cycle. The cell lysate was centrifuged at 38.850 g for 45 min at 4 °C, and the supernatant was loaded onto a 5-mL HisTrap HP column previously equilibrated with buffer A supplemented with 30 mM imidazole. The column was washed with five column volumes with buffer containing 50 mM Hepes, pH 7.0, 1 M NaCl, 1 mM DTT and 100 mM imidazole. Then the column was washed with buffer A supplemented with 100 mM imidazole and subsequently proteins were eluted with buffer A supplemented with 350 mM imidazole. Fractions containing target protein were pooled and concentrated with centrifugal filter units (Amicon Ultra-15, 50 kDa; Millipore, Massachusetts, USA). Concentrated protein was re-buffered to buffer B (50 mM Hepes, 50 mM NaCl, 1 mM DTT, pH 7.0) with a PD-10 desalting column. The protein solutions were shock frozen and stored at -80 °C if not used immediately.

Determination of molecular mass of Irc15p

The subunit molecular mass of purified Irc15p was determined by SDS-PAGE with a 12.5% separating gel and 5% stacking gel under reducing conditions described by Laemmli [14]. The molecular mass marker PageRuler™ (prestained protein ladder 10-180 kDa) from Thermo Fisher Scientific (Waltham, USA) was used.

To determine the native molecular mass of Irc15p size exclusion chromatography with Buffer A using a Superdex 200 10/300 GL column attached to an Äktapurifier™ system from GE Healthcare (Little Chalfont, UK) was performed. Protein elution was monitored at 280 nm and 450 nm. The column was calibrated with molecular mass standards according to the instructions from GE healthcare.

Determination of the flavin cofactor bound to Irc15p

To determine the nature of the flavin cofactor concentrated protein samples were treated with 8 M guanidine hydrochloride (pH 2 adjusted with concentrated HCl). Denatured protein was removed by centrifugation (13.000 g, 5 min) and the solution was neutralized with concentrated NaOH. To remove residual protein centrifugal filter units (Amicon Ultra-0.5 mL 10 kDa; Millipore, Massachusetts, USA) were used. The flow-through was concentrated at 50 °C under reduced pressure and subsequently analysed by HPLC (UltiMate® 3000 HPLC system from Dionex, California, USA) using an Atlantis® dC18 5 µM (4.6 x 250 mm) column. As liquid phase a 0.1% TFA solution and acetonitrile containing 0.1% TFA were used. The concentration of the

organic solvent was increased within 20 min from 0% to 95% in a linear gradient (T = 25 °C; flow rate = 1 ml/min). The samples were analysed using a diode array detector at 280, 370 and 450 nm. The retention times of authentic FAD, FMN and riboflavin were 9.05, 9.75 and 10.4 min, respectively.

Determination of the redox potential

The redox potential was determined by the dye-equilibration method using the xanthine/xanthine oxidase electron delivering system as described by Massey [15]. Reactions were carried out in buffer C (50 mM Hepes, 50 mM NaCl, pH 7) supplemented with methyl viologen (2,5 µM) as mediator, 500 µM xanthine, and xanthine oxidase in catalytic amounts (~40 nM) and lasted 0,5-2 h at 25 °C. The protein concentration for a typical experiment was ~10 µM. The concentrations given are final values after mixing in the flow cell. Experiments were performed with a SF-61SX2 stopped flow device from TgK Scientific Limited (Bradford-on-Avon, UK) equipped with an auto-shutter to reduce photochemical effects during the experiment. To maintain anoxic conditions the device was positioned in a glove box from Belle Technology (Weymouth, UK). Absorption spectra during the course of reduction were recorded with a KinetaScanT diode array detector from TgK Scientific Limited (Bradford-on-Avon, UK). Safranin T was used as a reference dye for the analysis (-289 mV). The amounts of oxidized and reduced Irc15p and safranin T were quantitated at 430 nm and 530 nm, respectively. The reduction-oxidation potentials were calculated from plots of $\log(Irc15p_{ox}/Irc15p_{red})$ versus $\log(dye_{ox}/dye_{red})$ according to Minnaert [16] using Excel 2010 (Microsoft, Redmond, WA, USA).

Homology modeling and sequence alignment

A structural model of Irc15p was generated using the Swiss Model server [17] with Lpd1p from *Saccharomyces cerevisiae* (PDB entry: 1V59) as template. Sequences for the alignment were taken from the *Saccharomyces* genome database [13] or from the UniProt database [18]. The alignment was generated with the program Clustal Omega [19].

Methods using UV-visible absorption spectroscopy

Absorption spectra were recorded with a Specord 200 plus spectrophotometer from Analytik Jena (Jena, Germany) at 25 °C using 1-cm quartz cuvettes.

Extinction coefficient: The extinction coefficient of Irc15p was determined according to [20]. Briefly, Irc15p bound FAD was released by addition of 0.2% SDS. Absorption spectra were recorded before and after denaturation of the enzyme. The calculation yielded an extinction coefficient of $11.900 \text{ M}^{-1} \text{ cm}^{-1}$ at 453 nm for Irc15p.

Anoxic photoreduction: Photoreduction was carried out as described in [20]. Briefly, $\sim 10 \text{ }\mu\text{M}$ Irc15p in 1 mL buffer B (50 mM Hepes, 50 mM NaCl, 1 mM DTT, pH 7.0) supplemented with 1 mM EDTA was deoxygenated by incubation for 2 h in a glove box from Belle Technology (Weymouth, UK). A 10 W LED floodlight (Lumineia) was used to reduce the cofactor by light irradiation. Absorption spectra were recorded after each reduction step until no further spectral changes were observed. Thereafter the sample was exposed to air and a spectrum was recorded after complete reoxidation.

Steady state kinetics: Initial-velocity kinetic measurements were performed in triplicates with NAD(P)H, the disulfide containing electron acceptors lipoic acid, glutathione and cystine and the artificial electron acceptors potassium ferricyanide, MQ (menadione), MTT [3-(4,5-dimethyl-2-thiazolyl)-2,5-diphenyl-2H-tetrazolium bromide] and DCPIP (2,6-dichlorophenol-indophenol). Reaction mixtures were setup in buffer C (50 mM Hepes, 50 mM NaCl, pH 7). All reactions were initiated by addition of 5 μL enzyme stock solution supplemented with 200 nM DTT to the reaction mixture – final enzyme concentrations were 10 nM. Controls were performed in the absence of enzyme. Rates of reduction with MQ, oxygen and disulfide containing substrates were determined by fitting the observed absorption change at 380 nm in the first minute using adapted extinction coefficients (NADH $\epsilon_{380 \text{ nm}} = 1.210 \text{ M}^{-1} \cdot \text{cm}^{-1}$ or NADPH $\epsilon_{380 \text{ nm}} = 1.280 \text{ M}^{-1} \cdot \text{cm}^{-1}$). For the other electron acceptors pertinent wavelengths and extinction coefficients were used (ferricyanide $\epsilon_{420 \text{ nm}} = 1.040 \text{ M}^{-1} \cdot \text{cm}^{-1}$; MTT $\epsilon_{578 \text{ nm}} = 13.000 \text{ M}^{-1} \cdot \text{cm}^{-1}$; DCPIP $\epsilon_{600 \text{ nm}} = 21.000 \text{ M}^{-1} \cdot \text{cm}^{-1}$) [21].

Determination of reductive/oxidative rates

The protein was deoxygenated by incubation for 2 h in a glove box from Belle Technology (Weymouth, UK) kept in nitrogen atmosphere. The reductive half-reaction was investigated by mixing protein ($\sim 20 \text{ }\mu\text{M}$) in buffer B with 25-2.500 μM NADH or 25-1.000 μM NAD(P)H. The concentrations given are final values after

mixing in the flow cell. Experiments were performed with a SF-61SX2 stopped flow device from TgK Scientific Limited (Bradford-on-Avon, UK) positioned in an anoxic glove box from Belle Technology (Weymouth, UK) at 4 °C. Changes in flavin absorption were followed with a PM-61s photomultiplier from TgK Scientific Limited (Bradford-on-Avon, UK) at 453 nm.

Thermal shift assay

Thermal shift assays were performed as described elsewhere [22]. 20 µL of ~13 µM Irc15p protein solution was pipetted into a white 96-well RT-PCR plate from Bio-Rad (California, USA). Two µL of a 1:500 dilution of SYPRO[®] orange from Molecular Probes (Oregon, USA) was added. The plates were sealed with an optical-quality sealing tape from Bio-Rad (California, USA) and heated in a CFX Connect™ Real-Time PCR detection system from Bio-Rad (California, USA) from 20 to 95 °C in increments of 0.5 °C/5 sec. Fluorescence changes of the dye were detected at a wavelength between 470 and 500 nm. Melting temperatures (T_m) were determined using cfx manager 3.0 software from Bio-Rad (California, USA).

Results

Biochemical characterization of Irc15p

Initially, Irc15p was produced with a C-terminal hexa-histidine tag as described by Keyes and Burke [2]. However, the protein could not be purified successfully due to weak binding to the Ni-NTA sepharose resin. Therefore, we employed a C-terminal nona-histidine tag enabling the successful purification of ~13 mg of protein from 1 l culture with a purity of >90 % as judged by visual inspection of SDS-PAGE and by using the program ImageJ (<http://imagej.nih.gov/ij/>) [23] (Figure 1, panel A). The presence of DTT in the buffer was critical to prevent the precipitation of Irc15p.

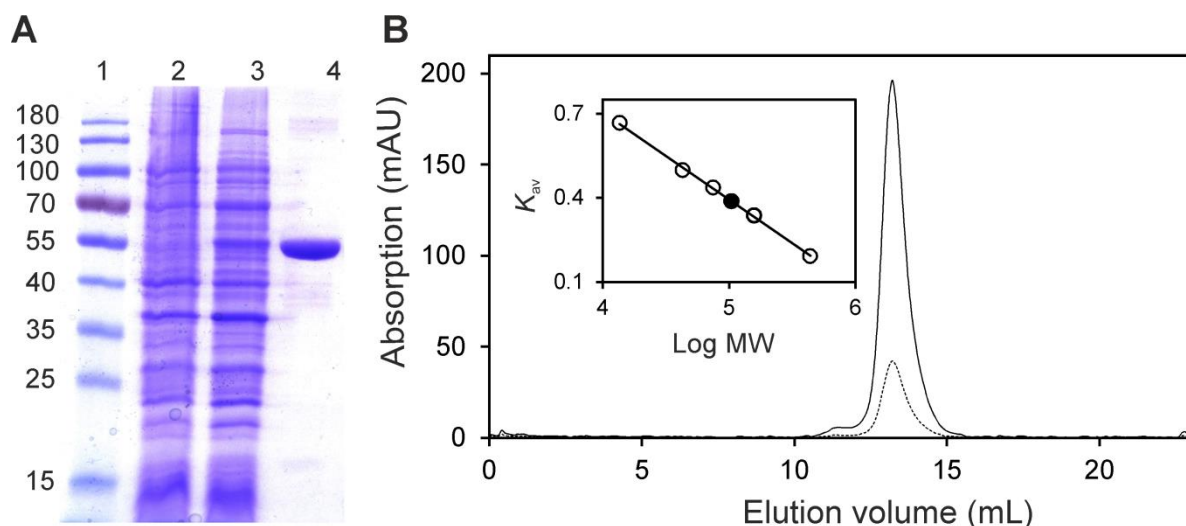


Figure 1. Determination of the purity and molecular mass of Irc15p using SDS-PAGE and analytical size exclusion chromatography. (A) Determination of purity and subunit molecular mass of Irc15p by SDS-PAGE after purification by affinity chromatography. Lane 1, PageRuler™ prestained protein ladder (10-180 kDa); lane 2, protein extract before induction; lane 3, protein extract after induction of *IRC15*; lane 4, protein fraction after purification by Ni-NTA-sepharose. The subunit molecular mass of Irc15p was estimated to ~55 kDa. (B) Determination of native molecular mass of Irc15p (solid and dotted line show the absorption at 280 nm and 450 nm, respectively) using analytical size exclusion chromatography. The insert shows a plot of the partition coefficient (K_{av}) against the logarithm of molecular mass of standard proteins (ferritin, 440 kDa; aldolase, 158 kDa; conalbumin, 75 kDa; ovalbumin, 43 kDa; ribonuclease A, 13.7 kDa). The calculated molecular mass of Irc15p (~ 113 kDa, black circle) indicates that Irc15p is present as a dimer.

Analytical size exclusion chromatography yielded a molecular mass of ~115 kDa confirming that Irc15p forms a homodimer as previously reported by Keyes and Burke [2]. The protein peak was associated with a yellow color indicating the presence of a flavin cofactor in agreement with the high sequence similarity to the FAD-dependent LPD (Figure 1, panel B).

To assess the chemical identity of the flavin cofactor, Irc15p was denatured and the released flavin was analyzed by HPLC. A peak was obtained at a retention time of 9.1 min closely corresponding to the retention time of authentic FAD (9.05 min). Furthermore, the purified protein showed the absorption characteristics of a flavoprotein with two distinct peaks at 377 and 453 nm with a shoulder at ~470 nm. Denaturation of the protein resulted in a slight bathochromic shift of the absorption maxima (Figure 2). Using an extinction coefficient of $11.300 \text{ M}^{-1} \text{ cm}^{-1}$ at 450 nm for free FAD [20] an extinction coefficient of $11.900 \text{ M}^{-1} \text{ cm}^{-1}$ at 453 nm was calculated for Irc15p. This extinction coefficient was used to determine the concentration of

Irc15p in further experiments. The A_{280}/A_{450} ratios of purified Irc15p were usually between 4.3 and 4.5.

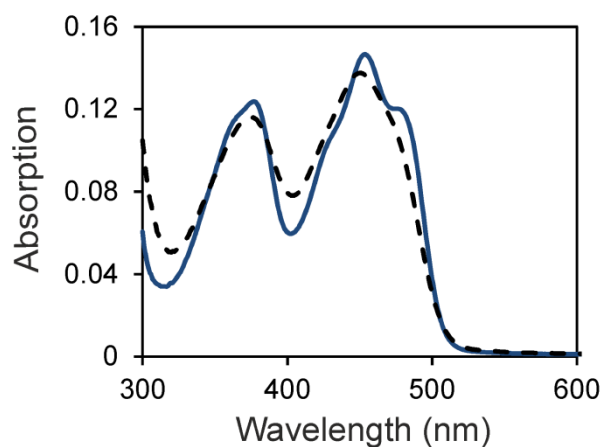


Figure 2. UV/Vis absorption spectroscopy. UV-visible absorption spectrum of Irc15p before (solid line) and after denaturation (dashed line). Denaturation of purified Irc15p was carried out in buffer B (50 mM Hepes, 50 mM NaCl, 1 mM DTT, pH 7.0) containing 0.2% SDS.

Photoreduction of Irc15p in the presence of EDTA led to the formation of the fully reduced flavin (hydroquinone) without the formation of a semiquinone radical (Figure 3). After reoxidation and removal of precipitated protein the obtained UV-vis absorption spectrum was similar to the initial spectrum indicating that reduction is fully reversible and does not give rise to chemical alterations of the flavin (Figure 3).

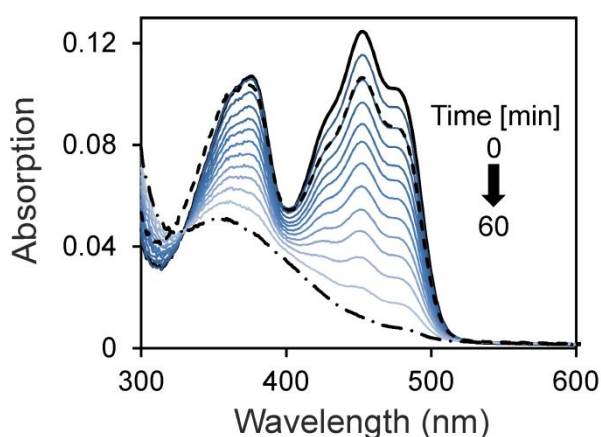


Figure 3. Absorption spectra observed during the anaerobic photoreduction of Irc15p in 50 mM Hepes, 50 mM NaCl, 1 mM DTT, pH 7.0. The solid black line represents the spectrum before irradiation. The reduction proceeds as indicated by the arrow with the dashed dotted line representing the final spectrum. After reoxidation by dioxygen the protein was partially denatured. The solution was cleared by centrifugation and the spectrum recorded (dashed line).

The redox potential of the FAD cofactor was determined with the xanthine/xanthine oxidase system in the presence of safranin T ($E_M = -289$ mV). According to the method of Minnaert [16] a plot of $\log(Irc15p_{ox}/Irc15p_{red})$ versus $\log(dye_{ox}/dye_{red})$ was used to estimate the redox potential to -313 ± 1 mV (six independent measurements). In agreement with the photoreduction, reduction of Irc15p occurred without formation of semiquinones and accordingly the slope of the logarithmic plot was close to unity indicating that the reference dye as well as the isoalloxazine moiety of the flavin takes up two electrons (Figure 4).

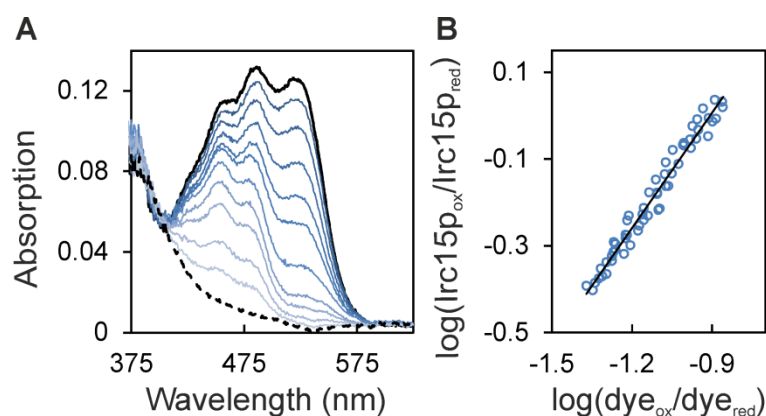


Figure 4. Redox potential determination of Irc15p in the presence of safranin T. (A) The absorption spectrum of the fully oxidized and fully reduced species are represented by a solid and dashed black line, respectively. Selected spectra of the course of reduction are represented in different shades of blue. Ten μ M Irc15p was reduced by the xanthine/xanthine oxidase electron delivering system in the presence of safranin T over a time period of ~ 100 min. Data points for evaluation were extracted at 430 nm and 530 nm for Irc15p and for the dye safranin T, respectively. (B) Double logarithmic plot of the concentration of oxidized/reduced Irc15p vs. the concentration of oxidized/reduced safranin T (Nernst plot).

Homology modelling and sequence alignment

The sequence identity and similarity of Irc15p and Lpd1p from *S. cerevisiae* is about 40% and 59%, respectively and several crucial amino acids and sequence motifs are conserved (Figure 5).

The microtubule-associated flavoprotein Irc15p from *Saccharomyces cerevisiae*

```

S. seoulensis Lpd -----MANDASTVFDLVILGGGSGGYAAALRGAQLGLDVALIEK---
S. cerevisiae Irc15p -----MGGEDEILSTM--EDFAAVYDVLVI GCGPGGF TAAMQASQAGLLTACVDQ--
E. coli Lpd -----MSTEIKTQVVVL GAGPAGY SAAFRCADLGLLETIVIVERY--
S. cerevisiae Lpd1p MLRIRSLNNKRAFSSVRTL TINKSHDVVII GGGPAGY VAAIKAAQLGFNTACVEK---
A. vinelandii Lpd -----MSQKFDVIVI GAGPGGY VAAIKSAQLGLKTALIEKYKG
                               ::::* * .*: **:: : : * : . . ::

S. seoulensis Lpd ----DKVGGTCLHKGCIPTKALLHAGEIADQARESEQFGVKA----TFEGIDVPAVQKYK
S. cerevisiae Irc15p ---RASLGGAYLVDGAVP SKTLLYESYLYRLLQQQELIEQRGTRLF--PAKFDMQAAQSAL
E. coli Lpd ----NTLGGVCLNVGCIPTSKALLHVAKVIEEAKA---LAEHGIV--FGEPKTDIDKIRTWK
S. cerevisiae Lpd1p ---RGKLGGTCLNVGCIPTSKALLNNSHLFHQMHT--AQKRGIDVNGDIKINVANFQKAK
A. vinelandii Lpd KEGKTALGGTCLNVGCIPTSKALLDSSYKFHEAHES--FKLHGIS--TGEVAIDVPTMIARK
                               :** . * * : * : * : * : . : : :

S. seoulensis Lpd DDVISGLYKGLQGLIASRKVTTYEGEGRSSPTSVDVNGQ-----RIEGRHVLL
S. cerevisiae Irc15p KHNIEELGNVYKRELSKNNVTYKGTAAFKDPHHEVIAQRGM-----KPFIVEAKYIVV
E. coli Lpd EKVINQLTGGLAGMAKGRKVKVNVNGLGKFTGANTLEVEGENG-----KTVINFDNAII
S. cerevisiae Lpd1p DDAVKQLTGGIELLFKKNKVTYKNGSFEDETKIRVTPVDGLEGTVEKDHI LDVKNII V
A. vinelandii Lpd DQIVRNLTGGVASLIKANGVTLEFEGHGLLAGKKVEVTAADGS-----SQVLDTENVIL
.. : * . * . * : . : : : : : : : : :

S. seoulensis Lpd ATGSVPKSLPGLQIDGDRIIISDHALVLDRVPKSAIILGGGVIGVEFASAWKSGFADVTV
S. cerevisiae Irc15p ATGSAVIQCPGVAIDNDKIIISDKALSLDYIPSRFTIMGGGTIGLEIACIFNNLGSRVTI
E. coli Lpd AAGSRPIQLPFI PHEDPR IWDSDALELKEVPERLLVMGGGIIGLEMGTVYHALGSQIDV
S. cerevisiae Lpd1p ATGSEVTPFPPIEIDEKIVSSTGALSLEKIPKRLTIIGGGIIGLEMGSVYSRLGSKVTV
A. vinelandii Lpd ASGSKPVEIPPAVDQDVIVDSTGALDFQNVPGKLGVI GAGVIGLEELGSVWARLGAEVTV
*:** * : * . * ** . : * : : * * ** : : : :

S. seoulensis Lpd IEGLKHLVPVEDENSSKLLERAFRKRGIKFSLGTFFFEKAEYTDQGVKVTLAD-----G
S. cerevisiae Irc15p VESQSEICQNMDNELASATKTLQCQGI AFLLDTRVQLAEADAAGQLNITLL--NKVSKKT
E. coli K12 Lpd VEMFDQVIPAADKDIVKVFTRISK--KFNLMLETKVTAVEAKEDGIYVTM--EGKKAPA
S. cerevisiae Lpd1p VEFQPQIGASMDGEVAKATQKFLKKQGLDFKLS TKVISAQRNDDKNVVEIVVEDTKTNQ
A. vinelandii Lpd LEAMDKFLPAVDEQVAKEAQKILTKQGLKILLGARVGTGEVKNKQVTVKVFVD---AEGE
: * .. * : . : : : * : . . :

S. seoulensis Lpd KEFEAEVLLVAVGRGPVSNQLGYEEQGVNID--RGYV--LVDEYMRNTVPTISAVGDLVP
S. cerevisiae Irc15p YVHHCVDVLMVSI GRRPLLKGLDISSIGL--DERDFVENVDVQTSLLKYPHIKPIGDVTL
E. coli Lpd EPQRYDAVLVAIGRVPGKNLDAGKAGVEVDDRGI---RVDKQLRNTVPHIIFAIGDIVI
S. cerevisiae Lpd1p ENLEAEVLLVAVGRRPYIAGLGAEKIGLEVDKRGR---VIDDQFNSKFPPIKVVGDVTF
A. vinelandii Lpd KSQAFDKLIVAVGRRPVTTDLLAADSGVTLDERGFI---YVDDYCATSVPGVYAI GDVVR
: : : : * * * . * : * * . : : : : : * : * : : :

S. seoulensis Lpd TLQLAHVGF AEGILVAERL--AGLKTVPIDYDGVPRVTVCHPEVASVGI TEAKAKEIYGA
S. cerevisiae Irc15p GPMLALKAEEQAIRAIQSIGCTG--SDGTSNCGFPPNVLYCQPQIGWVGYTEEGLAKARIP
E. coli Lpd QPMLAHKGVHEGHVAAEVI--AG--KKHYFDPKVPISIAVTEPEVAWVGLTEEKAKEKGIS
S. cerevisiae Lpd1p GPMLAHKAEEEGIAA VEML--KT--GHGHVNYNNI PSVMYSHPEVAWVGKTEEQLKEAGID
A. vinelandii Lpd GAMLAHKASEEGVVVAERI--AG--HKAQMNYDLIPAVIYTHPEIAGVGKTEQALKAEGVA
** . . . : : : : : * : * . * : : * *

S. seoulensis Lpd DKVVALKYS LAGNGKSKI-----LKTAGEIK--LVQVKDGA VGVVHMVGD RMGEQVGEA
S. cerevisiae Irc15p YQKGRVLF S--QNVRYNTLLPREENTTVSPFIKVLIDSRDMKILGVHMINDDANELL SQA
E. coli Lpd YETATFPWA--ASGRAI-----ASDCADGMTKLI FDKESHRI VIGGAI VGTNGGELLGEI
S. cerevisiae Lpd1p YKIGKFPFA--ANSRAK-----TNQDTEGFVKILIDSKTERILGAHI IGPNAGEMIAEA
A. vinelandii Lpd INVGVPFA--ASGRAM-----AANDTAGFVKVIADAKTDRVLGVHVI GPSAAELVQQG
: . : : . : . * : : . : * : :

S. seoulensis Lpd QLIYNWEALPAEVAQLIHAHPTQNEALGEAHLALAGKPLHAHD-----
S. cerevisiae Irc15p SMAVSLGLTAHDVCKVFPFHPHLSLSE SFKQAVQLAMANGTSPGVHVRE*-
E. coli Lpd GLAIEMGCDAEDIALTIHAHPTLHESVGLAAEVFEGSTIDLPNPKAKKK
S. cerevisiae Lpd1p GLALEYGASAE DVARVCHAHPTLSEAFK EANMAAYDKA IHC*-----
A. vinelandii Lpd AIAMEFGTSAEDLGMVFVHPALS EALHEAALVSG--HAHVANRKK---
: . : : . ** : * : *

```

Figure 5. Alignment of the Irc15p protein sequence with sequences of LPD from *S. cerevisiae*, *E. coli*, *Streptomyces seoulensis* and *Azotobacter vinelandii*. The mitochondrial targeting sequence of Lpd1p is highlighted in red. The amino acid signature near the redox-active disulfide is highlighted in yellow. The respective sequence in Irc15p is highlighted in green. The catalytic His-Glu diad is highlighted in blue. Other residues in the active site are highlighted in petrol. Residues involved in structural stabilization are highlighted in purple. Conserved sequence motifs (GxGxxG) which are part of the Rossmann-fold are highlighted in dark purple. Overall sequence identities and similarities of Irc15p and various LPDs to Lpd1p are: Irc15p (40% and 59%, respectively) *E. coli* LPD (41% and 57%, respectively), *Streptomyces seoulensis* LPD (37% and 55%, respectively) and *Azotobacter vinelandii* LPD (45% and 63%, respectively).

A structural model of Irc15p was generated using the Swiss model server [17] using Lpd1p from *S. cerevisiae* (PDB entry: 1V59) as template (Figure 6, panel A). A comparison of the close environment of the FAD cofactor from Irc15p (Figure 6, panel B) and Lpd1p (Figure 6, panel C) reflects a high sequence conservation: out of 16 residues that are within 4 Å of the flavin isoalloxazine ring only four are different. Notably, among these are the two cysteines, C46 and C49, which make up the dithiol/disulphide redox centre of Lpd1p. These are replaced by tyrosine and alanine, respectively. The two amino acid residues that compose the catalytic diad, i.e. H457 and E462 are conserved in both proteins [24].

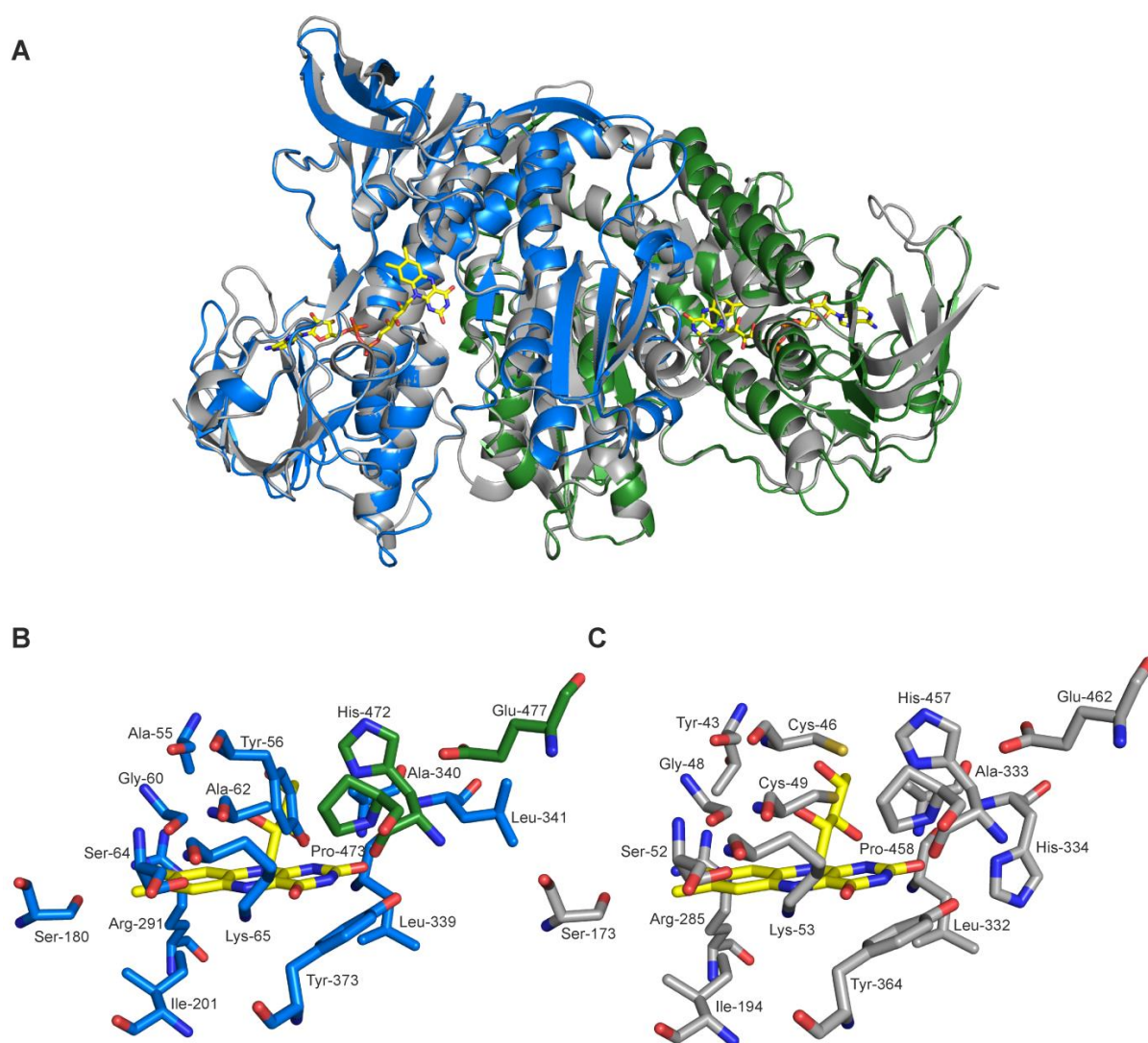


Figure 6. Overall structural similarity of Irc15p and LPD1p. **(A)** Structural superposition of LPD1p (grey, PDB code: 1V59) and Irc15p (blue/green). The FAD cofactor is shown as yellow sticks. Close-up view of the active sites of Irc15p **(B)** and LPD1p **(C)**. Residues close to the FAD isoalloxazine ring are shown as grey sticks for both protomers (Lpd1p) or in colors corresponding to the respective protomer (Irc15p). Figures were prepared with the software PyMOL [25].

Enzymatic properties and thermal stability of Irc15p

To gain information on the specificity of the electron donor the reductive half-reaction was studied using stopped-flow spectrophotometry. Reduction of Irc15p with NADH was fast and monophasic. The rate of reduction was analysed as a function of substrate concentration and fitted to a hyperbolic equation yielding a limiting reductive rate of $250 \pm 3 \text{ s}^{-1}$ and a dissociation constant of $100 \pm 5 \text{ }\mu\text{M}$ (Figure 7, panel A). As noted above, no semiquinone radical was observed (Figure 7, panel A, inset). In contrast to reduction by NADH, the reduction with NADPH exhibited two phases (Figure 7, compare panel B and C) and the bimolecular rate constant determined at $100 \text{ }\mu\text{M}$ NAD(P)H is an order of magnitude lower (NADH = $1,2 \cdot 10^6 \text{ M}^{-1} \text{ s}^{-1}$, NADPH = $3,4 \cdot 10^5 \text{ M}^{-1} \cdot \text{s}^{-1}$).

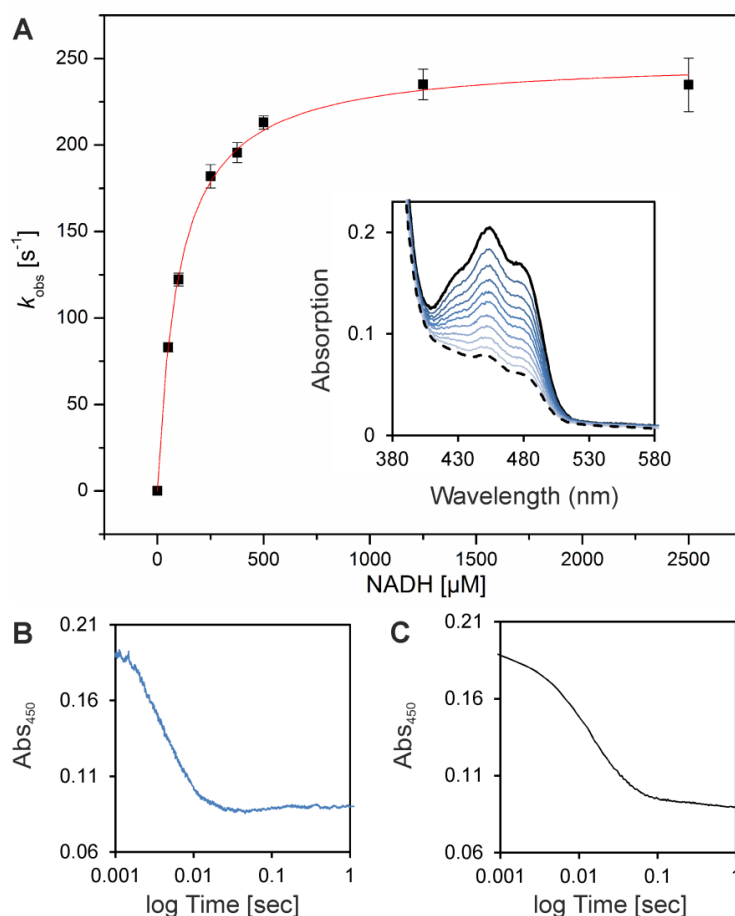


Figure 7 Presteady-state kinetics of Irc15p to determine reductive rates for NADH. **(A)** The rate of reduction was determined under anoxic conditions with the stopped flow device equipped with a diode array detector. At least three independent measurements were performed (error bars are shown as standard deviations). The inset shows selected absorption spectra of the reduction of $\sim 20 \text{ }\mu\text{M}$ Irc15p with $375 \text{ }\mu\text{M}$ NADH. **(B)** Absorption change at 450 nm of the reduction of $\sim 20 \text{ }\mu\text{M}$ Irc15p with $1250 \text{ }\mu\text{M}$ NADH determined. **(C)** Absorption change at 450 nm of the reduction of $\sim 20 \text{ }\mu\text{M}$ Irc15p with $1000 \text{ }\mu\text{M}$ NADPH.

To evaluate the enzymatic activity of Irc15p, assays with NAD(P)H and several potential electron acceptors were performed (Table 1). No activity was observed with substrate disulfides such as lipoic acid, glutathione or cystine. On the other hand, the enzyme showed diaphorase activity with the non-specific electron acceptors potassium ferricyanide, MTT, and DCPIP and quinone reductase activity with MQ. Furthermore the reduced cofactor was reoxidized by molecular oxygen, however at a comparatively sluggish rate. A clear preference for NADH as electron donor is only observed in steady-state assays employing potassium ferricyanide as electron acceptor.

Table 1. Specific activities of Irc15p with NAD(P)H [$\mu\text{mol}/\text{min}^{-1}/\text{mg}^{-1}$] as electron donor in comparison with the specific activity of LPD from *Streptomyces seoulensis* [26] and LPD from *S. cerevisiae* (in brackets) [27] with NADH. Reduction of ferricyanide, DCPIP and MTT was determined at 420, 600 and 500 nm, respectively. All other reactions were monitored at 380 nm.

Substrate	Specific Activity with NADH [$\mu\text{mol}/\text{min}^{-1}/\text{mg}^{-1}$] ^a	Specific Activity with NADPH [$\mu\text{mol}/\text{min}^{-1}/\text{mg}^{-1}$] ^a	Specific Activity of LPD with NADH [$\mu\text{mol}/\text{min}^{-1}/\text{mg}^{-1}$] ^c
Ferricyanide	179.5	17.9	7.9 (1670.0 ^d)
DCPIP ^b	3.9	4.7	61.4 (2.0 ^d)
MQ ^{*,b}	19.7	19.3	7.2
MTT [*]	1.6	1.3	-
Lipoic acid [*]	0	0	15.6
Cystine [*]	0	0	0.8
Glutathione [*]	0	0	0.2
Oxygen [*]	1.0	1.0	0

^aThe reaction mixture for the measurements of Irc15p contained 50 mM Hepes, pH 7.0, 50 mM NaCl, 10 nM DTT, 500 μM NAD(P)H, 500 μM electron acceptors (except MQ and DCPIP). ^bThe concentration of DCPIP and MQ were 50 and 200 μM , respectively. ^cThe reaction mixture for the measurements of LPD from *Streptomyces seoulensis* contained 50 mM sodium phosphate buffer, pH 7.4, 0.3 mM substrates and 0.2 mM NADH. ^dThe reaction mixture for the potassium ferricyanide assay of LPD1 from *Saccharomyces cerevisiae* contained 165 mM sodium acetate, pH 4.8, 0.7 mg/ml bovine serum albumin, 1mM EDTA, 600 μM NADH, 670 μM potassium ferricyanide. The DCPIP assay contained phosphate buffer, pH 7.2, 0.7 mg/ml bovine serum albumin, 1mM EDTA; 600 μM NADH and 40 μM DCPIP.

The potassium ferricyanide assay was further used to determine the influence of various pH values and salt concentrations on the enzymatic activity of Irc15p. The highest activity was observed at pH 7.0 without salt in the assay buffer. Below and above pH 7.0 the activity is reduced by about 14-49%, and the presence of salt decreased the activity at pH 7.0 by 40%.

The thermal stability of Irc15p was monitored using a thermal shift assay. However, the fluorescence of the non-covalently bound FAD can't be used for detection, so the experiment was performed with the fluorescent dye SYPRO[®] orange [22]. Under optimal conditions Irc15p displays a rather high thermal stability of about 70°C (Table 2).

Table 2. Activity and thermal stability of Irc15p at various pH and in the absence and presence of salt

Buffer composition	Activity [%]	T _m [°C]
50 mM Hepes, pH 6.0	51	70
50 mM Hepes, pH 7.0	100	69
50 mM Hepes, pH 8.0	86	62
50 mM Tris/HCl, pH 9.0	46	56
50 mM Hepes, pH 7.0, 150 mM NaCl	61	69

The reaction mixture for the activity assay contained also 10 nM DTT, 500 μM NADH and 500 μM ferricyanide.

Discussion

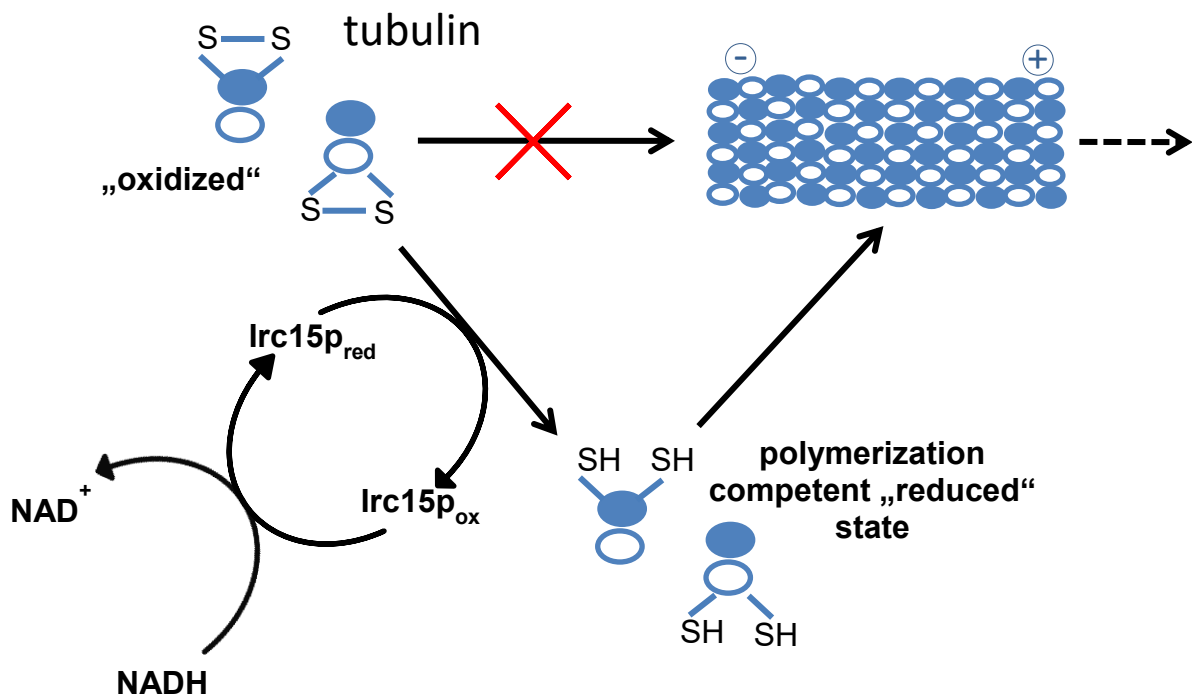
In this study, we have demonstrated for the first time that Irc15p is a flavoprotein with FAD as cofactor. Recombinant Irc15p features characteristic spectral properties that are similar to those reported for LPDs (Figure 2). In contrast to LPDs, reduction of Irc15p does not give rise to the typical charge transfer absorption at longer wavelength (~530 nm) owing to the lack of a pair of redox active cysteines near the FAD cofactor [26,28]. Instead, reduction by light as well as with NAD(P)H yielded the fully reduced hydroquinone FAD without the occurrence of a semiquinone radical (Figures 3 and 6).

The redox potential determined for Irc15p is shifted by 93 mV to -313 ± 1 mV compared to free flavin (= -220 mV). The redox potentials determined for LPD from *E. coli* were $E_{ox}/EH_2 = -264$ mV and $EH_2/EH_4 = -314$ mV and were assigned to the redox potentials of the disulfide/dithiol couple and the FAD/FADH₂ couple, respectively [28]. In order to confirm this assignment, Hopkins *et al.* [29] created two variants lacking either one of the two participating thiol groups, *i.e.* the variant C44S and C49S. The redox potentials of these variants were -379 and -345 mV, respectively, suggesting that the more negative redox potential determined for wild-type LPD belongs to the FAD/FADH₂ couple. Thus the redox potential of Irc15p is very similar to that of LPD suggesting that the environment of the FAD cofactors in these proteins is comparable.

Furthermore, we have demonstrated that the thermal stability of the protein is rather high (= 70 °C). This is not unusual as the reported melting temperature for lipoamide dehydrogenase from *Azotobacter vinelandii* is even higher (= 80 °C, [30]). Interestingly, it was shown that an exchange of Y16 to phenylalanine leads to a decrease of the melting temperature to 72 °C, since Y16 stabilizes the interaction of the subunits via hydrogen bond formation to H470 [31]. In Irc15p phenylalanine is found in position 16 and H470 is replaced by serine. Therefore, the lower melting temperature of Irc15p may be accounted for the amino acid changes in these positions.

To determine the substrate specificity of Irc15p the reductive half reaction was investigated using either NADH or NADPH. These measurements established a clear preference for NADH as electron donor proceeding with a limiting rate of $k_{red} = 250$ s⁻¹ (Figure 6). Thus, the limiting rate of Irc15p is an order of magnitude lower than that of lipoamide dehydrogenase (250 s⁻¹ at 4 °C vs. >3000 s⁻¹ at 21 °C) [32,33]. Since Irc15p is associated with microtubules and was shown to regulate their dynamics the rapid reduction by NADH sheds a new light on its potential role in processes such as mitosis. In recent years, several studies concluded that the NAD⁺/NADH ratio and the overall redox status are regulatory elements of the cell cycle and the dynamics of the cytoskeleton [34–36]. It was shown that the NAD⁺/NADH ratio is high during the G0 phase, decreases during the S phase before it increases again in the G2 phase. However, no information is available of the NAD⁺/NADH ratio during mitosis [35]. Furthermore, it has been shown that NAD⁺ has an influence on the stability and curvature of microtubules. Since it is not interacting

directly with the polymer it has been proposed, that NAD^+ affects microtubule binding proteins on the plus-end of the polymer [36]. How exactly the redox state influences the cell cycle and the cytoskeletal dynamics is not known, but several cell cycle regulating proteins as well as tubulin contain redox sensitive elements like cysteines or cofactors where modifications may occur [37,38]. Therefore, it is conceivable that reduced Irc15p interacts with these proteins and reduces oxidized groups, e.g. disulfides, to enable for example the polymerization of tubulins as shown in Scheme 1. This reactivity would clearly fit to the mode of action found in LPDs, where an internal disulfide in proximity to the isoalloxazine moiety of FAD is reduced to the dithiol via reduction of the flavin by NAD(P)H. In search for such an activity we tested a variety of disulfides, such as cystine, glutathione and lipoamide but we were unable to detect any reduction of these compounds (Table 1). However, we discovered that artificial electron acceptors such potassium ferricyanide, DCPIP, MTT and MQ were good to excellent electron acceptors (Table 1).



Scheme 1. Hypothetical role of Irc15p in the polymerization of tubulin subunits. Shown here is the reduction of putative disulfides located on tubulin by the action of reduced Irc15p at the expense of NADH.

A similar observation was reported for LpdA from *Mycobacterium tuberculosis*, which contains five homologs of flavoprotein disulfide reductases [39]. Apparently, LpdA does not reduce disulfide containing compounds but similar to Irc15p reduces

quinones [39]. Interestingly, LpdA lacks one of the two cysteines near the FAD and the catalytic His-Glu diad, in other words it shares the absence of the dithiol-disulfide redox center with Irc15p but on the other hand also lacks the catalytic diad, which is present in Irc15p. Since the catalytic diad is important in the oxidative half reaction of disulfide reductases, *i.e.* the formation of the internal disulfide by oxidation through the external disulfide (the “dithiol-disulfide exchange reaction”), its presence in Irc15p suggests that it has retained the ability to catalyze a similar reaction. Although our experimental data do not directly support the involvement of Irc15p in the reduction of disulfides, it is conceivable that the interaction of Irc15p with tubulin subunits unmask the catalytic machinery of Irc15p leading to the formation of a competent complex conducive to electron transfer from the reduced FAD to disulfides present in tubulin. Alternatively, Irc15p transfers the electrons to another yet unidentified electron acceptor. Further studies will be required to elucidate the nature of the electron acceptor and the role of the reduction in microtubule dynamics.

References

- [1] V. Gudipati, K. Koch, W.-D. Lienhart, P. Macheroux, The flavoproteome of the yeast *Saccharomyces cerevisiae*, *Biochim. Biophys. Acta* 1844 (2014) 535–44.
- [2] B.E. Keyes, D.J. Burke, Irc15 is a microtubule-associated protein that regulates microtubule dynamics in *Saccharomyces cerevisiae*, *Curr. Biol.* 19 (2009) 472–478.
- [3] A. Argyrou, J.S. Blanchard, Flavoprotein disulfide reductases: advances in chemistry and function, *Prog. Nucleic Acid Res. Mol. Biol.* 78 (2004) 89–142.
- [4] S.M. Miller, Flavoprotein disulfide reductases and structurally related flavoprotein thiol/disulfide-linked oxidoreductases, in: H. Russ, S. Miller, B. Palfey (Eds.), *Handb. Flavoproteins Vol. 2 Complex Flavoproteins, Dehydrogenases Phys. Methods*, Walter de Gruyter & Co, Berlin, 2012, pp. 165–201.

- [5] M. Kellis, B.W. Birren, E.S. Lander, Proof and evolutionary analysis of ancient genome duplication in the yeast *Saccharomyces cerevisiae*, *Nature* 428 (2004) 617–624.
- [6] K.P. Byrne, K.H. Wolfe, The yeast gene order browser: combining curated homology and syntenic context reveals gene fate in polyploid species, *Genome Res.* 15 (2005) 1456–1461.
- [7] C.E. French, B. Boonstra, K.A. Bufton, N.C. Bruce, Cloning, sequence, and properties of the soluble pyridine nucleotide transhydrogenase of *Pseudomonas fluorescens*, *J Bacteriol.* 179 (1997) 2761–2765.
- [8] B. Boonstra, C.E. French, I. Wainwright, N.C. Bruce, I. a N. Wainwright, The *udhA* Gene of *Escherichia coli* encodes a soluble pyridine nucleotide transhydrogenase, 181 (1999) 1030–1034.
- [9] R. Komuniecki, H.J. Saz, Purification of lipoamide dehydrogenase from *Ascaris* muscle mitochondria and its relationship to NADH:NAD⁺ transhydrogenase activity, *Arch. Biochem. Biophys.* 196 (1979) 239–247.
- [10] A. Argyrou, J.S. Blanchard, Mycobacterium tuberculosis lipoamide dehydrogenase is encoded by Rv0462 and not by the *lpdA* or *lpdB* genes, *Biochemistry* 40 (2001) 11353–11363.
- [11] C. Pashley, S. Kendall, Cloning in plasmid vectors, *Methods Mol. Biol.* 235 (2003) 121–135.
- [12] W.E. Swords, Chemical transformation of *E. coli*, *Methods Mol. Biol.* 235 (2003) 49–53.
- [13] J.M. Cherry, E.L. Hong, C. Amundsen, R. Balakrishnan, G. Binkley, E.T. Chan, K.R. Christie, M.C. Costanzo, S.S. Dwight, S.R. Engel, D.G. Fisk, J.E. Hirschman, B.C. Hitz, K. Karra, C.J. Krieger, S.R. Miyasato, R.S. Nash, J. Park, M.S. Skrzypek, M. Simison, S. Weng, E.D. Wong, *Saccharomyces* genome database: the genomics resource of budding yeast, *Nucleic Acids Res.* 40 (2012) 700–705.
- [14] U.K. Laemmli, Cleavage of structural proteins during the assembly of the head of bacteriophage T4, *Nature.* 227 (1970) 680–685.

- [15] V. Massey, A simple method for the determination of redox potentials, in: B. Curti, G. Zanetti, S. Ronchi (Eds.), *Flavin and Flavoproteins*, Walter de Gruyter & Co, Berlin, Como, 1990, pp. 59–60.
- [16] K. Minnaert, Measurement of the equilibrium constant of the reaction between cytochrome c and cytochrome a, *Biochim. Biophys. Acta* 110 (1965) 42–56.
- [17] K. Arnold, L. Bordoli, J. Kopp, T. Schwede, The SWISS-MODEL workspace: A web-based environment for protein structure homology modelling, *Bioinformatics* 22 (2006) 195–201.
- [18] UniProtConsortium, A. Bateman, UniProt: A hub for protein information, *Nucleic Acids Res.* 43 (2015) D204–D212.
- [19] F. Sievers, A. Wilm, D. Dineen, T.J. Gibson, K. Karplus, W. Li, R. Lopez, H. McWilliam, M. Remmert, J. Söding, J.D. Thompson, D.G. Higgins, Fast, scalable generation of high-quality protein multiple sequence alignments using Clustal Omega, *Mol. Syst. Biol.* 7:539 (2011) 1-6.
- [20] P. Macheroux, UV-Visible spectroscopy as a tool to study flavoproteins, *Methods Mol. Biol.* 131 (1999) 1–7.
- [21] C. Yan, J.K. Kepa, D. Siegel, I.J. Stratford, D. Ross, Dissecting the role of multiple reductases in bioactivation and cytotoxicity of the antitumor agent RH1, *Mol. Pharmacol.* 74 (2008) 1657–1665.
- [22] U.B. Ericsson, B.M. Hallberg, G.T. DeTitta, N. Dekker, P. Nordlund, Thermofluor-based high-throughput stability optimization of proteins for structural studies, *Anal. Biochem.* 357 (2006) 289–298.
- [23] W.S. Rasband, ImageJ, U. S. National Institutes of Health, Bethesda, Maryland, USA, <http://imagej.nih.gov/ij/>, 1997-2016.
- [24] J. Benen, W. Vanberkel, Z. Zak, T. Visser, C. Veeger, A. Dekok, Lipoamide dehydrogenase from *Azotobacter vinelandii* - site-directed mutagenesis of the His450-Glu455 diad - spectral properties of wild type and mutated enzymes, *Eur. J. Biochem.* 202 (1991) 863–872.

- [25] DeLano Warren Lyford, The PyMOL Molecular Graphics System Version 1.5.0.4, 2002.
- [26] H. Youn, J. Kwak, H.D. Youn, Y.C. Hah, S.O. Kang, Lipoamide dehydrogenase from *Streptomyces seoulensis*: biochemical and genetic properties, *Biochim. Biophys. Acta* 1388 (1998) 405–418.
- [27] P. Heinrich, H. Ronft, W. Schartau, G.-B. Kresze, Lipoamide dehydrogenase from baker's yeast - improved purification and some molecular, kinetic, and immunochemical properties, *Hoppe-Seyler's Z. Physiol. Chem.* 364 (1983) 41–50.
- [28] K.D. Wilkinson, C.H. Williams, Evidence for multiple electronic forms of two-electron-reduced lipoamide dehydrogenase from *Escherichia coli*, *J. Biol. Chem.* 254 (1979) 852–862.
- [29] N. Hopkins, C.H. Williams, Lipoamide dehydrogenase from *Escherichia coli* lacking the redox active disulfide: C44S and C49S. Redox properties of the FAD and interactions with pyridine nucleotides, *Biochemistry*.34 (1995) 11766–11776.
- [30] W.J.H. van Berkel, A.G. Regelink, J.J. BEINTEMA, A. de Kok, The conformational stability of the redox states of lipoamide dehydrogenase from *Azotobacter vinelandii*, *Eur. J. Biochem.* 202 (1991) 1049–1055.
- [31] J. Benen, W. van Berkel, C. Veeger, A. de Kok, Lipoamide dehydrogenase from *Azotobacter vinelandii* - the role of the C-terminus in catalysis and dimer stabilization, *Eur. J. Biochem.* 207 (1992) 499–505.
- [32] G. Matthews, P. Ballou, H. Williams, Reactions of pig heart lipoamide dehydrogenase with pyridine nucleotides, *J. Biol. Chem.* 254 (1979) 4974–4981.
- [33] J. Benen, W. Van Berkel, N. Dieteren, D. Arscott, C.W. Jr, C. Veeger, A. De Kok, Lipoamide dehydrogenase from *Azotobacter vinelandii*: site-directed mutagenesis of the His450-Glu455 diad - kinetics of wild-type and mutated enzymes, *Eur. J. Biochem.* 497 (1992) 487–497.

- [34] Y. Fa-Xing, D. Ru-Ping, G. Shuang-Ru, Z. Lei, L. Yan, Logic of a mammalian metabolic cycle: An oscillated NAD⁺/NADH redox signaling regulates coordinated histone expression and S-phase progression, *Cell Cycle*. 8 (2009) 773–779.
- [35] J. da Veiga Moreira, S. Peres, J.-M. Steyaert, E. Bigan, L. Paulevé, M.L. Nogueira, L. Schwartz, Cell cycle progression is regulated by intertwined redox oscillators, *Theor. Biol. Med. Model.* 12 (2015) 10.
- [36] W.T. Harkcom, A.K. Ghosh, M.S. Sung, A. Matov, K.D. Brown, P. Giannakakou, S.R. Jaffrey, NAD⁺ and SIRT3 control microtubule dynamics and reduce susceptibility to antimicrotubule agents, *Proc. Natl. Acad. Sci. USA* 111 (2014) E2443-2452.
- [37] S.G. Menon, P.C. Goswami, A redox cycle within the cell cycle: ring in the old with the new, *Oncogene* 26 (2007) 1101–1109.
- [38] C. Wilson, C. González-Billault, Regulation of cytoskeletal dynamics by redox signaling and oxidative stress: implications for neuronal development and trafficking, *Front. Cell. Neurosci.* 9:381 (2015) 1–10.
- [39] A. Argyrou, M.W. Vetting, J.S. Blanchard, Characterization of a new member of the flavoprotein disulfide reductase family of enzymes from *Mycobacterium tuberculosis*, *J. Biol. Chem.* 279 (2004) 52694–52702.

CHAPTER 3

Flavodoxin-like proteins and interacting proteins from *Saccharomyces cerevisiae*

3.1 Structure, biochemical and kinetic properties of recombinant Pst2p from *Saccharomyces cerevisiae*, a FMN-dependent NAD(P)H:quinone oxidoreductase

Karin Koch¹, Altijana Hromic², Marija Sorokina¹, Emilia Strandback¹, Manuel Reisinger², Karl Gruber² and Peter Macheroux^{1,*}

¹Institute of Biochemistry, Graz University of Technology, Petersgasse 12/2, 8010
Graz, Austria

²Institute of Molecular Biosciences, University of Graz, Humboldtstraße 50/3, 8010
Graz, Austria

*From the Graz University of Technology, Institute of Biochemistry, Petersgasse 12,
A-8010 Graz, Austria; Tel.: +43-316-873 6450, Fax: +43-316-873 6952,

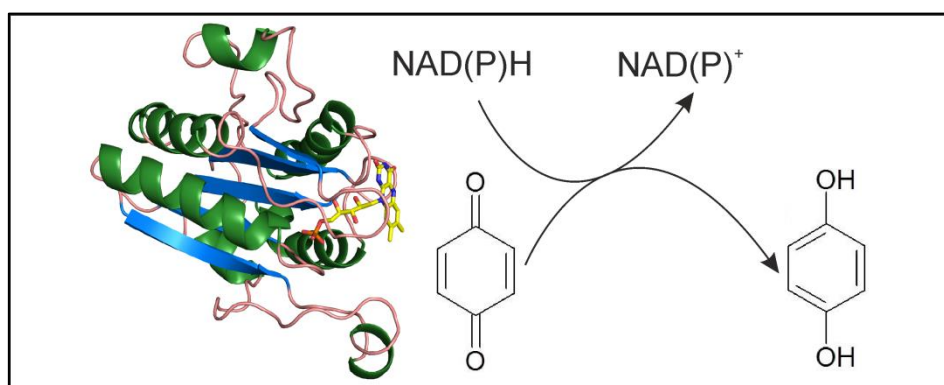
Email: peter.macheroux@tugraz.at

Author contributions

P.M. initiated the project; K.K., A.H., K.G. and P.M. designed the experiments and interpreted the data; K.K. and M.S. expressed PST2. K.K. purified Pst2p and performed analytical and biochemical experiments; K.K., M.S. and E.S. performed enzymatic experiments; K.K. performed the in vivo experiments; A.H., M.R. and K.G. crystallized Pst2p and determined the crystal structure; K.K., A.H., K.G. and P.M. wrote the manuscript.

Abstract

The genome of the yeast *Saccharomyces cerevisiae* encodes four flavodoxin-like proteins, namely Lot6p, Pst2p, Rfs1p and Ycp4p. Thus far only Lot6p was characterized in detail demonstrating that the enzyme possesses NAD(P)H:quinone oxidoreductase activity. In the present study, we heterologously expressed *PST2* in *Escherichia coli* and purified the produced protein to conduct a detailed biochemical and structural characterization. Determination of the three-dimensional structure by X-ray crystallography revealed that Pst2p adopts the flavodoxin-like fold and forms tetramers independent of cofactor binding. The lack of electron density for FMN indicated weak binding, which was confirmed by further biochemical analysis yielding a dissociation constant of $20 \pm 1 \mu\text{M}$. The redox potential of FMN bound to Pst2p was determined to $-89 \pm 3 \text{ mV}$ and is thus 119 mV more positive than that of free FMN indicating that reduced FMN binds ca. five orders of magnitude tighter to Pst2p than oxidized FMN. Due to this rather positive redox potential Pst2p is unable to reduce free FMN or azo dyes as reported for other members of the flavodoxin-like protein family. On the other hand, Pst2p efficiently catalyzes the NAD(P)H dependent two-electron reduction of natural and artificial quinones. The kinetic mechanism follows a ping-pong bi-bi reaction scheme. *In vivo* experiments with a *PST2* knock out and overexpressing strain demonstrated that Pst2p enables yeast cells to cope with quinone-induced damage suggesting a role of the enzyme in managing oxidative stress.



Highlights

- Heterologous production of the flavoprotein Pst2p from *Saccharomyces cerevisiae*
- The flavodoxin-like protein Pst2p forms tetramers independent of cofactor binding
- Reduced FMN binds ca. five orders of magnitude tighter to Pst2p than oxidized FMN
- Pst2p exhibits quinone reductase activity *in vitro* and *in vivo*

Keywords:

enzyme kinetics; flavodoxin-like protein; redox potential; UV-visible absorption spectroscopy; x-ray crystallography;

Chemical compounds studied in this article:

1,4-Benzoquinone (PubChem CID: 4650); Coenzyme Q1 (PubChem CID: 4462); Duroquinone (PubChem CID: 68238); Hydroquinone (PubChem CID: 785); Menadione (PubChem CID: 4055); NADH disodium salt (PubChem CID: 272471); NADPH tetra sodium salt (PubChem CID: 91654154);

Abbreviations

1,4-BQ, 1,4 benzoquinone; CoQ1, coenzyme Q1; DQH₂, duroquinole; DQ, duroquinone; *S. cerevisiae*, *Saccharomyces cerevisiae*; *E. coli*, *Escherichia coli*; EtOH, ethanol; HQ, hydroquinone; Lot6, low temperature-responsive 6; MQ, menadione; NQO1 or 2; NAD(P)H:quinone oxidoreductase 1 or 2; PDB, Protein Data Bank; Pst2, protoplasts-secreted 2; Rfs1, Rad55 suppressor; WrbA, tryptophan (W) repressor-binding protein;

Database

Atomic coordinates and structure factors have been deposited in the PDB database. Pst2p (PDB ID: 5MP4).

Introduction

The yeast flavoproteome comprises 68 proteins with 47 distinct biological functions. Despite having served as a model organism for decades, many of the flavoproteins are poorly characterized with regard to their biochemical and enzymatic properties. Within the yeast flavoproteome, the group of flavodoxin-like proteins comprises four members, namely Lot6p, Pst2p, Rfs1p and Ycp4p. However, only Lot6p was structurally, biochemically and enzymatically characterized [1]. In general, the flavodoxin-like protein superfamily comprises highly diverse members with regard to amino acid sequence, flavin cofactor, electron donor and acceptor as well as quaternary structure [2]. On the other hand, mammalian flavodoxin-like proteins, such as NQO1 and NQO2 are strictly homo-dimeric proteins, which possess a FAD-cofactor. The FAD cofactor can be reduced either by NAD(P)H or by dihydronicotinamide riboside and both enzymes catalyze the reduction of quinones, azo dyes and nitro compounds [3-6].

In the other kingdoms of life, quinone reductases more distantly related to NQO1 were found, for example WrbA from *Escherichia coli*, the founding member of a family of FMN-dependent proteins, which are present in archaea, bacteria, fungi and the *Viridiplantae* kingdom [7, 8 and references therein]. WrbA possesses FMN as cofactor and lacks the C-terminal subdomain present in NQO1 and is therefore able to form tetramers, assembled as a dimer of dimers [9]. Similar to NQO1, WrbA possesses NAD(P)H-dependent quinone reductase activity but no azo reductase activity [10,11].

The importance of quinone reductase activity *in vivo* is still under discussion. It was proposed that it protects the cell from oxidative stress provoked by exogenous toxic quinones and, on the other hand, may prevent cellular damage from lipid peroxidation by keeping endogenous quinones in their reduced form to maintain their anti-oxidative activity [12 and references therein]. In the past two decades, the redox activity of flavodoxin-like proteins was implicated also in other functions, such as the generation of reduced FMN for other enzymes [13], ubiquitin-independent proteasomal degradation [14 and references therein], superoxide scavenging [15] as well as the pathogenicity of *Candida albicans* [16], *Botrytis cinerea* [17] and *Pseudomonas aeruginosa* [18]. In addition to this functional diversity of flavodoxin-like proteins, it was shown that many species possess more than one flavodoxin-like

protein with distinct but overlapping functions [11 and references therein]. This complexity makes it difficult to define the cellular roles of flavodoxin-like proteins solely based on sequential or structural information.

In the present study we set out to express *PST2* from *S. cerevisiae* and purified the produced protein from *E. coli* for a detailed biochemical and structural characterization. X-ray crystallography confirmed a flavodoxin-like topology and kinetic analysis revealed that the enzyme is an efficient NAD(P)H:quinone oxidoreductase. However, due to the unusually positive redox potential, Pst2p lacks FMN and azo reductase activity. *In vivo*, Pst2p appears to confer resistance to some exogenous quinones whereas in other cases it renders yeast cells more sensitive.

Materials and Methods

Materials

All chemicals, reagents and enzymes were of highest quality and were from Sigma-Aldrich (St. Louis, USA), Roth (Karslsruhe, Germany) or Thermo Fisher Scientific (Waltham, USA), unless otherwise noted. Columns for affinity chromatography (Ni-NTA-sepharose), size exclusion chromatography (Superdex 200 10/300 GL) and buffer exchange (PD-10 desalting column) were from GE Healthcare (Little Chalfont, UK). *E. coli* strains Top10 and RosettaTM(DE3) were from Invitrogen (Carlsbad, USA) and Merck (Darmstadt, Germany), respectively. *S. cerevisiae* strains BY4741 (MATa, his3 Δ 1, leu2 Δ 0, met15 Δ 0, ura3 Δ 0) were from Euroscarf (Frankfurt, Germany) and correct depletion was ensured by colony PCR. The plasmids pET21a and pYES2 were from Merck (Darmstadt, Germany) and Invitrogen (Carlsbad, USA), respectively. The concentrations of holo- and apo-Pst2p and the following compounds were determined spectrophotometrically using molar extinction coefficients: Pst2p ($\epsilon_{453} = 10.600 \text{ M}^{-1} \text{ cm}^{-1}$, experimentally determined), apo-Pst2p ($\epsilon_{280} = 32.430 \text{ M}^{-1} \text{ cm}^{-1}$, based on amino acid sequence), NAD(P)H ($\epsilon_{340} = 6.220 \text{ M}^{-1} \text{ cm}^{-1}$), 1,4-BQ dissolved in EtOH ($\epsilon_{242} = 24.000 \text{ M}^{-1} \text{ cm}^{-1}$) [19], MQ dissolved in EtOH ($\epsilon_{333} = 2.450 \text{ M}^{-1} \text{ cm}^{-1}$) [20], DQ dissolved in EtOH ($\epsilon_{271\text{nm}} = 14.500 \text{ M}^{-1} \text{ cm}^{-1}$), CoQ1 solved in EtOH ($\epsilon_{278\text{nm}} = 14.500 \text{ M}^{-1} \text{ cm}^{-1}$) [21] and FMN ($\epsilon_{450} = 12.500 \text{ M}^{-1} \text{ cm}^{-1}$) [22].

Cloning of PST2 for large scale expression in E. coli and for yeast overexpression

All strains were generated using standard genetic techniques [23–25]. Briefly, genomic DNA from *S. cerevisiae* was extracted with yeast DNA extraction kit from VWR (Radnor, USA). According to the sequence for *PST2* from the *Saccharomyces* genome database [26] the following primers excluding the stop codon of the gene and including respective restriction sites for cloning were designed and synthesized from VBC (Vienna, Austria): fw_5'-GAGCCATATGCCAAGAGTAGCTATCATCATTTACACAC-3'; rev_5'-CCTGCTCGAGAACTTTGCAACGGTTTCGTAGAAAGTC-3'. To construct the heterologous expression vector pET1a(+)*PST2* introducing an additional C-terminal 6x-His tag the restriction enzymes NdeI/XhoI were used. Individual clones were sequenced before transforming the plasmid into *E. coli* RosettaTM(DE3) cells.

For overexpression of *PST2* in *S. cerevisiae* the construct was generated using PCR with pET1a(+)*PST2* as template to cover also the C-terminal 6xHis tag. The following primers including respective restriction sites were designed and synthesized from VBC (Vienna, Austria): (fw-5'-GAGCGGATCCCCAAGAGTAGCTATCATCATTTACACAC-3', rev-5'-GCTGCGGCCGCTCAGTGGTGGTGGTGGTG-3'). The restriction enzymes BamHI/NotI were used and the gene was ligated into the corresponding site of the vector pYES2, thus expressing C-terminal 6xHis tagged *PST2* under the control of the *GAL1* promoter. Individual clones were sequenced and *S. cerevisiae* BY4741Δ*PST2* cells were transformed from now on referred as *PST2* overexpression strain. Furthermore BY4717 and BY4741Δ*PST2* cells were transformed with empty pYES2 plasmid, from now on referred as wild-type and *PST2* knock out strain, respectively.

Heterologous expression of PST2 and purification of Pst2p

A single colony of *E. coli* Rosetta(DE3) comprising pET21a(+)*PST2* was used to inoculate a pre-culture that was aerobically incubated (37 °C, 16 h, 150 rpm) in lysogeny broth (bacto-tryptone 10 g/L, bacto-yeast extract 5 g/L, NaCl 5 g/L) supplemented with 100 µg/mL ampicillin and 20 µg/mL chloramphenicol. 1% pre-culture was used to inoculate the main-culture supplemented with 100 µg/mL ampicillin and 10 µg/mL chloramphenicol, which was incubated aerobically at 37 °C with agitation at 150 rpm until an OD_{600} of ~0,6 was reached. Expression of *PST2* was induced by addition of 0.5 mM isopropyl-thio-β-d-galactoside. The culture was

further incubated for 16 h at 20 °C. Cells were harvested by centrifugation at 4.500 x g at 4 °C and washed once with 1% saline solution. Cell pellets were resuspended in 4 mL/1g pellet buffer A (50 mM Hepes, 150 mM NaCl, pH 7.0) supplemented with 20 mM imidazole, 1 mM phenylmethylsulfonyl fluoride solved in dimethylsulfoxide, 10 µM riboflavin 5'-monophosphate sodium salt and further 1 µL of protease inhibitor cocktail for use in the purification of histidine-tagged proteins from Sigma-Aldrich (St. Louis, USA) was added per g of cell pellet. Cell disruption was achieved by sonication with a Labsonic L instrument from Braun Biotech. International (Berlin, Germany) with 120 Watt for 3 x 3 min in an ice-water bath with 3 min pauses between each cycle. The cell lysate was centrifuged at 38.850 x g for 45 min at 4 °C, and the supernatant was loaded onto a 5-mL HisTrap HP column previously equilibrated with buffer A supplemented with 20 mM imidazole. The column was washed with buffer A supplemented with 50 mM imidazole and subsequently proteins were eluted with buffer A supplemented with 300 mM imidazole. Fractions containing target protein were pooled and concentrated with centrifugal filter units (Amicon Ultra-15, 10 k; Millipore, Billerica, MA, USA). Concentrated protein was re-buffered to buffer B (50 mM Hepes, pH 7.0) with a PD-10 desalting column. The protein solutions were shock frozen and stored at -80 °C, if not used immediately.

Crystallization

Crystallization experiments were performed in microbatch plates using different commercial crystallization screens (i.e. the Index Screen from Hampton Research and the Morpheus Screen from Molecular Dimensions). Sitting drops were prepared by mixing 0.5 µL of the protein solution (at a concentration of 18 mg/mL) with an equal volume of mother liquor, which were pipetted using an ORYX 8 pipetting robot from Douglas Instruments. The trays were incubated at 20 °C. First crystal clusters were observed after one day, followed by further optimization using cross-seeding. Diffracting Pst2p crystals were obtained with 0.2 M ammonium acetate, 0.1 M HEPES pH 7.5, 25% w/v 3350 Index screen (condition F8). Crystals were flash cooled in liquid nitrogen using 20% glycerol for cryoprotection.

Structure determination and refinement

X-ray diffraction data were collected to a maximum resolution of 2.8 Å on beamline ID29 ($\lambda=0.972$ Å) at the ESRF Grenoble, France. The crystals were orthorhombic

(space group $P2_12_12_1$) with unit-cell dimensions $a=69.41$ Å, $b=110.56$ Å and $c=223.81$ Å. The data were processed using the XDS package [27] and programs from the CCP4 suite [28] and a randomly chosen set of 5% of the reflection was set aside for the calculation of R_{free} values. The structure was solved by molecular replacement using the structure of WrbA from *E. coli* in complex with 1,4-BQ (PDB code: 3B6K, 44% sequence identity) [29] as search template yielding eight chains in the asymmetric unit. Structure rebuilding and refinement were performed using the programs Coot [30] and PHENIX [31]. The electron density was improved by density modification and statistical phase improvement using the programs Parrot and Pirate from the CCP4 suite [28]. Non-crystallographic-symmetry (NCS) restraints were applied in the initial stages of the refinement but were removed for the final refinement cycles. Sufficiently clear electron density was observed for all amino acids except of the first methionine in all chains. Detailed statistics pertaining to data processing and structure refinement are summarized in Table 2. Atomic coordinates and structure factors have been deposited in the Protein Data Bank under accession number 5MP4.

Determination of molecular masses of Pst2p

Subunit molecular mass of purified Pst2p was determined by SDS-Page under reducing conditions with a 12.5% separating gel and 5% stacking gel described by Laemmli [32]. The used protein molecular mass marker was the PageRuler™ prestained protein ladder (10-180 kDa) from Thermo Fisher Scientific (Waltham, USA).

To determine the native molecular mass of Pst2p size exclusion chromatography with buffer A using a Superdex 200 10/300 GL column attached to an Äktapurifier™ system from GE Healthcare (Little Chalfont, UK) was performed. Protein elution was monitored at 280 nm and 450 nm wavelength. The column was calibrated with molecular mass standards according to the instructions from GE healthcare.

Apo-protein preparation

Apo-Pst2p was prepared as described in [33]. In brief, purified Pst2p was loaded on a 5-mL HisTrap HP column previously equilibrated with buffer A. The column was washed with buffer A supplemented with 2 M urea, and 2 M KBr until no cofactor was

noticed in the flow through and then re-equilibrated with 25 mL buffer A before eluting the protein. Fractions containing target protein were further processed as described for the holo-protein. Complete removal of the cofactor was verified spectrophotometrically.

Limited proteolysis

Limited proteolysis with 2 µg/mL trypsin from Promega, (Madison, USA) of 30 µM Pst2p or apo-Pst2p in buffer C was performed at 37°C. The reaction was stopped at various time points by adding SDS sample buffer and boiling at 95°C for 10 minutes. Samples were analysed by SDS-Page under reducing conditions with a 12.5% separating gel and 5% stacking gel.

Thermal shift assay

Thermal shift assays were performed as described elsewhere [34,35]. 20 µL of 0.5 mg/mL apo- or holo-Pst2p were pipetted into a white 96-well RT-PCR plate from Bio-Rad (California, USA). Five µL of a 1:500 dilution of SYPRO[®] orange from Molecular Probes (Oregon, USA) was added to apo-Pst2p. The plates were sealed with an optical-quality sealing tape from Bio-Rad (California, USA) and heated in a CFX Connect™ Real-Time PCR detection system from Bio-Rad (California, USA) from 20 to 95 °C in increments of 0.5 °C. Fluorescence changes of the intrinsic FMN of Pst2p or the dye in the case of apo-Pst2p were detected at a wavelength between 470 and 500 nm. Melting temperatures (T_m) were determined using cfx manager 3.0 software from Bio-Rad (California, USA).

Methods using UV-visible absorption spectroscopy

Absorption spectra were recorded with a Specord 200 plus spectrophotometer from Analytik Jena (Jena, Germany) at 25 °C using 1-cm quartz cuvettes.

Extinction coefficient

The extinction coefficient of Pst2p was determined according to the protocol described in reference [22]. Briefly, Pst2p bound FMN was released by addition of 0.2% SDS. UV-visible absorption spectra were recorded before and after denaturation of the enzyme. The calculation led to an extinction coefficient of 10.600 M⁻¹ cm⁻¹ at 453 nm for native Pst2p.

Difference titrations

Difference titrations were carried out in tandem quartz cuvettes as described in [33]. The cuvettes were filled with 800 μL of a ~ 50 μM protein solution (apo-Pst2p or Pst2p) in buffer C (50 mM Hepes, 50 mM NaCl, pH 7.0) in one chamber and 800 μL of buffer C in the other chamber. The titration experiments were performed by stepwise addition of 2-8 μM FMN (1 mM stock solution) to apo-Pst2p or by addition of 2-8 μM quinone (1-4 mM stock solution dissolved in 50% EtOH) to Pst2p. After careful mixing and incubation for 3 min an absorption spectrum was recorded (250–700 nm). The K_d values were determined by nonlinear hyperbolic fit in Origin 7.0 (OriginLab Corp., Northampton, MA, USA).

Anaerobic Photoreduction

Photoreduction was carried out as described in [22]. Briefly, ~ 20 μM Pst2p in 1 mL buffer C supplemented with 1 mM EDTA was deoxygenated by incubation for 2 h in a glove box from Belle Technology (Weymouth, UK). A 10 W LED floodlight (Lumineia) was used to reduce the cofactor by light irradiation. Spectra were recorded after each reduction step until no further spectral changes were observed. Thereafter the sample was exposed to air and a spectrum was recorded after complete reoxidation.

Steady state kinetics

Initial-velocity measurements were performed in triplicate with NAD(P)H, 1,4 BQ, MQ, duroquinone and CoQ1 by following the oxidation of NAD(P)H at 380 nm. Reaction mixtures were setup in 50 mM Hepes pH 7, 50 mM NaCl, 2% (v/v) EtOH. Substrate concentrations were as follows: NAD(P)H (30-500 μM) at a saturating concentration of 200 μM for MQ. Different quinone concentration, i.e. 1,4-BQ (5-155 μM), MQ (20-235 μM), DQ (12-317 μM) or Q1 (30-500) were measured at a saturating NADH concentration of 350 μM . For the investigation of the reaction mechanism of Pst2p various concentrations of NADH (30-350 μM) and MQ (20- 200 μM) were used. All reactions were initiated by addition of 5 μL enzyme stock solution, supplemented with 400 μM FMN, to the reaction mixture – final enzyme concentrations were 2-10 nM (final FMN concentration: 2 μM). Controls were performed in the absence of enzyme. For each concentration, at least three measurements were performed. Initial velocities were determined by fitting the absorption change at 380 nm in the first minute using the appropriate extinction

coefficients (NADH $\epsilon_{380} = 1.210 \text{ M}^{-1} \text{ cm}^{-1}$ or NADPH $\epsilon_{380} = 1.280 \text{ M}^{-1} \cdot \text{cm}^{-1}$). K_M and k_{cat} were determined by nonlinear hyperbolic fit in Origin 7.0 (OriginLab Corp., Northampton, MA, USA).

Determination of reductive/oxidative rates

The protein was deoxygenated by incubation for 2 h in a glove box from Belle Technology (Weymouth, UK). The reductive half-reaction was investigated by mixing protein (~25 μM) in buffer B with 25-1.250 μM NAD(P)H. The oxidative half-reaction was investigated by mixing reduced protein (~25 μM , reduced with 0,9 equivalents NADH) with 25-300 μM MQ, 25 μM 1,4-BQ and 25-100 μM DQ. These concentrations are final values after mixing in the flow cell. Experiments were performed with a SF-61SX2 stopped flow device from TgK Scientific Limited (Bradford-on-Avon, UK) positioned in an anaerobic glove box from Belle Technology (Weymouth, UK) at 4 °C. Changes in flavin absorption were followed with a PM-61s photomultiplier from TgK Scientific Limited (Bradford-on-Avon, UK) at 453 nm. Each concentration was measured in triplicates and the observed rate constants for different substrate concentrations (k_{obs}) were calculated using the exponential fitting function of the kinetic studio software (TgK Scientific Limited).

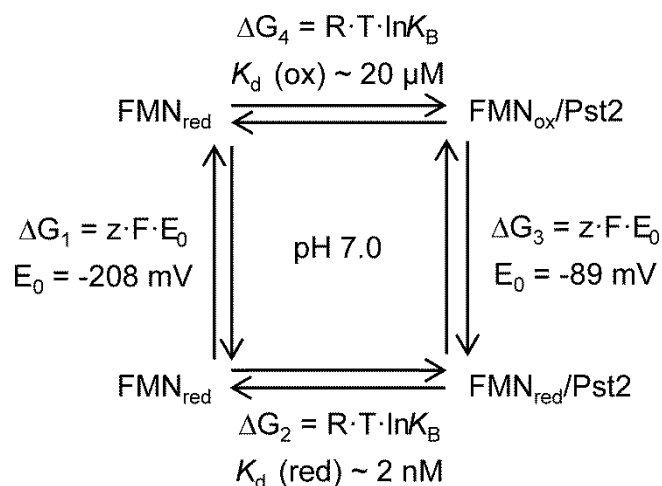
Redox potential

The redox potential was determined by the dye-equilibration method using the xanthine/xanthine oxidase electron delivering system as described by [36]. Reactions were carried out in buffer C supplemented with methyl viologen (2.5 μM) as mediator, 500 μM xanthine, and xanthine oxidase in catalytic amounts (~40 nM) and lasted 0.5-2 h. The protein concentration for a typical experiment was ~25 μM . These concentrations are final values after mixing in the flow cell. Experiments were performed with a SF-61SX2 stopped flow device from TgK Scientific Limited (Bradford-on-Avon, UK) equipped with an auto-shutter to reduce photochemical effects during the experiment. To maintain anaerobic conditions the device was positioned in a glove box from Belle Technology (Weymouth, UK). Spectra during the course of reduction were recorded with a KinetaScanT diode array detector from TgK Scientific Limited (Bradford-on-Avon, UK). Dyes used for analysis and their corresponding redox potentials were potassium indigotrisulfonate (-81 mV) and indigo carmine (-125 mV). Due to spectral changes of the used dyes during the

reduction process the amounts of oxidized and reduced Pst2p were quantified at the isosbestic points at 485 and 461 nm for potassium indigo-trisulfonate and for indigo carmine, respectively. The reduction oxidation potentials were calculated from plots of $\log([\text{ox}]/[\text{red}])$ of the protein versus $\log([\text{ox}]/[\text{red}])$ of the dye according to [37] using Excel 2010 (Microsoft, Redmond, WA, USA).

Determination of the dissociation constants for reduced FMN bound to Pst2p

The redox potential of free FMN (-208 mV) and the determined value for the FMN/FMNH₂ couple in Pst2p was used to calculate the K_d of the reduced flavin by using the determined K_d for the oxidized flavin according to the thermodynamic relationship shown in Scheme 1. The Gibbs energy for the binding affinity between the reduced cofactor and the enzyme was calculated according to the relationship $\Delta G_1 + \Delta G_2 = \Delta G_3 + \Delta G_4$.



Scheme 1. Thermodynamic relationships between redox potentials and dissociation constants.

Strain sensitivity and growth assay

A single colony of the respective strains was grown for 24 h in synthetic dextrose medium [0.67% amino acid free yeast nitrogen base, 2% carbon source, 0.01% (adenine, arginine, cysteine, leucine, lysine, threonine, tryptophan, uracil) 0.005% (aspartic acid, histidine, isoleucine, methionine, phenylalanine, proline, serine, tyrosine, valine) lacking uracil (SD-ura)]. About 20 mL of fresh synthetic galactose medium lacking uracil (SG-ura) was inoculated with pre culture to an OD₆₀₀ of 0,1. The culture was then grown for several hours to a final OD₆₀₀ of 1.0. Samples were

differentially diluted and plated on SG-ura plates supplemented with 1,4-BQ (50-250 μM), hydroquinone (500-2000 μM), DQ (25-100 μM) and were grown for 2–3 days in an incubator at 30 °C. Quinones were added from stocks made in pure EtOH to allow a homogenous distribution of the reagent in the agar medium. Final EtOH concentrations were 2% (v/v). To exclude growth differences, of the strains independent of the stressors, samples were also plated on SG-ura plates supplemented with the solvent and growth behavior in liquid media was monitored at OD_{600} .

Results

Biochemical characterization of Pst2p

PST2 from *S. cerevisiae* was heterologously expressed in *E. coli* and the produced protein was purified from crude extracts using Ni-NTA affinity chromatography. From 1 l culture about ~70 mg of enzyme was obtained with a high purity as judged by visual inspection of the SDS-gel (Figure 1, panel A).

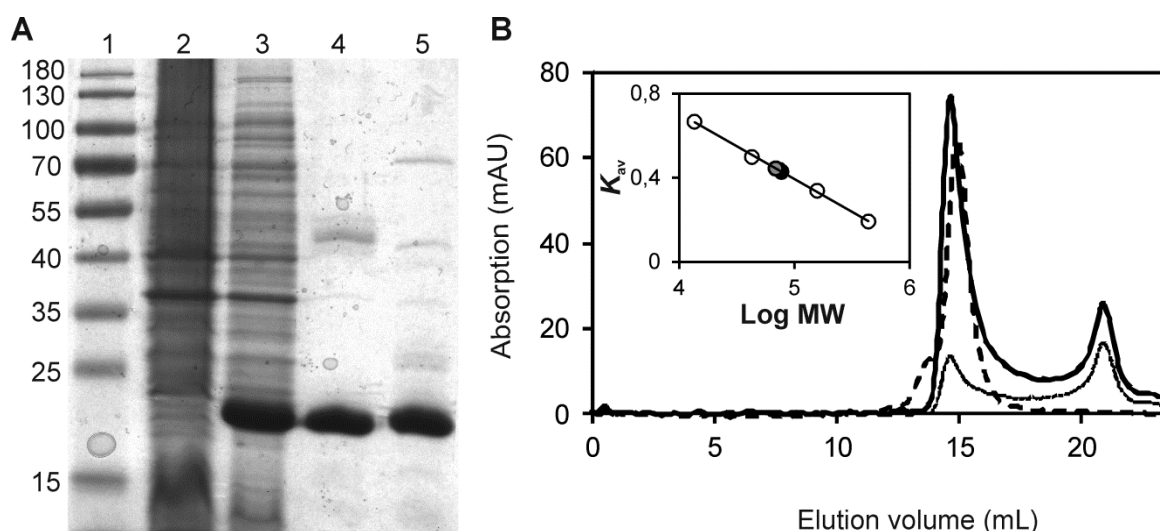


Figure 1. Determination of purity and molecular masses of Pst2p and apo-Pst2p using SDS-Page and analytical size exclusion chromatography. **(A)** Determination of purity and subunit molecular masses of Pst2p and apo-Pst2p by SDS-Page after purification by Ni-NTA-sepharose. Lane 1, PageRuler™ prestained protein ladder (10-180 kDa); lane 2, protein extract before induction; lane 3, protein extract after induction of Pst2p; lane 4, protein fraction after purification by Ni-NTA-sepharose; lane 5, protein fraction after apo-protein preparation. The subunit molecular mass of Pst2p was estimated to 22 kDa.

(B) Determination of native molecular mass of Pst2p (black, continuous line 280 nm and dotted line 450 nm) and apo-Pst2p (dashed line) using analytical size exclusion chromatography. The elution profile of Pst2p indicates that the protein lost most of the FMN cofactor during chromatography. The insert shows a plot of the partition coefficient (K_{av}) against the logarithm of molecular mass of standard proteins (ferritin, 440 kDa; aldolase, 158 kDa; conalbumin, 75 kDa; ovalbumin, 43 kDa; ribonuclease A, 13.7 kDa). The calculated molecular masses of Pst2p (86 kDa, black circle) and apo-Pst2p (78 kDa, grey circle) indicate that Pst2p is present in a tetrameric form and that oligomerization is independent of cofactor binding.

The purified protein showed the characteristics of a flavoprotein with two distinct absorption peaks at 378 and 453 nm with a shoulder at ~469 nm. Denaturation of the protein resulted in a slight bathochromic shift of the absorption maxima (Figure 2). Using an extinction coefficient of $12.500 \text{ M}^{-1} \text{ cm}^{-1}$ at 450 nm for free FMN an extinction coefficient of $10.600 \text{ M}^{-1} \text{ cm}^{-1}$ at 453 nm was calculated for Pst2p. This extinction coefficient was used to determine the Pst2p concentration in further experiments.

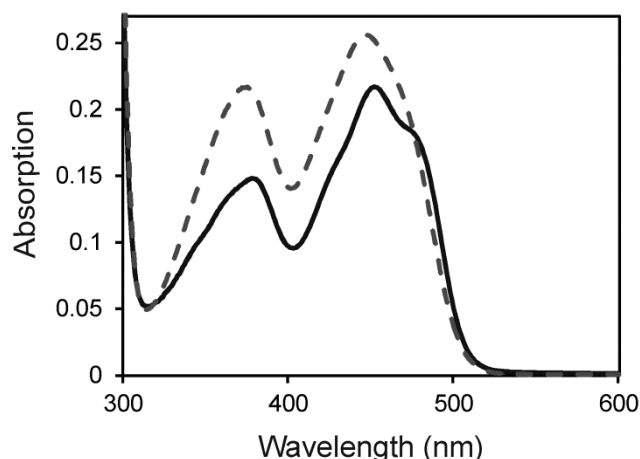


Figure 2. Spectra of native and denatured Pst2p. UV-visible absorption spectra of Pst2p before (solid line) and after denaturation (dashed line). Denaturation of purified Pst2p was carried out in buffer C (50 mM Hepes, 50 mM NaCl, pH 7.0) containing 0.2% SDS.

During purification we have noticed partial depletion of the cofactor, which is reflected by an increased absorption ratio at 280/450 nm (>9). However, reconstitution of apo-Pst2p was achieved by incubation with FMN and subsequent removal of free FMN by means of a PD10-column leading to an improved 280/453 ratio of 4.5, which is close to the theoretical value of 3. Similar observations were reported for several FMN-dependent enzymes, such as NAD(P)H:quinone oxidoreductases [7,11,38 and references therein]. Notably, the formation of tetramers

found in solution as well as in the crystals (see below) is independent of FMN binding (Figure 1, panel B). On the other hand, we found that the thermal stability of holo-Pst2p is clearly higher than that of the apo-Pst2p as the melting temperature of holo- and apo-Pst2p was determined to 58 and 51 °C, respectively. In addition, apo-Pst2p is more susceptible to limited proteolysis as shown in Figure 3. Taken together, these results suggest that FMN binding leads to a structural stabilization of the protomer but is not relevant for the assembly of the quaternary structure.

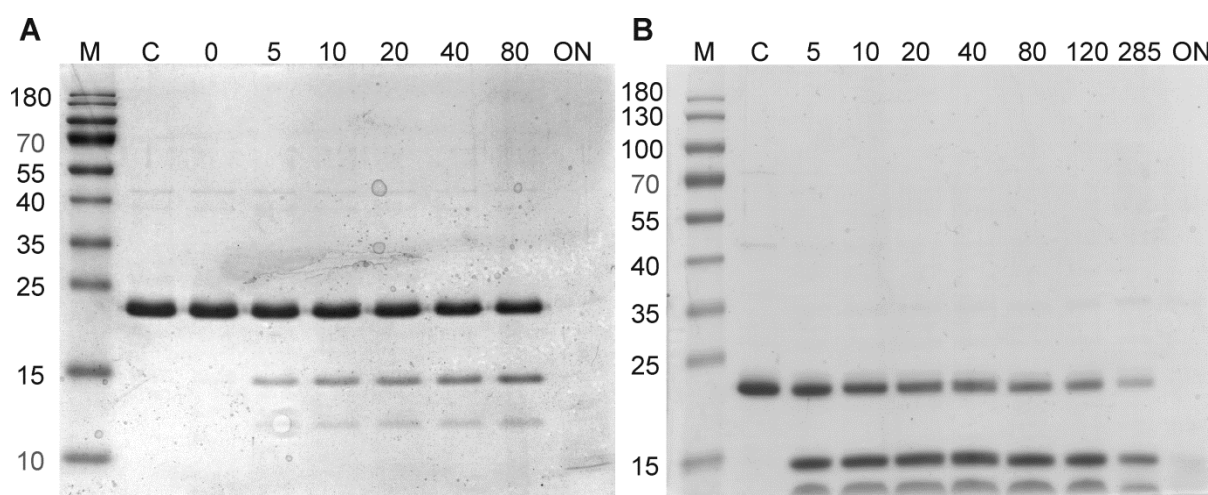


Figure 3. Limited trypsin proteolysis of Pst2p and apo-Pst2p. **(A)** SDS–Page showing a time course of trypsin digestion. The migration positions of the molecular weight marker (M) are indicated to the left of the gel. Lane 1, PageRuler™ prestained protein ladder (10-180 kDa); lane 2, protein without trypsin; lane 3-9 digestion times are given in minutes above the gel (ON, overnight). **(B)** SDS–Page showing trypsin digestion products of apo-Pst2p. The migration positions of the molecular weight marker (M) are indicated to the left of the gel. Lane 1, PageRuler™ prestained protein ladder (10-180 kDa); lane 2, protein without trypsin; lanes 3-10, digestion times are given in minutes above the gel (ON, overnight).

In order to determine the dissociation constant for the binding of FMN to apo-Pst2p, we followed the absorption changes occurring upon addition of FMN to the apo-protein. The obtained changes were fitted to a hyperbolic equation and indicated a binding ratio of one FMN molecule per subunit of apo-Pst2p with a dissociation constant of $20 \pm 1 \mu\text{M}$ (Figure 4, panel A). Similarly, we used difference titration experiments to determine the dissociation constants for menadione (MQ), duroquinone (DQ) and coenzyme Q1 (CoQ1). A representative titration of DQ with Pst2p is shown in Figure 4, panel B. The dissociation constants obtained for quinones were in the range of 139 to 226 μM and are summarized in Table 1 (right column).

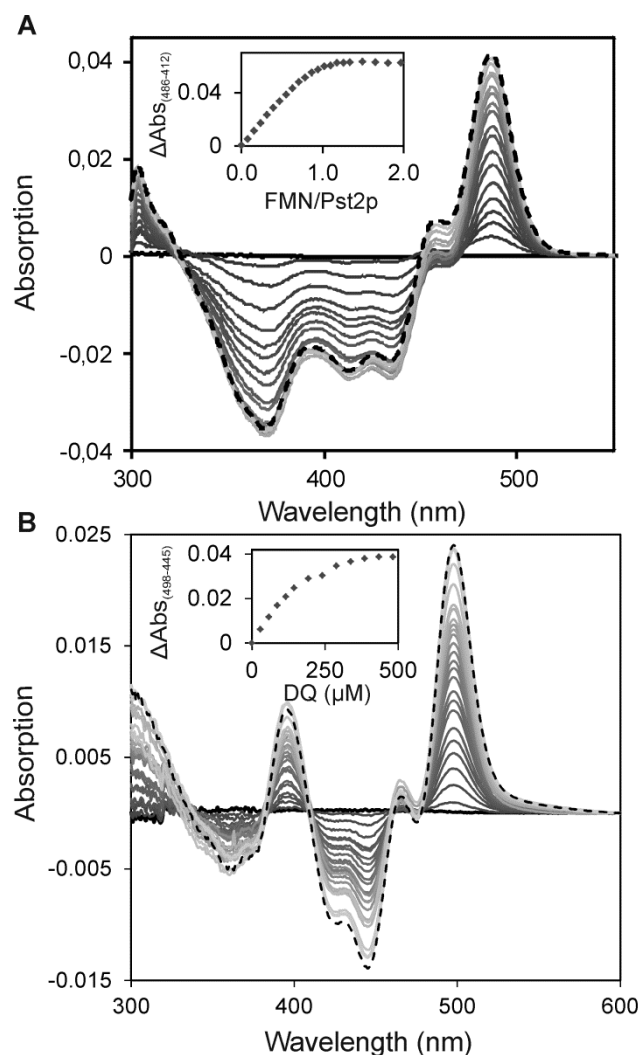


Figure 4. Binding of FMN and quinone substrates to Pst2p. **(A)** Difference titration of apo-Pst2p with FMN. 40 μM apo-Pst2p was titrated with FMN (0–90 μM) and absorption spectra were recorded from 300 to 550 nm. Representative and normalized spectra are depicted in different shades of grey. The final spectrum is shown as black dotted line. The inset shows a plot of the absorption change against the FMN/protein ratio. The data indicate a binding ratio of one FMN molecule per Pst2p subunit with a dissociation constant of $20 \pm 1 \mu\text{M}$. **(B)** Difference titration of Pst2p with DQ. 40 μM Pst2p was titrated with DQ (0–380 μM) and absorption spectra were recorded from 300 to 600 nm. Representative and normalized spectra are depicted in different shades of grey. The final spectrum is shown as black dotted line. The inset shows a plot of the absorption change as a function of DQ concentration. A hyperbolic fit to the experimental data yielded a dissociation constant of $199 \pm 12 \mu\text{M}$.

Table 1. Enzymatic activities and dissociation constants with several substrates determined with purified Pst2p. (n.o., not observed; n.d., not determined;)

Substrate	K_M^a [μM]	k_{cat}^a [s^{-1}]	k_{cat}/K_M^a [$\text{M}^{-1}\cdot\text{s}^{-1}$]	$k_{red/ox}^b$ [$\text{M}^{-1}\cdot\text{s}^{-1}$]	K_d^c [μM]
NADH*	67 ± 6	280 ± 8	$4.2 \cdot 10^6$	$5.8 \cdot 10^6 \pm 4.5 \cdot 10^5$	n. o.
NADPH*	104 ± 7	279 ± 7	$2.7 \cdot 10^6$	$1.9 \cdot 10^6 \pm 1.1 \cdot 10^5$	n. o.
MQ**	41 ± 3	268 ± 7	$6.5 \cdot 10^6$	$2.7 \cdot 10^6 \pm 7.8 \cdot 10^5$	139 ± 14
1,4-BQ**	15 ± 2	1119 ± 46	$7.5 \cdot 10^7$	$>10^6$ ^d	n. o.
DQ**	72 ± 5	380 ± 10	$6.8 \cdot 10^6$	$7.0 \cdot 10^6 \pm 5.6 \cdot 10^5$	199 ± 12
CoQ1**	91 ± 8	33 ± 1	$3.6 \cdot 10^5$	n. d.	226 ± 21

^aSteady-state kinetic constants were determined by UV–visible absorption spectroscopy in the presence of a saturating second substrate (MQ* or NADH**) at pH 7.0 and 25 °C; ^bRapid reaction data ($k_{red/ox}$) were determined with a stopped flow device at pH 7.0 and 4 °C; ^cDissociation constants were determined by UV–visible absorption difference spectroscopy at pH 7.0 and 25°C; ^dThe reduction of 1,4-BQ was complete within the dead time of the stopped-flow instrument (~5 ms).

Next, photoreduction of recombinant Pst2p was performed in the presence of EDTA by exposing the protein to light. Under the experimental conditions, FMN bound to Pst2p is continuously reduced to the hydroquinone (fully reduced flavin) (Figure 5).

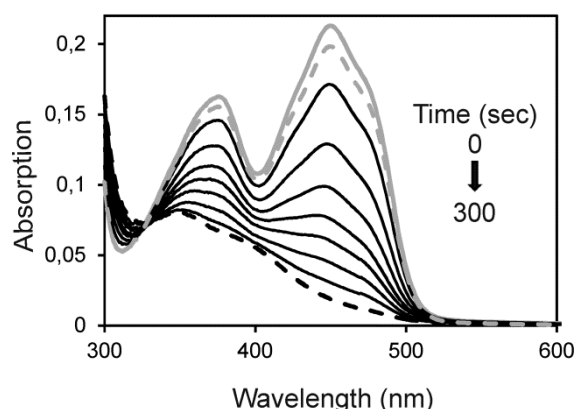


Figure 5. Absorption spectra observed during the anaerobic photoreduction of Pst2p in buffer C. The solid grey line represents the spectra before light illumination. For the time course of reduction selected spectra with decreasing absorption are shown in black, till complete reduction was achieved shown as dashed black line. After re-oxidation the initial spectra was restored (represented as dashed grey line).

Furthermore, the redox potential of the FMN cofactor was determined with the xanthine/xanthine oxidase system in the presence of suitable redox dyes, namely potassium indigotrisulfonate ($E_M = -81$ mV) and indigo carmine ($E_M = -125$ mV). As shown in Figure 6, a plot of $\log(\text{Pst2p}_{\text{ox}}/\text{Pst2p}_{\text{red}})$ versus $\log(\text{dye}_{\text{ox}}/\text{dye}_{\text{red}})$ was used to estimate the redox potential to -89 ± 3 mV [37]. In keeping with the reduction of the oxidized flavin directly to the hydroquinone observed in our photoreduction experiment, the slope of the logarithmic plot was close to unity indicating that both the reference dye and the flavin isoalloxazine ring are taking up two electrons. The redox potentials of the FMN/FMNH₂ couple free and bound to Pst2p as well as the dissociation constant of the oxidized FMN (20 μM) can be used to calculate the K_d of the reduced flavin by using the thermodynamic relationship shown in Scheme 1 (section 2.17. in Materials & Methods). This yields a K_d of 2 nM for the reduced flavin and thus reduced FMN binds 10,000 times tighter to Pst2p than oxidized FMN.

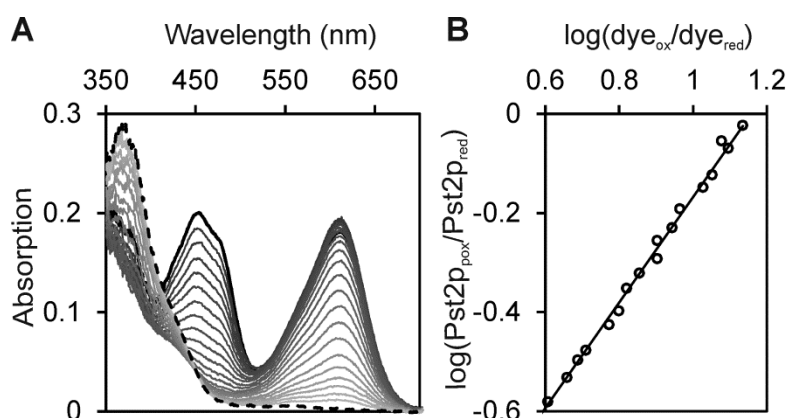


Figure 6. Redox potential determination of Pst2p in the presence of indigo carmine. **(A)** The fully oxidized spectrum is shown as black line the fully reduced spectrum is shown as dashed black line. Selected spectra of the course of reduction are represented in different shades of grey. ~ 20 μM Pst2p was reduced by the xanthine/xanthine oxidase system in the presence of indigo carmine over a time period of 50 min. Data points for evaluation were measured at 461 nm for the protein, where the dye shows no significant contribution to the absorbance. Data for the dye indigo carmine were extracted at 609 nm. Redox potential determinations with potassium indigotrisulfonate were done in a similar manner using values determined at 485 nm for the protein and 601 nm for the dye. Both dyes allowed estimating the redox potential to be -89 ± 3 mV. **(B)** Representation of the data evaluation.

Three dimensional structure of Pst2p

The X-ray crystal structure of Pst2p was determined at 2.8 Å resolution (Table 2). The orthorhombic crystal (space group $P2_12_12_1$) contained eight molecules in the asymmetric unit forming two tetramers. One of those tetramers is shown in Figure 7.

The assignment of the oligomeric state was also verified using the PDBePISA server [39]. This analysis revealed that each tetramer could be viewed as a dimer of dimers with stronger interactions within the dimers (approximately 1200 Å² interaction surface) as compared to the interaction between dimers (800 Å² interaction surface).

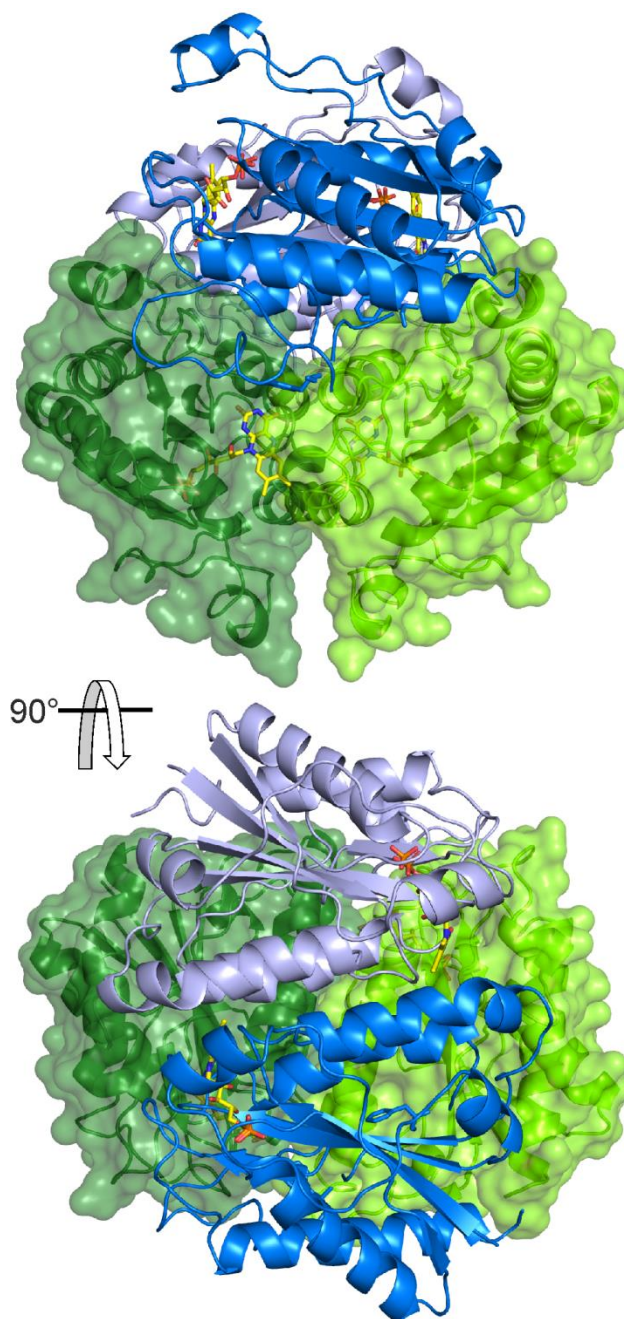


Figure 7. Tetrameric arrangement of Pst2p. The oligomeric state can be described as a dimer of dimers. One dimer is formed by the two green chains shown as surface model and the second by the two blue chains shown as cartoon model. From the respective FMN molecules only the density of phosphate could be observed. Depicted FMN molecules were implemented according to a structural superposition WrbA (PDB entry: 3B6I). Two views are presented, which are rotated by 90° around the x-axis. Figures were prepared with the software PyMOL [40].

Table 2. Data collection and refinement statistics. Values in parentheses are for the highest-resolution shell.

X-ray source	ID29, ESRF, Grenoble, France
Wavelength (Å)	0.972
Temperature	100 K
Space group	$P2_12_12_1$
Cell dimensions	
<i>a</i> , <i>b</i> , <i>c</i> (Å)	69.41, 110.56, 223.81
Resolution (Å)	46.17-2.79 (2.89-2.79)
Total no. reflections	208347 (19109)
No. unique reflections	43021 (4074)
Multiplicity	4.8 (4.7)
Completeness (%)	98.1 (94.5)
$\langle I/\sigma_I \rangle$	10.2 (1.8)
R_{merge} (%)	10.4 (83.4)
R_{meas} (%)	11.7 (93.5)
R_{pim} (%)	5.3 (40.9)
CC _{1/2}	0.998 (0.663)
CC*	0.999 (0.893)
Reflections used in refinement	43020 (4074)
$R_{\text{work}} / R_{\text{free}}$	0.2533 / 0.2855
No. atoms	11840
Protein	11800
Ligands	40
Mean B-factor (Å ²)	82.1
Wilson B-factor (Å ²)	66.9
R.m.s. deviations	
Bond lengths (Å)	0.003
Bond angles (°)	0.58
Ramachandran favored (%)	99.0
Ramachandran outliers (%)	0.0
Rotamer outliers (%)	1.02
Clashscore	7.73
PDB-entry	5MP4

The Pst2p protomer belongs to the flavodoxin-like fold family (CATH: 3.40.50.360) and exhibits the typical flavodoxin-fold consisting of five parallel β -strands forming a twisted β -sheet surrounded by α -helices with three additional loop regions. The chains in the asymmetric unit are very similar to each other with root-mean-square-deviations (rmsd) between 0.3 Å and 0.4 Å for all pairwise C α -atom superpositions calculated using the program PyMOL [40].

Although the solution of Pst2p used for crystallization as well as the crystals themselves were yellow, no clear electron density for the bound FMN was observed in the present structure, indicating either a lower occupancy or high flexibility of the cofactor. Residual density in the predicted FMN binding site was interpreted as phosphate in all chains. These phosphate ions are bound in the same location as the phosphate group of FMN bound in WrbA from *E. coli* [29] which was used as the search structure for molecular replacement and shares 44% sequence identity with Pst2p. A structural superposition of protomers of Pst2p and WrbA yielded a C α -rmsd of 0.9 Å underlining the close structural similarity of the two proteins (Figure 8, panel A). The structure of the complex of Pst2p with FMN modelled based on the comparison with WrbA revealed that each of the four cofactor binding sites is composed of residues from three protomers of the tetramer (Figure 8, panel B). WrbA is a dimeric/tetrameric, FMN-dependent flavoprotein originally described as a tryptophan repressor-binding protein promoting complex formation between the repressor and DNA. Sequence comparisons, however, showed homology to certain NAD(P)H:quinone oxidoreductase [41]. The close structural similarity of Pst2p and WrbA as well as the conservation of amino acid residues in the active site (Figure 8, panel C) suggest that Pst2p may also catalyze the reduction of quinones as previously reported for WrbA [29].

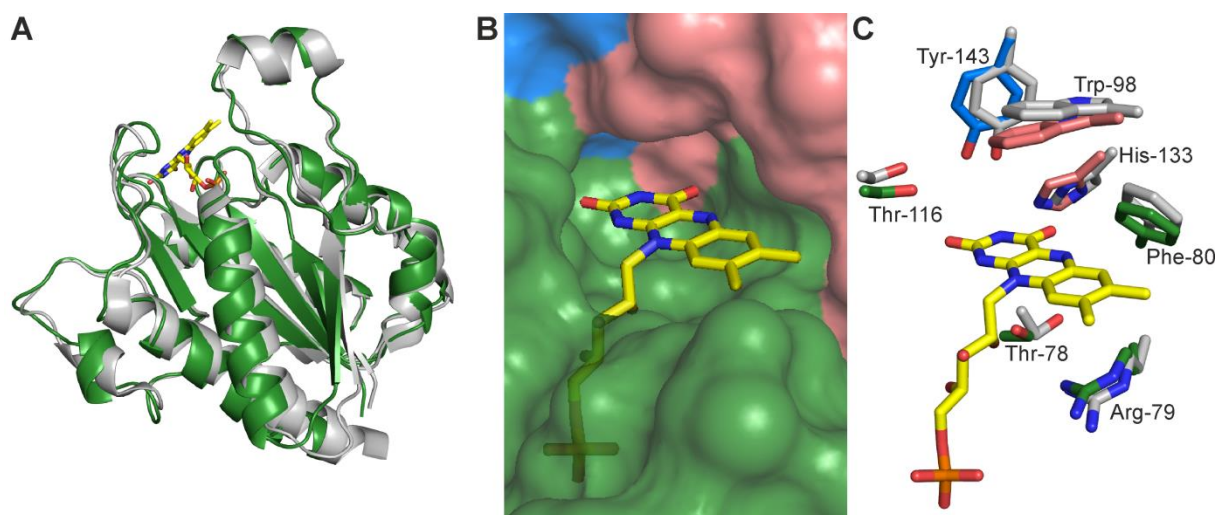


Figure 8. Overall structural similarity of WrbA with Pst2p. (A) Structural superposition of WrbA (grey, PDB code: 3B6I) and Pst2p (green). (B) Surface representation of Pst2p showing that residues from three protomers combine to create the active-site pocket. (C) Close-up view of the FMN binding site. Residues close to the FMN isoalloxazine ring are shown as grey sticks (WrbA) or in colors corresponding to the respective protomer (Pst2p). Figures were prepared with the software PyMOL (<http://www.pymol.org/>).

Characterization of the catalytic properties of Pst2p

To evaluate the enzymatic activity of Pst2p, assays were performed with NADH or NADPH as electron donor and several quinones were tested as electron acceptors. In all cases saturation kinetics were observed that were fitted to a single-phase hyperbolic equation (Figure 9). The extracted kinetic constants are given in Table 1.

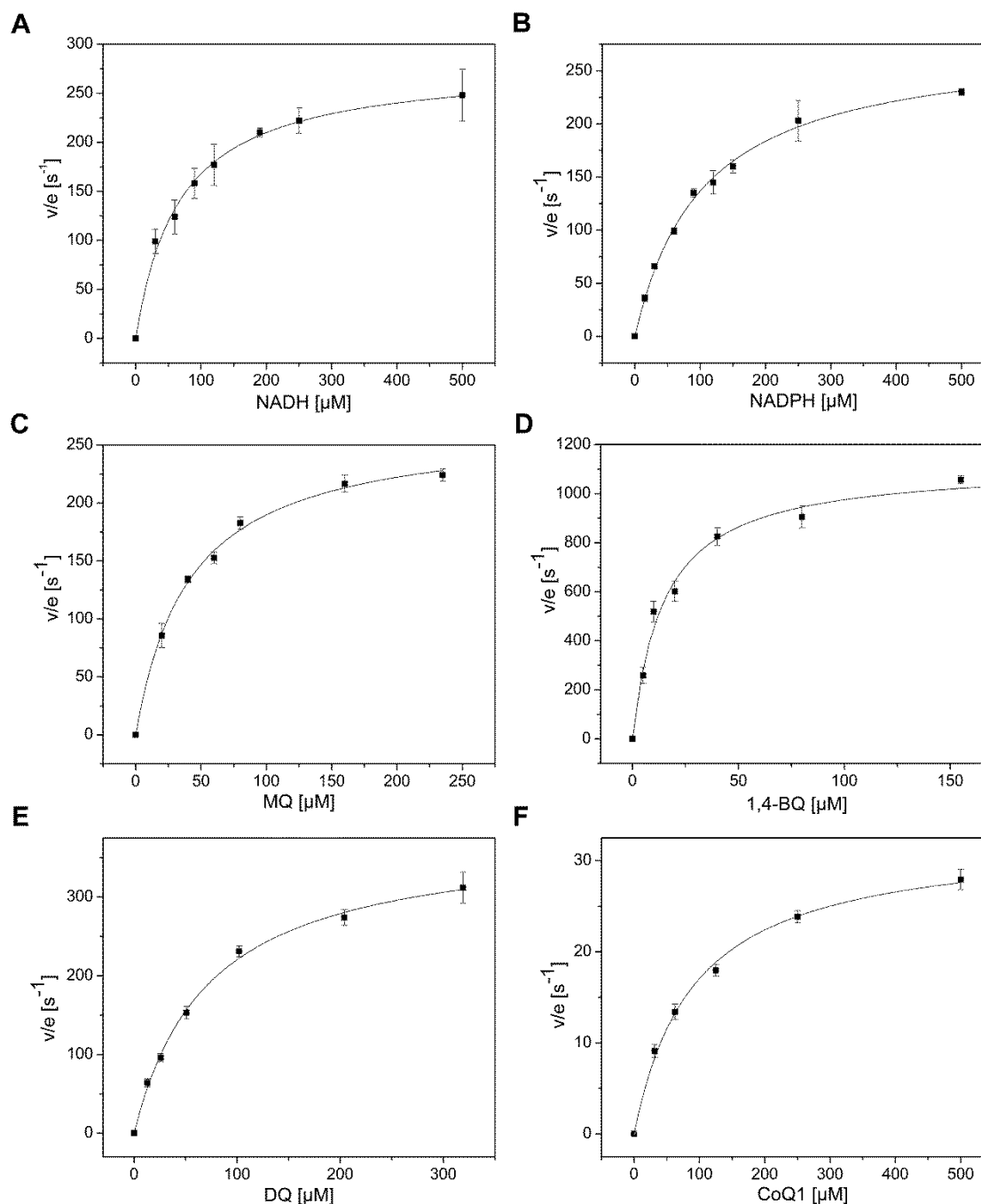


Figure 9. Steady state kinetics of Pst2p. Initial-velocity kinetic measurements were performed in triplicate with NAD(P)H, 1,4 BQ, MQ, DQ and coenzyme Q1 by following the oxidation of NAD(P)H at 380 nm. Reaction mixtures were setup in 50 mM HEPES pH 7, 50 mM NaCl, 2% (v/v) EtOH. Substrates were varied as follows: **(A)** NADH (30-500 μM) and **(B)** NADPH (30-500 μM) at a saturating MQ concentration (200 μM); **(C)** 1,4-BQ (5-155 μM), **(D)** MQ (20-235 μM), **(E)** DQ (12-317 μM) or **(F)** Q1 (30-500) at a saturating NADH concentration (350 μM).

The kinetic mechanism follows a ping-pong bi-bi reaction scheme (Figure 10, panel A) as it is the case for several other quinone reductases [2 and references therein]. Beside quinones, also FMN and different azo dyes, namely methyl orange, ethyl red

and Sudan Black were tested as substrates, but no significant activity with Pst2p was observed.

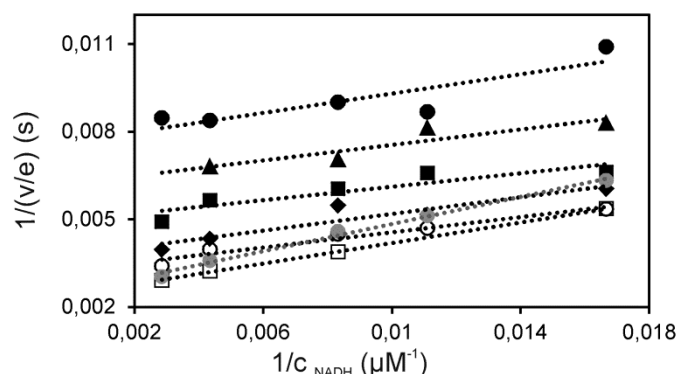


Figure 10. Determination of the kinetic mechanism of Pst2p. Rate of NADH oxidation as a function of MQ concentration. Double reciprocal plot of initial rates versus concentrations of NADH (30-350 μM) were NADH oxidation was determined at 380 nm at 25 °C in buffer C (50 mM Hepes, 50 mM NaCl, pH 7.0) at various concentrations of MQ (20 μM ●, 30 μM ▲, 40 μM ■, 60 μM ◆, 80 μM ○, 160 μM □, and 200 μM ●). The parallel lines in the double-reciprocal plot indicate a ping-pong bi-bi mechanism, with inhibitory effects at high MQ and low NADH levels.

To analyze the kinetic half reactions, Pst2p was mixed in a stopped-flow instrument at 4 °C with NAD(P)H, 1,4-BQ, DQ or MQ under anoxic conditions. For the reductive half reaction, concentrations of 25-250 μM of NADPH or NADH were used and FMN reduction was monitored at 453 nm. Bimolecular rate constants of $5.8 \times 10^6 \pm 4.5 \times 10^5 \text{ M}^{-1} \cdot \text{s}^{-1}$ for NADH and $1.9 \times 10^6 \pm 1.1 \times 10^5 \text{ M}^{-1} \cdot \text{s}^{-1}$ for NADPH were determined (Table 1). In accordance with the calculated catalytic efficiency ($k_{\text{cat}}/K_{\text{M}}$) obtained from steady state experiments NADH appears to be a marginally better reductant compared to NADPH. In order to investigate the oxidative half reaction, Pst2p was first reduced by the addition of 0.9 equivalents of NADH and then mixed with 1,4-BQ (25 μM), MQ (25–100 μM) and DQ (34-910 μM). The oxidation of the reduced FMN cofactor was monitored at 453 nm. Bimolecular rate constants of $2.7 \times 10^6 \pm 7.8 \times 10^5 \text{ M}^{-1} \cdot \text{s}^{-1}$ for MQ and $7.0 \times 10^6 \pm 5.6 \times 10^5 \text{ M}^{-1} \cdot \text{s}^{-1}$ for DQ were determined (Table 1). The reduction of 1,4-BQ was complete within the dead time of the stopped-flow instrument (~5 ms).

Examination of quinone sensitivity using PST2 knock out and overexpressing strains

The efficient reduction of quinones by Pst2p prompted the question whether it plays a role in the detoxification of quinones *in vivo*. In order to investigate this potential function of Pst2p, yeast cells in the logarithmic growth phase were exposed to various concentrations of 1,4-BQ (50-250 μ M), DQ (25-150 μ M) and MQ (25-150 μ M) under aerobic conditions on solid cultures (for details see Experimental Procedures). In the case of 1,4-BQ, yeast cells lacking *PST2* showed higher sensitivity whereas *PST2* overexpressing strains showed increased resistance (Figure 11, rows 2 and 3). Interestingly, the opposite result was obtained for DQ. In this case the *PST2* knock out strain is more resistant while the *PST2* overexpression strain shows a higher sensitivity compared to the wild type strain (Figure 11, rows 7-9). As shown before by North et al. [42] the *PST2* knock out strain shows also a higher sensitivity against hydroquinone compared to the wild type strain (Figure 11, rows 4-6). In contrast to 1,4-BQ and DQ, no growth differences were observed when MQ was employed as a quinone (Figure 11, rows 10-12).

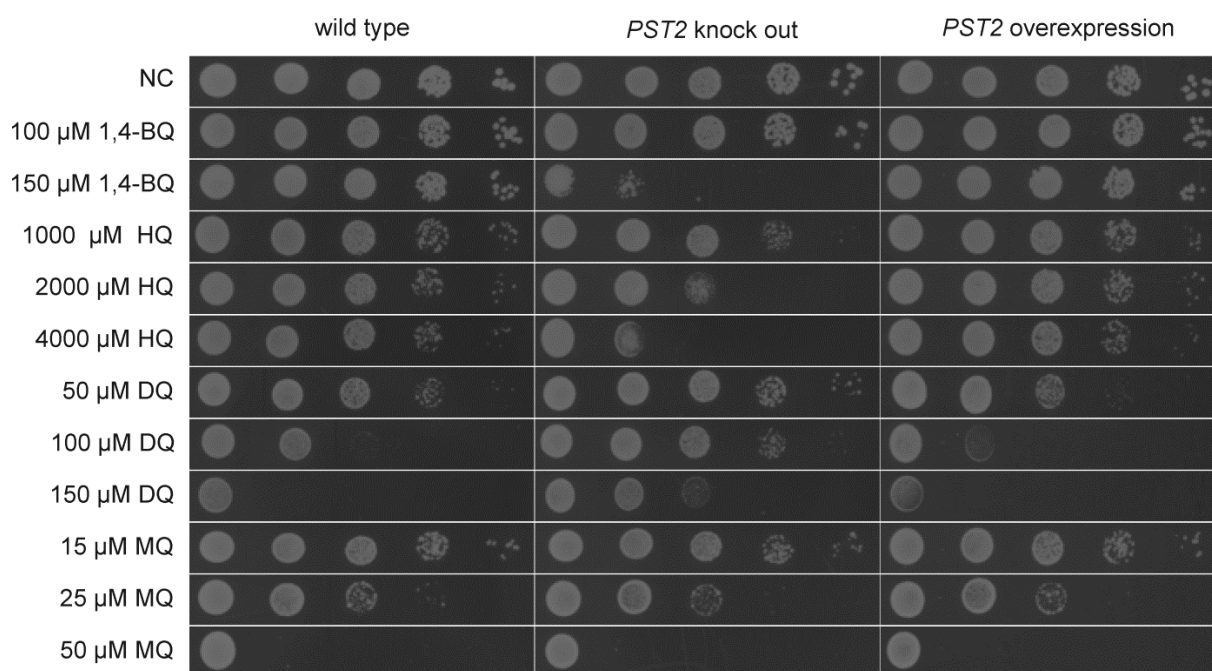


Figure 11. Spot assay on solid medium containing various quinones. Serial dilutions (10-fold) of yeast suspensions in logarithmic growth phase were spotted on SG-Ura containing various concentrations of 1,4-BQ, HQ, DQ or MQ solved in EtOH (2% end concentration). Negative controls (NC) including the solvent but no quinone were performed. Cells were grown for 2-3 days at 30 °C and photographs of the plates are shown.

Discussion

In this study we have demonstrated the expression of *PST2* from *S. cerevisiae* in *E. coli* and the purification and characterization of Pst2p, which turns out to be another member of the NAD(P)H-dependent quinone reductase family. Structure analysis revealed that Pst2p adopts the flavodoxin-like fold that is characteristic for the NAD(P)H-dependent FMN reductase family. Members of this family have an α/β subunit in addition to the α/β twisted open sheet fold that is characteristic for flavodoxins. Like other members of this family, namely YhdA from *Bacillus subtilis* [43], Azo1 from *Staphylococcus aureus* [44] and WrbA from *E. coli* [9], Pst2p is able to form stable tetramers in solution. However, in contrast to the mentioned proteins, tetramerization of Pst2p is independent of flavin binding since removal of the FMN cofactor does not affect the quaternary structure.

It is noteworthy that the redox potential of Pst2p is much more positive than that of free flavin (-89 ± 3 vs. -208 mV) and also significantly more positive than that for homologous enzymes like NQO1 (-159 mV) [46] or Lot6p (-172 mV) [38]. The redox potential of WrbA was not determined with accuracy because the dynamic equilibrium of the dimeric and tetrameric state of the protein appears to impede the measurements [7]. Clearly, the more positive redox potential indicates that reduced FMN binds much tighter than the oxidized cofactor. In fact, the dissociation constant of reduced FMN was calculated to 2 nM and is thus 10.000-fold more tightly bound than oxidized FMN (ca. 20 μ M) (Scheme 1). On the other hand, this also explains why reduced Pst2p lacks FMN reductase activity since this reaction is thermodynamically very unfavorable due to the redox potential difference to the free FMN_{ox}/FMN_{red} couple. This activity is clearly present in other members of the flavodoxin-like family such as Lot6p [38]. Another enzymatic activity, which was found with Lot6p but not with Pst2p is the capability to couple oxidation of NAD(P)H to the reduction of azo dyes [47]. As discussed by Ryan *et al.* [18], differences in the redox potential of various substrates can be partly responsible for the activity variations within the flavodoxin-like superfamily. The quinones investigated in this study cover a range of E° = 286 mV for 1,4-BQ [48] (best substrate) to E° = -13 mV for MQ [49] for which the enzymatic efficiency is an order of magnitude lower. However, the poorest substrate for Pst2p was CoQ1 (CoQ10 E° = 100 mV, [48]). In this case the low efficiency may be due to the bulky hydrophobic side chain that may interfere with

binding of the quinone to the active site. The redox potential of the azo dye methyl orange is also rather low (67 mV at pH 3 [50]), which may also contribute to the lack of activity. Recently, a study reporting the identification of novel azo reductases in *Pseudomonas aeruginosa* mentioned the importance of two structural differences between the classical azo reductase *PaAzoR1* and *PaWrbA*. *PaWrbA* lacks a β -hairpin that is important for substrate specificity in *PaAzoR1*. In addition, a tyrosine residue in the active site was replaced by arginine [11]. In the case of Pst2p, the structural features more closely resemble those in *PaWrbA* and are thus in agreement with the lack of an azo reductase activity. On the other hand, Lot6p features a similar active site as *PaAzoR1* (*i.e.* tyrosine rather than arginine) at the corresponding position. However, the β -hairpin structure is missing in Lot6p. Thus it appears that the active site composition is more relevant for azo reductase activity than the presence of the β -hairpin.

Several enzymes from *S. cerevisiae* have been shown to catalyze the two-electron reduction of quinones, such as the flavin-dependent enzymes Lot6p [38] and Ycp4p [42] and the flavin-independent enzyme Zta1 [51]. In the present study, we have shown that Pst2p is a very efficient NAD(P)H:quinone oxidoreductase rapidly reducing quinones such as 1,4-BQ, MQ, DQ and CoQ₁. Not surprisingly, deletion of *PST2* or its overexpression revealed significant effects with regard to the sensitivity against quinones in comparison to the wild-type strain (Figure 11). In the case of 1,4-BQ and HQ the *PST2* knock-out strain was more susceptible whereas the *PST2* overexpressing strain showed increased resistance. Interestingly, the inverse behavior was seen with DQ (compare rows 2-6 and 7-9 in Figure 11). This finding can be rationalized by the higher rate of auto-oxidation of DQ due to additional methyl groups present in comparison to 1,4-BQ. The increased rate of auto-oxidation causes extensive redox cycling and leads to the generation of semiquinones and reactive oxygen species [48,49]. Thus, the expression of *PST2* enhances the toxicity of DQ. Similar observations were reported for naphthoquinones [52–54]. It remains to be seen whether other electron acceptors exist and, if so, to define their biochemical roles in the yeast.

Acknowledgements

The authors are grateful for the support by the interuniversity program in natural sciences (NAWI Graz) and the FWF-funded doctoral program *Molecular Enzymology*

(W901). The authors thank the beamline staff of the European Synchrotron Radiation Facility (Grenoble, France) for their support during diffraction data collection.

References

- [1] V. Gudipati, K. Koch, W.-D. Lienhart, P. Macheroux, The flavoproteome of the yeast *Saccharomyces cerevisiae*, *Biochim. Biophys. Acta* 1844 (2014) 535–44.
- [2] S. Deller, P. Macheroux, S. Sollner, Flavin-dependent quinone reductases, *Cell. Mol. Life Sci.* 65 (2008) 141–160.
- [3] H.J. Prochaska, Purification and crystallization of rat liver NAD(P)H:(quinone-acceptor) oxidoreductase by cibacron blue affinity chromatography: Identification of a new and potent inhibitor, *Arch. Biochem. Biophys.* 267 (1988) 529–538.
- [4] R. Li, M.A. Bianchet, P. Talalay, L.M. Amzel, The three-dimensional structure of NAD(P)H:quinone reductase, a flavoprotein involved in cancer chemoprotection and chemotherapy: Mechanism of the two-electron reduction, *Proc. Natl. Acad. Sci. USA* 92 (1995) 8846–8850.
- [5] A.T. Dinkova-Kostova, P. Talalay, Persuasive evidence that quinone reductase type 1 (DT diaphorase) protects cells against the toxicity of electrophiles and reactive forms of oxygen, *Free Radical Biol. Med.* 29 (2000) 231–240.
- [6] R.J. Knox, S. Chen, Quinone reductase – mediated nitro-reduction: Clinical applications, *Methods Enzymol.* 382 (2004) 194–221.
- [7] R. Grandori, P. Khalifah, J.A. Boice, R. Fairman, K. Giovanielli, J. Carey, Biochemical characterization of WrbA, founding member of a new family of multimeric flavodoxin-like proteins, *J. Biol. Chem.* 273 (1998) 20960–20966.
- [8] E. V Patridge, J.G. Ferry, WrbA from *Escherichia coli* and *Archaeoglobus fulgidus* is an NAD(P)H:quinone oxidoreductase, *J. Bacteriol.* 188 (2006) 3498–3506.

- [9] J. Wolfova, I. Kuta, J. Brynda, J.R. Mesters, M. Lapkouski, M. Kutý, A. Natalello, N. Chatterjee, S. Chern, E. Ebbel, A. Ricci, R. Grandori, R. Ettrich, J. Carey, Structural organization of WrbA in apo- and holoprotein crystals, *Biochim. Biophys. Acta* 1794 (2009) 1288–1298.
- [10] I. Kishko, B. Harish, V. Zayats, D. Reha, B. Tenner, J. Carey, Biphasic kinetic behavior of *E. coli* WrbA, an FMN- dependent NAD(P)H:quinone oxidoreductase, *PLoS One* 7 (2012) e43902.
- [11] V. Crescente, S.M. Holland, S. Kayhyap, E. Polycarpou, E. Sim, A. Ryan, Identification of novel members of the bacterial azoreductase family in *Pseudomonas aeruginosa*, *Biochem. J.* 473 (2016) 549–558.
- [12] A. Atia, N. Alrawaiq, A. Abdullah, A review of NAD(P)H:quinone oxidoreductase 1 (NQO1); a multifunctional antioxidant enzyme, *J. Appl. Pharm. Sci.* 4 (2014) 118–122.
- [13] A. Morokutti, A. Lyskowski, S. Sollner, E. Pointner, T.B. Fitzpatrick, C. Kratky, K. Gruber, P. Macheroux, Structure and function of YcnD from *Bacillus subtilis*, a flavin-containing oxidoreductase, *Biochemistry* 44 (2005) 13724–13733.
- [14] S. Sollner, P. Macheroux, New roles of flavoproteins in molecular cell biology: An unexpected role for quinone reductases as regulators of proteasomal degradation, *FEBS J.* 276 (2009) 4313–4324.
- [15] D. Siegel, D.L. Gustafson, D.L. Dehn, J.Y. Han, P. Boonchoong, L.J. Berliner, D. Ross, NAD(P)H:quinone oxidoreductase 1: Role as a superoxide scavenger, *Mol. Pharmacol.* 65 (2004) 1238–1247.
- [16] L. Li, S. Naseem, S. Sharma, J.B. Konopka, Flavodoxin-like proteins protect *Candida albicans* from oxidative stress and promote virulence, *PLoS Pathog.* 11 (2015) e1005147.
- [17] E. Heyno, N. Alkan, R. Fluhr, A dual role for plant quinone reductases in host-fungus interaction, *Physiol. Plant.* 149 (2013) 340–353.
- [18] A. Ryan, E. Kaplan, J.-C. Nebel, E. Polycarpou, V. Crescente, E. Lowe, G.M. Preston, E. Sim, Identification of NAD(P)H quinone oxidoreductase activity in azoreductases from *P. aeruginosa*: azoreductases and NAD(P)H quinone

oxidoreductases belong to the same FMN-dependent superfamily of enzymes, PLoS One. 9 (2014) e98551.

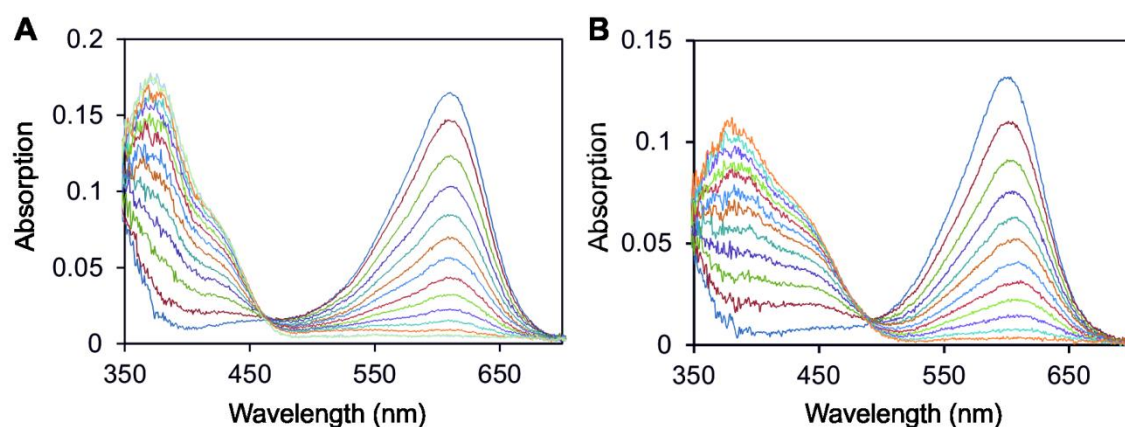
- [19] H. Du, R.A. Fuh, J. Li, L.A. Corkan, J.S. Lindsey, Technical and software note photochemCAD: A computer-aided design and research tool in photochemistry, Photochem. Photobiol. 68 (1998) 141–142.
- [20] J.C. Overeem, G.J.M. Kerk, Mollisin, a naturally occurring chlorine-containing quinone: Part III. The synthesis of dechloromollisin methyl ether and of related compounds, Recl. Des Trav. Chim. Des Pays-Bas. 83 (1964) 1005–1022.
- [21] M.A. Moxley, J.J. Tanner, D.F. Becker, Steady-state kinetic mechanism of the proline:ubiquinone oxidoreductase activity of proline utilization A (PutA) from *Escherichia coli*, Arch Biochem. Biophys. 516 (2011) 113–120.
- [22] P. Macheroux, UV-visible spectroscopy as a tool to study flavoproteins, Methods Mol. Biol. 131 (1999) 1–7.
- [23] C. Pashley, S. Kendall, Cloning in plasmid vectors, Methods Mol. Biol. 235 (2003) 121–135.
- [24] W.E. Swords, Chemical transformation of *E. coli*, Methods Mol. Biol. 235 (2003) 49–53.
- [25] R. Gietz, Yeast transformation by the LiAc/SS carrier DNA/PEG method, Methods Mol. Biol. 1205 (2014) 1–12.
- [26] J.M. Cherry, E.L. Hong, C. Amundsen, R. Balakrishnan, G. Binkley, E.T. Chan, K.R. Christie, M.C. Costanzo, S.S. Dwight, S.R. Engel, D.G. Fisk, J.E. Hirschman, B.C. Hitz, K. Karra, C.J. Krieger, S.R. Miyasato, R.S. Nash, J. Park, M.S. Skrzypek, M. Simison, S. Weng, E.D. Wong, *Saccharomyces* genome database: The genomics resource of budding yeast, Nucleic Acids Res. 40 (2012) 700–705.
- [27] W. Kabsch, Xds, Acta Crystallogr. 66 (2010) 125–132.
- [28] M.D. Winn, C. Charles, K.D. Cowtan, E.J. Dodson, A.G.W. Leslie, A. McCoy, J. Stuart, N. Garib, H.R. Powell, J. Randy, Overview of the CCP4 suite and current developments, Acta Crystallogr. 67 (2011) 235–242.

- [29] S.L.A. Andrade, E.V. Patridge, J.G. Ferry, O. Einsle, Crystal structure of the NADH:quinone oxidoreductase WrbA from *Escherichia coli*, *J. Bacteriol.* 189 (2007) 9101–9107.
- [30] P. Emsley, B. Lohkamp, Features and development of Coot, *Acta Crystallogr.* 66 (2010) 486–501.
- [31] P.D. Adams, V. Pavel, V.B. Chen, W. Ian, N. Echols, N.W. Moriarty, R.J. Read, D.C. Richardson, S. Jane, C. Thomas, PHENIX: a comprehensive Python-based system for macromolecular structure solution, *Acta Crystallogr.* 66 (2010) 213–221.
- [32] K. Laemmli, Cleavage of structural proteins during the assembly of the head of bacteriophage T4, *Nature.* 227 (1970) 680–685.
- [33] W.-D. Lienhart, V. Gudipati, M.K. Uhl, A. Binter, S.A. Pullido, R. Saf, K. Zangger, K. Gruber, P. Macheroux, Collapse of the native structure caused by a single amino acid exchange in human NAD(P)H:quinone oxidoreductase 1, *FEBS J.* 281 (2014) 4691–4704.
- [34] F. Forneris, R. Orru, D. Bonivento, L.R. Chiarelli, A. Mattevi, ThermoFAD, a Thermofluor-adapted flavin ad hoc detection system for protein folding and ligand binding, *FEBS J.* 276 (2009) 2833–2840.
- [35] U.B. Ericsson, B.M. Hallberg, G.T. DeTitta, N. Dekker, P. Nordlund, Thermofluor-based high-throughput stability optimization of proteins for structural studies, *Anal. Biochem.* 357 (2006) 289–298.
- [36] V. Massey, A simple method for the determination of redox potentials, in B. Curti, G. Zanetti, S. Ronchi (Eds.), *Flavin and Flavoproteins*, Walter de Gruyter & Co, Berlin, 1990, pp. 59-66.
- [37] K. Minnaert, Measurement of the equilibrium constant of the reaction between cytochrome c and cytochrome a, *Biochim. Biophys. Acta* 110 (1965) 42–56.
- [38] S. Sollner, R. Nebauer, H. Ehammer, A. Prem, S. Deller, B. a Palfey, G. Daum, P. Macheroux, Lot6p from *Saccharomyces cerevisiae* is a FMN-dependent reductase with a potential role in quinone detoxification, *FEBS J.* 274 (2007) 1328–39.

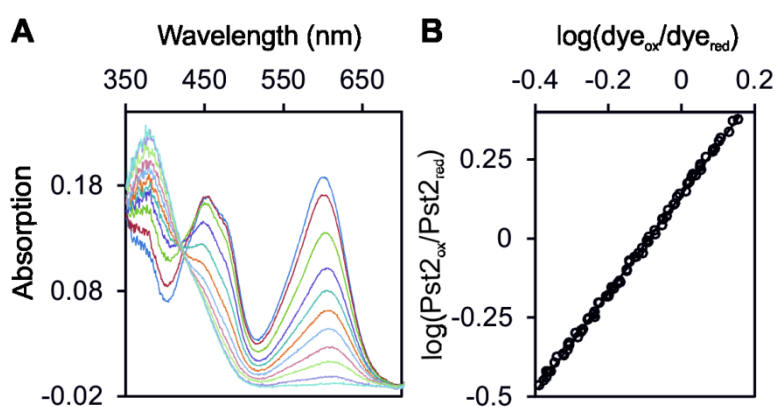
- [39] E. Krissinel, K. Henrick, Inference of macromolecular assemblies from crystalline state, *J. Mol. Biol.* 372 (2007) 774–797.
- [40] DeLano Warren Lyford, The PyMOL Molecular Graphics System Version 1.5.0.4, 2002.
- [41] J. Carey, J. Brynda, J. Wolfova, R. Grandori, T. Gustavsson, R. Ettrich, I.K. Smatanova, WrbA bridges bacterial flavodoxins and eukaryotic NAD(P)H:quinone oxidoreductases, *Protein Sci.* 16 (2007) 2301–2305.
- [42] M. North, V.J. Tandon, R. Thomas, A. Loguinov, I. Gerlovina, A.E. Hubbard, L. Zhang, M.T. Smith, C.D. Vulpe, Genome-wide functional profiling reveals genes required for tolerance to benzene metabolites in yeast., *PLoS One* 6 (2011) e24205.
- [43] J. Ren, L. Wen, X. Gao, CSS-Palm 2 . 0: an updated software for palmitoylation sites prediction, *Protein Eng. Des. Sel.* 21 (2008) 639–644.
- [44] S. Deller, S. Sollner, R. Trenker-el-Toukhy, I. Jelesarov, G.M. Gübitz, P. Macheroux, Characterization of a thermostable NADPH:FMN oxidoreductase from the mesophilic bacterium *Bacillus subtilis*, *Biochemistry* 45 (2006) 7083–7091.
- [45] H. Chen, S.L. Hopper, C.E. Cerniglia, Biochemical and molecular characterization of an azoreductase from *Staphylococcus aureus*, a tetrameric NADPH-dependent flavoprotein, *Microbiology* 151 (2016) 1433–1441.
- [46] G. Tedeschi, S. Chen, V. Massey, DT-Diaphorase: redox potential, steady-state, and rapid reaction studies, *J. Biol. Chem.* 270 (1995) 1198–1204.
- [47] D. Liger, M. Graille, C. Zhou, N. Leulliot, S. Quevillon-cheruel, K. Blondeau, H. Van Tilbeurgh, Crystal structure and functional characterization of yeast YLR011wp, an enzyme with NAD(P)H-FMN and ferric iron reductase activities, *J. Biol. Chem.* 279 (2004) 34890–34897.
- [48] P.A. Loach, Oxidation-reduction potentials, absorbance bands and molar absorbance of compounds used in biochemical studies., in: G.D. Fasman (Ed.), *Handb. Biochem. Mol. Biol. Phys. Chem. Data*, 3rd ed., CRC Press, Cleveland, 1976, pp. 122–130.

- [49] E. Denke, T. Merbitz-Zahradnik, O.M. Hatzfeld, C.H. Snyder, T.A. Link, B.L. Trumpower, Alteration of the midpoint potential and catalytic activity of the Rieske iron-sulfur protein by changes of amino acids forming hydrogen bonds to the iron-sulfur cluster, *J. Biol. Chem.* 273 (1998) 9085–9093.
- [50] J. Peral, M. Trillas, X. Doménech, Heterogeneous photochemistry - an easy experiment, *J. Chem. Educ.* 72 (1995) 565–566.
- [51] S. Porté, E. Crosas, E. Yakovtseva, J.A. Biosca, J. Farrés, M.R. Fernández, X. Parés, Chemico-biological interactions MDR quinone oxidoreductases: The human and yeast ζ -crystallins, *Chem. Biol. Interact.* 178 (2009) 288–294.
- [52] T.H. James, A. Weissberger, Oxidation processes. XI. The autoxidation of durohydroquinone, *J. Am. Chem. Soc.* 60 (1934) 98–104.
- [53] T.H. James, J.M. Snell, A. Weisberger, Oxidation processes. XII. The autoxidation of hydroquinone and of the mono-, di- and trimethylhydroquinones, *J. Am. Chem. Soc.* 60 (1938) 2084–2093.
- [54] B.R. Munday, Activation and detoxification of naphthoquinones by NAD(P)H:quinone oxidoreductase, *Methods Enzymol.* 382 (2004) 364–380.

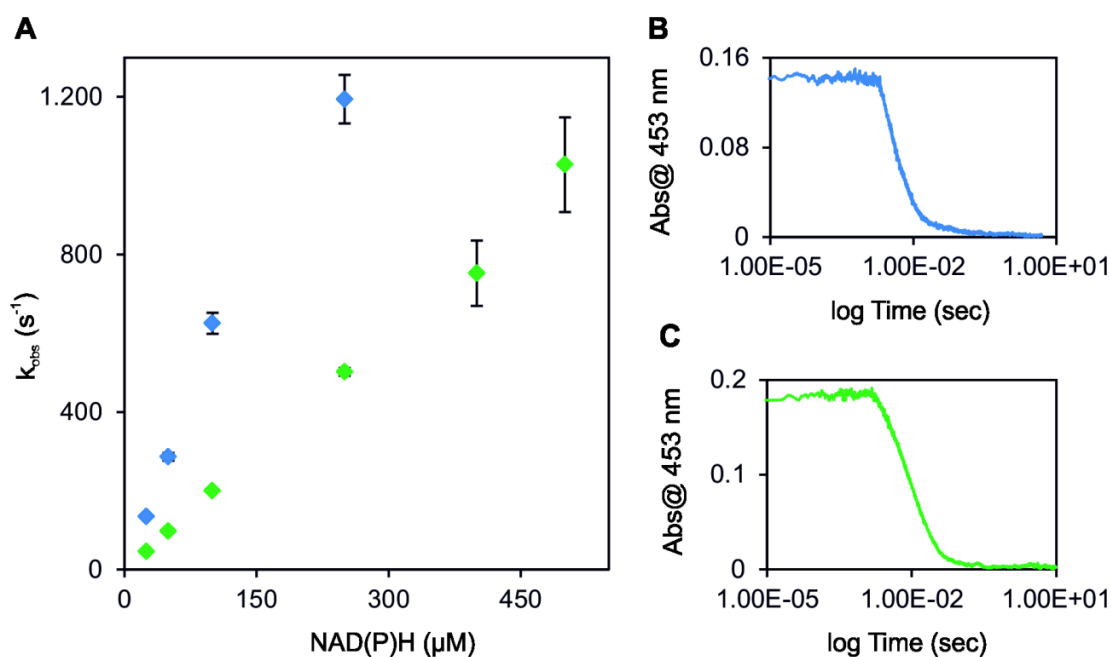
Supplementary information (unpublished figures)



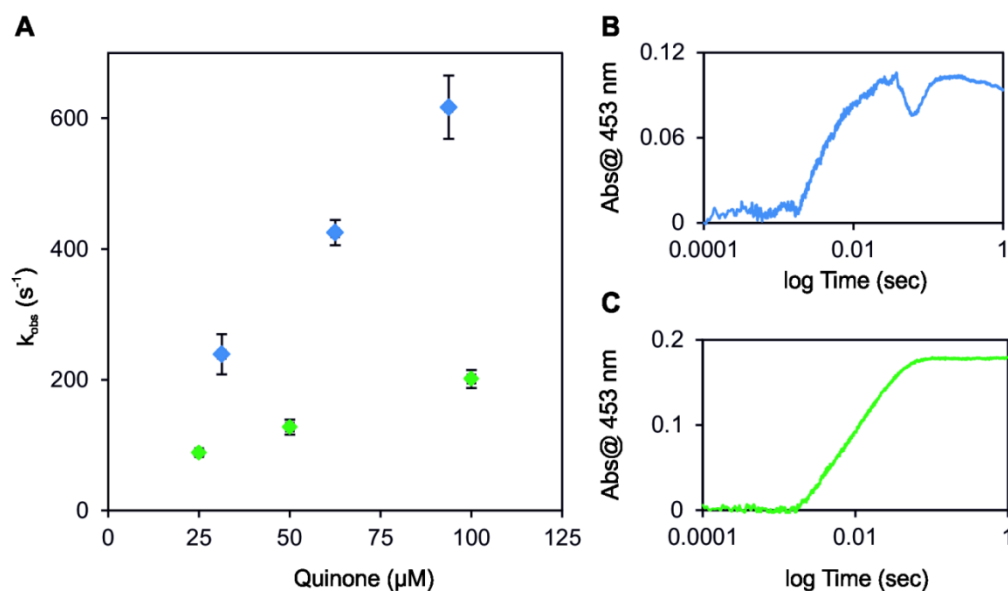
Supplementary Figure 1. Course of reduction of indigo carmine and indigotrisulfonate. **(A)** Reduction of indigo carmine by the xanthine/xanthine oxidase system over a time period of ~ 13 min. The dye shows a maximum absorption at 609 nm and an isosbestic point at 461 nm. **(B)** Reduction of indigotrisulfonate by the xanthine/xanthine oxidase system over a time period of ~ 10 min. The dye shows a maximum absorption at 601 nm and an isosbestic point at 485 nm.



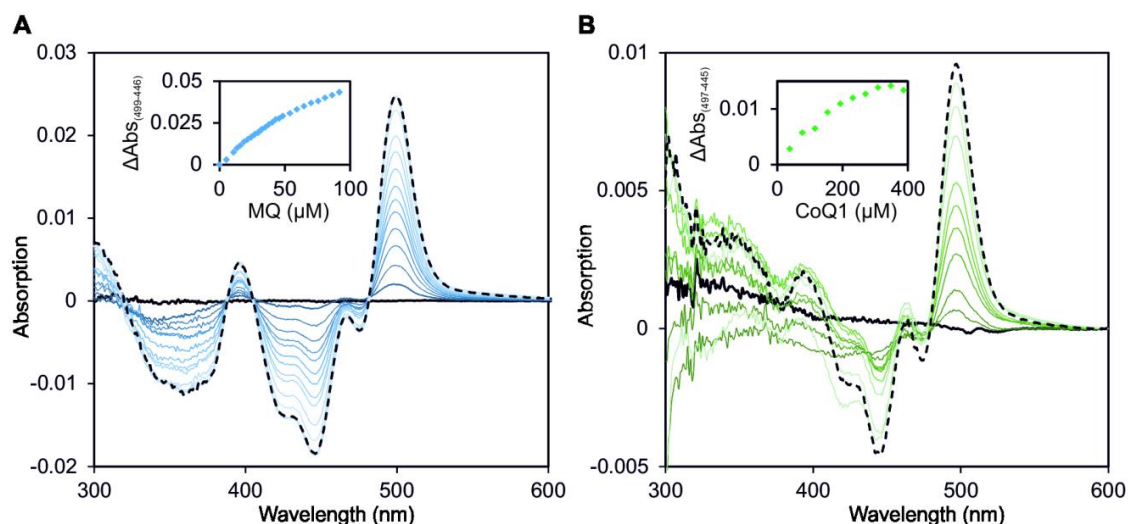
Supplementary Figure 2. Redox potential determination of Pst2p in the presence of indigotrisulfonate. **(A)** Selected spectra of the course of reduction. ~20 μ M Pst2p was reduced by the xanthine/xanthine oxidase system in the presence of indigotrisulfonate over a time period of 65 min. Data points for evaluation were measured at 485 nm for the protein, where the dye shows no significant contribution to the absorbance. Data for the dye indigotrisulfonate were extracted at 601 nm. Redox potential determinations with potassium indigo carmine were done in a similar manner using values determined at 461 nm for the protein and 609 nm for the dye. Both dyes allowed estimating the redox potential to be -89 ± 3 . **(B)** Representation of the data evaluation.



Supplementary Figure 3. Presteady-state kinetics of Pst2p to determine reductive Rates. **(A)** Reductive rates were determined for NADH (blue) and NADPH (green). At least three independent measurements were performed; error bars are shown as standard deviations. **(B)** Absorption change at 453 nm of the anoxic reduction of 25 μM Pst2p with 50 μM NADH. **(C)** Absorption change at 453 nm of the anoxic reduction of 25 μM Pst2 with 50 μM NADPH.



Supplementary Figure 4. Presteady-state kinetics of Pst2p to determine oxidative Rates. **(A)** Oxidative rates were determined for DQ (blue) and MQ (green). At least three independent measurements were performed; error bars are shown as standard deviations. **(B)** Absorption change at 453 nm of the anoxic oxidation of 20 μM Pst2p with 63 μM DQ. **(C)** Absorption change at 453 nm of the anoxic reduction of 25 μM Pst2p with 50 μM MQ.



Supplementary Figure 5. Binding of MQ and CoQ1 to Pst2p. **(A)** Difference titration of Pst2p with MQ. 40 μM Pst2p was titrated with MQ (0–100 μM) and absorption spectra were recorded from 300 to 600 nm using a UV/Vis spectrophotometer. Representative and normalized spectra are depicted in different shades of blue. The final spectrum is shown as black dotted line. The inset shows a plot of the absorption change as a function of MQ concentration. A hyperbolic fit to the experimental data yielded a dissociation constant of $139 \pm 14 \mu\text{M}$. **(B)** Difference titration of Pst2p with Coenzyme Q1. 40 μM Pst2p was titrated with DQ (0–387 μM) and absorption spectra were recorded from 300 to 600 nm using a UV/Vis spectrophotometer. Representative and normalized spectra are depicted in different shades of green. The final spectrum is shown as black dotted line. The inset shows a plot of the absorption change as a function of Coenzyme Q1 concentration. A hyperbolic fit to the experimental data yielded a dissociation constant of $226 \pm 21 \mu\text{M}$.

3.2 Expression and purification of the flavodoxin-like proteins Ycp4p and Rfs1p from Saccharomyces cerevisiae

Karin Koch, Marija Sorokina and Peter Macheroux

Institute of Biochemistry, Graz University of Technology, Petersgasse 12/2, 8010
Graz

Author contributions

P.M. initiated the project; K.K. and P.M. designed the experiments and interpreted the data; K.K. and M.S. expressed and purified Ycp4p, Rfs1p and TEV protease and performed analytical, biochemical and enzymatic experiments.

Abbreviations

DTT, dithiothreitol; *E. coli*, *Escherichia coli*; EtOH, ethanol; EDTA, ethylenediaminetetraacetic acid; HF, high-fidelity; MQ, menadione; Ni-NTA-sepharose; nickel-nitrilotriacetic acid-sepharose; OE-PCR, overlap extension polymerase chain reaction; Pst2, protoplasts-secreted 2; Rfs1, Rad55 suppressor 1; *S. cerevisiae*, *Saccharomyces cerevisiae*; TEV, *Tobacco etch* virus; WrbA, tryptophan (W) repressor-binding protein; Ycp4, yeast chromosomal protein 4;

Materials and Methods

Materials

All chemicals, reagents and enzymes were of highest quality and were from Sigma-Aldrich (St. Louis, USA), Roth (Karlsruhe, Germany) or Thermo Fisher Scientific (Waltham, USA), unless otherwise noted. Columns for affinity chromatography (Ni-NTA-sepharose; nickel-nitrilotriacetic acid), size exclusion chromatography (Superdex 200 10/300 GL) and buffer exchange (PD-10 desalting column) were from GE Healthcare (Little Chalfont, UK). *E. coli* strains Top10 and RosettaTM(DE3) were from Invitrogen (Carlsbad, USA) and Merck (Darmstadt, Germany), respectively. The plasmids pET21a(+) and pET28a(+) were obtained from Merck (Darmstadt, Germany). The concentrations of the following compounds were determined spectrophotometrically using molar extinction coefficients: NAD(P)H ($\epsilon_{340} = 6.220 \text{ M}^{-1} \text{ cm}^{-1}$), MQ dissolved in EtOH ($\epsilon_{333} = 2.450 \text{ M}^{-1} \text{ cm}^{-1}$) [1] and FMN ($\epsilon_{450} = 12.500 \text{ M}^{-1} \text{ cm}^{-1}$) [2]

Cloning of RFS1 and YCP4 for expression in E. coli with His-tag or solubility enhancing proteins

All strains were generated using standard genetic techniques [3,4]. Briefly, genomic DNA from *Saccharomyces cerevisiae* (*S. cerevisiae*) was extracted with yeast DNA extraction kit from VWR (Radnor, USA). According to the sequence for *RFS1* and *YCP4* from the *Saccharomyces* genome database [5] primers including respective restriction sites for cloning were designed (Table 1) and synthesized from VBC (Vienna, Austria). Vectors containing sequences for respective 6xHis-tagged fusion proteins (ZTZ, ZZ, DsbC, Gst, Trx, M11, GB1, DsbA, MBP or NusA) were kindly

provided by Dr. Andreas Winkler. To include the sequence for *YCP4* or *RFS1* the restriction enzymes NcoI and NotI were used. Since both genes contain the target sequence for NcoI the respective sequence was mutated by overlap-extension PCR (OE-PCR) without changing the amino acid sequence. Corresponding primers are listed in Table 1.

Table 1. List of primers used in this study.

Constructs with C-terminal 6xHis-tag (vector: pET21a)	
<i>YCP4_FW</i>	5'-GAGAC <u>ATATGG</u> TAAAGATAATTAC-3'
<i>YCP4_REV</i>	5'-CGTCTCGAGCATGACAGTACAGCAGGATAA-3'
<i>RFS1_FW</i>	5'-GAGCC <u>ATATGCC</u> GAAAGTCGCTATTTTGAT-3'
<i>RFS1_REV</i>	5'-CGTCTCGAGCAAATCTTTGATACGGTCGTAAAAGGC-3'
Constructs with N-terminal 6xHis-tag (vector: pET28a)	
<i>YCP4_FW</i>	5'-GAGAC <u>ATATGG</u> TAAAGATAATTAC-3'
<i>YCP4_REV</i>	5'-CGTCTCGAGTTACATGACAGTACAGCAGGA-5'
<i>RFS1_FW</i>	5'-GAGCC <u>ATATGCC</u> GAAAGTCGCTATTTTGAT-3'
<i>RFS1_REV</i>	5'-CGTCTCGAGTTACAAATCTTTGATACGGTCGTAAAAGGC-3'
Fusion constructs	
<i>YCP4_FW</i>	5'-GAGCC <u>ATGGG</u> TGTAAGATTGCGATAATTACTTACTCTACC-3'
<i>YCP4_overlap_FW</i>	5'-CTCTCCTTGGGGTGCTG-3'
<i>YCP4_overlap_REV</i>	5'-CAGCACCCCAAGGAGAG-3'
<i>YCP4_REV</i>	5'-GCTGCGGCCGCTTACATGACAGTACAGCAGGATAATAATC-3'
<i>RFS1_FW</i>	5'-GAGCC <u>ATGGG</u> TCGAAAGTCGCTATTTTGATTTATTCAG-3'
<i>RFS1_overlap_FW</i>	5'-GTTCTCTCCACGGCAAATTG-3'
<i>RFS1_overlap_REV</i>	5'-GCTGCGGCCGCTTAGAATCTTT-3'
<i>RFS1_REV</i>	5'-GCTGCGGCCGCTTACAAATCTTTGATACGGTCGTAAAAGG-3'

In the first step of the OE-PCR the fragments, which should be further assembled to fusion constructs, were amplified separately using primers with overlapping extensions. A 50 μ L reaction mixture contained 0.2 mM dNTPs, 1x high-fidelity (HF) buffer, 1 U HF-Phusion DNA polymerase, 10 pmol of forward and reverse primer and 100 ng of template DNA. The following program was used for the initial PCR: 30 sec at 98 °C, 35 cycles with 7.5 sec at 98 °C, 20 sec at 57 °C and 20 sec at 72 °C followed by a final extension step of 7 min at 72 °C. PCR products were purified from

agarose gels and consequently subjected to the second step of OE-PCR, where the two fragments were linked in a primerless amplification reaction via the overlapping linker region. A 50 μ L reaction mixture consisted of 0.2 mM dNTPs, 1x HF buffer, 1 U HF-Phusion DNA polymerase and the products of the first step in an equimolar range (1-10 ng of the largest fragment). In principle the same program was used as for the initial PCR with a reduced number of cycles (20). In the final step of the OE-PCR the assembled sequences were amplified by the addition of the two terminal primers by pipetting another reaction mixture directly to the PCR reaction mixture from the second step. 20 μ L of this mixture contained 1x HF buffer, 0.2 mM dNTPs, 1 U HF-Phusion DNA polymerase, and 10 pmol forward and reverse primer. The following program was used for the final step: initial denaturation for 30 sec at 98 °C, 35 cycles of 20 sec at 98 °C, 20 sec at 57 °C, and 20 sec at 72 °C, followed by a final extension step of 7 min at 72 °C. The PCR products were purified from agarose gels and cloned into the respective fusion protein vectors. Individual clones were sequenced before transforming the plasmid into *Escherichia coli* (*E. coli*) RosettaTM(DE3) cells.

Expression and purification of TEV protease (protease from Tobacco etch virus)

The vector encoding TEV protease was kindly provided by Dr. Klaus Zangger and was transformed into *E. coli* BL21(DE3). A single colony was used to inoculate a pre-culture that was aerobically incubated (37 °C, 16 h, 150 rpm) in lysogeny broth (bacto-tryptone 10 g/L, bacto-yeast extract 5 g/L, NaCl 5 g/L) supplemented with 100 μ g/mL ampicillin. 1% pre-culture was used to inoculate the main-culture supplemented with 100 μ g/mL ampicillin, which was incubated aerobically at 37 °C with agitation at 150 rpm until an OD_{600} of ~0,6 was reached. Expression of TEV protease was induced by addition of 0.5 mM isopropyl-thio- β -d-galactoside. The culture was further incubated for 16 h at 20 °C. Cells were harvested by centrifugation at 4.500 x *g* at 4 °C and washed once with 1% saline solution.

Cell pellets were resuspended in 4 mL/1g pellet buffer A [50 mM Tris/HCl, 150 mM NaCl, 2 mM DTT (dithiothreitol), pH 8.0] supplemented with 10 mM imidazole, 1 mM phenylmethylsulfonyl fluoride solved in dimethylsulfoxide, 1 mg/mL lysozyme and further 1 μ L of protease inhibitor cocktail for use in the purification of histidine-tagged proteins from Sigma-Aldrich (St. Louis, USA) was added per g of cell pellet. Cell disruption was achieved by sonication with a Labsonic L instrument from Braun Biotech. International (Berlin, Germany) with 120 Watt for 3 x 3 min in an ice-water

bath with 3 min pauses between each cycle. The cell lysate was centrifuged at 38.850 x g for 45 min at 4 °C, and the supernatant was loaded onto a 5-mL HisTrap HP column previously equilibrated with buffer A supplemented with 10 mM imidazole. The column was washed with buffer A supplemented with 10 mM imidazole and 1 M NaCl, then washed with buffer A supplemented with 20 mM imidazole and subsequently proteins were eluted with buffer A supplemented with 330 mM imidazole and 10% glycerol. Fractions containing target protein were pooled and concentrated with centrifugal filter units (Amicon Ultra-15, 10 k; Millipore, Billerica, MA, USA). Concentrated protein was re-buffered to buffer B 50 mM Hepes, pH 7.0 supplemented with 5 mM DTT, 10% glycerol, with a PD-10 desalting column. The protein solutions were shock frozen and stored at -80 °C, if not used immediately.

Expression and purification of Rfs1p and Ycp4p fusion proteins

A single colony *E. coli* RosettaTM(DE3) cells containing the respective vector was used to inoculate a pre-culture that was aerobically incubated (37 °C, 16 h, 150 rpm) in lysogeny broth (bacto-tryptone 10 g/L, bacto-yeast extract 5 g/L, NaCl 5 g/L) supplemented with 100 µg/mL ampicillin. 1% pre-culture was used to inoculate the main-culture supplemented with 100 µg/mL ampicillin, which was incubated aerobically at 37 °C with agitation at 150 rpm until an OD_{600} of ~0,6 was reached. Expression of TEV protease was induced by addition of 0.5 mM isopropyl-thio-β-d-galactoside. The culture was further incubated for 16 h at 20 °C. Cells were harvested by centrifugation at 4.500 x g at 4 °C and washed once with 1% saline solution.

Cell pellets were resuspended in 4 mL/1g pellet buffer C (50 mM Hepes, 150 mM NaCl, pH 7.0) supplemented with 1 mM phenylmethylsulfonyl fluoride solved in dimethylsulfoxide, 1 mg/mL lysozyme and further 1 µL of protease inhibitor cocktail for use in the purification of histidine-tagged proteins from Sigma-Aldrich (St. Louis, USA) was added per g of cell pellet. Cell disruption was achieved by sonication with a Labsonic L instrument from Braun Biotech. International (Berlin, Germany) with 120 Watt for 3 x 3 min in an ice-water bath with 3 min pauses between each cycle. The cell lysate was centrifuged at 38.850 x g for 45 min at 4 °C, and the supernatant was loaded onto a 5-mL HisTrap HP column previously equilibrated with buffer C. The column was washed with buffer C supplemented with 20 mM imidazole, subsequently proteins were eluted with buffer C supplemented with 300 mM imidazole. Fractions

containing target protein were pooled and concentrated with centrifugal filter units (Amicon Ultra-15, 10 k; Millipore, Billerica, MA, USA). Concentrated protein was re-buffered to buffer B (50 mM Hepes, pH 7.0) with a PD-10 desalting column. The protein solutions were shock frozen and stored at $-80\text{ }^{\circ}\text{C}$, if not used immediately.

Separation of the fusion proteins and Ycp4p or Rfs1p was achieved by digestion with a hexahistidine-tagged TEV-protease. The digestion was performed overnight at $4\text{ }^{\circ}\text{C}$. The reaction mixture contained 50 mM Hepes, pH 7.0, 0.5 mM EDTA (ethylenediaminetetraacetic acid), 1 mM DTT and 1 μg TEV protease per 10 μg fusion protein. After digestion the buffer was exchanged using centrifugal filter units (Amicon Ultra-15, 10 k; Millipore, Billerica, MA, USA) to remove EDTA and the solution was subsequently loaded onto the Ni-NTA column, where the 6xHis-tagged TEV protease and fusion protein bound again, while untagged Ycp4p and Rfs1p remained in the flow through. The protein solutions containing target protein were concentrated with centrifugal filter units (Amicon Ultra-15, 10 k; Millipore, Billerica, MA, USA) and were shock frozen and stored at $-80\text{ }^{\circ}\text{C}$, if not used immediately.

Determination of molecular masses

Subunit molecular mass of purified proteins was determined by SDS-Page under reducing conditions with a 12.5% separating gel and 5% stacking gel described by Laemmli [6]. The used protein molecular mass marker was the PageRuler™ prestained protein ladder (10-180 kDa) from Thermo Fisher Scientific (Waltham, USA).

To determine native molecular masses size exclusion chromatography with buffer A using a Superdex 200 10/300 GL column attached to an Äktapurifier™ system from GE Healthcare (Little Chalfont, UK) was performed. Protein elution was monitored at 280 nm and 450 nm wavelength. The column was calibrated with molecular mass standards according to the instructions from GE Healthcare.

Methods using UV-visible absorption spectroscopy

Absorption spectra were recorded with a Specord 200 plus spectrophotometer from Analytik Jena (Jena, Germany) at $25\text{ }^{\circ}\text{C}$ using 1-cm quartz cuvettes.

The activity of 10 μg Ycp4p in the presence of NAD(P)H, FMN and MQ was tested under different conditions. NAD(P)H consumption was monitored at 390 nm.

Limited proteolysis

Ycp4p in buffer C was subjected to limited proteolysis at 37 °C by the addition of trypsin from Promega (Wisconsin, USA) to a final concentration of 2 µg·mL⁻¹. The reaction was stopped by adding SDS sample buffer to aliquots of the reaction mixture and immediately boiling at 95 °C for 10 min. The samples were analysed using 12.5% SDS-Page.

Sequence alignment

Sequence alignments of Pst2p, Rfs1p and Ycp4p with the FMN-dependent NQO WrbA from *E. coli* were performed with the program Clustal Omega [7]. Sequences for the yeast proteins were obtained from the *Saccharomyces* genome database [5]. The sequence from WrbA was obtained from the UniProt database [8].

Results

Trials to express and purify Ycp4p and Rfs1p with C-or N-terminal 6x-Histag resulted in either almost no soluble protein or in a protein solution with a very low purity. Therefor expression and purification of the proteins in combination with N-terminal 6xHis-tagged solubility enhancing fusion proteins, namely ZTZ, ZZ, DsbC, Gst, Trx, M11, GB1, DsbA, MBP and NusA was performed. In the case of Rfs1p only MBP and NusA fusion resulted in a stable fusion protein. Nevertheless all processing steps lead to significant loss of protein, which made it impossible to go on with the studies on this protein. Furthermore there was no cofactor detected at all steps (Figure 1).

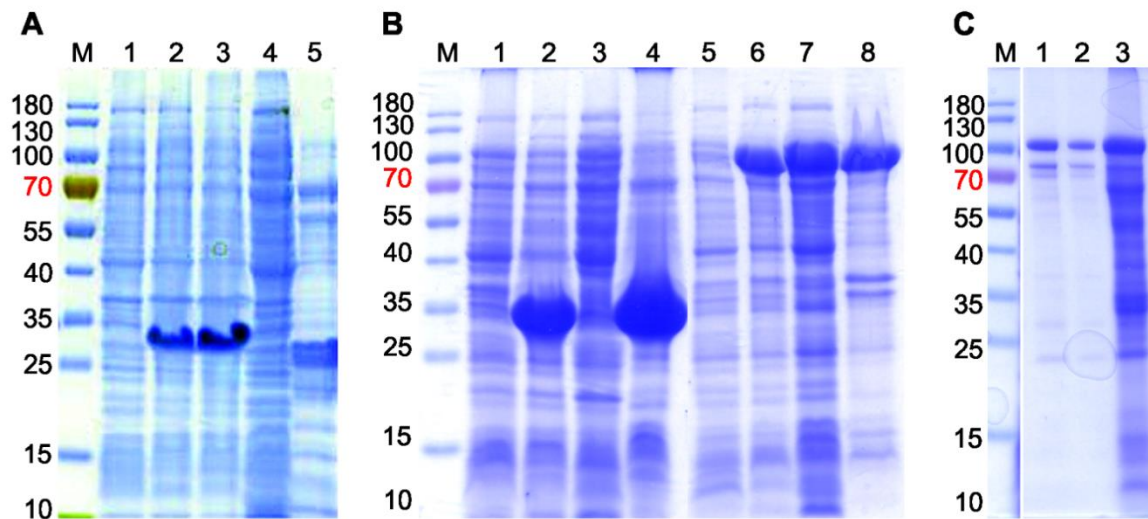


Figure 1. Rfs1p solubility and purification trials. **(A)** Expression and purification of C-terminal 6xHis-tagged Rfs1p. Lane M, PageRuler™ prestained protein ladder (10-180 kDa), lane 1, protein extract before induction; lane 2 protein extract after induction of Rfs1p; lane 3, insoluble fraction; lane 4, soluble fraction; lane 5, protein fraction after purification by Ni-NTA-sepharose. The subunit molecular mass of Rfs1p was estimated to be ~30 kDa. **(B)** Expression and purification of Rfs1p in combination with 6xHis-tagged fusion proteins, namely Disulfide bond formation protein A (DsbA) and N-utilization substance protein A (NusA). Lane M, PageRuler™ prestained protein ladder (10-180 kDa); lane 1, protein extract before induction; lane 2 protein extract after induction of Rfs1p-DsbA; lane 3, soluble fraction; lane 4, insoluble fraction; lane 5, protein extract before induction; lane 6, protein extract after induction of Rfs1p-NusA; lane 7, soluble fraction; lane 8, insoluble fraction **(C)** Lane M, PageRuler™ prestained protein ladder (10-180 kDa); lane 1, elution fraction Rfs1p-NusA; lane 2, soluble Rfs1p-NusA sample after buffer exchange via PD10 column; lane 3, precipitated sample eluted from PD10 column.

In the case of Ycp4p all fusion proteins increased the expression levels in comparison to simple His-tagged Ycp4p (Figure 2). Also the purification of Ycp4p-MBP was possible and furthermore also the separation of the two proteins by incubation with TEV protease overnight at 4 °C and removal of the His-tagged fusion protein and the His-tagged TEV protease by another Ni-NTA purification step were successful.

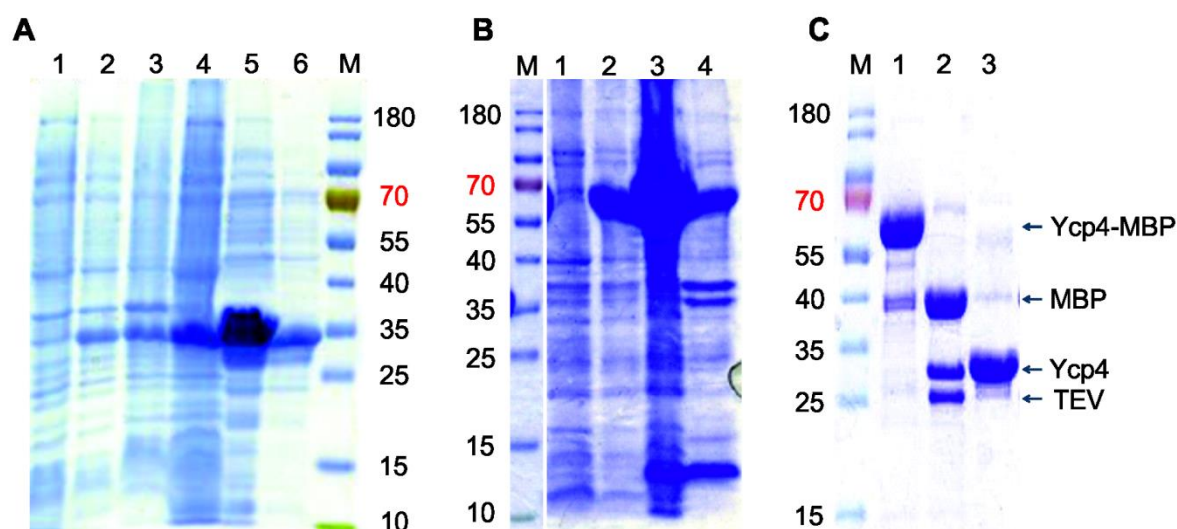


Figure 2. Ycp4p solubility and purification trials. **(A)** Expression and purification of C-terminal 6xHis-tagged Ycp4p. Lane 1, protein extract before induction; lane 2 protein extract after induction of *YCP4*; lane 3, insoluble fraction; lane 4, soluble fraction; lane 5, protein fraction after purification by Ni-NTA-sepharose; lane 6, precipitated protein after concentration; lane M, PageRuler™ prestained protein ladder (10-180 kDa). The subunit molecular mass of Ycp4p was estimated to be ~35 kDa. **(B)** Expression and purification of Ycp4p in combination with a 6xHis-tagged fusion protein, namely maltose binding protein (MBP). Lane M, PageRuler™ prestained protein ladder (10-180 kDa); lane 1, protein extract before induction; lane 2 protein extract after induction of Ycp4p; lane 3, soluble fraction; lane 4, insoluble fraction. **(C)** Separation of MBP and Ycp4p by digestion with a hexahistidine-tagged TEV-protease followed by another Ni-NTA purification step. Lane M, PageRuler™ prestained protein ladder (10-180 kDa); lane 1, Ycp4p-MBP uncuted; lane 2, Ycp4p-MBP after digestion with TEV protease at 4 °C overnight; lane 3, flow through of the second Ni-NTA purification step. No cofactor was observed during the purification process.

Analytical size exclusion chromatography indicated a size of ~175 kDa for Ycp4p, which means either that Ycp4p is present as pentamer or hexamer or it forms soluble aggregates (Figure 3).

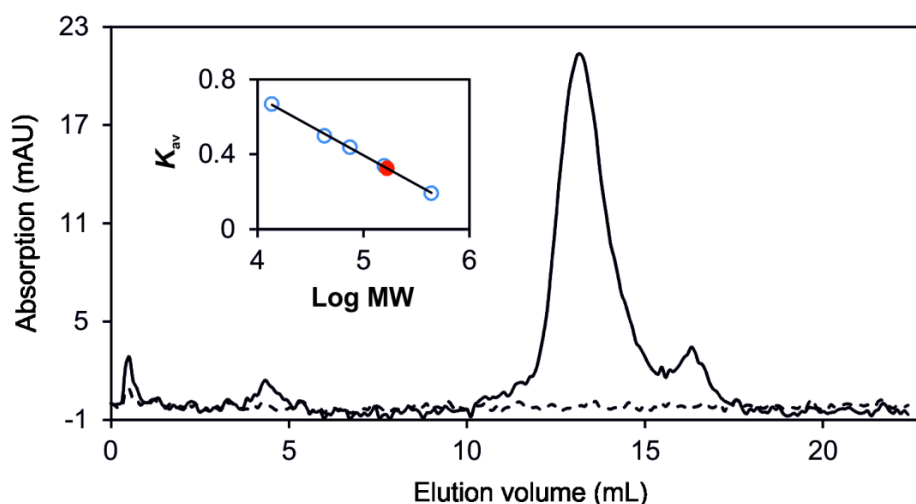


Figure 3. Determination of native molecular mass of Ycp4p (black, continuous line 280 nm and dashed line 450 nm) using analytical size exclusion chromatography. The elution profile of Ycp4p indicates that the protein lost the cofactor completely during passing the column. The insert shows a plot of the partition coefficient (K_{av}) against the logarithm of molecular mass of standard proteins (ferritin, 440 kDa; aldolase, 158 kDa; conalbumin, 75 kDa; ovalbumin, 43 kDa; ribonuclease A, 13.7 kDa). The calculated molecular mass of Ycp4p (~ 175 kDa, red circle) indicates that Ycp4p is present in a pentameric or hexameric form or forms soluble aggregates.

However, no cofactor was observed during the purification process. Trials to saturate Ycp4p afterwards with FMN and clarification of the sample from residual FMN with PD10-column were unsatisfactory (280/450 ~ 15-20; Value for Pst2p ~ 4.5). A spectral analysis of Ycp4p further indicates that no cofactor is bound to the protein, since the spectra of native and denatured sample look almost identical (Figure 4).

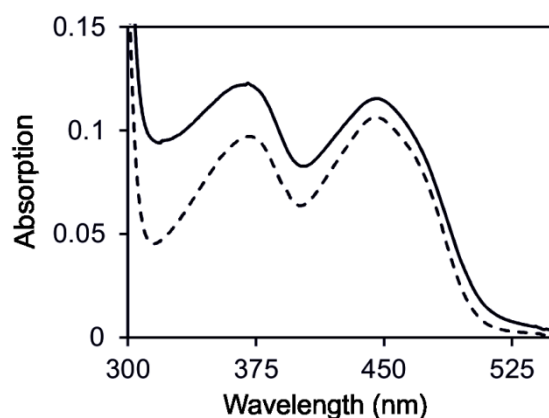


Figure 4. UV-visible absorbance spectra of Ycp4p before (solid line) and after denaturation (dashed line). Denaturation of purified Ycp4p was carried out in buffer C (50 mM Hepes, 50 mM NaCl, pH 7.0) containing 0.2 % SDS.

Nevertheless it could be demonstrated that Ycp4p has some FMN- and quinone reductase activity if the reaction mixture is supplemented with FMN (Figure 5).

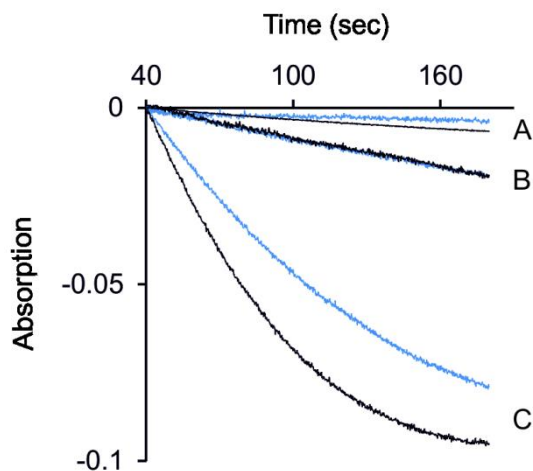


Figure 5. Activity of 10 μg Ycp4p with NADH (blue) or NADPH (black) was tested under different conditions. NAD(P)H consumption was monitored at 390 nm. A, 300 μM NAD(P)H, 200 μM MQ; B, 300 μM NAD(P)H, 100 μM FMN; C, 300 μM NAD(P)H, 100 μM FMN, 200 μM MQ; The results indicate that free FMN can directly be reduced by Ycp4 (B) but enhances also the efficiency if other substrates are converted (compare A and C).

A possible explanation for the unsatisfactory results with Ycp4p could be that the prolonged C-terminal part of Ycp4p destabilizes the whole protein. In order to investigate if this could be the case, limited proteolysis with trypsin at 37 °C with Ycp4p was performed, which revealed that one part of Ycp4p was digested within 20 min. The remaining fragment with a size of ~ 20 kDa showed a high stability and could still be observed after overnight digestion (Figure 6). The results indicate that indeed the prolonged C-terminal part can lead to an overall destabilization of Ycp4p. Further experiments would be necessary, as complete in-gel tryptic digestion of the protein bands from the limited proteolysis experiment with a subsequent peptide mass fingerprinting by MALDI-TOF MS to verify the identity of the C-terminus and the N-terminus followed by expression of truncated versions of Ycp4p.

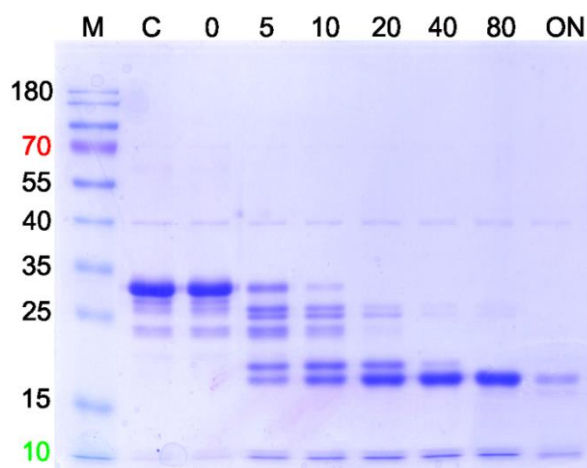


Figure 6. Limited proteolysis of Ycp4p with trypsin. SDS-Page showing trypsin digestion products of Ycp4p. The migration positions of the molecular weight marker (M) are indicated to the left of the gel. Lane 1, PageRuler™ prestained protein ladder (10-180 kDa); lane 2, protein suspension without trypsin; lane 3-9 digestion times are given in minutes above the gel (ON – overnight).

Discussion

During our studies we could demonstrate that *PST2* from *S. cerevisiae* can be heterologously expressed and the produced protein purified from *E. coli*. Similar expression experiments with *RFS1* and *YCP4* from *S. cerevisiae* were unsuccessful. Sequence alignments of WrbA from *E. coli* with Pst2p, Rfs1p and Ycp4p displayed a high homology of the proteins from 34-45%. Major differences are only present in form of an extension within a loop region in the case of Rfs1p and a C-terminal extension in the case of Ycp4p (Figure 7). Parameters computed with the program ProtParam (<http://www.expasy.org/tools/protparam.html>) revealed that within this 50 residues a high content of basic residues is present (22,2%) resulting in a really high pI of this segment of around 9.35. Further a palmitoylation site can be predicted at C243 (C244) with CSS-Palm [9]. Therefore it is very likely that this whole region is involved in membrane binding which was further reported from previous studies [10-12], but it is also possible that this segment led to solubility problems during expression and purification. Nevertheless only minor changes within the residues close to the redox-active isoalloxazine ring system were observed with the aligned proteins. Replacements were observed at R79K, T116I in the case of Rfs1p and at T116S in the case of Ycp4p. Therefore we suggest that all three proteins within *S. cerevisiae* show a similar activity.

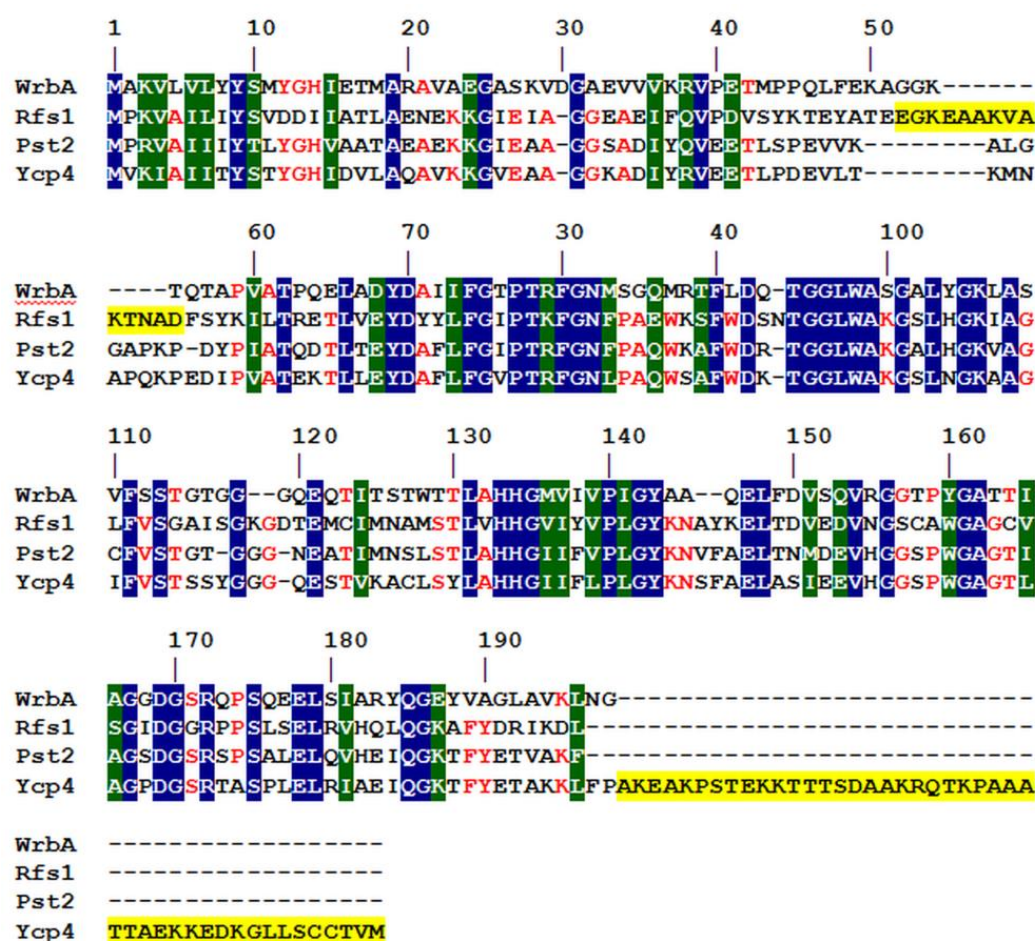


Figure 7. Sequence alignment of WrbA from *E. coli* with Pst2p, Rfs1p and Ycp4p from *S. cerevisiae*. Sequences were obtained from the *Saccharomyces* genome database. The overall sequence homology between WrbA and the yeast proteins is 34% (Rfs1p) to 45% (Pst2p and Ycp4p). Highly conserved regions are highlighted in blue, lower conserved regions are highlighted in green. Residues which are identical in three out of four proteins are depicted in red. Regions which are significantly different within the three yeast proteins are highlighted in yellow. Alignments were made with Clustal Omega.

References

- [1] J.C. Overeem, G.J.M. Kerk, Mollisin, a naturally occurring chlorine-containing quinone: Part III. The synthesis of dechloromollisin methyl ether and of related compounds, *Recl. Des Trav. Chim. Des Pays-Bas.* 83 (1964) 1005–1022.
- [2] P. Macheroux, UV-visible spectroscopy as a tool to study flavoproteins, *Methods Mol. Biol.* 131 (1999) 1–7.
- [3] C. Pashley, S. Kendall, Cloning in plasmid vectors, *Methods Mol. Biol.* 235 (2003) 121–135.

- [4] W.E. Swords, Chemical transformation of *E. coli*, *Methods Mol. Biol.* 235 (2003) 49–53.
- [5] J.M. Cherry, E.L. Hong, C. Amundsen, R. Balakrishnan, G. Binkley, E.T. Chan, K.R. Christie, M.C. Costanzo, S.S. Dwight, S.R. Engel, D.G. Fisk, J.E. Hirschman, B.C. Hitz, K. Karra, C.J. Krieger, S.R. Miyasato, R.S. Nash, J. Park, M.S. Skrzypek, M. Simison, S. Weng, E.D. Wong, *Saccharomyces* genome database: The genomics resource of budding yeast, *Nucleic Acids Res.* 40 (2012) 700–705.
- [6] K. Laemmli, Cleavage of structural proteins during the assembly of the head of bacteriophage T4, *Nature.* 227 (1970) 680–685.
- [7] F. Sievers, A. Wilm, D. Dineen, T.J. Gibson, K. Karplus, W. Li, R. Lopez, H. McWilliam, M. Remmert, J. Söding, J.D. Thompson, D.G. Higgins, Fast, scalable generation of high-quality protein multiple sequence alignments using Clustal Omega, *Mol. Syst. Biol.* 7:539 (2011) 1-6.
- [8] UniProtConsortium, A. Bateman, UniProt: A hub for protein information, *Nucleic Acids Res.* 43 (2015) D204–D212.
- [9] J. Ren, L. Wen, X. Gao, C. Jin, Y. Xue, X. Yao, CSS-Palm 2.0: an updated software for palmitoylation sites prediction, *Protein Eng. Des. Sel.* 21 (2008) 639-644.
- [10] F. Delom, W. Szponarski, N. Sommerer, J.C. Boyer, J.M. Bruneau, M. Rossignol, R. Gibrat, The plasma membrane proteome of *Saccharomyces cerevisiae* and its response to the antifungal calcofluor. *Proteomics* 6 (2006) 3029-3039.
- [11] G. Grossmann, J. Malinsky, W. Stahlschmidt, M. Loibl, I. Weig-Meckl, W.B. Frommer, M. Opekarová, W. Tanner, Plasma membrane microdomains regulate turnover of transport proteins in yeast, *J. Cell Biol.* 183 (2008) 1075-1088.
- [12] F. Cardona, H. Orozco, S. Friant, A. Aranda, M.I. del Olmo. The *Saccharomyces cerevisiae* flavodoxin-like proteins Ycp4 and Rfs1 play a role in stress response and in the regulation of genes related to metabolism. *Arch. Microbiol.* 193 (2011) 515-525.

3.3 Overexpression of the yeast bZIP transcription factor Yap4p, an interaction protein of the flavodoxin-like protein Lot6p

Karin Koch, Karin Athenstaedt, Venugopal Gudipati, Karl-Heinz Grillitsch and Peter Macheroux

Institute of Biochemistry, Graz University of Technology, Petersgasse 12/2, 8010

Author contributions

P.M. initiated the project; K.K., K.A., K.-H. G., V.G. and P.M. designed the experiments and interpreted the data; K.K. performed all experiments discussed in this chapter except the analysis of individual sterols which was performed by K.-H.G. K.A. guided K.K. through the lipid methods.

Abbreviations

bZIP, basic leucine zipper; *E. coli*, *Escherichia coli*; GLC, gas liquid chromatography ; Lot6, low temperature responsive 6; *S. cerevisiae*, NQO1, NAD(P)H:quinone oxidoreductase 1; *Saccharomyces cerevisiae*; SE, sterol esters; TF, SD-ura; synthetic dextrose media lacking uracil; SG-ura; synthetic galactose media lacking uracil; transcription factor; TG, triacylglycerols; Yap, yeast activator protein;

Introduction

The genome of the yeast *Saccharomyces cerevisiae* encodes for ca. 209 transcription factors (TFs) [1]. Transcription factors have the ability to bind short DNA sequence motifs and thereby affect gene expression in a positive or negative way [2]. Due to specific binding domains most TFs can be subdivided into six main families: these domains are the zinc cluster (57 proteins), the zinc finger (41 proteins), the basic leucine zipper (bZIP) (15), the homeodomain (12), the GATA domain (10) and the basic helix-loop-helix (8) [1]. In yeast it is difficult to define the regulatory network from specific TFs since most of them are not essential under normal growth conditions. This can be attributed to the fact that many TFs regulate an overlapping subset of genes [1]. Furthermore the ability to form heterodimers which confer different DNA sequence specificities complicate this issue [3].

With 15 members the family of bZIP proteins is the second largest group of dimerizing TFs within the yeast *S. cerevisiae* [1]. The uniform bZIP-motif is 60-80 amino acids long with two clusters of basic amino acids at the N-terminal side and an amphiphatic sequence with a leucine at every seventh position at the C-terminal side. While the basic region is involved in DNA binding the leucine zipper is responsible for dimerization of the TF [3]. Within the family most members (8) can be further divided into the subfamily of yeast activator proteins (Yap) which play a role under various stress conditions, such as oxidative stress (Yap1/3/4) [4–6], cadmium stress (Yap2) [7], arsen stress (Yap1/8) [7], osmotic stress (Yap4/6) [8,9] nitrogen depletion (Yap5/7) [10,11] and DNA damage response (Yap1/2/4/5/6) [12,13]. Further specific family members are involved in the regulation of iron metabolism (Yap1/5) [7] and cell cycle (Yap4/6) [14–16]. Despite the similarities within the family members this variety of functionalities originates from small differences in the DNA binding motif

(TTAn(x)TAA) [12], the binding pattern (constant or transient binding, rapid or slow induction) [9], the mode of action [activation (Yap1) or repression of gene expression or both (Yap2/4/5/6)] [12], activation signals (e.g. phosphorylation of Yap4p [17] or disulfid bond formation of Yap1p [18]), and regulation of other transcription factors (Yap4/6) [19].

YAP4 was initially described as chromosome instability mutant (CIN5) [14] and as transcription factor which is involved in the regulation of gene expression under osmotic stress (HAL6) [20]. As mentioned above *YAP4* expression is upregulated in several stress and non-stress related processes and the protein gets modified by phosphorylation under these conditions which increases the stability of the protein but does not influence its functionality under stress conditions [6,8,21]. Yap4p has a close homolog Yap6p which has a sequence identity of 20 % and an overlapping functionality [7]. However, the exact role of these two proteins in the transcriptional network is mainly unclear. In former studies Yap4p gained attention since evidences suggested that this largely unstructured protein can be rescued in a redox-dependent manner from degradation by the 20S proteasome by binding to the NAD(P)H:quinone reductase Lot6p [22]. A process which is also described in humans, were NAD(P)H:quinone oxidoreductase 1 (NQO1) physically interacts with transcription factors like p53 or p73 and the 20S proteasome, which prevents the ubiquitin-independent degradation of these intrinsically disordered proteins. The degradation of the proteins can occur also in an ubiquitin-dependent process, which is not influenced by the presence of NQO1 [23].

During former studies in our laboratory Sonja Sollner, Wolf-Dieter Lienhart and Venugopal Gudipati set out to express and purify Lot6p as well as the 20S proteasome to high purity (data not shown). However, the instability of Yap4p and the low purity prevented a detailed structural investigation of the proposed mechanism and interaction of these three proteins. Expression and purification of Yap4p from *E. coli* [24] as well as from *S. cerevisiae* [25] were unsatisfactory. In the present study it was set out to express Yap4p with a solubility enhancing fusion protein (maltose binding protein) and in combination with Yap6p to investigate if Yap4p expression and purification can be improved by these strategies. However, no improvement could be achieved.

From the expression studies in *S. cerevisiae* we came to know that strong overexpression of *YAP4* in *S. cerevisiae* leads to significant changes in the cell cycle

prior to mitosis and to an accumulation of lipid droplets [25]. This prompted us to investigate the importance of phosphorylation on the growth behaviour as well as on stress resistance. The phosphorylation mutants exhibit the same growth defect as the *YAP4* overexpressing strain and were also less sensitive against oxidative stress compared to the wild type strain. Further the neutral lipid content was analysed to determine if specific changes occur if *YAP4* is overexpressed. During the exponential growth phase the content of sterol esters (SE) and triacylglycerols (TG) was increased, while at the stationary phase only a higher SE content was observed, whereby all sterol precursors showed elevated levels. Several genes of the ergosterol biosynthesis pathway contain regulatory elements within their promoter regions, however, higher mRNA levels in the *YAP4* overexpressing strain were only observed for genes which encode for oxygen-dependent enzymes. Interestingly also the sterol ester hydrolases *YHE1* and *YHE2* exhibit higher mRNA levels, which stands in contrast to the increased content of sterol esters within the overexpressing strain.

Materials and Methods

Materials

All chemicals were of highest quality and were obtained from Sigma-Aldrich (St. Louis, USA) or Carl Roth (Karlsruhe, Germany), unless otherwise noted. The *E. coli* strain Top10 was purchased from Invitrogen (Carlsbad, USA). The *E. coli* strains BL21(DE3) and RosettaTM(DE3) were obtained from Merck (Darmstadt, Germany). The chaperone plasmid set was obtained from Takara Bio Europe (Saint-Germain-en-Laye, France). The *S. cerevisiae* strains BY4741 (MATa, his3 Δ 1, leu2 Δ 0, met15 Δ 0, ura3 Δ 0) were from Euroscarf (Frankfurt, Germany) and correct depletion was ensured by colony PCR with GoTaq[®] DNA polymerase from Promega (Madison, USA). Following plasmids were used: pMAL-c4E from NEB (Ipswich, USA), pET21a(+) and pET28a(+) from Merck (Darmstadt, Germany) and pYES2 from Invitrogen (Carlsbad, USA). Restriction enzymes, Phusion high-fidelity DNA polymerase and T4 DNA Ligase were obtained from Thermo Fisher Scientific (Waltham, USA).

Molecular cloning

All strains were generated using standard genetic techniques [26–28]. Briefly, genomic DNA from *S. cerevisiae* was extracted with yeast DNA extraction kit from VWR (Radnor, USA). According to the sequence for *YAP4* and *YAP6* from the *Saccharomyces* genome database [29] primers for cloning were designed and synthesized from VBC (Vienna, Austria): Primers for *YAP4-MBP* expression (pMAL-c4e) to produce N-terminal MBP-tagged Yap4p: fw_5'-ATGTTAATGCAAATAAAAATGGACAATC-3'; rev_5'-CTTCAAGCTTATTCTTTAATTTCGAC-3' Primers for *YAP6* expression [pET28a(+)] to produce untagged protein: fw_5'-GAGCCCATGGAGATGCAAACCCTCCGTTGATTTCG-3'; rev_5'-CCTGCTCGAGTTACGTGGCACTATCCGAGTGTC-3'. The pET21a(+)*YAP4* plasmid was used from a previous study from Sonja Sollner *et al.* [22], the primers to express C-terminal 6xHis-tagged Yap4p were fw_5'-GGAATTCCATATGTTAATGCAAATAAAAATGGACAATC-3'; rev_5'-CCGCTCGAGTTCTTTAATTTTCGACTTTAATGATTCAATC-3'. Plasmids containing Yap4 and several mutants of it (YIplac211-*YAP4TAP*; mutants: S89A, T192A, T192AS196A, S196A, K242AR243A) were kindly provided from Prof. Claudina Rodrigues-Pousada. The mutants were sub cloned into the pYES2 vector using the primers, for expression of N-terminal 9xHis-tagged Yap4p [25] (fw_5'AGATAAAGCTTATGCACCATCACCACCATCACCATTTAATGCAAA TAAAATGG-3'; 9xHis_Yap4_rev 5'-GTGGTGGTGGTGGTGGTCTCGAGTTATTCTTTAATTTTCGACTTTAATGATTC-3'). The code for the respective restriction enzymes was included in the primer sequences. Restriction and blunt end (pMAL-c4E) or sticky end (pET-vectors and pYES2) ligation were performed according to the protocols from Thermo Fisher Scientific (Waltham, USA). Individual clones were sequenced before transforming the plasmids into various expression strains (*E. coli* or *S. cerevisiae*).

Heterologous expression of YAP4 (fusionprotein and co-expression)

A single colony of *E. coli* BL21(DE3) comprising pET21a(+)*YAP4* and pET28a(+)*YAP6* or pMAL-c4E-*YAP4* was used to inoculate a pre-culture that was aerobically incubated (37 °C, 16 h, 150 rpm) in lysogeny broth (bacto-tryptone 10 g/L, bacto-yeast extract 5 g/L, NaCl 5 g/L) supplemented with 100 µg/mL ampicillin and 50 µg/mL kanamycin (co-expression) or only with 100 µg/mL ampicillin (fusionprotein). 1% ONC was used to inoculate the main-culture supplemented with 100 µg/mL

ampicillin, which was incubated aerobically at 37 °C with agitation at 150 rpm until an OD_{600} of ~0,6 was reached. Expression of the genes was induced by addition of 0.5 mM isopropyl-thio- β -d-galactoside. The culture was further incubated for 16 h at 20 °C. Cells were harvested by centrifugation at 4.500 x g at 4 °C and washed once with 1% saline solution.

Purification of Yap4p (fusionprotein)

Purification was performed as described in the protocol from NEB (Ipswich, USA - pMAL™ Protein Fusion and Purification System). Cell pellets were resuspended in 4 mL buffer A /g pellet (20 mM Tris-HCl, pH 7.0, 200 mM NaCl, 1 mM EDTA); buffer was supplemented with 1 mM phenylmethylsulfonyl fluoride solved in dimethylsulfoxide, and further 1 μ L of protease inhibitor cocktail for use in the purification of histidine-tagged proteins from Sigma-Aldrich (St. Louis, USA) was added per g of cell pellet. Cell disruption was achieved by sonication with a Labsonic L instrument from Braun Biotech. International (Berlin, Germany) with 120 Watt for 3 x 3 min in an ice-water bath with 3 min pauses between each cycle. The cell lysate was centrifuged at 38.850 x g for 45 min at 4 °C, and the supernatant was loaded onto a 15 ml amylose column previously equilibrated with buffer A. The column was washed with buffer A and subsequently proteins were eluted with buffer A supplemented with 10 mM maltose. Fractions containing target protein were pooled and concentrated with centrifugal filter units (Amicon Ultra-15, 10 k; Millipore, Billerica, MA, USA). Concentrated protein was re-buffered to buffer A with a PD-10 desalting column. Cleavage of the fusion protein was achieved by digestion with enterokinase (0.5 ng/50 μ g fusionprotein). Digestion was completed within four hours at 4 °C. Separation of the proteins was achieved by rebinding MBP to the amylose resin, while Yap4p was in the flow through. The protein solutions were shock frozen and stored at -80 °C, if not used immediately.

Purification of Yap4p (co-expression)

Initial steps of purification were carried out as for the fusionprotein purification. Except that buffer B (50 mM Hepes, pH 7.0, 150 mM NaCl) was used and supernatant was loaded onto a 5-mL HisTrap HP column previously equilibrated with buffer B. The column was washed with buffer B supplemented with 10 mM imidazole and subsequently proteins were eluted with buffer B supplemented with 300 mM

imidazole. Fractions containing target protein were pooled and concentrated with centrifugal filter units (Amicon Ultra-15, 10 k; Millipore, Billerica, MA, USA). Concentrated protein was re-buffered to buffer C (50 mM Hepes, pH 7.0) with a PD-10 desalting column. The protein solutions were shock frozen and stored at $-80\text{ }^{\circ}\text{C}$, if not used immediately.

Neutral lipid analysis

Total cell extracts for lipid analysis were prepared from yeast cells grown to the early logarithmic or early stationary phase in induction medium. Cells were harvested by centrifugation at $2500 \times g$ for 5 min at $4\text{ }^{\circ}\text{C}$. The cells were washed with ddH₂O and frozen at $-70\text{ }^{\circ}\text{C}$ for one hour. Cells were resuspended in ddH₂O and lysis was performed by vigorous shaking in the presence of glass beads for 3x3 min at $4\text{ }^{\circ}\text{C}$. Lipids from total cell extracts were isolated by the method of Folch *et al.* [30] using chloroform/methanol (2:1; vol/vol). Lipid extracts were applied to thin layer chromatography plates (silica gel 60). Lipid extracts were applied to thin layer chromatography (TLC) plates (silica gel 60). Chromatograms were developed in an ascending manner in a solvent system containing light petroleum/diethyl ether/acetic acid (20:20:0.8; per vol.) to 1/3 of the distance, briefly dried and further developed using a second solvent system containing light petroleum/diethyl ether (39.2:0.8; v/v) to 2/3 of the distance. To visualize the separated neutral lipid bands the TLC plates were immersed for 6 sec in a solution containing 0.63 g MnCl₂·4H₂O, 60 mL water, 60 mL methanol, and 4 mL concentrated sulfuric acid. Afterwards the plates were incubated in a heating chamber at $105\text{ }^{\circ}\text{C}$ for 30 min. Triacylglycerols and sterol esters were quantified by densitometric scanning at 275 and 400 nm, respectively, using a Shimadzu dual wavelength chromatoscanner CS-930 (Kyoto, Japan). Triolein from Nu-Check Prep (Waterville, USA) and ergosterol from Sigma-Aldrich (St. Louis, USA) were used as standards.

After alkaline hydrolysis of the lipid extract [31] individual sterols were analysed by gas liquid chromatography (GLC). GLC was performed on a Hewlett-Packard 5890 equipped with a flame ionization detector operated at 320°C , using a capillary column (Hewlett-Packard 5; 30 m with 0.32 mm and 0.25 μm film thickness). After a 1-min hold at $150\text{ }^{\circ}\text{C}$, the temperature was increased to $310\text{ }^{\circ}\text{C}$ at $10\text{ }^{\circ}\text{C}/\text{min}$. The final temperature was held for 10 min. Nitrogen was used as the carrier gas, and 1 μl

aliquots of samples were injected onto the column. Cholesterol from Sigma-Aldrich (St. Louis, USA) was used as internal standard.

RNA isolation and real time PCR

Total RNA from cells grown to the early exponential phase (OD_{600} 0.8-1) in induction medium at 30 °C was isolated using the RNeasy kit from Qiagen (Hilden, Germany) following the manufacturer's instructions (including on-column digestion with DNaseI). Reverse transcription was performed with iScript™ cDNA synthesis kit from Biorad (California, USA) according to the instructions. Real time PCR was performed with the SsoAdvanced™ Universal SYBR® Green supermix from Biorad (California, USA) as described by the manufacturer (amplification temperature 61.2 °C). Reactions were performed in 96-well plates sealed with an optical-quality sealing tape from Bio-Rad (California, USA) and amplification was performed in a CFX Connect™ Real-Time PCR detection system from Bio-Rad (California, USA). Differences in mRNA expression relative to a control (*ACT1*) were quantified with the $\Delta\Delta C_t$ method [32]. The used primers are listed in Table 1.

Table 1. List of primers used in this study for real time PCR

<i>ACT1</i>	fw_5'-CCAGCCTTCTACGTTTCCATCCAAG-3' rev_5'-GACGTGAGTAACACCATCACCGGA-3'
<i>ARE1</i>	fw_5'-CCACCTGCTCTTCGACATGATTCC-3' rev_5'-GGTCAACTCCGCCACGCAATTCAA-3'
<i>ARE2</i>	fw_5'-TATCCTGTAGCAATGAGAGCATTGGCT-3' rev_5'-ATAAACCTGGGACGATATCAACGAG-3'
<i>ERG3</i>	fw_5'-GCAGGTGCCATTCTGTTTG-3' rev_5'-ACACGTAGCTGAGACTAGCC-3'
<i>ERG7</i>	fw_5'-TTCCATGGTCCACAGGGTATG-3' rev_5'-ACTACCTGGAACGCACTCG-3'
<i>ERG9</i>	fw_5'-TGACTTGTTGCGTCACTTCC-3' rev_5'-GTCGTAGTCGTGGACGGT-3'
<i>ERG11</i>	fw_5'-TGCACCATCCATTGCACTCT-3' rev_5'-CCGACGGAATAAGAGGAGGC-3'
<i>TGL1</i>	fw_5'-GACATGGAAGACAACCTCATCCAACGCATG-3' rev_5'-GACCTCATCCGCTTCATCAGCTTGTAC-3'
<i>YHE1</i>	fw_5'-GAAGTTGATGCAATGGTGGCTGTCAC-3' rev_5'-GTCTGAAAACCACTTAACATTGTGGGGAAC
<i>YHE2</i>	fw_5'-GCAATGGTGGTTGTACCTCTTCCTAATAAG-3' rev_5'-CTGTCATCATCATTCTTGGCAATAGGAAACCATG-3'
<i>YAP4</i>	fw_5'-TGCATCACACGCACCATTTG-3' rev_5'-GGAAGGTTAGTCGTGGCACT-3'

Yeast growth assay

A single colony of the respective strains was grown for 24 h in synthetic dextrose medium [0.67% amino acid free yeast nitrogen base, 2% carbon source, 0.01% (adenine, arginine, cysteine, leucine, lysine, threonine, tryptophan, uracil), 0.005% (aspartic acid, histidine, isoleucine, methionine, phenylalanine, proline, serine, tyrosine, valine) lacking uracil (SD-ura)] with orbital shaking (200 rpm) at 30°C. About 100 mL of fresh synthetic galactose medium lacking uracil (SG-ura) was inoculated with pre culture to an OD₆₀₀ of 0.1. Cell growth in induction medium was monitored by OD₆₀₀ readings all six hours for up to 96 hours. Measuring points are mean values of three replicates.

Colony forming unit (Cfu) assay

Respective strains were grown to early exponential phase (OD₆₀₀ 0.8-1) in induction medium at 30 °C with orbital shaking (200 rpm). At this point various concentrations (0.3 mM, 1 mM and 3 mM) of H₂O₂ were added to the culture and the cells were allowed to grow for three more hours. To assess the viability, the cultures were serially diluted and plated on YPD plates. Cultures were differentially diluted, plated on YPD (10 g/L yeast extract, 20 g/L tryptone, 20 g/L glucose) and were grown for 2–3 days in an incubator at 30 °C The number of colonies was determined after incubation for 2-3 days at 30°C. Untreated samples were used as control. All tests were performed at least in triplicate.

Results

Expression and purification of Yap4p (fusion protein and co-expression)

Previous attempts to express *YAP4* and purify the protein to adequate purity to perform co-crystallization experiments with Lot6p were insufficient [24,25]. Since expression and purification from *E. coli* as well as from *S. cerevisiae* failed, *YAP4* expression with an attached fusion protein (MBP) in *E. coli* was performed with the expectation to increase protein expression, folding and stability [33]. However, fusion protein expression leads only to a marginal better expression level. Further it could be demonstrated with size exclusion chromatography that the fusion protein mainly forms soluble aggregates (elution at void volume) (Figure 1, panel B). Varying

conditions and the presence of chaperones did not improve expression of soluble protein. Even if separation of Yap4p and MBP by cleavage of the fusion protein with enterokinase was successful (Figure 1, panel A), Yap4p precipitated after this reaction.

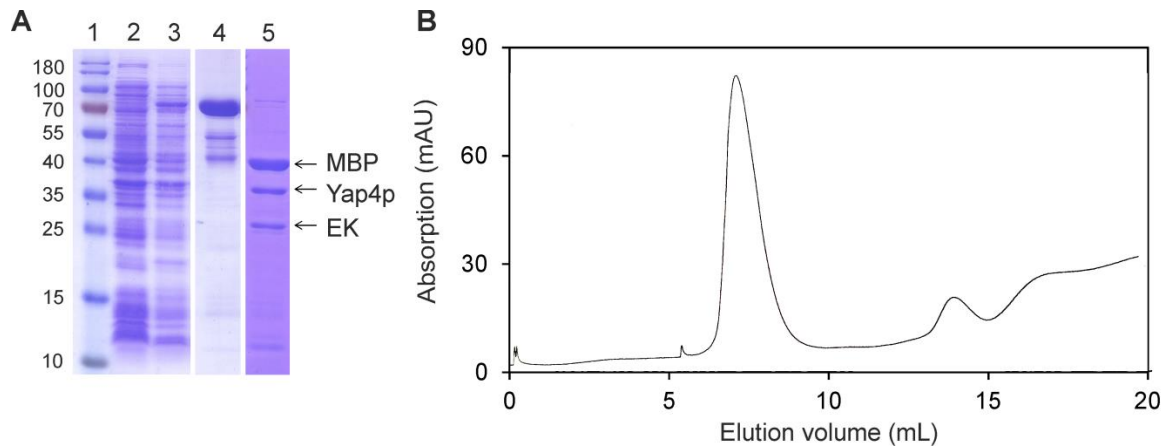


Figure 1. Determination of molecular masses of denatured and native MBP-Yap4p fusionprotein. **(A)** Determination of purity and molecular masses of MBP-Yap4p fusionprotein and the individual proteins after cleavage with enterokinase. Lane 1, PageRuler™ prestained protein ladder (10-180 kDa); lane 2, protein extract before induction; lane 3, protein extract after induction; lane 4, protein fraction after purification by Ni-NTA-sepharose; lane 5, sample after cleavage of the fusionprotein with enterokinase (EK). The molecular mass of the fusion protein was estimated to be ~80 kDa. **(B)** The elution of the fusionprotein occurred in the void volume (2000 kDa) indicating that it forms soluble aggregates.

Since it was reported that bZIP proteins have the ability to form heterodimers [3,34] co-expression of *YAP4* and its closest homolog *YAP6* was performed to investigate if a heterodimer can be formed and if it shows better folding and stability. Unfortunately, no stabilization of His-tagged Yap4p could be achieved by co-expression (Figure 2, panel A and B). Again a variation of the conditions and the presence of chaperones did not improve expression and solubility.

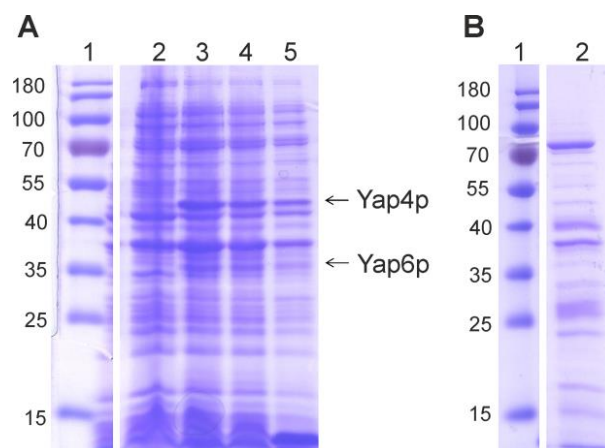


Figure 2. Coexpression of 6xHis-tagged Yap4p and untagged Yap6p in *E. coli*. **(A)** Lane 1, PageRuler™ prestained protein ladder (10-180 kDa); lane 2, protein extract before induction; lane 3, protein extract after induction; lane 4, soluble protein fraction; lane 5, insoluble. **(B)** Lane 1, PageRuler™ prestained protein ladder (10-180 kDa); lane 2, protein fraction after purification by Ni-NTA-sepharose.

Analysis of neutral lipids in total cell extracts and gene expression regulation of cells lacking or overexpressing YAP4

Before it could be demonstrated by fluorescence microscopy that the *YAP4* overexpressing strain exhibits a higher amount of lipid droplets in the early exponential phase [25]. This prompted us to analyse the neutral lipid content of cells lacking or overexpressing *YAP4* at the early exponential phase (Figure 3, panel A) as well as in the early stationary phase (Figure 3, panel B). During logarithmic growth the $\Delta YAP4$ strain showed comparable amounts of SE and TG to the wild type strain, in contrast to the *YAP4* overexpressing strain which comprises double the amount of SE and TG. In the stationary growth phase TG levels in all strains were comparable, while the SE content was still ~1.5 fold increased in the *YAP4* overexpressing strain.

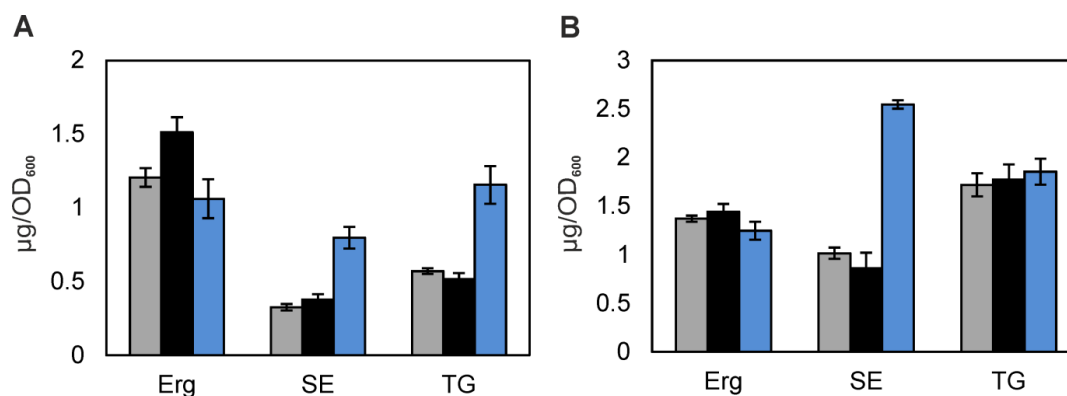


Figure 3. Effect of depletion or overexpression of *YAP4* on neutral lipid composition. For lipid analysis cells were grown on SG-U containing at 30°C to the mid-log phase (a) and the early stationary phase (b). Total lipids from wild type (grey), $\Delta YAP4$ (black) and *YAP4* overexpression strains were extracted, separated and analysed by TLC. Amounts of SE and TG are shown as $\mu\text{g}/\text{OD}_{600}$. Data are mean values of three independent experiments. Error bars indicate the standard deviation.

To investigate the SE composition, individual sterols were analysed by GLC in the sample of the logarithmic growth phase (Figure 4, panel A) and the stationary growth phase (Figure 4, panel B). Particular sterol precursors showed elevated levels in the *YAP4* overexpressing strain, namely squalene, 4-methylzymosterol, episterol and lanosterol, while in the stationary phase all sterol precursors were abundant in a higher amount in comparison to the wild type and the $\Delta YAP4$ strain.

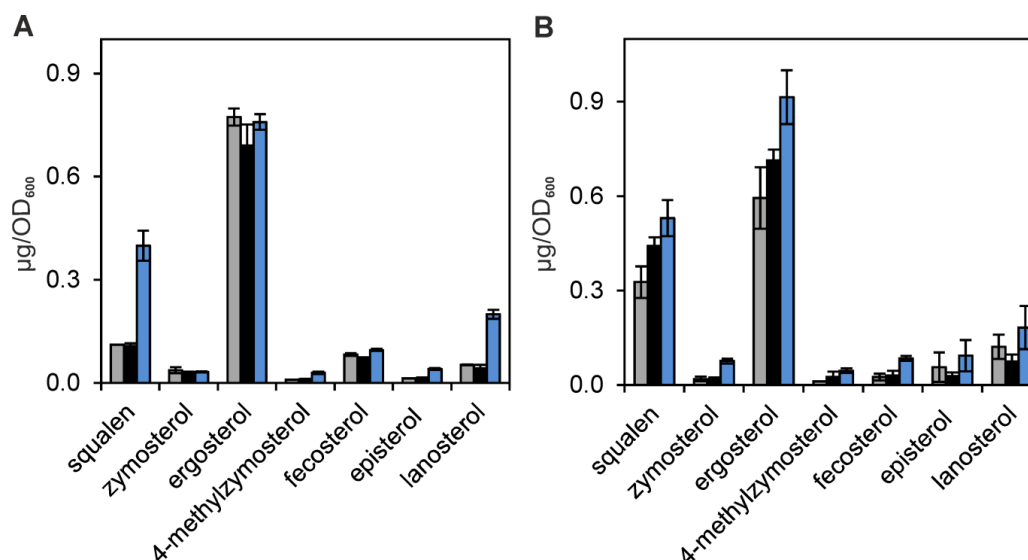


Figure 4. Sterol composition of yeast cells in logarithmic (A) and stationary growth phase (B). Cells were grown on SG-U containing at 30°C. Total lipids from wild type (grey), $\Delta YAP4$ (black) and *YAP4* overexpression strains were extracted and subjected to MS analysis of sterols. Amounts of individual sterols are shown as $\mu\text{g}/\text{OD}_{600}$. Data are mean values of two independent experiments. Error bars indicate the standard deviation.

The YEASTRACT database was used to investigate whether genes involved in the ergosterol biosynthesis pathway contain the Yap4p targeting sequence (TTACATAA [12]) [35]. This approach revealed 17 potential target genes (*ERG28*, *ERG4*, *ERG25*, *ERG11*, *NSG1*, *ERG9*, *ERG3*, *ATG26*, *HMG2*, *ERG13*, *ERG5*, *ERG8*, *CYB5*, *MVD1*, *HES1*, *KES1*, *ERG7*, *GRE2*). The involvement of the corresponding proteins in squalene and lanosterol synthesis prompted us to determine the expression levels of *ERG9* and *ERG7*, further the expression level of genes encoding for two oxygen-dependent enzymes (*ERG3* and *ERG11*) was determined by real-time PCR. Further primers for *ARE1* and *ARE2* (sterol ester synthases), *TGL1*, *YHE1* and *YHE2* (sterol ester hydrolases) were kindly provided by Prof. Günther Daum and Dr. Karin Athenstaedt. Furthermore the mRNA levels of *YAP4* in wild type and overexpression strain were determined. Increased mRNA levels were determined for *ERG3*, *ERG11* and *YEH2* (2-fold) and *YEH1* (5-fold) (Figure 5). The mRNA level of *YAP4* was ~30 times higher in the overexpression strain than in the wild type strain.

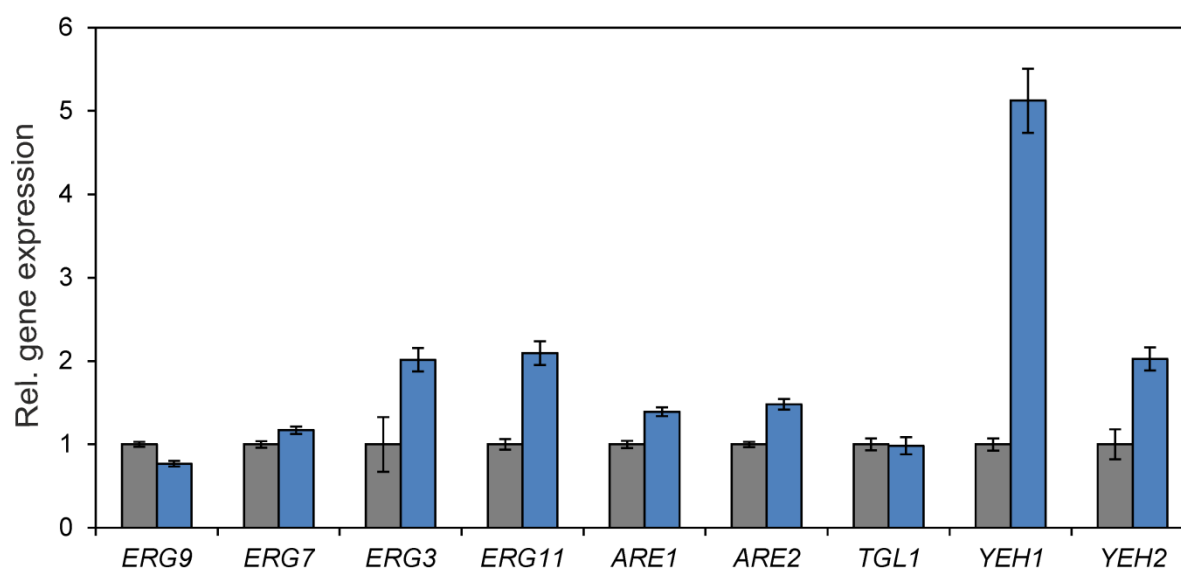


Figure 5. Gene expression of genes involved in ergosterol biosynthesis (*ERG9*, *ERG7*, *ERG3* and *ERG11*), SE formation (*ARE1* and *ARE2*) and SE hydrolysis (*TGL1*, *YEH1* and *YEH2*). Relative gene expression of the genes in wild type (grey) and *YAP4* overexpressing strain was quantified by real-time PCR. The wild type value was set to 1. Data are mean values from three independent experiments with the respective deviation.

Growth and stress resistance of YAP4 mutants

Growth assays from former studies demonstrated that *YAP4* overexpression under control of *GAL1* promoter in yeast leads to significant growth defects because the cell cycle is delayed at G_0/G_1 phase [25] (Figure 6, panel A).

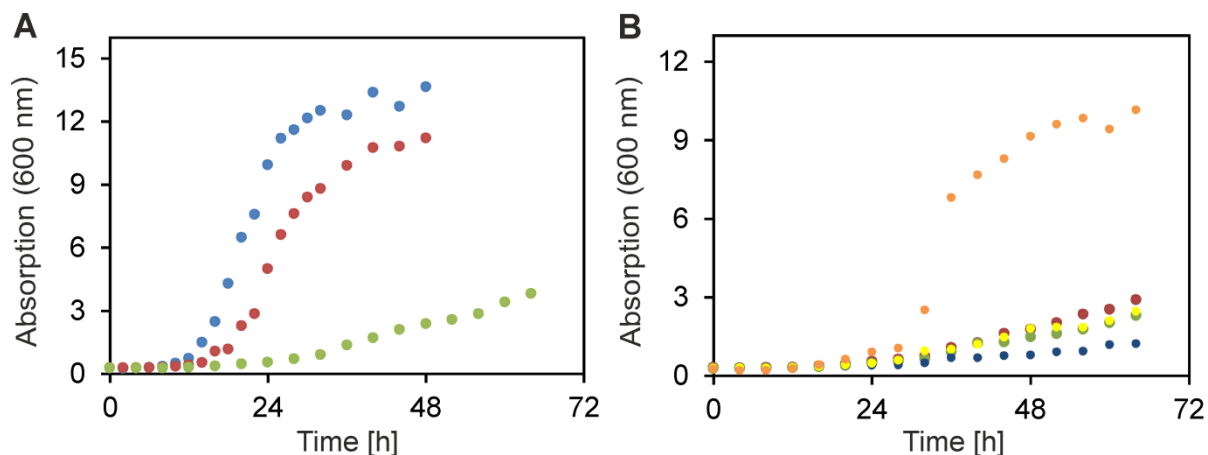


Figure 6. Effect of depletion or overexpression of *YAP4* and *YAP4* phosphorylation and DNA binding mutants on cell growth. **(A)** • wild type • $\Delta YAP4$ • *YAP4* overexpression strain **(B)** • Yap4p-S89A, • Yap4p-T192A, • Yap4p-S196A, • Yap4p-T192AS196A, • Yap4p-K242AR243A. Growth was monitored by measuring the absorbance at OD_{600} every six hours. The shown data points were generated as mean values of three replicates.

To investigate whether mutation of phosphorylation sites (S89A, T192A, S196A, T192AS196A) or within the basic DNA binding region (K242AR243A) affects the cell growth, assays with respective strains were conducted (Figure 6, panel B). All phosphorylation mutants displayed an impaired growth. The growth behaviour of the K242AR243A mutant was comparable to the wild type strain. However, the lag-phase is prolonged within this mutant. Despite the prediction to be a nuclear localization signal, it could be demonstrated that Yap4p*K242AR241A has no impairment in its localization, but it displayed a reduced stress resistance [17]. The author concluded that mutations within the basic region abolish the ability of Yap4p to bind to DNA and therefore Yap4p cannot perform its function in gene expression regulation. This conclusion is further supported by our growth assay.

Previous studies demonstrated that *YAP4* overexpressing cells are less sensitive against oxidative stress [25] and that the protein gets phosphorylated under these stress condition at the positions T192, S196 [21] and S89 [6]. To investigate the

sensitivity of the cells if phosphorylation at the respective sites is abolished, cells harbouring *YAP4* mutants were exposed to oxidative stress (H_2O_2) (Figure 7).

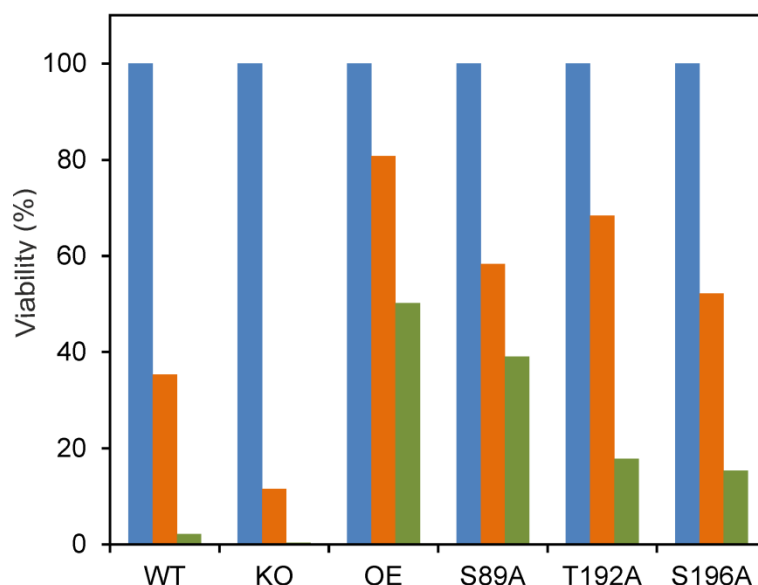


Figure 7. Effect of depletion or overexpression of *YAP4* and *YAP4* phosphorylation mutants on oxidative stress resistance. Cells grown to early exponential phase in SG-U containing at 30°C were treated with various amounts of H_2O_2 (0 mM blue; 0.3 mM orange; 3 mM green) over three hours. After the treatment appropriate quantities were plated onto YPD and colonies were counted after 2-3 days.

All phosphorylation mutants exhibited a higher viability than the wild type strain. In the presence of 3 mM H_2O_2 S89A displayed comparable viability to the *YAP4* overexpressing strain (~40% vs. 50%), the mutation of T192 and S196 were more pronounced (~15% viability). This points out that phosphorylation of T192 and S196 are from higher importance than phosphorylation of S89, which corresponds to the results from *Pereira et al.* [21].

Discussion

Expression experiments in *E. coli* were carried out to purify Yap4p to an adequate purity to perform co-crystallization experiments with Lot6p and the 20S proteasome. The experiments were unsuccessful due to the low stability of Yap4p under all tested conditions, which most likely can be attributed to the high flexibility of the protein. Former trials to express Yap4p in *S. cerevisiae* were also unsuccessful, but revealed

a significant growth defect if *YAP4* expression is under control of the very strong *GAL1* promoter. However, under control of the weaker copper promoter (*CUP1*) no significant growth differences were observed (data not shown), which indicates that growth inhibition occurs only at very high Yap4p contents. Interestingly, this effect was only observed with *YAP4* and *YAP6* overexpression, while overexpression of other YAP members had no influence on the growth rate [36]. On the one hand this indicates an involvement of Yap4p and Yap6p in cell cycle regulation as reported also from other groups [15,16]. On the other hand this strategy was used to identify new target genes of transcription factors [37] which prompted us to investigate the observed differences in neutral lipid content. During exponential as well as stationary growth phase a significant accumulation of SE was noticed. However, this accumulation could not be assigned to a particular step within the ergosterol biosynthesis pathway since several ergosterol precursors exhibited higher levels. Furthermore, mRNA levels from potential target genes of Yap4p encoding for proteins from the ergosterol biosynthesis pathway were analysed, which revealed a slight increase of gene expression from oxygen-dependent proteins (*ERG3* and *ERG11*) while other genes were unaffected (*ERG7* and *ERG9*). Even if no direct regulatory effect of Yap4p on the expression of genes encoding for sterol formation (*ARE1* and *ARE2*) and hydrolysis (*YEH1*, *YEH2*, and *TGL1*) was expected, the mRNA levels of the corresponding genes were determined and surprisingly indicated an upregulation of sterol ester hydrolases (*YEH1* 5-fold, *YEH2* 2-fold), which stands in contrast to the increased content of sterol esters in the overexpressing strain. Yeh2p was assigned as the SE hydrolase with the highest activity [38], however, Yeh1p is the major SE hydrolase under heme-deficient conditions, which imitates anaerobic conditions [39]. Taking into consideration that especially an accumulation of sterol precursors occurred which are substrates of oxygen-dependent enzymes, it can be assumed that *YAP4* overexpressing cells, respond to hypoxia a stress condition where it is supposed that Yap4p is required [40,41].

Yap4p is phosphorylated under several stress conditions [6,8,21]. If expression of *YAP4* is under the control of the *GAL1* promoter, Yap4p is also phosphorylated [25], which indicates that strong overexpression of *YAP4* triggers stress response. Growth assays with *YAP4* phosphorylation mutants revealed that this modification is not required to induce growth inhibition and has only marginal influences on stress resistance.

In conclusion, Yap4p is supposed to be one of the major regulators in the Yap-mediated network with potential target sites in several functional categories, including the ones where we observed significant differences, namely cell cycle progression, neutral lipid content and stress response [7,12]. However, since various studies imply the coordination of metabolic activities, cell cycle progression and stress resistance in *S. cerevisiae* [42–46] as well as in other organisms [47–49] it is difficult to say if all three explored categories are directly influenced by Yap4p or if changes occurred because of synergistic effects.

References

- [1] T.R. Hughes, C.G. de Boer, Mapping yeast transcriptional networks, *Genetics* 195 (2013) 9–36.
- [2] S. Latchman, Transcription factors: An overview, *Int. J. Biochem. Cell Biol.* 2725 (1997) 1305.
- [3] C. Vinson, M. Myakishev, A. Acharya, A.A. Mir, J.R. Moll, M. Bonovich, Classification of human B-ZIP proteins based on dimerization properties, *Mol. Cell. Biol.* 22 (2002) 6321–6335.
- [4] J. Lee, C. Godon, D. Spector, J. Garin, M.B. Toledano, G. Lagniel, J. Labarre, Yap1 and Skn7 control two specialized oxidative stress response regulons in yeast, *J. Biol. Chem.* 274 (1999) 16040–16046.
- [5] M. North, V.J. Tandon, R. Thomas, A. Loguinov, I. Gerlovina, A.E. Hubbard, L. Zhang, M.T. Smith, C.D. Vulpe, Genome-wide functional profiling reveals genes required for tolerance to benzene metabolites in yeast, *PLoS One.* 6 (2011) e24205.
- [6] T. Nevitt, J. Pereira, C. Rodrigues-Pousada, YAP4 gene expression is induced in response to several forms of stress in *Saccharomyces cerevisiae*, *Yeast* 21 (2004) 1365–1374.
- [7] C. Rodrigues-Pousada, R.A. Menezes, C. Pimentel, The Yap family and its role in stress response, *Yeast* 27 (2010) 245–258.

- [8] T. Nevitt, J. Pereira, D. Azevedo, P. Guerreiro, C. Rodrigues-Pousada, Expression of YAP4 in *Saccharomyces cerevisiae* under osmotic stress, *Biochem. J.* 379 (2004) 367–74.
- [9] L. Ni, C. Bruce, C. Hart, J. Leigh-Bell, D. Gelperin, L. Umansky, M.B. Gerstein, M. Snyder, Dynamic and complex transcription factor binding during an inducible response in yeast, *Genes Dev.* 23 (2009) 1351–1363.
- [10] C. a Ball, K. Dolinski, S.S. Dwight, M. a Harris, L. Issel-Tarver, A. Kasarskis, C.R. Scafe, G. Sherlock, G. Binkley, H. Jin, M. Kaloper, S.D. Orr, M. Schroeder, S. Weng, Y. Zhu, D. Botstein, J.M. Cherry, Integrating functional genomic information into the *Saccharomyces* genome database, *Nucleic Acids Res.* 28 (2000) 77–80.
- [11] A.P. Gasch, P.T. Spellman, C.M. Kao, O. Carmel-Harel, M.B. Eisen, G. Storz, D. Botstein, P.O. Brown, Genomic expression programs in the response of yeast cells to environmental changes, *Mol. Biol. Cell.* 11 (2000) 4241–57.
- [12] K. Tan, H. Feizi, C. Luo, S.H. Fan, T. Ravasi, T.G. Ideker, A systems approach to delineate functions of paralogous transcription factors: role of the Yap family in the DNA damage response, *Proc. Natl. Acad. Sci. USA.* 105 (2008) 2934–9.
- [13] T. Furuchi, H. Ishikawa, N. Miura, M. Ishizuka, K. Kajiya, S. Kuge, A. Naganuma, Two nuclear proteins, Cin5 and Ydr259c, confer resistance to cisplatin in *Saccharomyces cerevisiae*, *Mol. Pharmacol.* 59 (2001) 470–4.
- [14] M.A. Hoyt, T.I.M. Stearns, D. Botsteint, Chromosome instability mutants of *Saccharomyces cerevisiae* that are defective in microtubule-mediated processes, *Mol. Cell. Biol.* 10 (1990) 223–234.
- [15] W.-S. Wu, W.-H. Li, Systematic identification of yeast cell cycle transcription factors using multiple data sources, *BMC Bioinformatics* 9 (2008) 522 (1-13).
- [16] S.B. Haase, C. Wittenberg, Topology and control of the cell-cycle-regulated transcriptional circuitry, *Genetics* 196 (2014) 65–90.
- [17] J. Pereira, Dissertation: Deciphering the role of Yap4 phosphorylation under stress conditions, 2008.

- [18] S. Kuge, N. Jones, A. Nomoto, Regulation of yAP-1 nuclear localization in response to oxidative stress, *EMBO J.* 16 (1997) 1710–1720.
- [19] S.E. Hanlon, J.M. Rizzo, D.C. Tatomer, J.D. Lieb, M.J. Buck, The stress response factors Yap6, Cin5, Phd1, and Skn7 direct targeting of the conserved co-repressor Tup1-Ssn6 in *S. cerevisiae*, *PLoS One.* 6 (2011).
- [20] I. Mendizabal, G. Rios, J.M. Mulet, R. Serrano, I.F. De Larrinoa, Yeast putative transcription factors involved in salt tolerance, *FEBS Lett.* 425 (1998) 323–328.
- [21] J. Pereira, C. Pimentel, C. Amaral, R.A. Menzes, C. Rodrigues-Pousada, Yap4 PKA- and GSK3-dependent phosphorylation affects its stability but not its nuclear localization, *Yeast.* 26 (2009) 641–653.
- [22] S. Sollner, M. Schober, A. Wagner, A. Prem, L. Lorkova, B.A. Palfey, M. Groll, P. Macheroux, Quinone reductase acts as a redox switch of the 20S yeast proteasome, *EMBO Rep.* 10 (2009) 5–10.
- [23] G. Asher, P. Tsvetkov, C. Kahana, A mechanism of ubiquitin-independent proteasomal degradation of the tumor suppressors p53 and p73, *Genes Dev.* 19 (2005) 316–321.
- [24] M. Schober, Master thesis: The transcription factor Yap4p and its interaction with the quinone reductase Lot6p, 2008.
- [25] K. Koch, Master Thesis: Cellular role of the yeast bZip transcription factor Yap4p, 2012.
- [26] C. Pashley, S. Kendall, Cloning in plasmid vectors, *Methods Mol. Biol.* 235 (2003) 121–135.
- [27] W.E. Swords, Chemical transformation of *E. coli*, *Methods Mol. Biol.* 235 (2003) 49–53.
- [28] R. Gietz, Yeast transformation by the LiAc/SS carrier DNA/PEG method, *Methods Mol. Biol.* 1205 (2014) 1–12.

- [29] J.M. Cherry, E.L. Hong, C. Amundsen, R. Balakrishnan, G. Binkley, E.T. Chan, K.R. Christie, M.C. Costanzo, S.S. Dwight, S.R. Engel, D.G. Fisk, J.E. Hirschman, B.C. Hitz, K. Karra, C.J. Krieger, S.R. Miyasato, R.S. Nash, J. Park, M.S. Skrzypek, M. Simison, S. Weng, E.D. Wong, *Saccharomyces* genome database: the genomics resource of budding yeast, *Nucleic Acids Res.* 40 (2012) 700–705.
- [30] J. Folch, M. Lees, G.. H. Sloane Stanley, A simple method for the isolation and purification of total lipides from animal tissues, *J. Biol. Chem.* 55 (1987) 999–1033.
- [31] T.A. Lewis, R.J. Rodriguez, L.W. Parks, Relationship between intracellular sterol content and sterol esterification and hydrolysis in *Saccharomyces cerevisiae*, *Biochim. Biophys. Acta* 921 (1987) 205–212.
- [32] K.J. Livak, T.D. Schmittgen, Analysis of relative gene expression data using real-time quantitative PCR and the $2^{-\Delta\Delta CT}$ method, *Methods* 25 (2001) 402–408.
- [33] K.D. Pryor, B. Leiting, High-level expression of soluble protein in *Escherichia coli* using a His6-tag and maltose-binding-protein double-affinity fusion system, *Protein Expr. Purif.* 10 (1997) 309–319.
- [34] R.P. Johnson, S.W. Craig, Crystal structure of the heteromdimeric bZIP transcription factor c-Fos-c-Jun to DNA, *Nature* 373 (1995) 257–261.
- [35] M.C. Teixeira, P. Monteiro, P. Jain, S. Tenreiro, A.R. Fernandes, N.P. Mira, M. Alenquer, A.T. Freitas, A.L. Oliveira, I. Sá-Correia, The YEASTRACT database: a tool for the analysis of transcription regulatory associations in *Saccharomyces cerevisiae*, *Nucleic Acids Res.* 34 (2006) D446–D451.
- [36] K. Yoshikawa, T. Tanaka, Y. Ida, C. Furusawa, T. Hirasawa, H. Shimizu, Comprehensive phenotypic analysis of single-gene deletion and overexpression strains of *Saccharomyces cerevisiae*, *Yeast.* 28 (2011) 349–361.

- [37] G. Chua, Q.D. Morris, R. Sopko, M.D. Robinson, O. Ryan, E.T. Chan, B.J. Frey, B.J. Andrews, C. Boone, T.R. Hughes, Identifying transcription factor functions and targets by phenotypic activation, *Proc. Natl. Acad. Sci. USA* 103 (2006) 12045–50.
- [38] R. Köffel, R. Tiwari, L. Falquet, The *Saccharomyces cerevisiae* YLL012/YEH1, YLR020/YEH2, and TGL1 genes encode a novel family of membrane-anchored lipases that are required for steryl ester hydrolysis, *Mol. Cell. Biol.* 25 (2005) 1655–1668.
- [39] R. Köffel, R. Schneiter, Yeh1 constitutes the major steryl ester hydrolase under heme-deficient conditions in *Saccharomyces cerevisiae*, *Eukaryot. Cell.* 5 (2006) 1018–1025.
- [40] T.A. Knijnenburg, J.H. de Winde, J.-M. Daran, P. Daran-Lapujade, J.T. Pronk, M.J.T. Reinders, L.F.A. Wessels, Exploiting combinatorial cultivation conditions to infer transcriptional regulation, *BMC Genomics* 8 (2007) 25:1-14.
- [41] A.N. Shah, D. Cadinu, R.M. Henke, X. Xin, R.G. Dastidar, L. Zhang, Deletion of a subgroup of ribosome-related genes minimizes hypoxia-induced changes and confers hypoxia tolerance, *Physiol. Genomics* 43 (2011) 855–872.
- [42] M.J. Brauer, C. Huttenhove, E.M. Airoidi, R. Rosenstein, J.C. Matese, D. Gresham, V.M. Boer, O.G. Troyanskaya, D. Botstein, Coordination of growth rate, cell cycle, stress response and metabolic activity in yeast, *Mol. Biol. Cell.* 19 (2008) 357–367.
- [43] C. Lu, M.J. Brauer, D. Botstein, Slow growth induces heat-shock resistance in normal and respiratory-deficient yeast, *Mol. Biol. Cell.* 20 (2009) 891–903.
- [44] C.F. Kurat, H. Wolinski, J. Petschnigg, S. Kaluarachchi, B. Andrews, K. Natter, S.D. Kohlwein, Cdk1/Cdc28-dependent activation of the major triacylglycerol lipase Tgl4 in yeast links lipolysis to cell-cycle progression, *Mol. Cell.* 33 (2009) 53–63.
- [45] N. Chauhan, M. Visram, A. Cristobal-Sarramian, F. Sarkleti, S.D. Kohlwein, Morphogenesis checkpoint kinase Swe1 is the executor of lipolysis-dependent cell-cycle progression, *Proc. Natl. Acad. Sci.* 112 (2015) E1077–E1085.

- [46] K.K. Sharma, H. Schuhmann, P.M. Schenk, High lipid induction in microalgae for biodiesel production, *Energies*. 5 (2012) 1532–1553.
- [47] H.W. Yen, Z. Zhang, Effects of dissolved oxygen level on cell growth and total lipid accumulation in the cultivation of *Rhodotorula glutinis*, *J. Biosci. Bioeng.* 112 (2011) 71–74.
- [48] M. Sanchez-Alvarez, Q. Zhang, F. Finger, M.J.O. Wakelam, C. Bakal, Cell cycle progression is an essential regulatory component of phospholipid metabolism and membrane homeostasis., *Open Biol.* 150093 (2015) 1–15.
- [49] M. Dottermusch, T. Lakner, T. Peyman, M. Klein, G. Walz, E. Neumann-Haefelin, Cell cycle controls stress response and longevity in *C. elegans*, *Aging (Albany NY)* 8 (2016) 2100–2126.

APPENDIX

Additional Publication

Human flavodoxin-like protein NQO1

Catalytic competence, structure and stability of the cancer associated R139W variant of the human NAD(P)H:quinone oxidoreductase 1 (NQO1)

Wolf-Dieter Lienhart^{1‡}, Emilia Strandback^{1‡}, Venugopal Gudipati¹, Karin Koch¹, Alexandra Binter¹, Michael K. Uhl², David M. Rantasa¹, Benjamin Bourgeois³, Tobias Madl³, Klaus Zangger⁴, Karl Gruber² and Peter Macheroux^{1*}

¹Institute of Biochemistry, Graz University of Technology, Petersgasse 12/2, 8010 Graz, Austria

²Institute of Molecular Biosciences, University of Graz, Humboldtstraße 50/3, 8010 Graz, Austria

³Institute of Molecular Biology and Biochemistry, Medical University of Graz, Harrachgasse 21/3, 8010 Graz, Austria

⁴Institute of Chemistry, University of Graz, Heinrichstraße 28, 8010 Graz, Austria

*From the Graz University of Technology, Institute of Biochemistry, Petersgasse 12, A-8010 Graz, Austria; Tel.: +43-316-873 6450, Fax: +43-316-873 6952,

Email: peter.macheroux@tugraz.at

Author contributions

‡ The first two authors have contributed equally to this work. K.G. and P.M. initiated the project; W.-D.L., E.S., V.G., M.K.U., K.Z., K.G. and P.M. designed the experiments and analysed the data; W.-D.L., E.S. and V.G. expressed and purified NQO1; M.K.U. and K.G. crystallized NQO1 and determined the crystal structure; W.-D.L., E.S., V.G., K.K., A.B. and D.M.R. performed analytical and biochemical experiments, and determined dissociation constants as well as kinetic parameters; K.Z. performed NMR-experiments; T.M. and B.B. performed and interpreted SAXS measurements; W.-D.L., E.S., V.G., M.K.U., K.Z., K.G. and P.M. wrote the manuscript.

Manuscript accepted

Abstract

The human NAD(P)H:quinone oxidoreductase 1 (NQO1; EC 1.6.99.2) is an essential enzyme in the antioxidant defence system. Furthermore, NQO1 protects tumour suppressors like p53, p33^{ING1b} and p73 from proteasomal degradation. The activity of NQO1 is also exploited in chemotherapy for the activation of quinone-based treatments. Various single nucleotide polymorphisms are known, such as *NQO1**2 and *NQO1**3 yielding protein variants of NQO1 with single amino acid replacements, *i.e.* P187S and R139W, respectively. While the former NQO1 variant is linked to a higher risk for specific kinds of cancer, the role, if any, of the arginine 139 to tryptophan exchange in disease development remains obscure. On the other hand, mitomycin C resistant human colon cancer cells were shown to harbour the *NQO1**3 variant resulting in substantially reduced enzymatic activity. However, the molecular cause for this decrease remains unclear. In order to resolve this issue, recombinant NQO1 R139W has been characterized biochemically and structurally. In this report we show by X-ray crystallography and 2D-NMR spectroscopy that this variant adopts the same structure both in the crystal as well as in solution. Furthermore, the kinetic parameters obtained for the variant are similar to those reported for the wild-type protein. Similarly, thermostability of the variant was only slightly affected by the amino acid replacement. Therefore, we conclude that the previously reported effects in human cancer cells cannot be attributed to protein stability or enzyme activity. Instead it appears that loss of exon 4 during maturation of a large fraction of pre-mRNA is the major reason of the observed lack of enzyme activity and hence reduced activation of quinone-based chemotherapeutics.

Introduction

NAD(P)H:quinone oxidoreductase 1 (NQO1; EC 1.6.99.2) [1] is an important enzyme in the human antioxidant defence system. Among other functions, the dimeric flavoprotein is catalysing the conversion of quinones to hydroquinones preventing the formation of semiquinone radicals [2]. Yet another important role is the regulation and stabilisation of various tumour suppressors like p33^{ING1b}, p53 and p73. This effect appears to be related to the interaction of NQO1 with the 20S proteasome in a NADH dependent manner [3,4]. Single nucleotide polymorphisms result in the expression of different protein variants of NQO1. The two most prevalent variants in the human population are *NQO1*2* (*NQO1 609C>T*; *NQO1 P187S*; allelic frequency: 0.22-0.47) and *NQO1*3* (*NQO1 465C>T*; *NQO1 R139W*; allelic frequency: 0.00-0.05), which are connected to a higher risk for specific cancers [5-11]. Several studies have focused on *NQO1*2* and have shown a reduction or even a loss of the enzymatic activity of *NQO1 P187S* [12-14]. Furthermore, this single nucleotide polymorphism (SNP) gives rise to reduced stability of the protein and to a loss of the FAD cofactor. On the other hand, the involvement of *NQO1*3* in the development of cancer is currently unclear. Initial observations indicated that splicing of the transcript of *NQO1*3* yields mature mRNA lacking exon 4, which consequently leads to the loss of the FAD binding domain [15]. In the mitomycin C resistant tumour cell lines HCT 116-R30A solely the mRNA of *NQO1*3* could be detected while in the mitomycin C sensitive HCT 116 cell line mRNAs of *NQO1*1* and *NQO1*3* were detectable [16]. These findings led to the assumption that the higher cancer risk for the *NQO1*3* polymorphism might be caused by erroneous splicing of the pre-mRNA derived from *NQO1*3*. As a matter of fact, the nucleotide transition found in *NQO1*3* disrupts the consensus sequence of the 5' splicing site required for the correct splicing by the spliceosome and thus rationalizes the observations mentioned above [11]. Since the full length mRNA of *NQO1*3* is still representing one to two thirds of the whole mRNA [11], it is unclear if the higher risk for specific cancers can be explained solely by erroneous splicing. Thus far enzyme activities were determined only in cell extracts [11] or with the unspecific redox dye DCPIP [17] but not with a quinone substrate. Moreover, information concerning the potential impact of the R139W exchange on structural properties of the enzyme is currently not available.

A loss of enzymatic activity is increasing the toxicity of benzene as well as aggravating the cancer treatment of patients [18]. The broad substrate specificity of NQO1 allows the activation of chemotherapeutic prodrugs, like mitomycin C or β -lapachone. Since various tumours are upregulating the NQO1 levels, these chemotherapeutics are acting more specific on cancer than healthy cells [19-21]. The success of the prevalent cancer treatment with cisplatin is also affected by the NQO1 activity. One limitation for the use of cisplatin is the induced nephrotoxicity. Activation of NQO1 can improve the negative effects of the treatment to the kidneys while a loss of enzyme activity can cause an accelerated damage of the renal system [22]. Taken together the status of NQO1 expression and activity is essential for the success of quinone-based chemotherapies and therefore detailed biochemical and structural studies are paramount to generate a sound basis for the development and design of cancer intervention strategies.

In order to remedy the current lack of sound biochemical information on the NQO1 R139W variant, we have undertaken a biochemical, enzymatic and structural investigation to fully comprehend the effect of this widely occurring variant of the human enzyme.

Materials and Methods

Materials

All chemicals and reagents were of the highest purity commercially available from Sigma-Aldrich (St. Louis, MO, USA) and Merck (Darmstadt, Germany). Ni-NTA-agarose columns were obtained from GE Healthcare (Little Chalfont, UK).

*Molecular cloning of *nqo1*, protein expression and purification*

The cloning of NQO1 and the generation of the NQO1 R139W variant as well as the expression and purification was carried out according to the already described procedure from Lienhart and Gudipati *et al.* [14]. The wild type gene of NQO1 in a pET28a vector was modified with the Quick Change II XL Site-Directed Mutagenesis Kit (Agilent, Santa Clara, CA, USA) according the provided manual with gene specific primers from Eurofins (Luxembourg).

Apoprotein preparation and UV/Vis absorption difference titration

Apoprotein preparation and difference titration spectra were conducted as described by Lienhart and Gudipati *et al.* [14]. The measurements were made with a Specord 200 plus spectrophotometer (Analytik Jena, Jena, Germany) at 25 °C in Tandem cuvettes (Hellma Analytic, Müllheim, Germany). 800 µl of NQO1 R139W (45 µM) in the sample cell was titrated with 0-42 µl (in 2 µl intervals) and 52 µl and 62 µl in (10 µl intervals) of a FAD stock solution (1 mM). At the same time the same volume of FAD as in the sample cell was added to the buffer chamber in the reference cell and the same amount of buffer was also added to the protein chamber in the reference cell to adjust the volumes of cells. For analysis, the sum of the absolute values at 436 nm and 455 nm were plotted against the FAD/protein molar ratio.

Small-angle X-ray scattering.

SAXS data for solutions of the FAD-free and bound forms of wild type NQO1 were recorded with an in-house SAXS instrument (SAXSspace, Anton Paar, Graz, Austria) equipped with a Kratky camera, a sealed X-ray tube source and a one-dimensional Mythen2 R 1k hybrid photon coupling detector (Dectris). The scattering patterns were measured with a 60-min exposure time (20 frames, each 3 min) with a solute concentration of 300 µM. Radiation damage was excluded on the basis of a comparison of individual frames of the 60-min exposures, wherein no changes were detected. A range of momentum transfer of $0.010 < s < 0.63 \text{ \AA}^{-1}$ was covered ($s = 4\pi \sin(\theta)/\lambda$, where 2θ is the scattering angle, and λ is the X-ray wavelength, in this case 1.5 Å). All SAXS data were analyzed with the ATSAS package (version 2.8). The data were processed with SAXSQuant (version 3.9) and desmeared with GNOM [23]. The forward scattering ($I(0)$), the radius of gyration, (R_g), the maximum dimension (D_{\max}) and the interatomic distance distribution function ($(P(r))$) were computed with GNOM [23]. The masses of the solutes were evaluated based on their Porod volume.

Isothermal titration microcalorimetry (ITC)

A VP-ITC system (MicroCal, GE Healthcare, Little Chalfont, UK) was used for calorimetric determination of the dissociation constants for FAD. The experiments were performed at 10 °C or 25 °C in 50 mM HEPES, pH 7.0 buffer or 50 mM sodium phosphate buffer with 150 mM NaCl, pH 7.0. The solutions were degassed before measurements. The titration experiments were performed with either apo-protein

solution or FAD solution in the syringe and in each case the other solution in the sample cell. The concentrations of FAD and the apo-protein (concentration of NQO1 protomers) were determined spectrophotometrically. The first measurement point is rejected while the remaining data points were analysed assuming a single site or a two site binding model with Origin version 7.0 (MicroCal) for ITC data analysis [14]. To remove aggregated protein solutions were centrifuged at 21.130 g for 20 minutes at 22 °C.

Steady state kinetics

Steady state parameters for NQO1 WT and NQO1 R139W were determined using a Specord 200 plus spectrophotometer (Analytik Jena, Jena, Germany) at 25 °C. NADH was used as electron donor and menadione as electron acceptor for the assays. The concentrations of all components were determined spectrophotometrically. For the assay with variation of NADH the reaction mixture contained 2.5 nM WT NQO1 or the R139W variant, 200 µM menadione ($\epsilon_{333\text{nm}} = 2,450 \text{ M}^{-1}\text{cm}^{-1}$, dissolved in ethanol, final concentration in the cuvette 1% v/v) and 1-10 mM NADH ($\epsilon_{340\text{nm}} = 6,220 \text{ M}^{-1}\text{cm}^{-1}$) in 50 mM HEPES containing 150 mM NaCl, pH 7.0 and for the variation of menadione 2 nM NQO1 WT or NQO1 R139W, 10 mM NADH, 10-160 µM menadione (dissolved in ethanol, final concentration in the cuvette 1% v/v) in 50 mM HEPES containing 150 mM NaCl, pH 7.0. The reaction mixtures were incubated for 3 minutes at 25 °C and then the reaction was initiated by addition of the enzyme and the decrease in absorption of NADH was measured at 400 nm (determined for these measurements) due to the high concentrations of NADH that were needed. In the case of measurements as a function of NADH concentration the slope corresponding to the first 60 s was used for the analysis whereas in the case of menadione variation only 10 s was used for analysis due to the fast reaction. The kinetic parameters were determined using the KALEIDAGRAPH software (Synergy Software, Reading, PA, USA).

Transient kinetics

The rates of the reductive half reactions were determined using a Hi-Tech (SF-61DX2) stopped-flow device (TgK Scientific Limited, Bradford-on-Avon, UK), placed in a glovebox from Belle Technology (Weymouth, UK), at 25 °C. Buffer were first flushed with nitrogen and thereafter incubated in the glove box. In the same way

enzyme and substrate solutions were deoxygenated in the glove box and diluted to the desired concentration. During the experiments, enzyme was rapidly mixed with substrate and reduction of the FAD cofactor was measured by monitoring changes at 455 nm with a photomultiplier detector (PM-61s, TgK Scientific Limited, Bradford-on-Avon, UK). For these measurements 40 μ M protein was mixed with 50-2500 μ M NADH or NADPH in 50 mM HEPES buffer containing 50 mM NaCl at pH 7.0. Initial rates were analysed with a hyperbolic function using the KINETIC STUDIO software (TgK Scientific).

Crystallization and structure determination of NQO1 R139W

NQO1 R139W at 6.1 mg/ml in 50 mM HEPES (pH 7.5) was crystallized by the microbatch method in a precipitating solution containing 200 mM Li_2SO_4 , 100 mM BisTris (pH 6.5), 25% w/v PEG 3350 (Hampton Research Index Screen, condition 75), and incubated at 289 K. The total drop volume was 1 μ L, with equal amounts of protein and precipitant solution. Yellow crystals grew to full size (~ 100 μ m) within 2 months. Crystals were harvested from their mother liquor with CryoLoops™ (Hampton Research), and flash-cooled in liquid nitrogen.

A complete diffraction dataset was collected up to 2.09 Å resolution from a single triclinic crystal (space group *P*1) at the Swiss Light Source (SLS) of the Paul Scherrer Institute in Villigen, Switzerland (beamline X06DA). The data were processed using the program XDS [24]. The calculated Matthews coefficient [25] indicated the presence of four molecules per asymmetric unit. The structure was determined by molecular replacement using the program PHASER [26] and the wild type structure of NQO1 (PDB code: 1QBG) as search template.

R_{free} values were computed from 5% randomly chosen reflections which were not used during refinement [27]. Structure refinement and model rebuilding were carried out with the programs PHENIX [28] and COOT [29,30] by alternating real-space fitting against σ_A -weighted $2F_o - F_c$ and $F_o - F_c$ electron density maps and least square optimizations. Validation of the structure was carried out with the program MOLPROBITY [31] yielding a Ramachandran plot with 97.0% of the residues in favoured regions, 3.0% in allowed and none in disallowed regions. Prediction of the biologically active form of NQO1 R137W was done using the PISA server [32]. Figures were created using the program PyMOL (<http://www.pymol.org>).

The final model was refined to $R = 16.9\%$ and $R_{\text{free}} = 20.1\%$. Details of the data reduction and structure refinement are listed in Table 4.

Limited proteolysis

NQO1 and NQO1 R139W (30 μM in 50 mM HEPES and 150 mM NaCl buffer at pH 7.5) were partially digested with trypsin (Promega, Madison, WI, USA) with a final concentration of 2 $\mu\text{g/ml}$ at 37 °C. The reaction was stopped after 5 and 10 minutes by addition of SDS sample buffer to aliquots of the reaction mixture and immediately boiled at 95 °C for 10 min. The samples were analysed by SDS-PAGE with precast gradient gels (Thermo Scientific, Waltham, MA, USA) (Figure 8) [14,17,33,34].

¹⁵N-Labeling of NQO1 and NQO1 R139W

Minimal medium containing 6.8 g/l Na_2HPO_4 , 3 g/l KH_2PO_4 , 0.5 g/l NaCl, 1 g/l $^{15}\text{NH}_4\text{Cl}$, 3 g/l glucose, 1 $\mu\text{g/l}$ biotin, 1 $\mu\text{g/l}$ thiamin, 50 $\mu\text{g/ml}$ kanamycin and 1 ml 1000x microsals [150 mM CaCl_2 , 20 mM, FeCl_3 , 50 mM H_3BO_3 , 150 μM CoCl_2 , 800 μM CuCl_2 , 1.5 mM ZnCl_2 , 15 μM $(\text{NH}_4)_6\text{Mo}_7\text{O}_{24}\cdot 4\text{H}_2\text{O}$] was used for protein expression as described in Lienhart and Gudipati *et al.* [14].

NMR spectroscopy

All NMR experiments were carried out with a Bruker Avance III 700 MHz spectrometer using a cryogenically cooled 5 mm TXI probe with z-axis gradients at 298 K. Samples containing between 20-40 mg/ml NQO1 or NQO1 R139W in 50 mM HEPES, pH 6.5 in 90% H_2O and 10% D_2O were used. For the ^1H - ^{15}N HSQC spectra, data matrices of 2048 x 160 points were acquired and zero filled to 4k x 256 points prior to Fourier transformation. Sixty degree phase shifted squared sine bell window functions were applied in both dimensions [14].

Thermal stability

The melting points were determined with a CFX Connect™ Real-Time PCR Detection System (Bio-Rad Laboratories, Inc.; Hercules; California; USA) by detecting the fluorescence change of SYPRO® Orange Protein Gel Stain (1:5000) or the fluorescence change caused by the release of the FAD cofactor during heating [35]. The tested proteins (100 μM for FAD and 10 μM for SYPRO® Orange, measured in duplicates) have been dialysed in water over night and mixed with concentrated buffer and salt solutions to obtain all tested conditions.

Results

Expression and basic biochemical characterisation of the R139W variant

Heterologous expression of the NQO1 R139W variant in *E. coli* BL21 yielded similar amounts of soluble protein as was previously reported for wild-type NQO1 [14]. Preparations of the R139W variant showed the typical yellow colour indicating that the protein tightly binds the FAD cofactor in stark contrast to the P187S variant that was isolated largely as an apo-protein [14]. Further analysis showed that wild-type NQO1 and the R139W variant have nearly identical absorption spectra with maxima at 375 and 450 nm (Figure 1). In addition, titration of apo-proteins with FAD gave rise to a similar difference absorption spectrum indicating that the FAD binding pockets provided by wild-type NQO1 and the R139W variant are comparable (Figure 1).

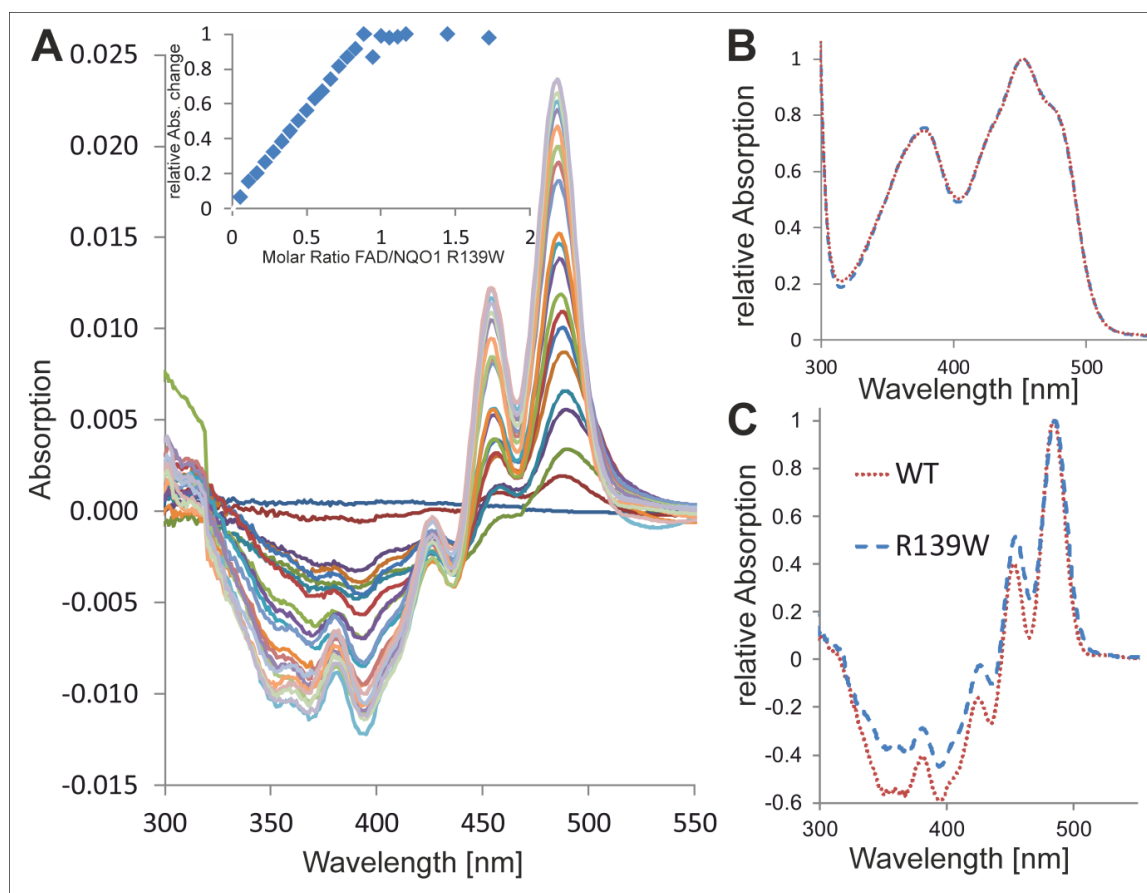


Figure 1. UV-visible and difference titration absorption spectra of wild-type NQO1 and NQO1 R139W. A: Difference titration spectra of 800 μ l NQO1 R139W (45 μ M) with 0-42 μ l in 2 μ l intervals FAD (1 mM). The insert shows the change of the absolute absorption values at 436 nm and 455nm against the FAD/protein molar ratio with two additional points (with additional 10 μ l FAD each) compared to the main figure. B: Absorption spectra of wild-type NQO1 and NQO1 R139W normalised to the maximum at 450 nm. C: Difference titration spectra of wild-type NQO1 and NQO1 R139W with protein/FAD ratio of 1 normalised to the maximum at 480 nm

The melting points of the NQO1 WT and NQO1 R139W variant were determined in different buffers and showed a decrease of 2 °C for the R139W variant. Measurements with SYPRO® Orange of the holo- and apo-form of the proteins showed a decrease of the melting points for the apoprotein. The small differences of the melting points observed between FAD and SYPRO® Orange may indicate that the latter has an adverse effect of thermal stability by promoting the unfolding of the protein (Table 1).

Table 1. Thermostability measurements. Melting points were determined with a CFX Connect™ Real-Time PCR Detection System under different buffer and salt conditions of NQO1 and NQO1 R139W with FAD or SYPRO® Orange as fluorescent reporter. Melting points are given in °C (values given are the average of two independent measurements).

Buffer	NQO1	NQO1 R139W
50 mM potassium phosphate, pH 7	54.0	52.0
50 mM sodium phosphate, pH 7	54.0	52.0
50 mM Tris/Cl, pH 7	54.5	52.5
50 mM HEPES, pH 7	56.0	54.0
Holoprotein in 50 mM HEPES, pH 7 +SYPRO® Orange	52.8	51.2
Apoprotein in 50 mM HEPES, pH 7 +SYPRO® Orange	50.8	48.5

Isothermal titration calorimetry and small-angle X-ray scattering

To obtain quantitative information on the binding affinity of the FAD cofactor to the R139W variant isothermal titration calorimetry experiments were conducted. As reported recently, reproducible measurements are obtained by titration of a fixed concentration of FAD with apo-protein [14]. The raw data could be nicely fitted to a one binding site model [14] (Figure 2). The average of three measurements was used to determine the K_D values for the NQO1 R139W variant as 155 ± 27 nM, which is 2.5-fold higher than the K_D for wild-type enzyme [14]. Thus it can be concluded that the arginine to tryptophan replacement has only a marginal effect on the binding affinity of the FAD cofactor.

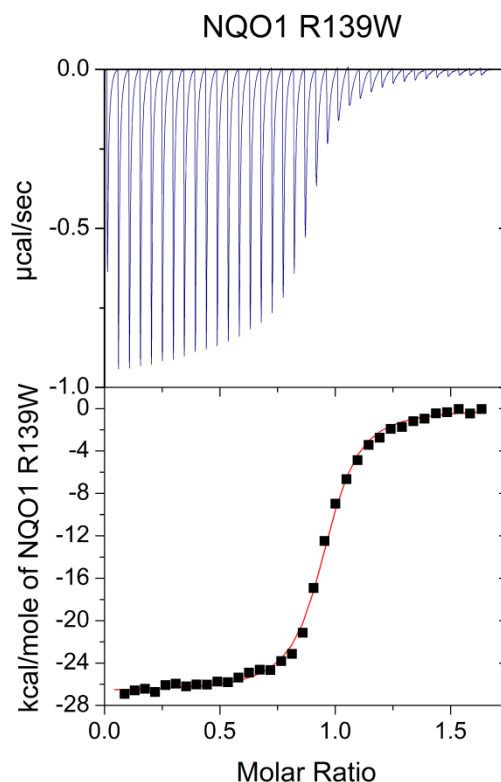


Figure 2. ITC measurement of NQO1 R139W. NQO1 R139W: 35 injections with 6 μl of 298 μM NQO1 R139W apoprotein solution in 29 μM FAD solution and 300 seconds spacing (top) at 25 $^{\circ}\text{C}$. From three independent measurements under the same conditions the dissociation constant was calculated to $K_D = 155 \pm 27$ nM. Data was fitted using the one binding site model.

In this context it is important to note, that the experimental set-up of the ITC experiment is critical to obtain reliable data both in terms of stoichiometry and the dissociation constant. In principal, reversal of the order of titration should not influence the outcome of the experiment in terms of the model used to fit the raw data. However, when apo-proteins (wild-type as well as the R139W variant) were titrated with FAD the raw data could not be satisfactorily fitted with a one binding site model. Instead, the raw data were best fitted to a two binding site model, a result that is difficult to reconcile with the structural identity of the two FAD binding pockets in the homodimeric protein (Figure 3; data with wild-type).

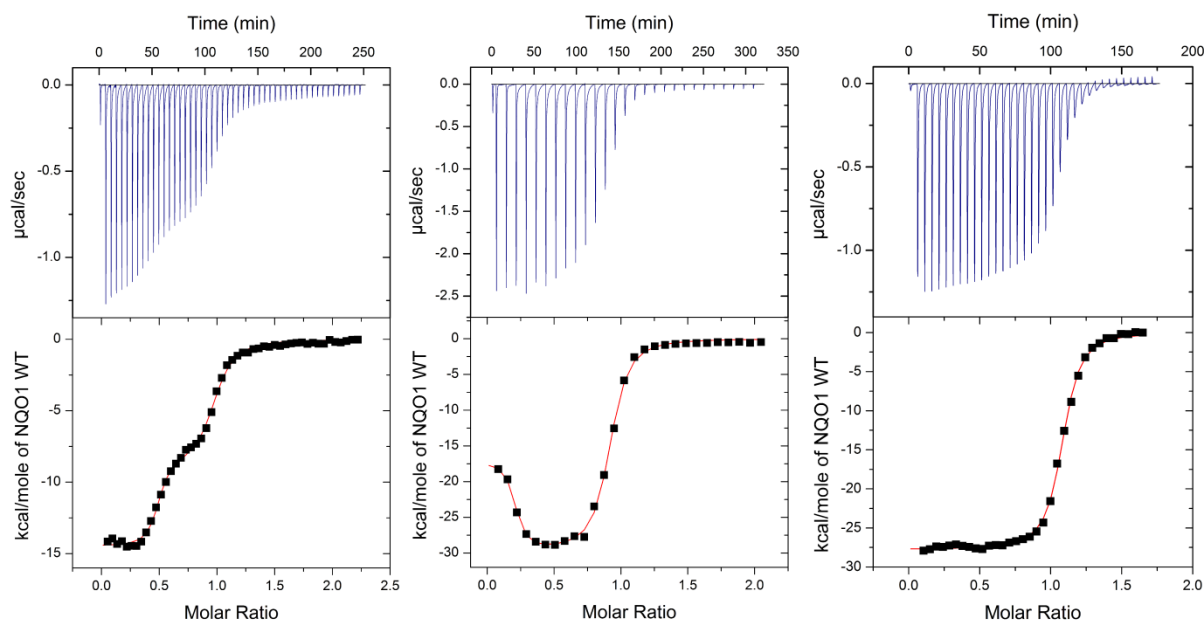


Figure 3. ITC measurements of NQO1 wild-type in HEPES buffer. The left and the middle measurements were conducted with apo-NQO1 in the sample cell of the microcalorimeter and FAD in the injection syringe. Data was fitted using the two binding site model. Left: First injection with 2 μ l and 49 injections with 6 μ l of 477 μ M FAD solution in 49.4 μ M NQO1 apo-protein solution and 300 seconds spacing at 25 $^{\circ}$ C. The determined K_D and N values are: $K_{D1} = 9,2$ nM; $K_{D2} = 780$ nM; $N1 = 0,47$; $N2 = 0,5$. Middle: First injection with 2 μ l and 27 injections with 10 μ l of 457 μ M FAD solution in 46.8 μ M NQO1 apo-protein solution and 600 seconds spacing at 25 $^{\circ}$ C. The determined K_D and N values are: $K_{D1} = 4$ nM; $K_{D2} = 295$ nM; $N1 = 0,18$; $N2 = 0,71$

The right measurement was conducted with FAD in the sample cell of the microcalorimeter and apo-NQO1 in the injection syringe. Data was fitted using the one binding site model. First injection with 2 μ l and 34 injections with 6 μ l of 284 μ M NQO1 apoprotein solution in 29 μ M FAD solution and 300 seconds spacing at 25 $^{\circ}$ C. From three independent measurements under the same conditions the dissociation constant was calculated to $K_D = 64 \pm 23$ nM.

Interestingly, we observed that variable amounts of protein had apparently precipitated during the experiment. Thus, a possible source for the irreproducibility observed with this particular experimental set-up appears to be the instability of apo-proteins in the microcalorimeter cell where constant stirring is required over the entire time course of the experiment. Similarly, when wild-type NQO1 was constantly stirred in an optical cuvette, we observed a gradual increase at 600 nm indicating denaturation and finally precipitation of protein. After removal of the precipitated protein by centrifugation the residual protein appeared to be intact as it behaved similar to unstirred protein in size exclusion chromatography. Attempts to stabilize the apo-proteins by lowering the temperature (e.g. 4 $^{\circ}$ C) or testing different buffers

influenced the overall shape of the obtained raw data but failed to improve the reproducibility of the experiment. Importantly, SAXS measurements of wild-type NQO1 showed that the protein forms a dimer in solution both in the holo- and the apo-form, with the holo-protein being more compact compared to the more extended apo-protein (radius of gyration 2.5 and 2.94 nm, Figure 4). Thus, the dimeric apo-protein seems to be partially open or unfolded as a consequence of FAD depletion.

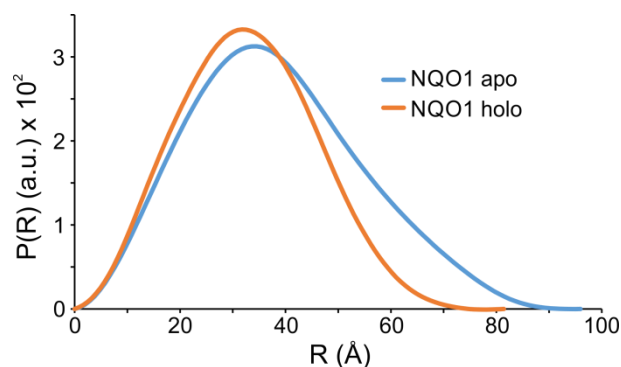


Figure 4. SAXS Measurement of NQO1. SAXS data showing a comparison of the experimental radial density distribution ($P(r)$) of apo- and holo-NQO1 in cyan and orange, respectively.

Kinetic measurements

The reductive rates for the NQO1 R139W variant, with NADH and NADPH as reducing co-substrates, were determined. As shown in Table 2, the limiting values for reduction are comparable to those determined earlier for wild-type NQO1 [14]. Interestingly the observed transients showed a biphasic behaviour with a second slower substrate-independent rate, which might have been caused by product release. The oxidative half reaction of the NQO1 R139W variant was completed within the dead time of the stopped flow device as was reported previously for the wild-type and the NQO1 P187S variant [14].

In addition, we have determined steady-state kinetic parameters for WT enzyme and the R139W variant using NADH and menadione as reducing and oxidising substrate, respectively. As summarised in Table 3 and seen in Figure 5, the values for k_{cat} and K_{M} are virtually identical for WT enzyme and the R139W variant for both NADH and menadione again indicating that the single amino acid replacement does not affect the kinetic properties.

Table 3. Steady state kinetic parameters for NQO1 and NQO1 R139W. Kinetic parameters with standard deviations determined for NQO1 and NQO1 R139W, using NADH as electron donor and menadione as electron acceptor.

	NADH			Menadione		
	$k_{cat,app}$ (s^{-1})	$K_{M,app}$ (mM)	$k_{cat,app}/K_{M,app}$ ($mM^{-1}s^{-1}$)	k_{cat} (s^{-1})	K_M (μM)	k_{cat}/K_M ($\mu M^{-1}s^{-1}$)
NQO1 WT	1590 ± 52	3.22 ± 0.27	494 ± 44	1830 ± 82	11.6 ± 2.2	158 ± 31
NQO1 R139W	1580 ± 73	3.31 ± 0.38	478 ± 60	1730 ± 100	10.6 ± 2.8	162 ± 44

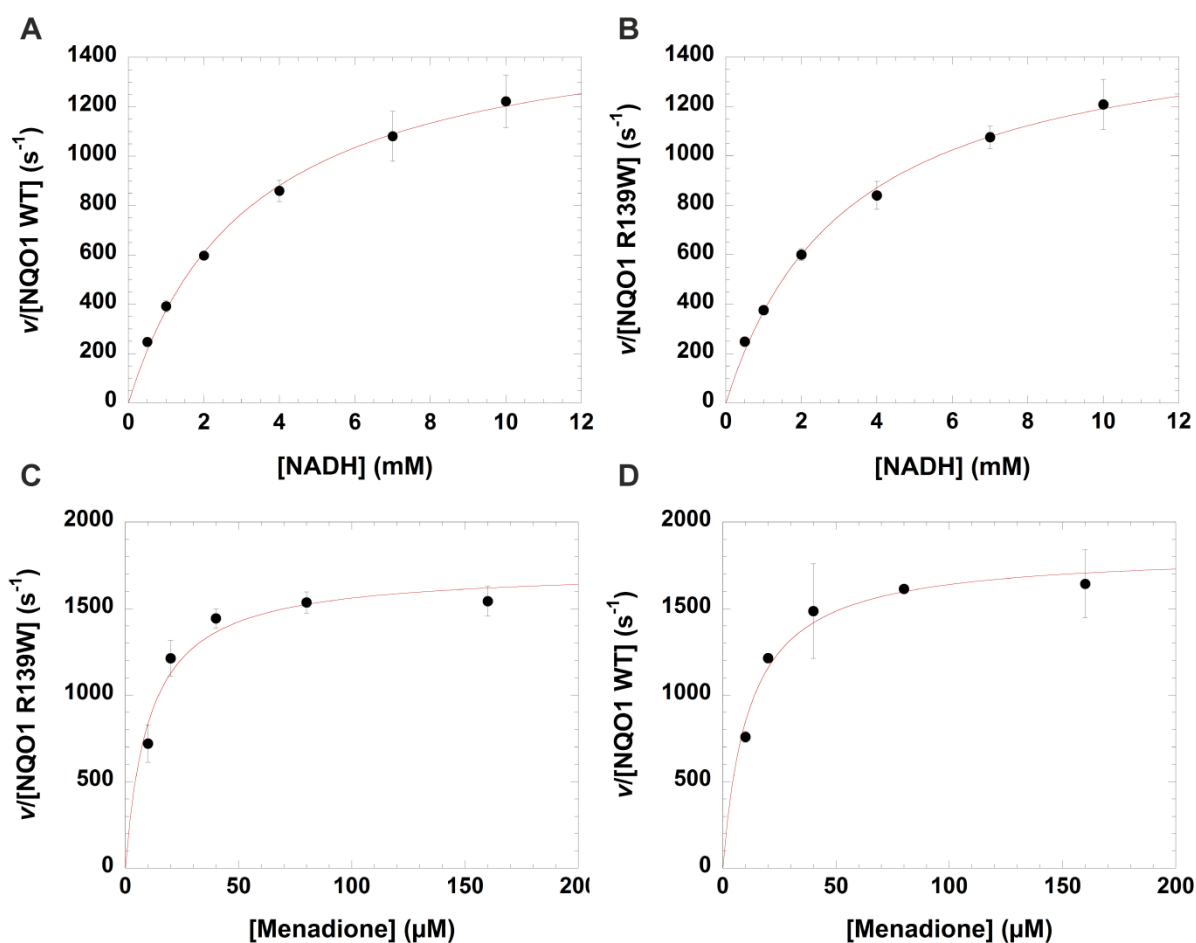


Figure 5. Steady state kinetics of NQO1 WT and NQO1 R139W. In the case of variation of NADH, the velocity v over the enzyme concentration is plotted against NADH concentration for NQO1 WT (A) and NQO1 R139W (B). For the variation of menadione, the velocity v over the enzyme concentration is plotted against menadione concentration for NQO1 WT (C) and NQO1 R139W (D). Standard deviations are shown with error bars.

Structural studies: X-ray crystallography, NMR-spectroscopy and partial proteolysis

To gain further insight into the structural properties of the R139W variant the crystal structure of this protein was solved (see Materials & Methods and Table 4).

Table 4. Data collection and refinement statistics.

	NQO1 R139W
Data collection	
X-ray source	SLS-X06DA
Wavelength (Å)	1.0
Temperature	100 K
Space group	<i>P</i> 1
Cell dimensions	
<i>a</i> , <i>b</i> , <i>c</i> (Å)	54.61, 59.93, 99.83
α , β , γ (°)	100.37, 92.85, 90.22
Resolution (Å)*	49.03-2.09 (2.17-2.09)
Total reflections	194450 (16603)
Unique reflections	67587 (5937)
Multiplicity*	2.9 (2.8)
Completeness (%)*	97.1 (86.89)
R_{meas}	0.093 (0.339)
R_{merge}	0.076 (0.296)
$\langle I/\sigma_I \rangle^*$	12.27 (4.1)
CC _{1/2} *	0.995 (0.906)
CC*	0.999 (0.975)
Refinement	
Resolution (Å)	49.03-2.09
$R_{\text{work}} / R_{\text{free}}$	0.1693 / 0.2013
No. of atoms	
Protein	8659
Cofactor/ligands	240
Water	1052
Mean B-factors (Å ²)	
Protein	23.40
Cofactor/ligands	26.60
Water	32.30
All atoms	24.40
R.m.s. deviations	
Bond lengths (Å)	0.004
Bond angles (°)	0.95
Ramachandran outliers (%)	0
PDB-entry	5A4K

The structure was determined to 2.1 Å and contains four protein chains in the asymmetric unit. These crystallographically independent molecules are very similar to each other, indicated by an average root-mean-square-deviation (rmsd) of 0.14 Å for a superposition of (on average) 224 out of 271 C α -atoms. The subunit structure of the R139W variant is also virtually identical to the wild-type structure with the exception of the amino acid replacement at position 139 (Figure 6). The respective average rmsd in this case is 0.18 Å for a superposition of 230 out of 271 C α -atoms.

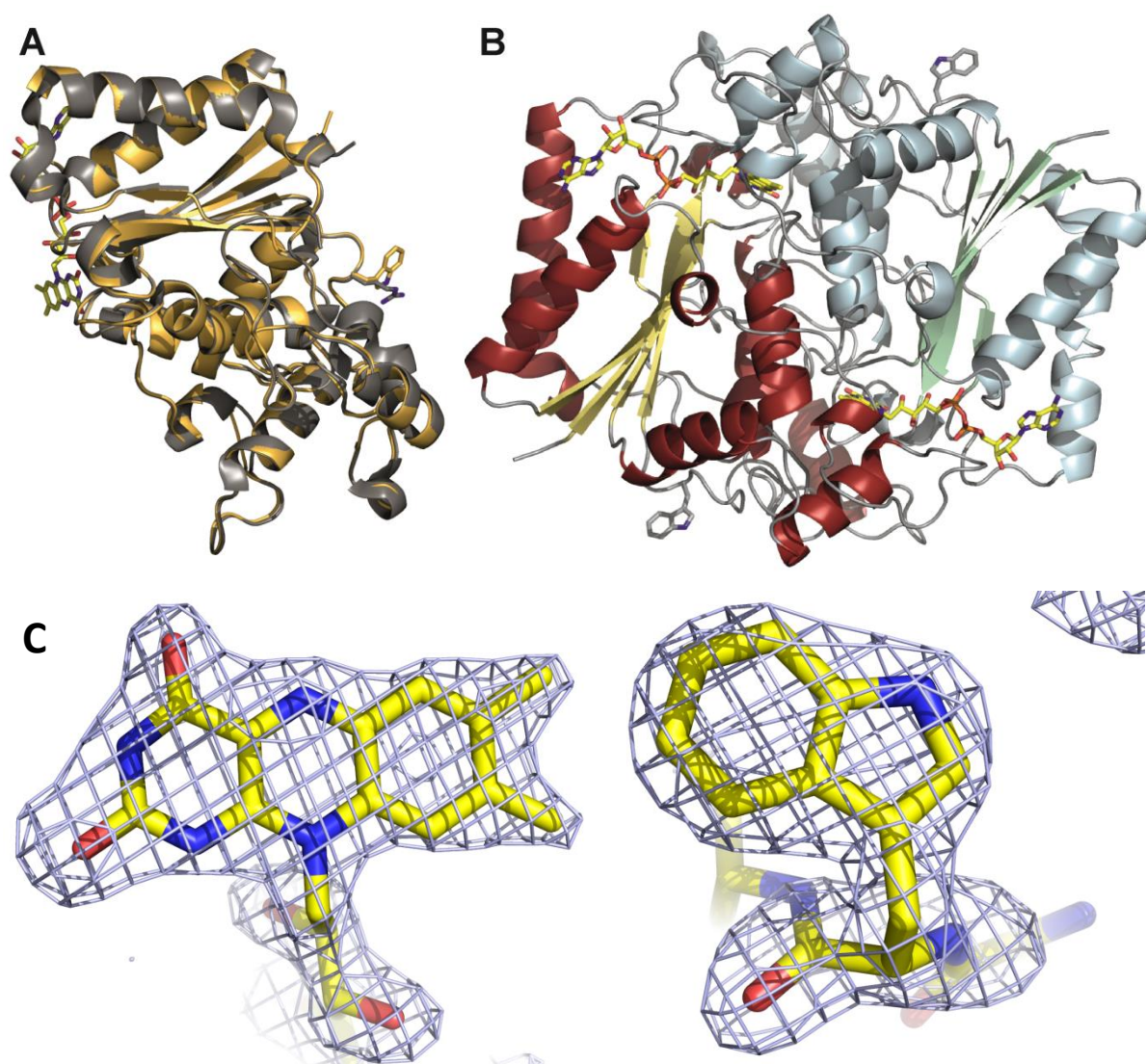


Figure 6. Crystal structure of NQO1 R139W. Panel A: Cartoon model of the superposition of NQO1 and NQO1 R139W with the arginine and tryptophan residue (right) and the FAD (left) shown as a stick model. Panel B: Cartoon model of the NQO1 R139W homodimer with the tryptophan residue and the FAD shown as a stick model. Panel C: $F_o - F_c$ omit electron density contoured at 3σ for the isoalloxazine moiety of FAD bound to one of the subunits (left) and for tryptophan 139 (right).

Recently, it was shown for the NQO1 P187S variant that despite adopting the same structure in the crystal it behaved very differently in solution as evidenced by 2D HSQC NMR-spectroscopy [14] (Figure 7, insert). Thus the R139W variant was also analysed using this technique. As shown in Figure 7, the 2D HSQC spectra of NQO1 (red) and NQO1 R139W (black) are again nearly identical with the exception of an additional signal found in the region typical for a nitrogen of the indole ring in tryptophan side chains (marked by an arrow in Figure 7). Minor shifts observed for a few signals are typical for a single amino acid exchange. Identical line-widths also indicate that the flexibilities of the two proteins are essentially unchanged.

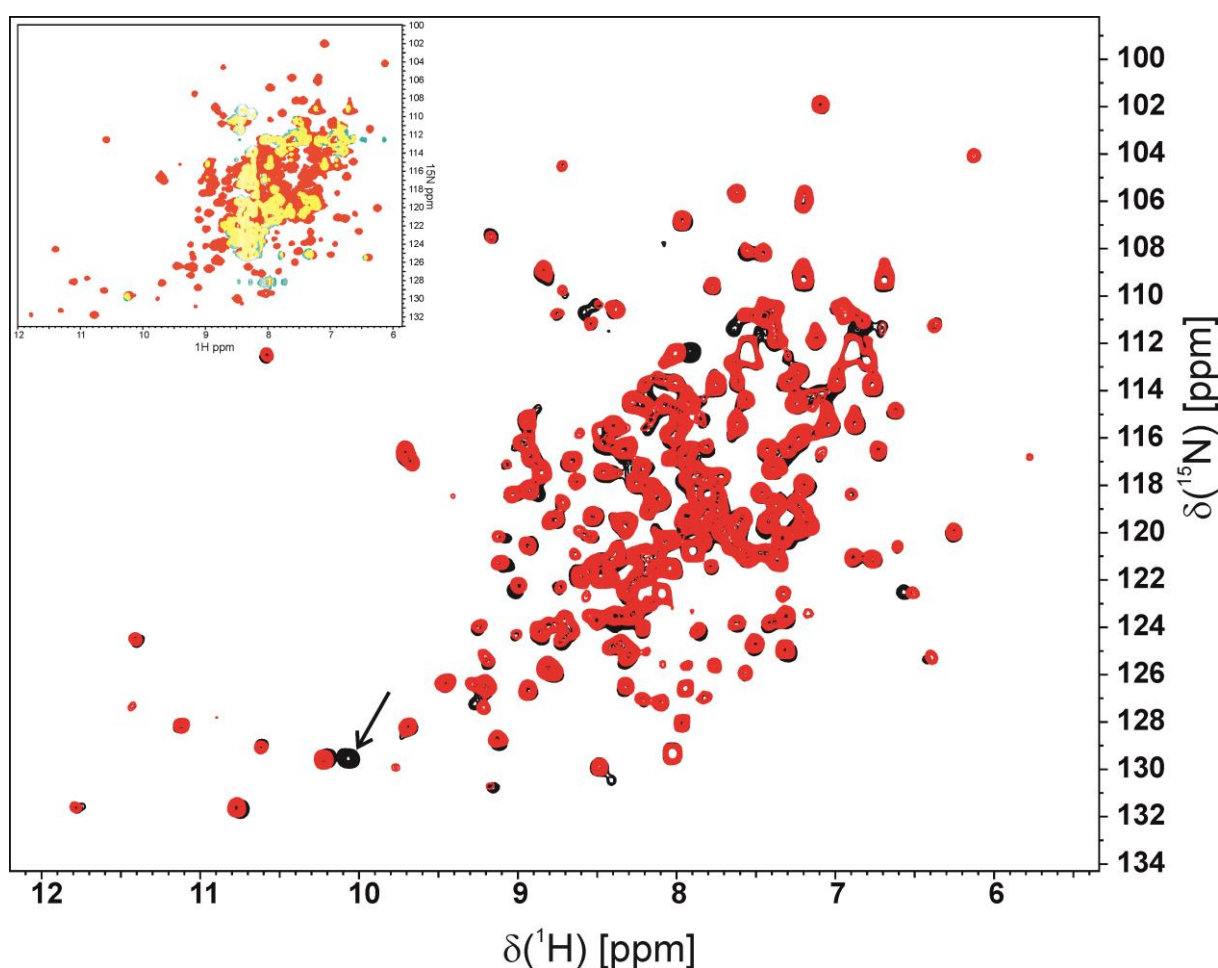


Figure 7. 2D ^1H - ^{15}N HSQC spectra. Overlay of the 2D ^1H - ^{15}N HSQC spectrum of NQO1 R139W (black) and wild-type (red). An additional tryptophan side chain NH signal is visible in the R139W variant and indicated by an arrow. All other signals are almost identical in the HSQC spectrum of the R139W variant and wild-type, respectively, indicative of a very similar structure. A few minor shift differences result from residues close to residue 139. The insert in the upper left corner shows an overlay of the NMR spectra of NQO1 WT (red) and NQO1 P187S (green) where overlapping areas are marked yellow.

Recently, we also demonstrated that limited tryptic digestion can be used to monitor the structural flexibility of NQO1 variants, i.e. the unstable and partially unfolded P189S variant. In the case of the R139W variant no difference in the digestion pattern compared to WT was detectable in agreement with the NMR-spectroscopic results (Figure 8).

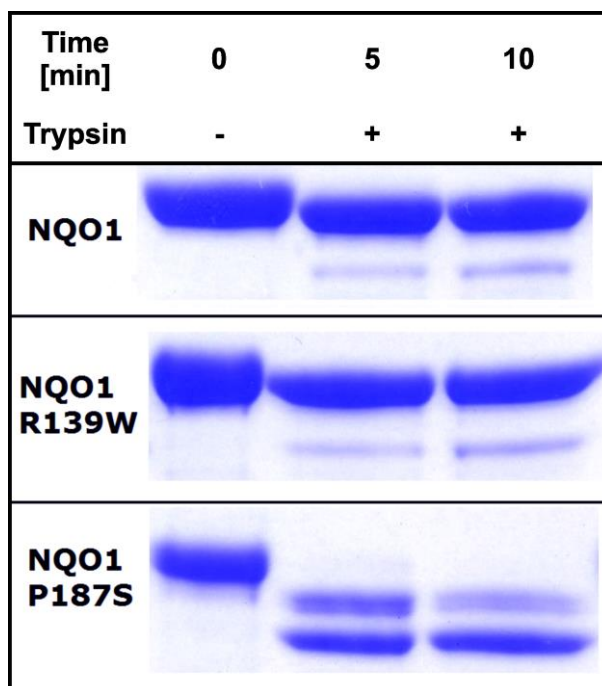


Figure 8. Trypsin digestion of different NQO1 variants. Comparison of Trypsin digestion of three NQO1 variants without addition of Trypsin (0 minutes) and two measurements after addition of Trypsin (5 and 10 minutes).

Discussion

NQO1 constitutes an important enzyme of the cellular defence system and plays a central role in the activation of quinone-based chemotherapeutics. The occurrence of genetic variants in the human population necessitates the proper evaluation of the biochemical properties of the resulting protein variants. Previous studies on the P187S protein variant (encoded by *NQO1*2*) demonstrated that this single amino acid exchange causes strong destabilization of the tertiary structure leading to a substantial loss of function [14,17]. Astonishingly, it could be demonstrated that the variant adopts a very similar crystal structure, while in solution the protein is present largely in an unfolded state [14]. This very unusual and unexpected behaviour of the

P187S variant prompted us to initiate a parallel study on the R139W variant caused by a single nucleotide transition in the *nqo1* gene (*NQO1*3*).

Initial analysis of the recombinant R139W variant by UV-visible absorption spectroscopy indicated that the affinity of the FAD cofactor as well as the nature of the cofactor binding site were not or only marginally affected by the arginine to tryptophan replacement (Figure 1). Further studies by ITC intended to obtain dissociation constants for FAD binding revealed that the apo-proteins of both wild-type and the R139W variant precipitated during the experiment, probably due to the damaging effect of shearing forces exerted by constant mixing in the sample cell. As a consequence, this particular experimental set-up resulted in non-reproducible and erroneous results leading to artefacts for the stoichiometry as well as binding affinities. SAXS measurements showed that the apo-protein is not as compact as the holo-protein but still forms a dimer (Figure 4). This may result in a lowered stability against shearing forces as well as in a lowered melting point (Table 1). Similar experiments were recently reported for wild-type NQO1 as well as the P187S and R139W variants and a sequential two site binding model was assumed to fit the data despite the fact that there is neither biochemical nor structural evidence that the two observed binding sites in the homodimeric protein are interdependent or different [17,33]. Depending on the experimental set-up the ratio of the two assumed binding sites was variable rendering the sequential binding site mode unlikely. Importantly, our ITC studies clearly demonstrate that these experimental artefacts can be avoided by simply reversing the order of the titration leading to reproducible data that is in accordance to the biochemical and structural background. We believe that this observation may also have implications for other biochemical systems investigated by ITC where one binding partner (in most cases this will be the macromolecule rather than the small ligand) is unstable under the experimental conditions. In the case of flavoproteins it is well-known that apo-proteins are much less stable than the holo-proteins in part due to the damaging effects required to prepare the apo-protein as well as the intrinsic destabilisation of the overall protein structure due to depletion of the flavin prosthetic group (mostly FMN or FAD) [36].

The detailed biochemical and structural analysis of the R139W variant revealed only minor differences in comparison to wild-type NQO1. Similarly, pre-steady state measurements yielded almost identical bimolecular rate constants for both enzyme variants (Table 2). The reductive half reaction was extremely fast

making it impossible to determine a reliable dissociation constant of NAD(P)H in our experimental setup. This indicates a low affinity of the pyridine nucleotides resulting in high K_D values as was already shown for the rat liver NQO1 [37]. Also, steady state measurements with the two enzyme variants produced comparable results. Interestingly, our measurements demonstrated that turnover hyperbolically increased with higher concentrations of NADH of up to 10 mM (!) suggesting that a canonical Michaelis-complex is not formed. This is in stark contrast to previous studies that reported K_M values in the order of about 50 to 300 μ M. However, these studies have only covered a very low concentration range of NADH and thus failed to recognize the non-classical behaviour of the enzyme [17,38]. These findings from pre-steady state and the steady state kinetic measurements indicate that NADH rapidly reduces the FAD cofactor of NQO1 without prior formation of a Michaelis-complex.

While the crystal structure of the previously studied variant NQO1 P187S was similar to the wildtype structure the NMR measurements revealed considerable movements of the residues [14]. In the case of the NQO1 R139W variant we found that the crystal structure as well as the solution structure, as evidenced by NMR-spectroscopy, is virtually identical to the wildtype protein (Figure 7). Self-association of the R139W variant caused by the higher hydrophobicity could not be observed in size exclusion chromatography. Nevertheless, we cannot exclude that under cellular conditions self-association may take place or the surface changes result in altered interaction with other proteins like the tumour suppressor p53. Tryptic digestion shows a comparable stability of NQO1 WT and NQO1 R139W in contrast to the faster degradation of NQO1 P187S as was already shown and confirmed in previous studies [14,17]. The NQO1 R139W variant only slightly differentiates from the NQO1 WT concerning FAD affinity (ca. 2.5 times weaker binding) and thermostability, by ca. 2 °C. Thus it can be safely concluded that the expression of this variant in humans has no adverse effect on the level of NQO1 activity. Therefore, the observed effects are most probably primarily caused by erroneous splicing of the premature mRNA, leading to the loss of exon 4 and thus reducing the amount of correctly spliced NQO1 in the cell [11].

Acknowledgements

This work was supported by the Austrian Fonds zur Förderung der wissenschaftlichen Forschung (FWF) through project P22361 to PM and KG and project P28854) to TM. Additional funding was received by the PhD programs “Molecular Enzymology” (W901) and “Molecular Basis of Cardiovascular Disease” (W1226) to KZ, KG, PM and to TM, respectively. We also thank the interuniversity program in natural sciences, NAWI Graz, for financial support.

References

- [1] W.D. Lienhart, V. Gudipati, P. Macheroux, The human flavoproteome. *Arch. Biochem. Biophys.* 535 (2013) 150-162.
- [2] D. Ross, D. Siegel, NAD(P)H:quinone oxidoreductase 1 (NQO1, DT-diaphorase), functions and pharmacogenetics, *Methods Enzymol.* 382 (2004) 115-144.
- [3] M. Garate, R.P. Wong, E.I. Campos, Y. Wang, G. Li, NAD(P)H quinone oxidoreductase 1 inhibits the proteasomal degradation of the tumour suppressor p33(ING1b), *EMBO Rep.* 9 (2008) 576-581.
- [4] G. Asher, P. Tsvetkov, C. Kahana, Y. Shaul, A mechanism of ubiquitin-independent proteasomal degradation of the tumor suppressors p53 and p73, *Genes Dev.* 19 (2005) 316-321.
- [5] K.T. Kelsey, D. Ross, R.D. Traver, D.C. Christiani, Z.F. Zuo, M.R. Spitz, M. Wang, X. Xu, B.K. Lee, B.S. Schwartz, J.K. Wiencke, Ethnic variation in the prevalence of a common NAD(P)H quinone oxidoreductase polymorphism and its implications for anti-cancer chemotherapy, *Br. J. Cancer* 76 (1997) 852-854.

- [6] A. Gaedigk, R.F. Tyndale, M. Jurima-Romet, E.M. Sellers, D.M. Grant, J.S. Leeder, NAD(P)H:quinone oxidoreductase: polymorphisms and allele frequencies in Caucasian, Chinese and Canadian Native Indian and Inuit populations, *Pharmacogenetics* 8 (1998) 305-313.
- [7] M. Eguchi-Ishimae, M. Eguchi, E. Ishii, D. Knight, Y. Sadakane, K. Isoyama, H. Yabe, S. Mizutani, M. Greaves, The association of a distinctive allele of NAD(P)H:quinone oxidoreductase with pediatric acute lymphoblastic leukemias with MLL fusion genes in Japan, *Haematologica* 90 (2005) 1511-1515.
- [8] M. Krajcinovic, H. Sinnett, C. Richer, D. Labuda, D. Sinnett, Role of NQO1, MPO and CYP2E1 genetic polymorphisms in the susceptibility to childhood acute lymphoblastic leukemia, *International Journal of Cancer* 97 (2002) 230-236.
- [9] R.K. Mandal, K. Nissar, R.D. Mittal, Genetic variants in metabolizing genes NQO1, NQO2, MTHFR and risk of prostate cancer: a study from North India, *Mol. Biol. Rep.* 39 (2012) 11145-11152.
- [10] J.J. Freriksen, J. Salomon, H.M. Roelofs, R.H. Te Morsche, J.W. van der Stappen, P. Dura, B.J. Witteman, M. Lacko, W.H. Peters, Genetic polymorphism 609C>T in NAD(P)H:quinone oxidoreductase 1 enhances the risk of proximal colon cancer, *J. Hum. Genet.* 59 (2014) 381-386.
- [11] S.S. Pan, Y. Han, P. Farabaugh, H. Xia, Implication of alternative splicing for expression of a variant NAD(P)H:quinone oxidoreductase-1 with a single nucleotide polymorphism at 465C>T, *Pharmacogenetics* 12 (2002) 479-488.
- [12] R.D. Traver, D. Siegel, H.D. Beall, R.M. Phillips, N.W. Gibson, W.A. Franklin, D. Ross, Characterization of a polymorphism in NAD(P)H: Quinone oxidoreductase (DT-diaphorase), *Br. J. Cancer* 75 (1997) 69-75.
- [13] D. Siegel, A. Anwar, S. Winski, J. Kepa, K. Zolman, D. Ross, Rapid polyubiquitination and proteasomal degradation of a mutant form of NAD(P)H:Quinone oxidoreductase 1, *Mol. Pharmacol.* 59 (2001) 263-268.

- [14] W.D. Lienhart, V. Gudipati, M.K. Uhl, A. Binter, S.A. Pulido, R. Saf, K. Zangger, K. Gruber, P. Macheroux, Collapse of the native structure caused by a single amino acid exchange in human NAD(P)H:quinone oxidoreductase 1, *FEBS Journal* 281 (2014) 4691-4704.
- [15] P.Y. Gasdaska, H. Fisher, G. Powis, An alternatively spliced form of NQO1 (DT-diaphorase) messenger RNA lacking the putative quinone substrate binding site is present in human normal and tumor tissues, *Cancer Res.* 55 (1995) 2542-2547.
- [16] L.T. Hu, J. Stamberg, S. Pan, The NAD(P)H:quinone oxidoreductase locus in human colon carcinoma HCT 116 cells resistant to mitomycin C, *Cancer Res.* 56 (1996) 5253-5259.
- [17] A.L. Pey, C.F. Megarity, D.J. Timson, FAD binding overcomes defects in activity and stability displayed by cancer-associated variants of human NQO1, *Biochim. Biophys. Acta* 1842 (2014) 2163-2173.
- [18] D.W. Nebert, A.L. Roe, S.E. Vandale, E. Bingham, G.G. Oakley, NAD(P)H:quinone oxidoreductase (NQO1) polymorphism, exposure to benzene, and predisposition to disease: a HuGE review, *Genet. Med.* 4 (2002) 62-70.
- [19] A. Begleiter, N. El-Gabalawy, L. Lange, M.K. Leith, L.J. Guziec, F.S. Guziec Jr., A Model for NAD(P)H:Quinoneoxidoreductase 1 (NQO1) Targeted Individualized Cancer Chemotherapy, *Drug Target Insights* 4 (2009) 1-8.
- [20] D. Siegel, C. Yan, D. Ross, NAD(P)H:quinone oxidoreductase 1 (NQO1) in the sensitivity and resistance to antitumor quinones, *Biochem. Pharmacol.* 83 (2012) 1033-1040.
- [21] Z. Dai, A.C. Papp, D. Wang, H. Hampel, W. Sadee, Genotyping panel for assessing response to cancer chemotherapy. *BMC Med Genomics* 1 (2008) 24-8794-1-24.

- [22] G.T. Gang, Y.H. Kim, J.R. Noh, K.S. Kim, J.Y. Jung, M. Shong, J.H. Hwang, C.H. Lee, Protective role of NAD(P)H:quinone oxidoreductase 1 (NQO1) in cisplatin-induced nephrotoxicity, *Toxicol. Lett.* 221 (2013) 165-175.
- [23] D. Svergun, Determination of the regularization parameter in indirect-transform methods using perceptual criteria, *Journal of applied crystallography* 25 (1992) 495-503.
- [24] W. Kabsch, XDS. *Acta Crystallogr.* 66,(2010) 125-132.
- [25] Collaborative Computational Project N4, The CCP4 suite: programs for protein crystallography, *Act. Crystallogr.* 50 (1994) 760-763.
- [26] A.J. McCoy, R.W. Grosse-Kunstleve, P.D. Adams, M.D. Winn, L.C. Storoni, R.J. Read Phaser crystallographic software, *J. Appl. Crystallogr.* 40 (2007) 658-674.
- [27] G.J. Kleywegt, A.T. Brunger, Checking your imagination: applications of the free R value, *Structure* 4 (1996) 897-904.
- [28] P.D. Adams, P.V. Afonine, G. Bunkoczi, V.B. Chen, I.W. Davis, N. Echols, J.J. Headd, L.W. Hung, G.J. Kapral, R.W. Grosse-Kunstleve, A.J. McCoy, N.W. Moriarty, R. Oeffner, R.J. Read, D.C. Richardson, J.S. Richardson, T.C. Terwilliger, P.H. Zwart, PHENIX: a comprehensive Python-based system for macromolecular structure solution, *Acta Crystallogr.* 66 (2010) 213-221.
- [29] P. Emsley, K. Cowtan, Coot: model-building tools for molecular graphics, *Acta Crystallogr.* 60 (2004) 2126-2132.
- [30] P. Emsley, B. Lohkamp, W.G. Scott, K. Cowtan, Features and development of Coot, *Acta Crystallogr.* 66 (2010) 486-501.
- [31] V.B. Chen, W.B. Arendall 3rd, J.J. Headd, D.A. Keedy, R.M. Immormino, G.J. Kapral, L.W. Murray, J.S. Richardson, D.C. Richardson, MolProbity: all-atom structure validation for macromolecular crystallography, *Acta Crystallogr.* 66 (2010) 12-21.

- [32] E. Krissinel, K. Henrick, Inference of macromolecular assemblies from crystalline state, *J. Mol. Biol.* 372 (2007) 774-797.
- [33] M.C. Encarnacion, R.J. Palomino-Morales, J.E. Fuchs, P.G. Esperanza, M.T. Noel, E. Salido, D.J. Timson, A.L. Pey, Conformational dynamics is key to understanding loss-of-function of NQO1 cancer-associated polymorphisms and its correction by pharmacological ligands, *Sci. Rep.* 6 (2016) 20331.
- [34] S. Chen, P.S. Deng, J.M. Bailey, K.M. Swiderek, A two-domain structure for the two subunits of NAD(P)H:quinone acceptor oxidoreductase, *Protein Sci.* 3 (1994) 51-57.
- [35] F. Forneris, R. Orru, D. Bonivento, L.R. Chiarelli, A. Mattevi, ThermoFAD, a Thermofluor-adapted flavin ad hoc detection system for protein folding and ligand binding, *FEBS J.* 276 (2009) 2833-2840
- [36] M.H. Hefti, J. Vervoort, W.J. van Berkel, Deflavination and reconstitution of flavoproteins, *Eur. J. Biochem.* 270 (2003) 4227-4242.
- [37] G. Tedeschi, S. Chen, V. Massey, DT-diaphorase. Redox potential, steady-state, and rapid reaction studies, *J. Biol. Chem.* 270 (1995) 1198-1204.
- [38] S. Pan, G.L. Forrest, S.A. Akman, L. Hu, NAD(P)H:Quinone oxidoreductase expression and Mitomycin C resistance developed by human colon cancer HCT 116 cells, *Cancer Research* 55 (1995) 330-335.

CURRICULUM VITAE

Personal Information

Name: Karin Maria Koch
Address: Körösisstraße 48c/24,
8010 Graz
E-Mail: karin.maria.koch@gmail.com
Tel.: +43/680/4064949
Date and place of birth: 15th April 1985 in Spittal/Drau
Citizenship: Austria



Education

Since 09/2012 PhD Studies of Natural Sciences at the Graz University of Technology; Branch of the Study: Biochemistry
04/2010-07/2012 Master Studies of Biochemistry and Molecular Biomedicine at the Karl-Franzens University Graz, Degree: MSc
09/2005-04/2010 Bachelor Studies of Molecularbiology at the Karl-Franzens University Graz, Degree: Bakk. rer. nat.
09/2001-07/2005 Secondary School for Agricultur and Nutrition Pitzelstätten in Klagenfurt
09/1999-07/2001 Home Economics School Schloss Oberlorenzen in St. Lorenzen
09/1995-07/1999 Secondary Modern School in St. Katharein/Lmg.
09/1991-07/1995 Elementary School in Tragöß

Research activities

- 09/2012-03/2017 Work on PhD-project entitled "*Flavoproteins from Saccharomyces cerevisiae*" at the Institute of Biochemistry, Graz University of Technology (Supervisor: Prof. Peter Macheroux)
- 10/2011-05/2012 Master thesis project entitled "*Cellular role of the yeast bZip transcription factor Yap4p*" at the Institute of Biochemistry, Graz University of Technology (Supervisor: Prof. Peter Macheroux)
- 05/2011-07/2011 Project entitled "*Role of PBX2, TGF- β 1,2,3 and SMAD4 in the pathogenesis of nephroblastomas*" at the Institute of Pathology, Medical University Graz (Supervisor: Dr. Barbara Gürtl-Lackner)

Other occupational activities

- 09/2012-10/2016 University assistant with teaching assignment at the Graz University of Technology
- Supervision of laboratory courses in the field of Biochemistry and Immunological methods
 - Mentoring of Bachelor and Master students
 - Supervision of courses within the framework of the "Children university"

Other Qualifications

Foreign Languages: English (Fluent, spoken and written)

Italian (Basics)

Computer Skills: MS-Office (Word, Excel, Power Point)
Skills in Bioinformatics (Databases, Sequence analysis, PyMOL, etc.)

Driving Licence B

PUBLICATION LIST

Publications in reviewed journals

K. Koch, P. Macheroux, Microtubule-associated Irc15p from *Saccharomyces cerevisiae* is an FAD-dependent NADH dehydrogenase, (2017) Manuscript in preparation

K. Koch, A. Hromic, M. Sorokina, E. Strandback, M. Reisinger, K. Gruber, P. Macheroux, Structure, biochemical and kinetic properties of recombinant Pst2p from *Saccharomyces cerevisiae*, a FMN-dependent NAD(P)H:quinone oxidoreductase, (2017) Manuscript submitted

W.-D. Lienhart[‡], E. Strandback[‡], V. Gudipati, **K. Koch**, A. Binter, M.K. Uhl, D.M. Rantasa, B. Bourgeois, T. Madl, K. Zangger, K. Gruber, P. Macheroux, Catalytic competence, structure and stability of the cancer associated R139W variant of the human NAD(P)H:quinone oxidoreductase 1 (NQO1), FEBS J. (2017), Manuscript accepted, DOI: 10.1111/febs.14051.

[‡] The first two authors have contributed equally to this work.

K. Koller, M. Pichler, **K. Koch**, M. Zandl, V. Stiegelbauer, I. Leuschner, G. Hoefler, B. Guertl, Nephroblastomas show low expression of microR-204 and high expression of its target, the oncogenic transcription factor MEIS1, *Pediatr. Dev. Pathol.* 17 (2014) 169-75.

V. Gudipati, **K. Koch**, W.-D. Lienhart, P. Macheroux, The flavoproteome of the yeast *Saccharomyces cerevisiae*, *Biochim. Biophys. Acta* 1844 (2014) 535–44.

Poster presentations on international conferences

K. Koch, P. Macheroux, The protective/regulative role of the antioxidant enzyme Irc15 on the microtubule network of *S. cerevisiae*, 8th European Meeting on OxiZymes, Wageningen (Netherlands), 2016.

K. Koch, P. Macheroux, Biochemical and structural characterization of the microtubule-associated protein Irc15, 27th International conference on yeast genetics and molecular biology, Levico Terme (Italy), 2015.

K. Koch, J. Repelnig, P. Macheroux, New insights in flavodoxin-like proteins from *S. cerevisiae*, Enzyme Mechanisms by Biological Systems, Manchester (Great Britain), 2014.

K. Koch, K. Athenstaedt, V. Gudipati, P. Macheroux, A novel role for the yeast bZIP transcription factor Yap4p in the regulation of sterol biosynthesis, FEBS Congress, St. Petersburg (Russia), 2013.

V. Gudipati, W.-D. Lienhart, **K. Koch**, J. Dohmen, P. Macheroux, Yeast quinone reductase Lot6p mediates the degradation of transcription factor Yap4p by the 20S proteasome, FEBS Special Meeting on Protein Quality Control and Ubiquitin Systems in Health and Disease, Kusadasi (Turkey), 2012.

Other poster presentations

K. Koch, A. Hromic, M. Sorokina, M. Reisinger, K. Gruber, P. Macheroux NAD(P)H:quinone oxidoreductases from *Saccharomyces cerevisiae*, 8th ÖGMBT Annual Meeting, Graz (Austria), 2016.

K. Koch, A. Hromic, M. Sorokina, M. Reisinger, K. Gruber, P. Macheroux, The flavodoxin-like proteins Pst2 and Ycp4 from *Saccharomyces cerevisiae* belong to the FMN-dependent NAD(P)H:quinone oxidoreductases, 16th DocDay - NAWI Graz Doctoral School of Molecular Biosciences and Biotechnology, Graz (Austria), 2016.

K. Koch, P. Macheroux, Biochemical and structural characterization of the microtubule-associated protein Irc15, 14th DocDay - NAWI Graz Doctoral School of Molecular Biosciences and Biotechnology, Graz (Austria), 2015.

V. Gudipati, W.-D. Lienhart, **K. Koch**, P. Macheroux, Yeast quinone reductase Lot6p and its interactions with 20S proteasome and Yap4p, Enzymes & Signals - A research summit of the DK Molecular Enzymology and the DK Molecular Mechanisms of Cell Signaling, Graz (Austria), 2012.